RESOLUTION LIMITS IN

ELECTRON BEAM LITHOGRAPHY.

A Thesis
submitted to the Faculty of Engineering
of the University of Glasgow
for the degree of

Doctor of Philosophy

by

Stephen Anthony Rishton, B.Sc.(Eng).

February 1984.

Acknowledgements

I wish to express my thanks to all of the academic, technical, and computing staff of the Department who were involved in this project, and to my fellow research students.

In particular, I thank Professor J. Lamb, and Dr. P.J.R. Laybourn as Acting Head of Department, for the provision of the laboratory and computing facilities, and my supervisor Professor C.D.W. Wilkinson, and Dr. S.P. Beaumont for their enthusiastic advice and encouragement during the project.

I thank H. Anderson and all of his Mechanical Workshop staff, including J. Purves who has unfortunately left due to illness, for their expert manufacturing of many components, often at very short notice.

I am grateful to J. Crichton, J. Clark, G. Boyle, L. Hobbs, F. Regan, B. Miller, K. Piechowiak, R. Harkins, P. Watters, R. Darkin, J. Young, and J. Simms for their practical assistance during the project, and to the computer staff for retieving many lost files.

I acknowledge many useful discussions with C.E. Binnie and W.S. Mackie during the project, and I thank K.Y. Lee for providing some results for use in this thesis. I thank B. Singh for his collaboration in the work on arsenic trisulphide resist.

During this work I was in receipt of an SERC grant, and a CASE award with British Telecom Research Laboratories. I wish to thank my supervisor at BTRL, Dr. M.E. Jones, together with C. Dix, P. Hendy, and P. Flavin, for their support. I also thank J. Bizzell and M. Holmes of the Rutherford Appleton Laboratory, for

useful discussions on the practical applications of the electron beam measurement technique, and Professor H.E. Smith of Massachusetts Institute of Technology for providing <110> silicon wafers.

I am grateful to Professor R. Ferrier of the Natural Philosophy Department, Glasgow University for allowing the use of equipment, and to G.R. Morrison, J.N. Chapman, A.J. Craven, and P. Nicholson, also of the Natural Philosophy Department, for performing the high resolution HB5 measurements and for their very useful advice.

I thank Dr. A.N. Broers for introducing me to the subject of electron beam lithography.

Finally I thank my family and friends, and Siew Peng Lim, for their support.

Contents

Summary

This work is applicable to the resolution limits of electron beam lithography in thin resist layers on thin support membranes, in particular using poly(methyl methacrylate) (PMMA) as the electron beam resist. On thin support membranes it is generally found that the ultimate resolution of PMMA is about 10 nanometres, whereas on solid substrates the resolution for arbitrary patterns is usually of the order of 100 nanometres, due to the large numbers of high energy electrons backscattered from the substrate.

It has been proposed that secondary electron production within the resist, and the subsequent "energy spreading" caused by the higher-energy secondaries having a significant range in the material, is responsible for the ultimate resolution of PMMA on thin substrates. In this work, the range over which electrons of a given energy are able to expose the resist was measured by a direct method. The material was exposed by means of a low energy, constant current density electron beam, and after development the loss of thickness was measured. Electron ranges measured by this method are directly applicable to the study of resolution limits in lithography.

The energy distribution of secondary electrons created in the resist by inelastic collisions of high energy primary electrons was estimated by electron energy loss spectroscopy. These measurements were combined with the low energy electron range data in a Monte-Carlo program to simulate line exposures on a nanometre scale. The simulation program has been used to suggest how improvements in resolution and the minimum spacing of features might be brought about.

Measurements of the effective resist contrast on a macroscopic

scale were made, in order to optimise the development process for very high resolution lithography in PMMA. A cross-linking positive methacrylate resist was also characterised macroscopically.

The linewidth-exposure dose relationship for fine line exposures in very thin PMMA was measured. In most cases the exposures were performed by an electron beam of nominal diameter similar to the minimum linewidths obtained. An accurate method of measuring electron beams of less than 10 nanometres in diameter has been developed, in order to ascertain the effect on linewidths of the electron beam profile. This method involves scanning the electron beam across an etched silicon edge, and detecting the transmitted current. The technique is also found to be of use in producing consistent measurements of larger diameter electron beams in commercial lithographic equipment.

Using the low energy electron exposure system designed for the measurement of secondary electron ranges in PMMA, some further work was performed on the sensitivity to low energy electrons of the amorphous chalcogenide glass resist arsenic trisulphide, enabling some conclusions to be drawn on the exposure mechanism of this material.

CHAPTER 1

Introduction

1.1 Significance of the resolution limits of electron beam lithography

The principal use of electron beam lithography at present is in the production of reticles for the semiconductor industry, which are then reproduced by optical projection. The resolution of optical lithography is limited by the wavelength of the radiation to hundreds of nanometres, and electron beam lithography can quite easily better this by some considerable margin, so its theoretical resolution limit is not usually called into question; speed and coverage area are more significant factors.

In the manufacture of digital electronics, the expertise available in optical lithography provides the gradual improvements in performance necessary for growth of the industry, while it seems increasingly unlikely that other techniques of patterning semiconductor wafers directly, such as x-ray, ion beam, and electron beam lithography, will become competitive in mass production, mainly for reasons of speed and the cost of equipment. However, the current popularity being enjoyed by Boolean logic, on which most modern electronics is based, may not continue indefinitely. Future techniques may require the use of devices which are small on an atomic scale, whereas at present the size of a device is only one factor in the performance versus cost relationship. The finest resolution of any lithographic process is achieved by electron beam lithography, yet it has not approached the theoretical limit set by the smallest focused electron probe that can be formed (less than 1 nanometre). The success of attempts to fabricate structures with dimensions of

the order of 10nm will rely on a detailed knowledge of the interaction of the electron beam and resist on this scale, and the present work is a study of this interaction.

1.2 The scanning electron microscope

The apparatus for electron beam lithography is based on the scanning electron microscope (SEM), in which a finely focused beam of electrons is scanned over an area of a specimen to be examined. A review of the early development of the SEM was given recently by Oatley[1.1]. The first scanning electron microscope was a transmission instrument which was constructed in Germany in the 1930's by von Ardenne[1.2,1.3], but the instrument was not used extensively in this form since it could not compete in resolution and ease of use with the conventional transmission electron microscope arrangement. Scanning electron microscopes for the examination of thick specimens became practical in the early 1950's when sensitive secondary electron detectors were developed[1.4-1.6], but the first commercial SEM, the Cambridge Instrument Company's "Stereoscan", was not marketed until 1965.

The basic theory of electron beam diameter, lens aberration, and probe current and brightness (current into unit solid angle) was given by K.C.A. Smith[1.7]. At present, commercial SEM's are available which can form electron probes of about 5nm diameter, but scanning transmission electron microscopes (STEM's) are also available commercially, which may have probe diameters as small as 0.5nm (in the case of the Vacuum Generators HB5 instrument).

1.3 Scanning electron beam lithography

At an early stage in the development of scanning electron microscopy (1960), it was demonstrated by Mollenstedt and

Speidel[1.8] that patterning of a thin membrane (in this case collodion) could be achieved with a resolution of about 20nm. In 1965 Broers demonstrated 150nm wide metal lines on a solid silicon substrate by the beam-induced polymerisation of organic contamination (residual vacuum pump oil) onto the specimen, and subsequent ion etching[1.9]. A similar technique was later used to achieve 8nm metal features on thin silicon nitride substrates[1.10].

Organic contamination as an electron resist suffers from very poor sensitivity, and from depletion when closely spaced features are attempted. The development of poly(methyl methacrylate) (PMMA) as an electron beam resist[1.11] has led to more practical high-resolution electron beam lithography. Using a double-layer PMMA resist structure (to provide undercut profiles) and lift-off processing, it has been possible to achieve metal lines 10nm wide on thin substrates[1.12,1.20]. In this case the exposures were made using an 8nm beam, but the resolution has not been bettered using a beam of less than 1nm diameter[1.13]. The linewidth limit is significantly greater when closely-spaced line exposures are made[1.12,1.13].

On thick substrates the resolution of electron beam lithography can be poorer than on thin membranes due to significant backscattering of high-energy electrons from the substrate[1.14]. However, the use of PMMA and lift-off processing has enabled silicon MOS transistors with gate lengths as short as 100nm to be fabricated[1.15]; with very high electron acceleration potentials (120kV) it has been possible to reduce the effect of backscattering to such an extent that 10nm linewidths have been achieved on solid gallium arsenide[1.16]. Such high resolution lithography on solid substrates presents problems of examination and alignment, and it may be more practical to manufacture semiconductor devices of dimensions smaller than 100nm on thin semiconductor membranes[1.12].

The amorphous nature of the inorganic resists arsenic trisulphide and germanium selenium glass has aroused interest in these materials for high resolution lithography, but the results from these materials have not approached the resolution of PMMA[1.17,1.18]. Langmuir-Blodgett films have recently been patterned with lines as narrow as 10nm [1.19], although the image transfer to metal from such films may prove to be more difficult than from PMMA.

Very fine, high brightness electron beams have been used to cut 2nm wide lines through thin crystals of sodium chloride[1.21] and various metal beta-aluminas[1.22]. The direct cutting technique, however, necessitates much longer exposure times than conventional exposure-development techniques. Patterns cut in these materials have not been transferred to other materials in order to form useful structures, and the method is not yet considered to be a practical lithographic process.

1.4 Outline of the work presented

The main body of the work presented will be concerned with the characterisation of the various effects involved in the exposure of PMMA by electron beams, and will be particularly applicable to very high resolution lithography (ie. less than 0.1 micron linewidths) on thin substrates. A consistent method for the measurement of sub-10nm-diameter electron beams is presented; measurements are made to optimise the effective resist contrast in the development process; the numbers of secondary electrons generated in the resist (by the collision of primary electrons - see figure 1.1) are estimated by electron energy loss spectroscopy, and the ranges over which such low-energy electrons are able to expose the resist are measured. These measurements are brought together in a Monte-Carlo model which should be more

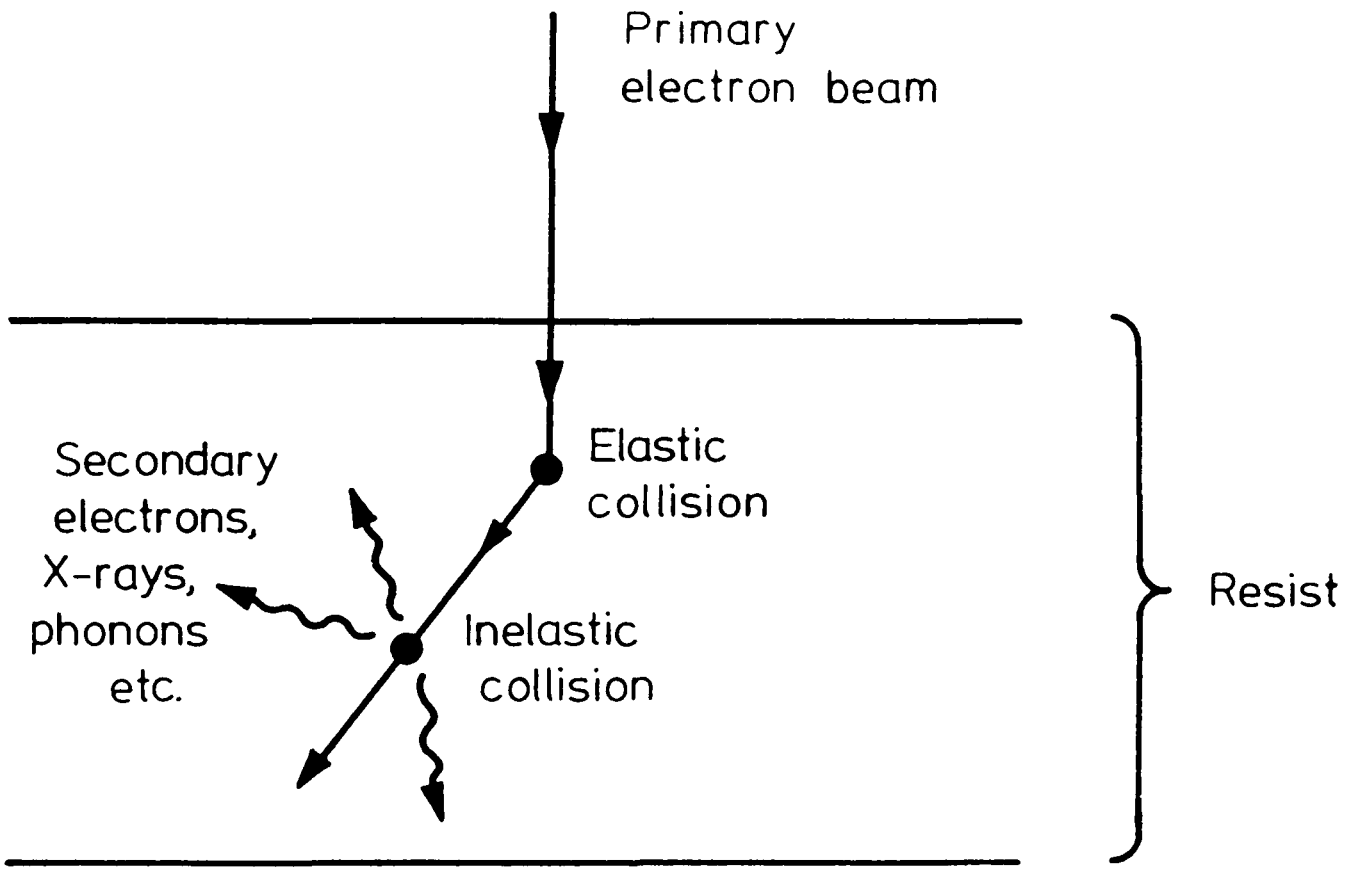

Fig. 1.1 Electron beam exposure of resist.

accurate than one based on theoretical predictions. The results of simulations of single-line exposures using the model are compared with those of experimental exposures, with both 8nm and very fine (less than 1nm) electron beams.

Some results are also presented on the low-energy electron exposure of the inorganic resist arsenic trisulphide; these results represent a further use of the low-energy exposure system used to measure the range of secondary electrons in PMMA.

References

1.1 C.W. Oatley "The early history of the scanning electron microscope"
J. Appl. Phys. 53(2), R1-R13, 1982.

1.2 M. von Ardenne "The scanning electron microscope: Theoretical fundamentals"
Z. Phys. 109, 553-572, 1938.

1.3 M. von Ardenne "The scanning electron microscope: Practical construction"
Z. Tech. Phys. 19, 407-416, 1938.

1.4 A.S. Baxter "Detection and analysis of low energy disintegration particles"
Ph.D. Thesis, Cambridge University, 1949.

1.5 D. McMullan "An improved scanning electron microscope for opaque specimens"
Proc. IEE II 100, 245-259, 1953.

1.6 D. McMullan "The scanning electron microscope and the electron-optical examination of surfaces"

Electron. Eng. (England) 25, 46-50, 1953.

1.7 K.C.A. Smith; Ph.D. Thesis, Cambridge University, 1956.

1.8 G. Mollenstedt and R. Speidel; Physikalische Blatter 16, 192, 1960.

1.9 A.N. Broers; Proceedings of the First International Conference on Electron and Ion Beam Science and Technology, 191-204, ed. R.A. Bakish, Wiley 1965.

1.10 A.N. Broers, W.W. Molzen, J.J. Cuomo, and N.D. Wittels "Electron-beam fabrication of 80 angstrom metal structures" Appl. Phys. Lett. 29(9), 596-598, 1976.

1.11 I. Haller, M. Hatzakis, and R. Scrinivasan; IBM J. Res. Develop., 12, 251, 1968.

1.12 W.S. Mackie; Ph.D. Thesis, Glasgow University, 1984.

1.13 A.N. Broers "Resolution limits of PMMA resist for exposure with 50kV electrons"
J. Electrochem. Soc.: Solid-state science and technology; 128(1), 166-170, 1981.

1.14 S.P. Beaumont, B. Singh, and C.D.W. Wilkinson "Very high resolution electron beam lithography - Thin films, or solid substrates?"
Tenth International Conference on Electron and Ion Beam Science and Technology, Ed. R. Bakish, Montreal, 1982

1.15 C.E. Binnie; Ph.D. Thesis, Glasgow University, 1984.

1.16 H.G. Craighead, R.E. Howard, L.D. Jackel, and P.M. Mankiewich "10-nm linewidth electron beam lithography on GaAs"

Appl. Phys. Lett. 42(1), 38-40, 1983.

1.17 B. Singh, S.P. Beaumont, P.G. Bower, and C.D.W. Wilkinson "New inorganic resist system for high resolution lithography" Appl. Phys. Lett. 41(9), 889-891, 1982.

1.18 B. Singh, S.P. Beaumont, P.G. Bower, and C.D.W. Wilkinson "Sub-50-nm lithography in amorphous Se-Ge inorganic resist by electron beam exposure" Appl. Phys. Lett. 41(10), 1002-1004, 1982.

1.19 A.N. Broers and M. Pomerantz "Rapid writing of fine lines in Langmuir-Blodgett films using electron beams" Thin Solid Films, 99, 323-329, 1983.

1.20 S.P. Beaumont, T. Tamamura, and C.D.W. Wilkinson; Proceedings of Microcircuit Engineering 80, Amsterdam, 1980.

1.21 M. Isaacson and A. Murray; J. Vac. Sci. Technol. 19, 1117, 1981.

1.22 M.E. Mochel, C.J. Humphreys, J.A. Eades, J.M. Mochel, and A.M. Petford "Electron beam writing on a 20 angstrom scale in metal beta-aluminas" Appl. Phys. Lett. 42(4), 392-394, 1983.

CHAPTER 2

Measurement of electron beam profiles

2.1 Introduction

The accurate measurement of the diameter of the focused spot of an electron beam is important in electron beam lithography, as the spot size influences the minimum width of line which can be written by a given electron beam machine. Metal lines 10nm wide have been produced using lift-off processing of lines written in PMMA by our Philips scanning electron microscope with a nominal spot diameter of 8nm. Quantitative information on an electron beam of this order of size is very important in assessing such results. As well as measuring the nominal spot diameter of the beam, it is also useful to measure any significant "tails" in the beam shape, outside the nominal diameter, which could affect the minimum line spacing and the exposure latitude that can be achieved in lithography.

Scanning electron microscope columns in general, and those used in e-beam lithography machines in particular, have no facilities for imaging the spot formed by the final (objective) lens. In order to measure the beam diameter, resort is therefore made either to resolution tests, where the minimum edge-to-edge or centre-to-centre spacing observable in the image of a suitable test specimen is taken as a measure of spot diameter, or to edge definition measurements where the reflected or transmitted current is measured as the beam is scanned across a sharp edge. The former method is recognised as being somewhat arbitrary, as the result is specimen-dependent. The latter is potentially capable of yielding more quantitative information about beam size and shape, and should allow consistent measurements to be made by

different observers. The sharp edge employed must be straight and opaque to electrons to a distance within the accuracy that is required of the measurement. Using edges etched in metal foils, it is very difficult to achieve simultaneously a sharp edge and sufficient thickness of film to provide adequate opacity. Cleaver and Smith[2.1] have made spot measurements of about 20 to 30 nanometres using etched copper foils, and it has been found that 20nm is approximately the resolution limit of this method. A slightly rounded edge will tend to scatter electrons into the detector, and it is found that the signal trace varies rapidly as the beam is moved along the specimen, indicating considerable irregularities in the edge.

2.2 Use of vertical etched silicon edges for beam measurement.

In this chapter the use of anisotropically etched silicon to provide the sharp edge is considered. Silicon is an ideal material to provide edges that are straight to well within the dimensions that are required in most electron beam measurements, because it can readily be etched along crystal planes. It is also a convenient material to use since it can be etched to the specimen dimensions required. A standard <100> silicon wafer can be etched along the (111) planes to form tapered edges. Etched holes in silicon of this orientation have been used by Iida and Everhart[2.2] as registration marks for electron beam lithography, and they estimate that the etched edges are sufficiently sharp to measure electron beam diameters less than 10nm. However, it is found that when a <100> wafer is mounted horizontally, the tapered edge of the silicon is too thin and hence transparent to electrons close to the edge, and cannot be used for high resolution beam measurements. Whilst edge transparency can be reduced by coating the silicon with gold-palladium or molybdenum, this does not provide better resolution than an etched copper foil, probably because of the granularity and edge rounding

effect of the coating material.

To take advantage of the silicon specimen having a plane etched face, it can be tilted to bring the etched face almost vertical, as shown in the arrangement of figure 2.1. This results in the edge transparency problem being avoided without coating the specimen. An alternative method of obtaining vertical etched faces is to use <110> oriented silicon, in which some of the (111) planes are orthogonal to the plane of the wafer.

Most of the experiments described here were conducted with <100> silicon because it is more readily available, but it will be shown that the results with either orientation of material are very similar, and <110> silicon is more convenient in use since it is mounted almost horizontally under the beam.

Figure 2.2 shows transmission electron micrographs of an etched edge in <100> silicon, (a) with the specimen mounted horizontally, the thickness extinction contours indicating that the edge is transparent to electrons, and (b) with the specimen tilted to bring the etched edge almost vertical, resulting in a sharp edge that is opaque to electrons. In this chapter it is shown that when a vertical silicon edge is used for beam diameter measurement, the resolution limit is usually better than 5nm provided that a tilting stage is available so that the angle of the silicon specimen can be optimised. It will also be shown that in less critical applications the specimen mounting angle can be preset, leading to the possibility of a "plug-in" specimen which might be used in a routine for setting up the beam. The silicon specimens used can also provide a simple method of astigmatism correction.

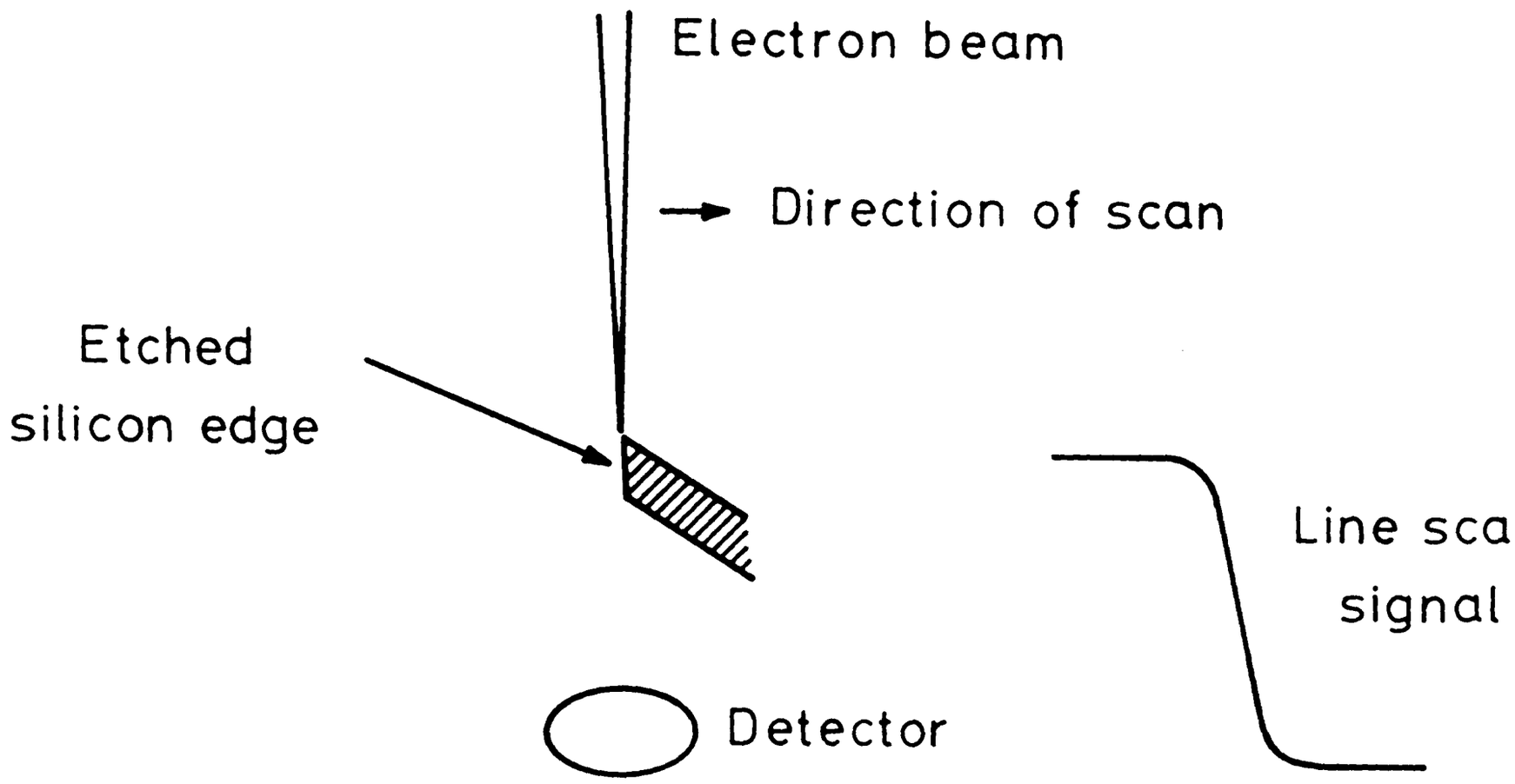

Fig. 2.1 Measurement of an electon beam using a tilted, etched silicon edge and a transmission detector. The line scan signal from the detector represents an integral of the electron beam profile.

a.

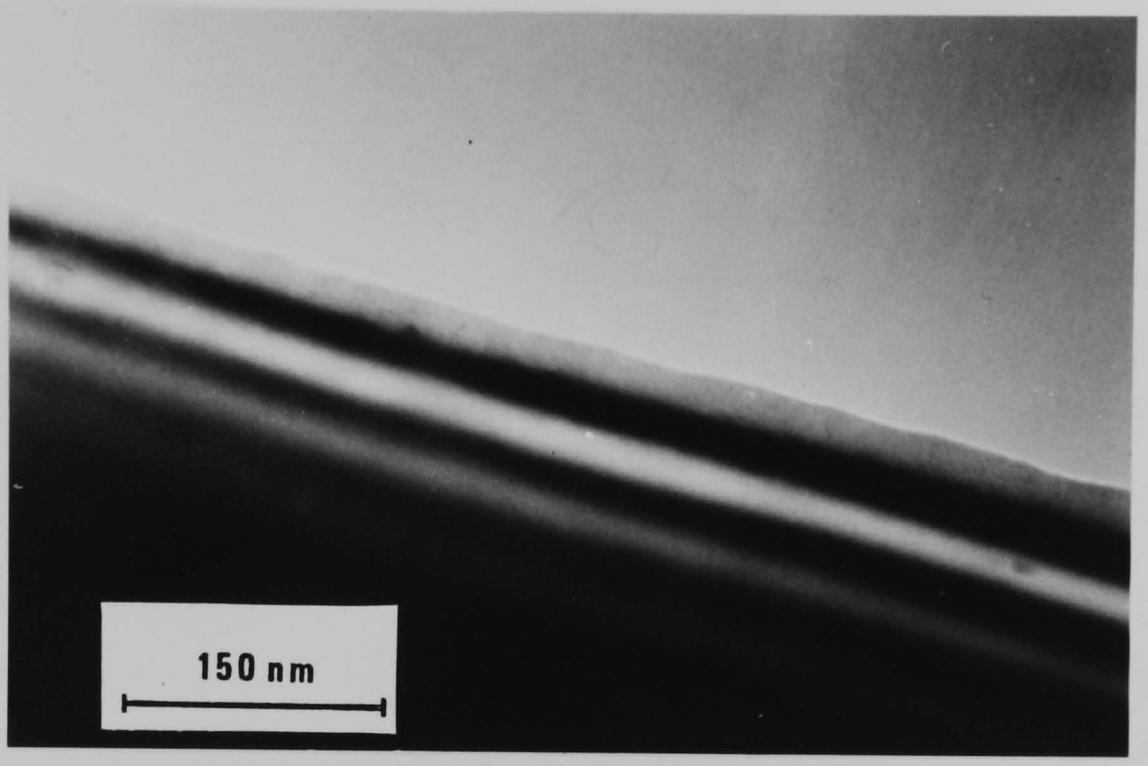

b.

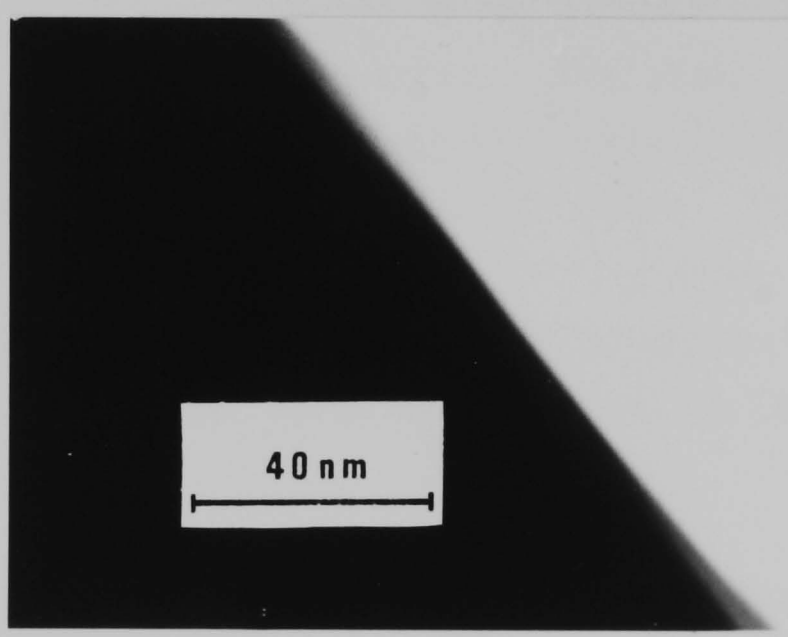

Fig. 2.2 Transmission electron micrographs of a preferentially-etched edge in <100> silicon, (a) with the specimen mounted horizontally, the thickness extinction contours indicating the edge to be transparent to electrons, and (b) with the specimen tilted to bring the etched face almost vertical, resulting in a sharp edge that is opaque to electrons.

2.3 Manufacture of silicon edge specimens in <100> and <110> material

Most of the process steps for etching <100> and <110> silicon are identical. The wafers are scribed into 10mm square dice which are then polished down to approximately 100 microns. This reduces the etch time and the depth of the etched face, and enables the finished specimens to be mounted in most electron microscope specimen stages. Both faces of the die are polished, then oxidised to a thickness of about one micron in wet oxygen at 1150°C for four hours.

Conventional photolithography is used to remove the oxide in the areas to be etched. The resist employed is Shipley AZ 1350J, and is spin-coated onto both sides of the wafer. After development the resist is baked at 175°C for 30 minutes to enable it to withstand the silicon dioxide etch. The oxide is etched using a commercial silicon dioxide etch, rather than hydrofluoric acid which attacks the photoresist. The etch pattern used for <100> silicon is shown in figure 2.3, and includes break lines to divide the die into 3mm diagonal chips. The rectangular area in each chip is aligned along the (111) planes. Misalignment within about one or two degrees causes "stepping" of the etched edges but does not appear to be detrimental to the performance of the specimen.

The silicon is etched by the low-temperature S-etch described by Reisman et al.[2.3], which yields a very high 100:111 etch rate ratio of about 33:1 when used at 50°C, and gives exceptionally smooth etched faces. The etch consists of 220ml ethylene diamine, 29.4ml deionised water, and 35.3g pyrocatechol, and is catalysed with 1.32g pyrazine. To avoid the irregular etch structure described by Reisman et al.[2.4] the etch bath is heated to 115°C for one hour before use. The etch bath is contained in a reflux system, with nitrogen bubbling through the solution, and

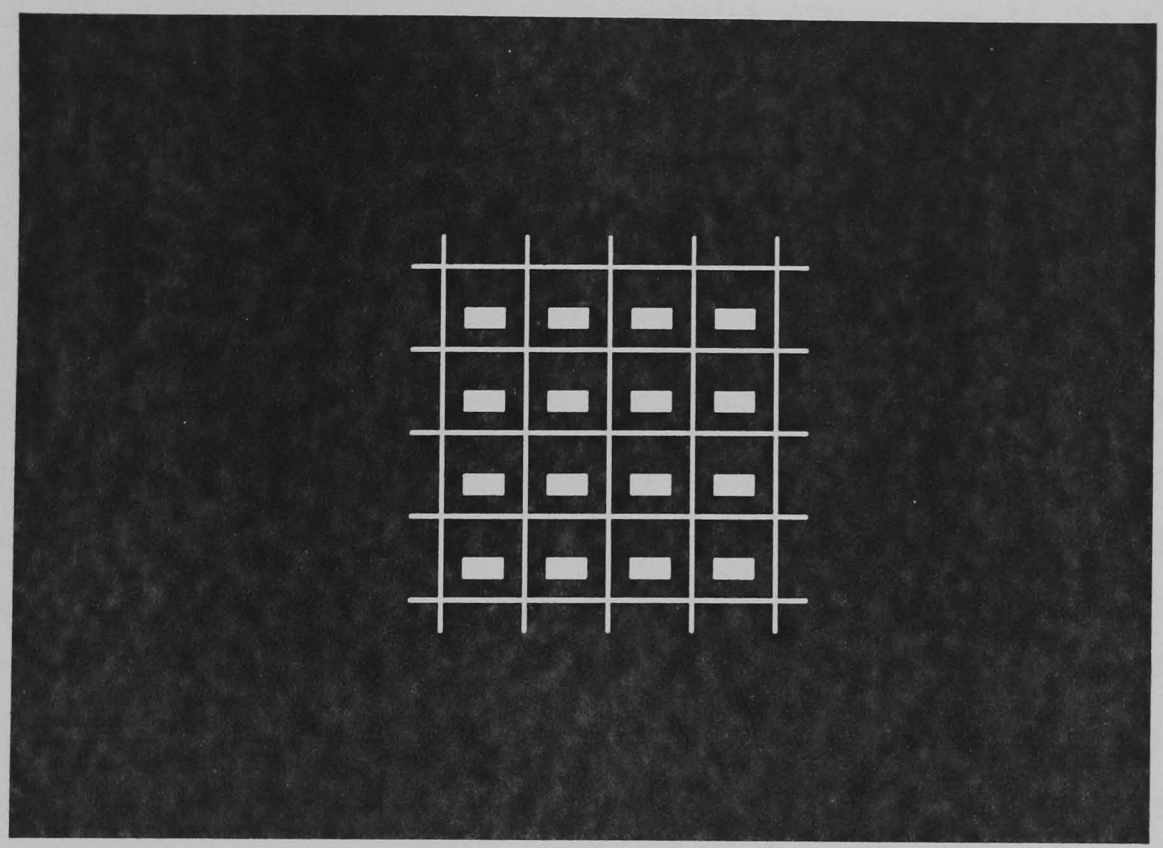

Fig. 2.3 Mask design used for etching the <100> silicon edge specimens, to fit a 10mm square wafer. The rectangular holes etch completely through the silicon to form the edges, while the thin lines etch to form break lines in the silicon to assist in dicing the wafer.

magnetic stirrer agitation. The bath temperature is automatically controlled to within 0.2°C. The etch rate at 50°C in the <100> direction is about 4.5 microns per hour. In order to avoid contamination deposits, the silicon is transferred to boiling deionised water for ten seconds on completion of the etch and then rinsed in cold deionised water, as described by Reisman et al.[2.3] The rectangular hole in the oxide etches back through the silicon in the <100> direction along the (111) planes. After etching completely through the silicon, four tapered smooth faces are produced. The process is summarised in figure 2.4.

In etching <110> silicon it was found to be preferable to start from a pattern of circular holes, as shown in figure 2.5(a). Because of the very slow etch rate in the <111> direction, the etching process "finds" the (111) planes as it proceeds. Since the etching is fastest in the <100> direction, parts of the pattern in <110> silicon are etched through at different rates. The corners of intersecting (111) faces are the last to etch through, and it is these corners that are useful in astigmatism correction (see section 2.5). The etching of 120 micron thick <110> silicon specimens was completed after approximately 40 hours. Figure 2.5(b,c) shows a fully-etched <110> specimen, and figure 2.5(d,e) shows a batch of 16 <110> specimens.

The silicon dioxide is left as a protective layer until the specimens are to be used, when it is etched away in dilute hydrofluoric acid. If the specimen becomes contaminated in use, it can be cleaned in a mixture of concentrated sulphuric acid and hydrogen peroxide. This will oxidise a thin layer of silicon, which should be etched away again in dilute hydrofluoric acid.

2.4.1 Estimation of spot size and shape from the signal trace

A recorded trace from the transmission detector in the Philips

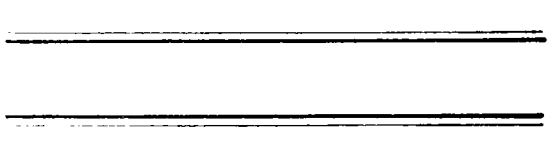

SiO_2 1um
Si 100um
SiO_2 1um

Oxidised thin silicon wafer, polished on both sides.

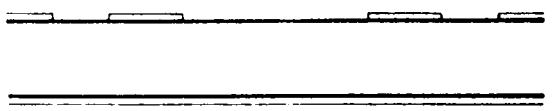

Pattern oxide by photolithography and wet chemical etching, forming windows and break lines.

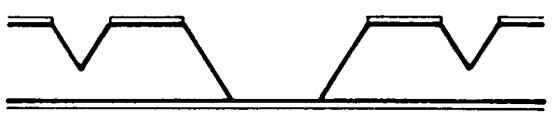

Preferentially etch through silicon, using low temperature S-etch.

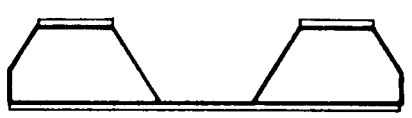

Dice wafer into individual specimens. SiO_2 remains as a protective layer.

Etch away SiO_2 before use.

Fig. 2.4 Summary of process steps in the manufacture of etched silicon edge specimens (‹100› silicon).

a.

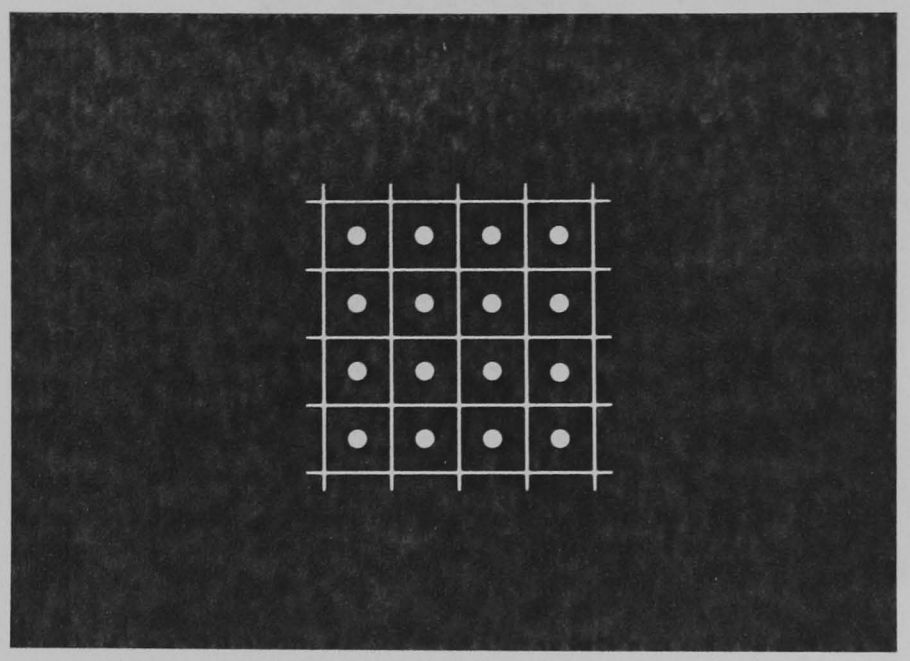

b.

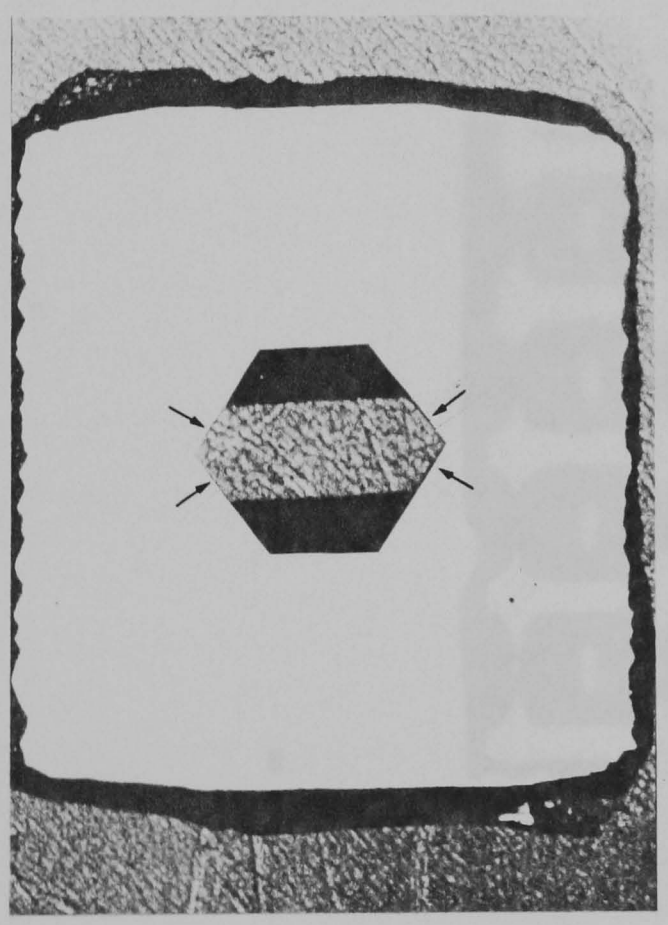

c.

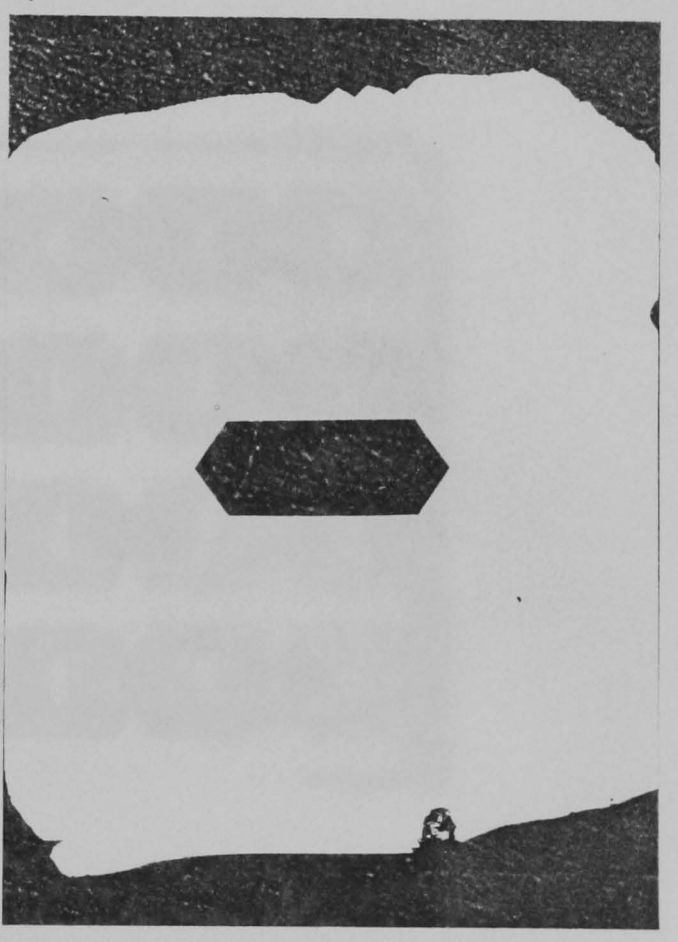

Fig.2.5(a) Mask design used for etching <110> specimens, to fit a 10mm square wafer. The etching process "finds" the (111) planes because of the very slow etch rate in the <111> direction; (b) Optical micrograph of the back polished face of a fully etched <110> specimen, the arrows indicating the vertical (111) planes. The electron beam is arranged to impinge on the opposite polished face shown in (c)

d.

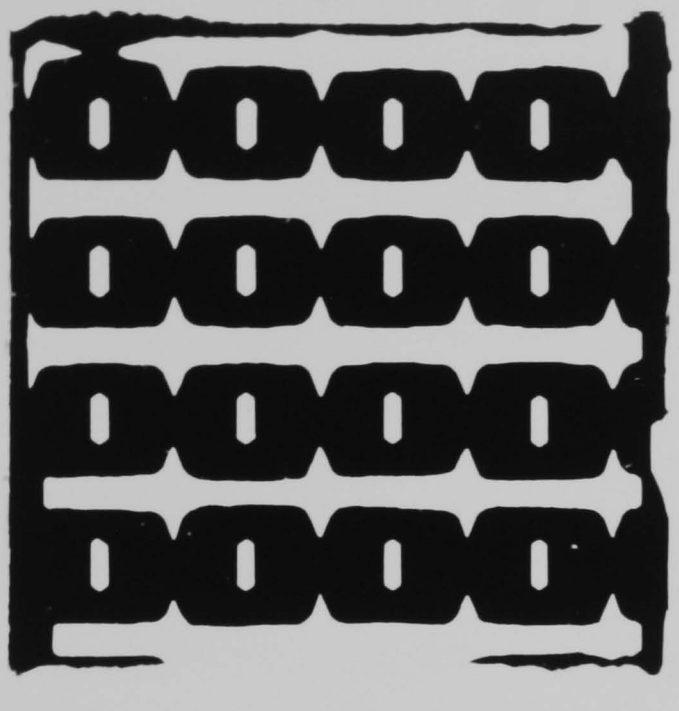

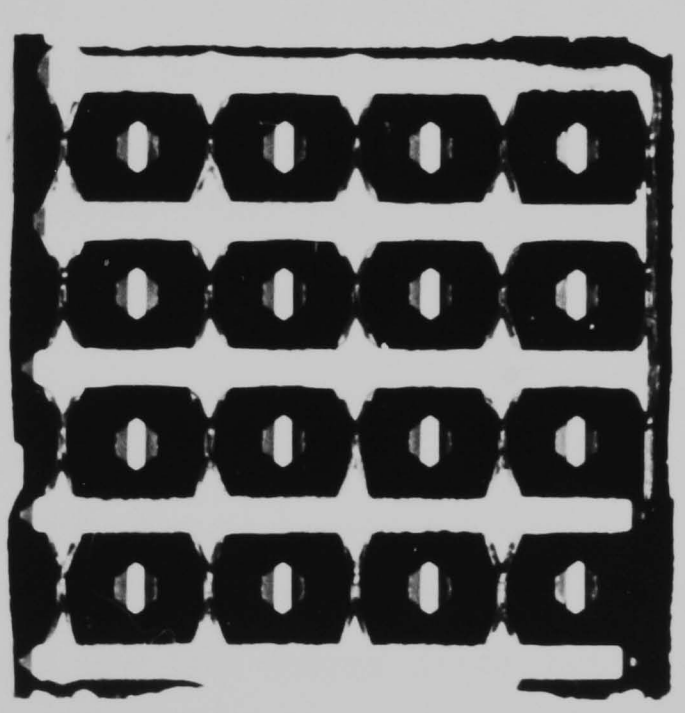

e.

Fig. 2.5 (d,e) A batch of 16 ‹110› specimens, etched from a 10mm square wafer. (d) Top face, towards beam.

(e) Bottom face, towards detector.

SEM 500, working at 50keV and adjusted for minimum beam diameter (the "dot" setting on the spot size control), is shown in figure 2.6. The <100> silicon specimen was held by a circlip onto a 32.5^{o} wedge as shown in figure 2.7, and the tilt adjustment on the SEM stage was used to maximise the slope of the signal trace. The measurement would usually be made as quickly as the recording method will allow (in this case a 64 millisecond line scan) to avoid problems of stage drift and, in the case of a very high current density beam, specimen contamination. It will be noted that the trace does not show any evidence of specimen irregularity. From this trace, the horizontal distance between the 25% and 75% signal levels is determined and divided by the magnification factor. The spot size is often estimated as being twice this distance, in this case approximately 9nm.

This estimation of the spot size can be converted to the 50% current density diameter (ie. the diameter at which the current density falls to 50% of its central level) by multiplying by the factor 0.865 (see Appendix). This gives a spot diameter for the Philips microscope of about 8nm, which is as specified for the instrument.

The definition of residual current "tails" in the beam shape will of course depend on the purpose of the measurement. The Appendix shows the relationship between the recorded trace, which could be digitised for processing by microcomputer, and the current distribution in the spot and the charge distribution in a scanned line. In particular, the charge distribution in a scanned line is easily derived and is useful in the context of lithography, since it determines the beam's contribution to linewidth and line spacing limits. It is found that the low-signal end of the trace (ie. where most of the beam is impinging on the specimen) contains about 3% of the total current, scattered out of the etched face of the silicon, decaying gradually as the beam is moved up to several tens of nanometres onto the specimen. The

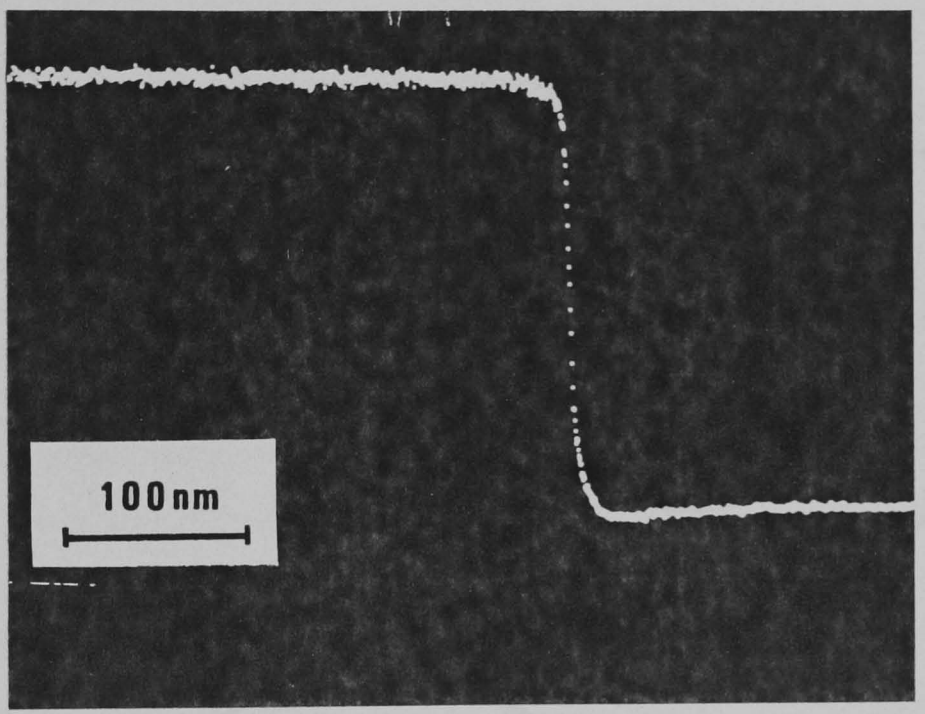

Fig. 2.6 Line scan across etched silicon edge in Philips SEM 500. Represents a spot diameter of approximately 8nm (see text).

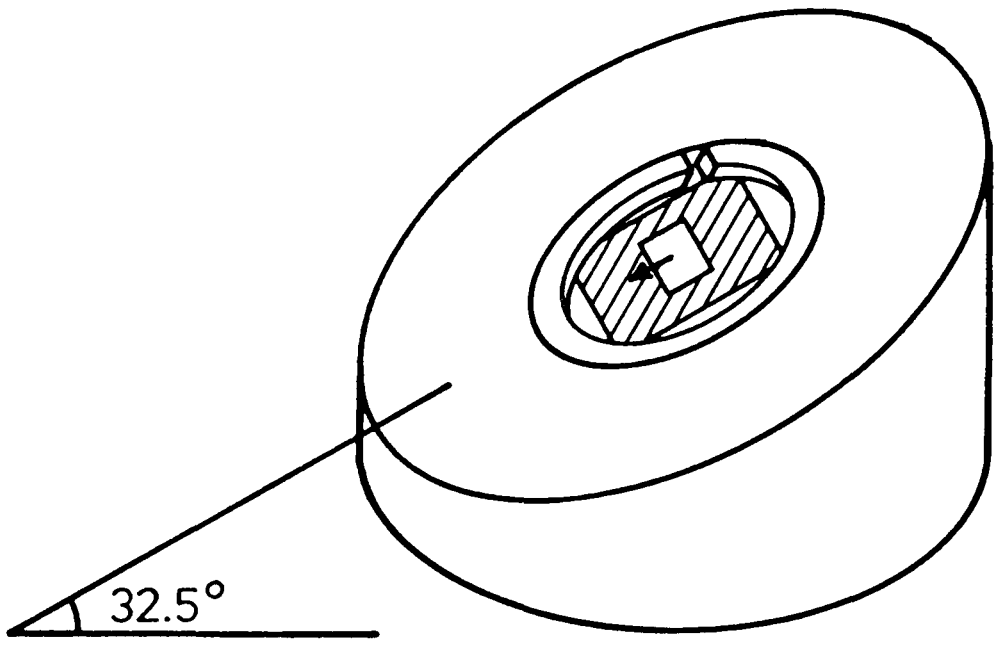

Fig. 2.7 Mounting of a ‹100› specimen in the Philips SEM 500 using a 32.5° wedge. The arrow indicates the electron beam scan across the edge. ‹110› specimens are mounted almost horizontally and do not require a special holder.

high-signal end of the trace does not suffer from this inaccuracy, since in this case most of the current does not impinge on the specimen; therefore any measurement of the beam tails should be based on this part of the trace.

The Monte-Carlo simulation (chapter 7) requires a distribution equivalent to the charge (ie. exposure dose) in a scanned line. Since digitisation of the signal trace was not implemented, this was approximated by matching a distribution to the signal trace as follows.

By shifting the scan position while the silicon edge was being scanned continuously, it was estimated that in the Philips SEM 500 working at 50kV and minimum spot size (the "dot" setting), 99% of the current is transmitted when the silicon edge is 15nm from the centre of the beam. In the case of a truly gaussian beam of the same nominal diameter (8nm 50% current density) the 99% transmission point would be 8nm from the centre of the beam (derived from equation 2.2 in the Appendix). The signal appeared to be still falling rapidly at this point, so the tail, although extending from the true gaussian distribution, becomes insignificant within a short distance of it. The charge distribution was first approximated to a pure gaussian distribution with a gaussian half-width of 4.84nm (equivalent to a 50% current density of 8nm - see appendix). This was integrated to give the equivalent signal trace for such a beam being transmitted past a sharp edge (figure 2.8(a)). To the resulting distribution was added a low-level tail distribution T(x) according to

$$T(x) = \frac{H}{1 + (x/W)^P} \qquad (2.1)$$

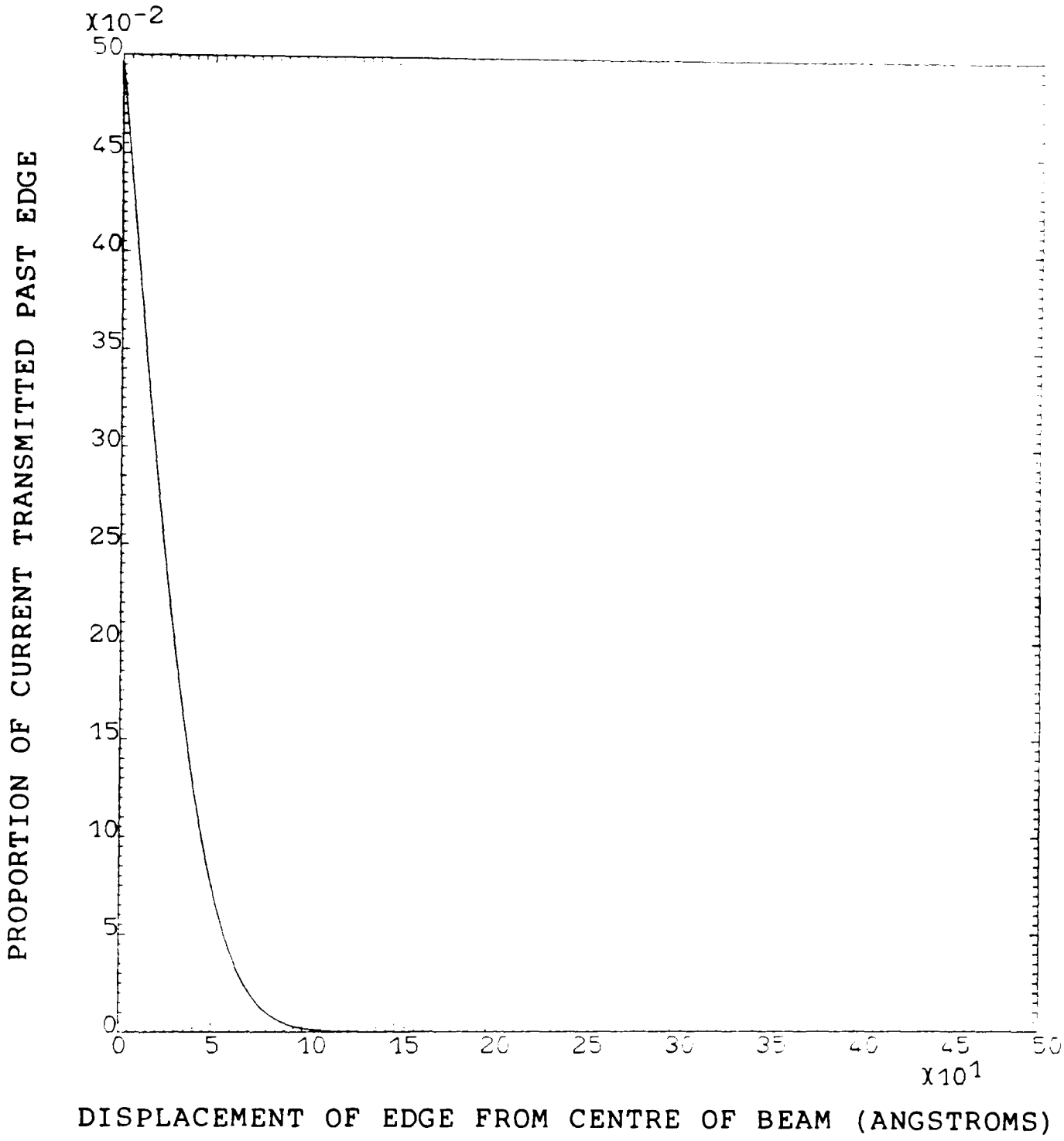

Fig. 2.8(a) Current transmitted past a sharp edge, simulated for a pure gaussian beam (8nm diameter at the 50% current density points).

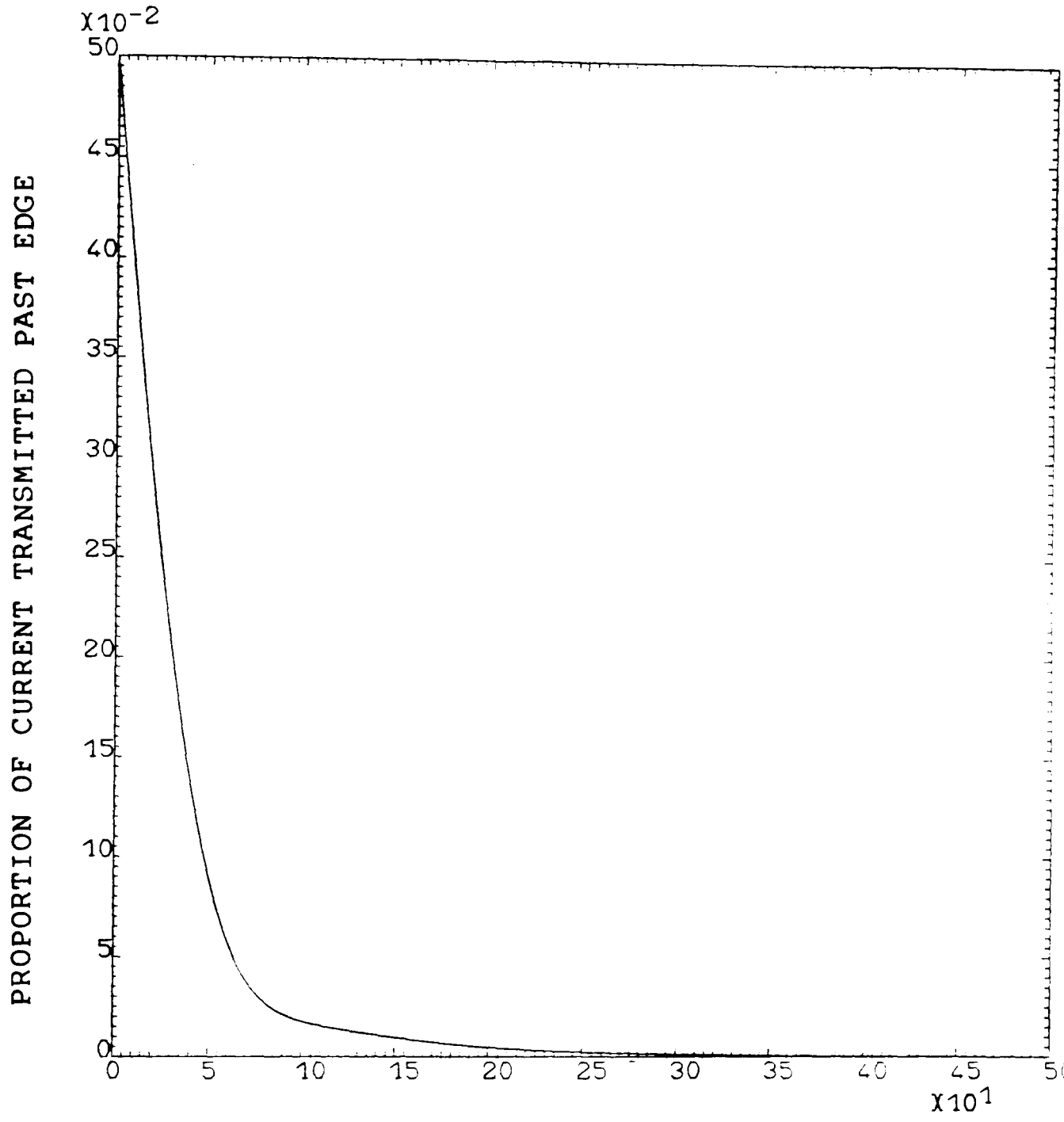

Fig. 2.8(b) Current transmitted past a sharp edge, simulated for a gaussian 8nm diameter beam, with added tails approximating to those observed experimentally in the Philips SEM 500 (see text).

where H = height
W = width, and
P = power of the distribution.

The tail contribution T(x) will be equal to H at the centre of the beam (x=0), and H/2 at distance x=W from the centre. In order to disturb the central gaussian core as little as possible, H is made small and W is larger than the gaussian width. In practice, H was taken as 2% of the full signal and W was 15nm, to match the measured 99% signal level point. It was found that taking power P=4 resulted in a realistic decay in signal level beyond 15nm, compared with that observed by shifting the scan as above, and the contribution of the tail distribution across the entire gaussian width would then be almost constant at 2%. It was not possible to compare the simulated trace with the recorded trace directly, because of linear distortions in the display tube. The resulting composite simulated line-scan is shown in figure 2.8(b); this was then differentiated, resulting in the charge distribution shown in figure 2.9, which could be supplied as a numerical distribution to the Monte-Carlo program for simulation of exposures in the Philips microscope.

2.4.2 Resolution limit of the method

In practice the ability to use etched silicon edges for beam profile measurement will often depend on the accuracy required in mounting the specimen, since in many cases a specimen tilt facility will not be available and the specimen mounting angle will be preset, perhaps in a specially machined holder.

Figure 2.10 shows the measured spot size against tilt angle using <100> silicon in the Philips SEM, for a 50keV beam with a convergence semi-angle of 0.57^{o}. As the etched face is brought almost vertical it is found that the detected signal level is

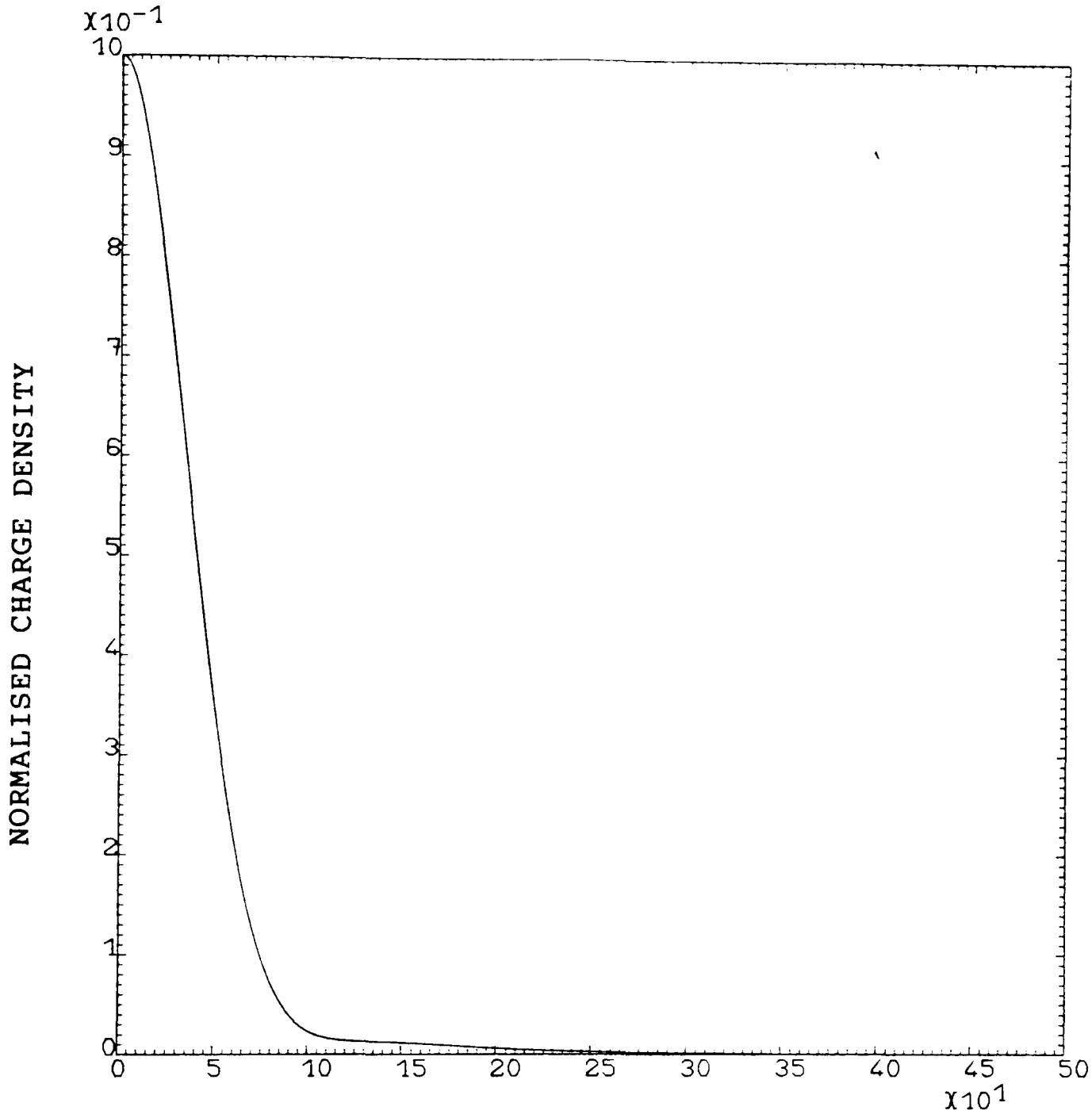

Fig. 2.9 Charge density in a scanned line, deposited by a gaussian 8nm electron beam with added tails, as indicated in figure 2.8(b).

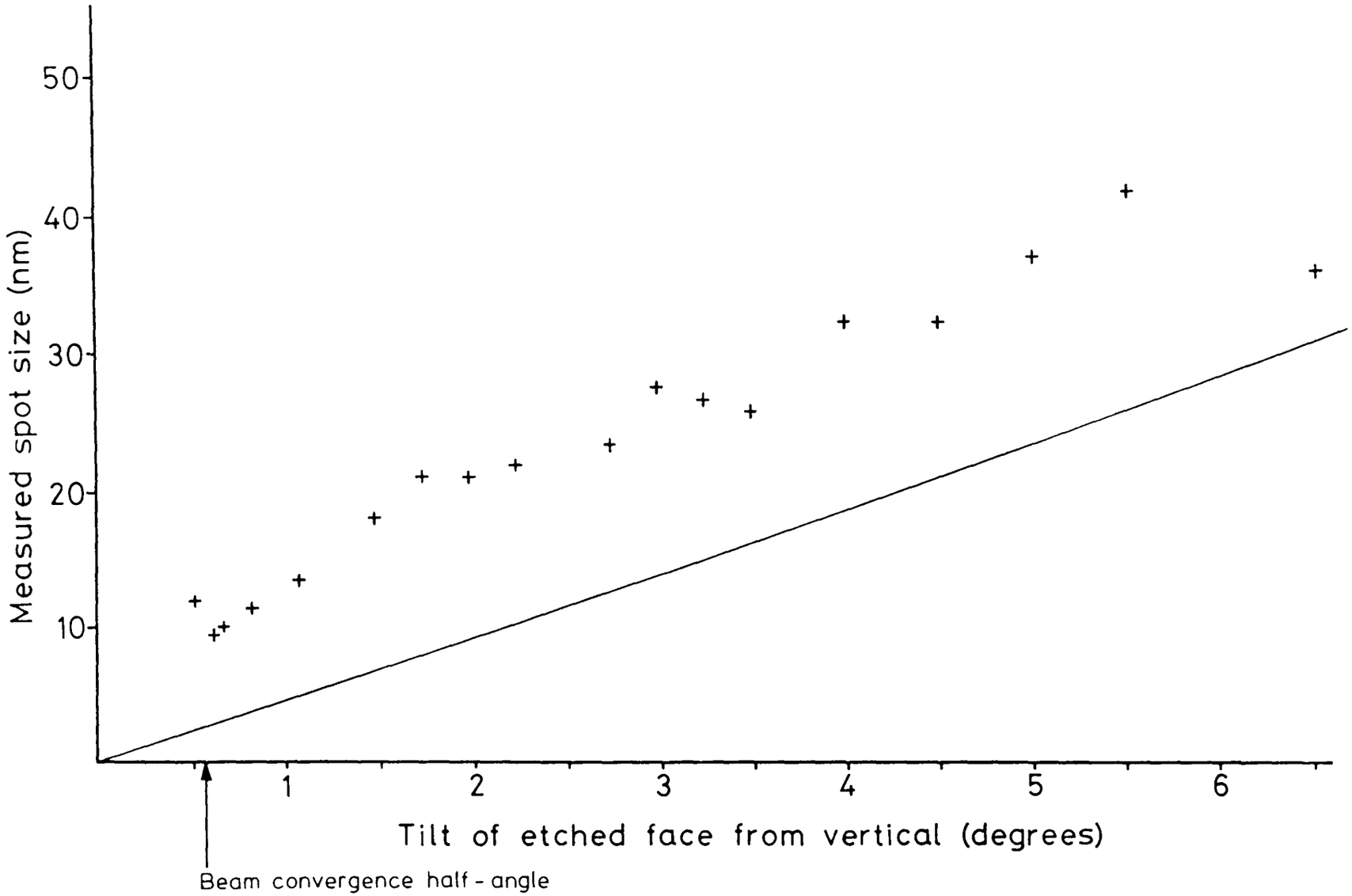

Fig.2.10 Variation of measured spot size in the Philips SEM 500 with tilt of the etched face from vertical, for <100> silicon. The resolution limit for the particular beam energy (50keV) can be estimated from the beam convergence half-angle and the penetration through untilted silicon, as indicated by the solid line.

reduced as shown in figure 2.11. This is because the beam, as it diverges beyond the focal plane, is obscured or scattered away from the detector by the etched face. Hence the optimum angle of the specimen is not with the etched face vertical, but at the convergence semi-angle of the beam. The origin in figure 2.10 was found by determining the tilt angle at which the transmitted signal just began to fall, and assuming that the etched face was then tilted precisely to the convergence semi-angle of the beam. Such a setting can only be achieved if the etched face is very smooth and free of deposits, as is the case when the silicon is etched by the method described above.

Since the measurements made are between the 25% and 75% signal levels, it is useful to know the thickness of silicon that 25% of the electrons will penetrate without large-angle scattering (ie. greater than the detector acceptance angle). A scan with a 50kV beam across a horizontally mounted (ie. untilted) <100> specimen is shown in figure 2.12. From this it can be determined that the signal has fallen to 25% of its initial level where the silicon is 0.30 microns thick. With a tilted specimen the distance from the edge to the point at which the silicon is 0.30 microns thick is approximately 0.30 tan θ (the exact relationship is shown in figure 2.14), where θ is the angle of the etched face from vertical; this limit is indicated by the solid line in figure 2.10 and it is assumed to be the resolution limit for a particular angle. The penetration was measured for a 50keV beam, and with a collection half-angle of about 5^{o}. The measured penetration increases with the electron potential, and also depends on the collection angle of the detector. For an accurate determination of the resolution limit in a particular case, therefore, a transmission trace should be taken with a <100> specimen mounted horizontally, under the same conditions as the beam profile trace is taken.

The absolute resolution that can be achieved if the tilt angle is

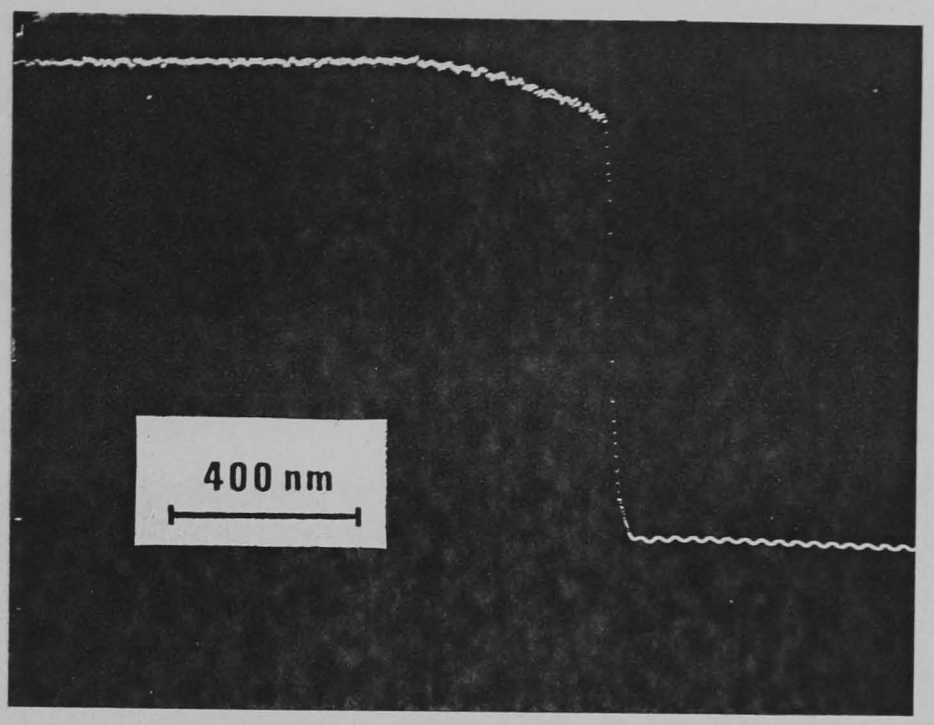

Fig.2.11 Effect of tilting the silicon edge 0.15° beyond the beam convergence half-angle. The 100% signal level begins to fall since the beam, diverging beyond the focal plane at the top face, hits the etched side-wall of the silicon.

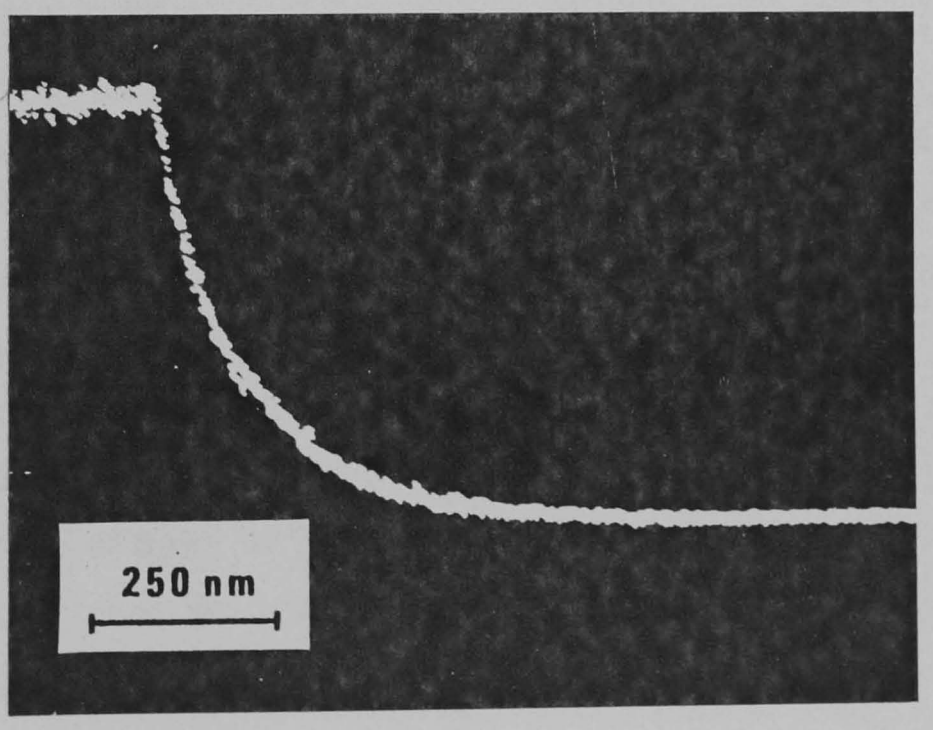

Fig.2.12 Line scan across untilted <100> specimen at 50kV, used to estimate the resolution limit of the measurements (see text).

adjusted critically depends then on the beam convergence angle; for the Philips SEM working at 50kV with a 200 micron aperture the absolute resolution of the method should be about 3nm. It might be noted at this point that dedicated electron beam lithography machines usually have longer working distances and hence potentially smaller convergence angles (depending on the objective aperture in use), so the resolution could be significantly better than this provided that the edge specimen is mounted with sufficient accuracy.

<110> specimens are found to behave in a very similar manner, as shown by the measured beam diameter against tilt relationship in figure 2.13. Edges in <110> silicon still suffer from transparency because, as with the <100> specimens, the etched face must be tilted slightly away from vertical to avoid impingement by the diverging beam. Since the silicon edge is slightly thicker for a given tilt angle (the geometry is shown in figure 2.14), there is an improvement of about 6% in the estimated resolution at 5^{o} tilt. For tilts of less than 1^{o} (which would usually be used) the improvement in resolution is less than 1%.

Because of the finite etch rate of the silicon in the <111> direction, the etched face of the <110> specimens is not quite orthogonal to the plane of the wafer. It is found that the etched face is usually at an angle of 1.5-2^{o} to the vertical, there being some variation in the orientation of the wafers. To achieve high resolution measurements in a machine without a tilting stage, a selection of thin tapered shims (shaped like washers) can be made, to place in the 3mm mounting recess under the specimen, in order to provide the necessary adjustment of the mounting angle.

Measurements to verify the resolution limit of the method have been made in the Vacuum Generators HB5 scanning transmission

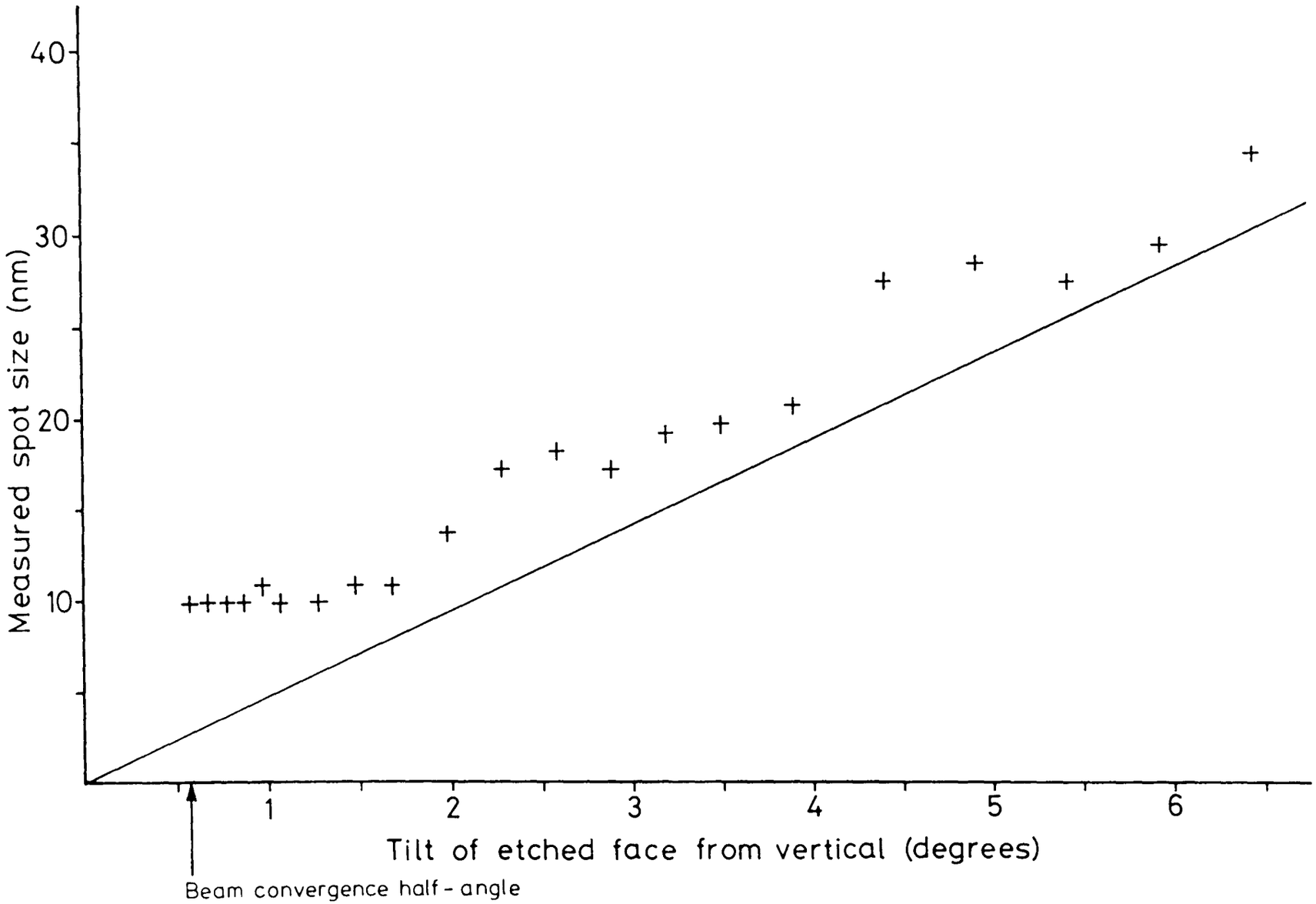

Fig. 2.13 Variation of measured spot size in the Philips SEM 500 with tilt of the etched face from vertical, for <110> silicon. The solid line indicates the estimated resolution limit at 50kV, as in figure 8.

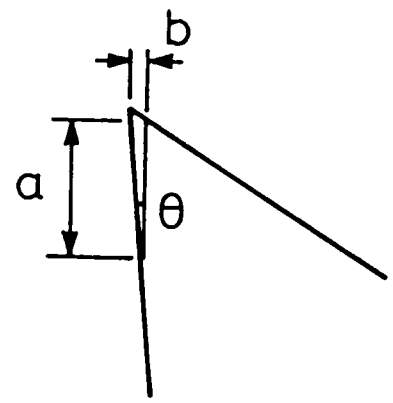

⟨100⟩ silicon

$$\frac{a}{b} = \frac{1}{\tan\theta} - \tan(32{\cdot}6^\circ - \theta)$$

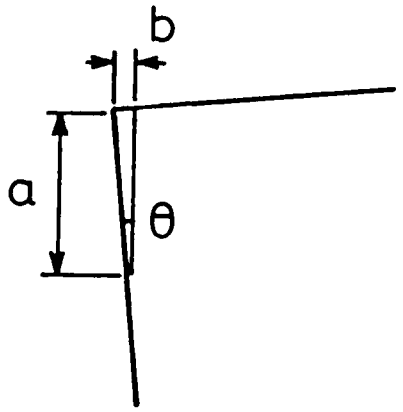

⟨110⟩ silicon

$$\frac{a}{b} = \frac{1}{\tan\theta} + \tan\theta$$

Fig. 2.14 Thickness of the edges of ‹100› and ‹110› silicon specimens, as seen by an electron beam from above.

electron microscope in the Natural Philosophy Department, Glasgow University, which has a nominal spot diameter of 0.5nm. Figure 2.15 shows a trace across a <100> specimen in which the slope has been maximised by adjusting the tilt angle of the specimen until the maximum signal level just began to fall. The trace indicates a spot diameter of approximately 4nm. The accelerating potential was 40kV and the convergence half angle was 0.48°. From this the resolution limit of the measurement can be estimated to be 3nm, which is in good agreement with the experiment. In making measurements in such an instrument in which the detection angle can be varied, it is necessary to keep the electron collection angle relatively wide, so that the imaging is effectively incoherent and edge-diffraction effects are avoided.

2.4.3 Alternative methods of detection.

Although it has been found that a secondary electron detector will produce useful measurements greater than about 25nm, the results are not very consistent as the beam is moved along the specimen, because of irregularities in the top polished face. It is therefore preferred in all cases to use some form of transmission detector, which can simply be a Faraday cup (or alternatively a metal plate) placed below the the specimen. Often the scan must be made slowly because of the limited bandwidth of most specimen current amplifiers, but experiments have been conducted using a Faraday cup connected to a Keithley Model 302 electrometer operational amplifier, which was found to provide sufficient bandwidth to enable the use of conveniently short scan times (ie. several scans per second). A photodiode has been suggested as another possible detector.

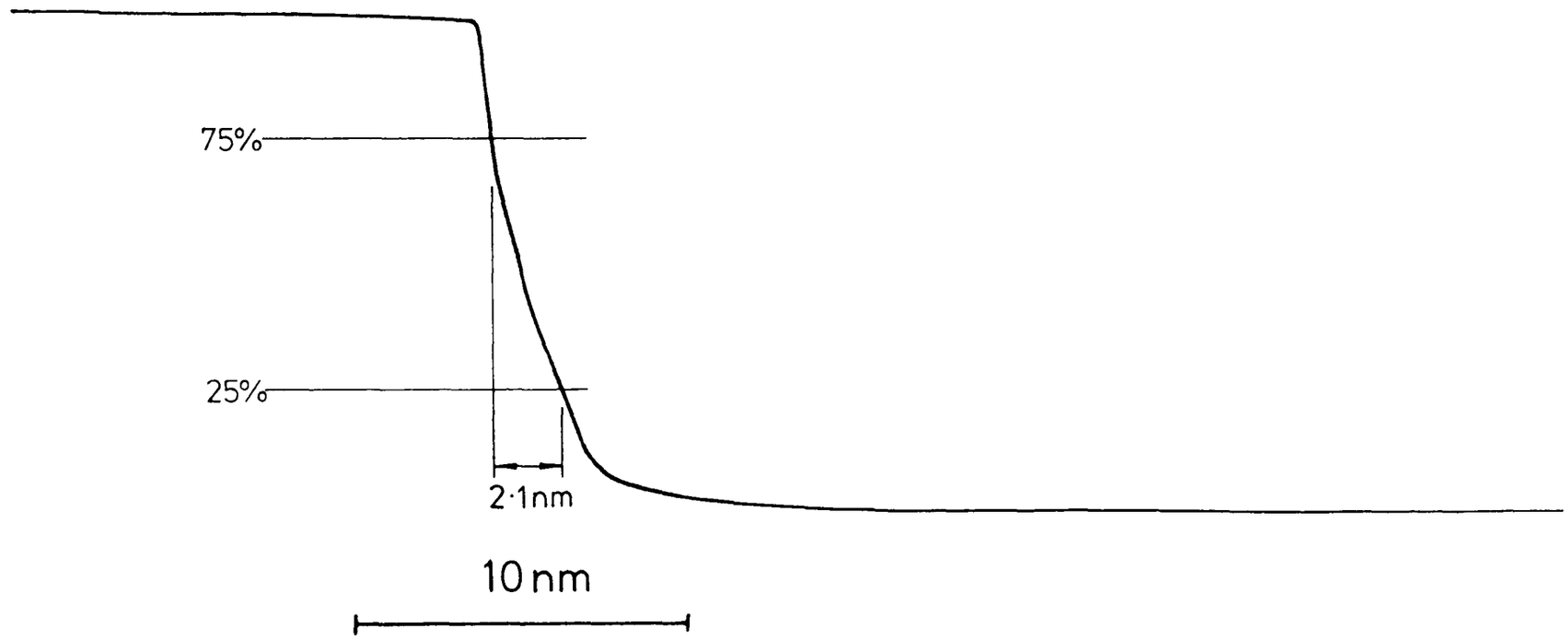

Fig.2.15 Line scan across etched silicon edge in Vacuum Generators HB5 scanning transmission electron microscope. Indicates a spot diameter of about 4nm, but the effect of the exponential decay in transmission through the edge can be seen clearly.

2.5 Use of etched edge specimens for astigmatism correction

A fully etched <110> specimen has a six-sided hole in which two of the corners are formed by vertical (111) faces intersecting at 109.5°. Such a corner can be used to provide two edges at once for correction of astigmatism.

A scan is made across one of the corners formed by two meeting (111) faces (see figure 2.5), and this produces two beam profile traces on the display at the same time (figure 2.16). Astigmatism is usually indicated by one slope peaking at a different objective current than the other. However, since the beam is measured in only two directions (unfortunately it is not possible to provide more than two orientations of anisotropically etched vertical silicon edges in the same specimen), an astigmatic beam could be symmetrical along the bisector of these two directions. This would be evident in the two slopes being less steep than expected (perhaps previously recorded), and also in the slopes peaking less rapidly as the objective is adjusted through focus. Experiment has shown that adjusting the stigmator controls as the objective is run through focus produces the same stigmator settings as a skilled operator using an ideal specimen placed in the same focal plane. An automatic astigmatism correction routine could be envisaged to follow such an iterative procedure, and then vary the objective through focus while measuring the two slopes and comparing them with a standard performance table.

If necessary, <100> silicon specimens can also be used for astigmatism correction. Two intersecting etched faces can both be brought vertical by tilting the specimen approximately 45° to the horizontal. A suitable method of mounting the specimen is shown in figure 2.17.

a.

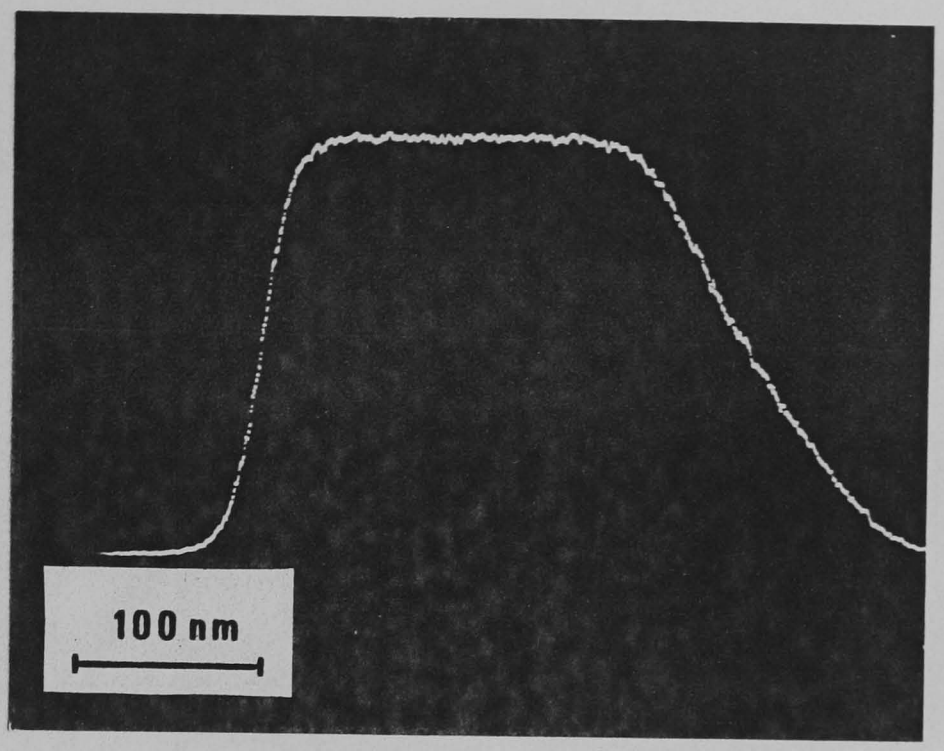

b.

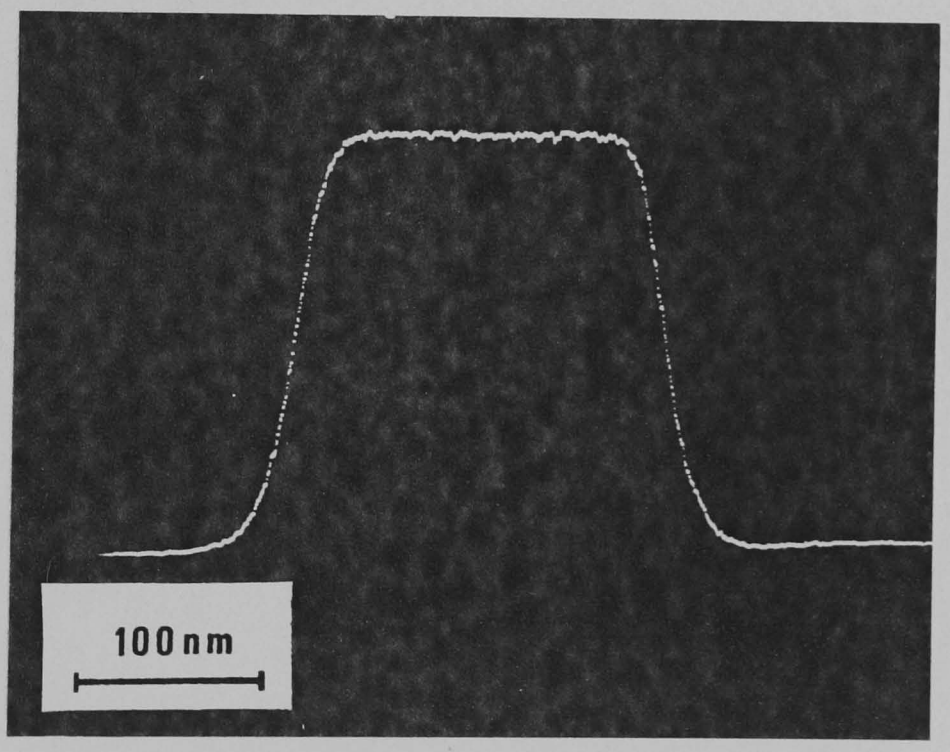

Fig.2.16 Use of silicon etched edge specimen for astigmatism correction; (a) astigmatism present; (b) astigmatism corrected.

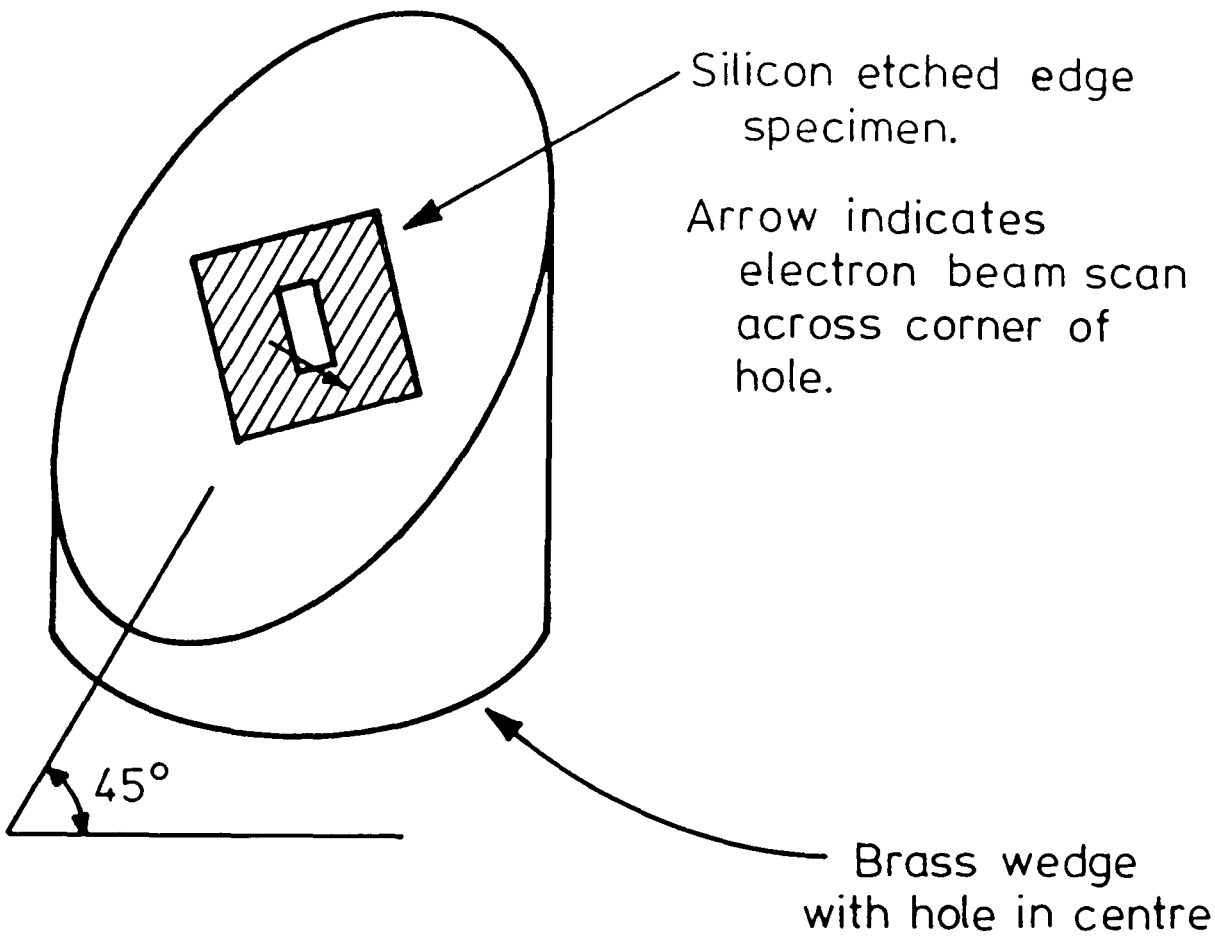

Fig. 2.17 Mounting of ‹100› silicon specimen for use in astigmatism correction.

2.6 Conclusion

Preferentially-etched silicon edges can be used to provide accurate measurements of electron beam diameters of 10 nanometres and larger, and sometimes of smaller diameter beams with lower accelerating potentials and narrow convergence angles. The edges are found to produce higher resolution and more consistent measurements than commonly-used edges such as etched metal foils, and yield more quantitative information than point-to-point resolution tests. Using the methods described here it is possible to estimate the resolution limit of the method in a particular case, and also the accuracy required in setting the angle of tilt of the specimen.

For use in electron beam fabrication equipment it would be possible to batch-fabricate specimens which could be mounted into preset holders to provide automatic measurement of the beam diameter and correction of astigmatism.

It would normally be preferred to use <110> silicon since it is mounted almost horizontally and is therefore more convenient to use, but standard <100> silicon is found to provide very similar resolution.

Appendix. Measurement of spot diameter from the transmission signal trace

Since the beam profile may not be gaussian the definition of spot diameter becomes arbitrary. It is convenient to assume that the beam is gaussian but may in addition have tails, and if only the central, steep part of the trace is measured then the tails can be specified separately. The measurement we make from the trace is of the distance between the 25% and 75% signal levels. This can be converted to a gaussian diameter as follows.

The current density of a gaussian beam is given (in rectangular coordinates) by

$$J = J_o \, e^{-x^2/w^2} \, e^{-y^2/w^2} \qquad (2.2)$$

where J_o is the maximum current density, and
$2w$ is the gaussian width (to the 1/e points).

As the beam is scanned over the edge, part of it is obscured from the detector as shown in figure 2.18. The transmitted current can be obtained by integrating equation 2.2 over the area that is not obscured. The 25% and 75% transmission points are at $x_1 = +0.48w$ and $x_1 = -0.48w$ respectively. Hence the gaussian width $2w$ is calculated by multiplying the 25% to 75% distance by the factor 2.09. Other definitions of beam diameter can be obtained; the 50% current density diameter is calculated by multiplying the 25% to 75% distance by the factor 1.74. Examples are shown in figure 2.19.

The relationships given above assume that the beam profile is gaussian, but since the beam does not usually deviate greatly from the gaussian close to the centre they can be used in general to define consistently the nominal beam diameter. However, in order to specify "tails" in the beam profile which are further from the centre of the beam, we need to derive the current density distribution J(r) with radius r. For any circularly symmetrical beam, this is related to the current transmitted past an edge $I(x_1)$ according to

$$I(x_1) = \int_{r=x_1}^{+\infty} J(r) \; 2r \; \cos^{-1}(x_1/r) \; dr \qquad (2.3)$$

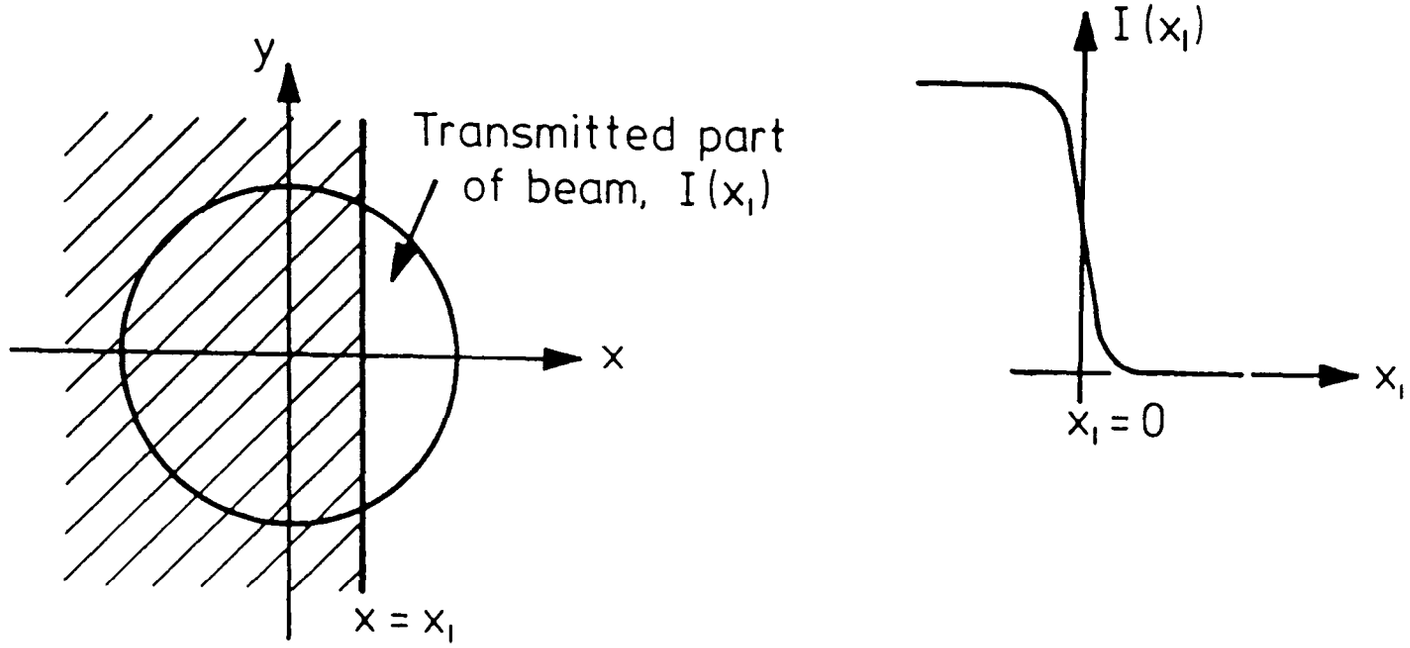

Fig.2.18 Representation of beam partly obscured by a perfectly sharp edge.

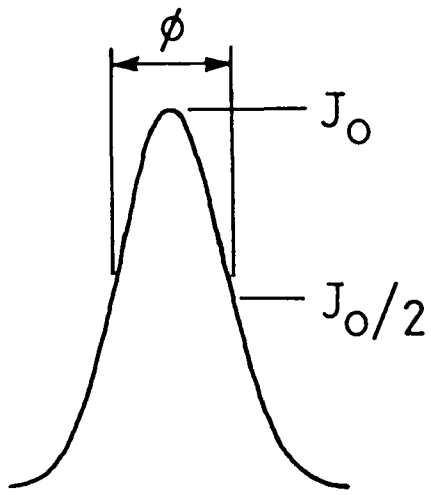

If 50% current density diameter ϕ = 10nm

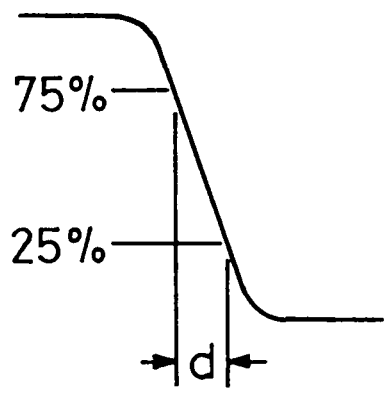

then distance between 25% and 75% transmission points d = 5·8nm

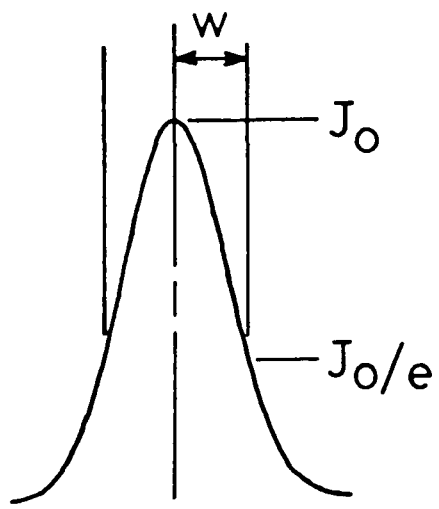

and gaussian width 2w = 12nm.

Fig. 2.19 Relationship between different definitions of spot diameter for a gaussian electron beam.

This is a Fredholm equation of the first kind, which is difficult to solve numerically for the general current density distribution J(r). However, more useful in lithography is the distribution of charge density across a scanned line. Imagine the beam shown in figure 2.18 to be scanned at a constant rate in the y direction from $-\infty$ to $+\infty$. The beam profile is then already integrated in the y direction and so the charge density distribution across the scanned line, $Q(x_1)$ is simply given by

$$I(x_1) \propto \int_{x=x_1}^{+\infty} Q(x)\, dx \qquad (2.4)$$

or $$Q(x_1) \propto dI(x_1) / dx_1 \qquad (2.5)$$

The distribution $Q(x_1)$ is in fact identical to the current density distribution J(r) in the gaussian case, since the x and y terms are separable. $Q(x_1)$ is easy to obtain by differentiating the transmitted signal trace, and it might be possible to use a derivative processor (fitted to most SEM's) to do this, although in most cases the bandwidth is too limited and noise is a problem. Digitisation of the trace would be preferable, since a small microcomputer could be used to average several traces before calculating the derivative, in order to reduce the effect of noise.

References

2.1 J.R.A. Cleaver and K.C.A. Smith; "Optical characteristics of a field emission scanning microscope"
Scanning Electron Microscopy: systems and applications 1973.

2.2 Y. Iida and T.E. Everhart; "High-contrast registration marks for electron-beam pattern exposure on (100) silicon"

J. Vac. Sci. Technol. 15(3), 917-920, 1978.

2.3 A. Reiseman, M. Berkenblit, S.A. Chan, F.B. Kaufman, and D.C. Green; "The controlled etching of silicon in catalyzed Ethylenediamine-Pyrocatechol-Water solutions"
J. Electrochem. Soc.: Solid-state science and technology; 126(8), 1406-1415, 1979.

2.4 A. Reisman, M. Berkenblit, C.J. Merz, A.K. Ray, and D.C. Green; "Anomalous etch structures using Ethylenediamine-Pyrocatechol-Water based etchants and their elimination"
J. Electrochem. Soc.: Solid-state science and technology; 1208, 1980.

CHAPTER 3

Exposure range of low energy electrons in PMMA

3.1 Introduction

It is believed that secondary electrons produced by the primary beam play a significant role in limiting the resolution of PMMA as an electron resist. Murata, Kyser, and Ting[3.1] have suggested that fast (keV) secondary electrons are important since they have longer ranges than lower energy electrons; however, relatively few high energy secondaries are produced in high resolution lithography on thin substrates. Broers[3.2] suggests on the contrary that low energy secondaries are significant since electrons of about 5eV and above are able to expose the resist and may have ultimate ranges of the order of tens of nanometres.

The aim of this work was to establish the exposure range in PMMA of low energy electrons by a direct method. The resist was exposed by a low energy beam, developed, and the depth to which the exposed area had dissolved in the developer was measured (see figure 3.1). Hence it was possible to determine the range over which the electrons were capable of exposing the resist, this being termed the exposure range, a useful parameter in simulating the effect of secondary electrons during the exposure of the electron resist by a high energy beam.

Since it had been suggested that the electron range increases significantly at very low energy, it was necessary to develop equipment which was capable of exposing resist by an electron beam of energy as low as 5eV, known from UV exposure experiments to be the lowest energy required to cause bond scission in PMMA[3.3].

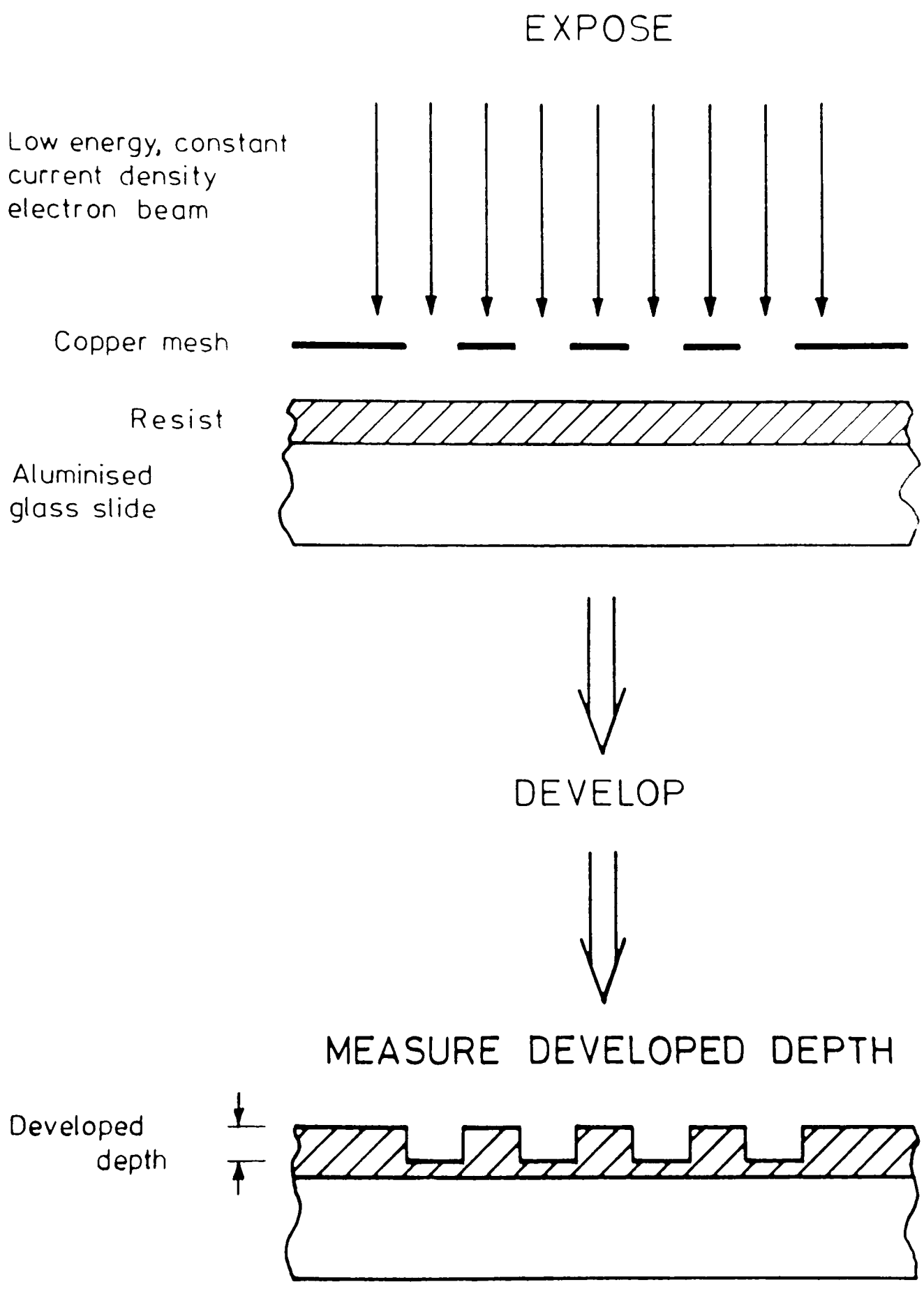

Fig. 3.1 A direct method of measuring the range over which low energy electrons are capable of exposing resist.

3.2 Experimental Method

The original form of the apparatus used the electrode structure of a small cathode ray tube to focus a low energy beam onto a specimen of the resist (see figure 3.2). For very low energy exposures (less than 100eV) the beam in such a column becomes very unstable, since some organic contamination is always present on the inside metal surfaces of the column, and is able to charge slowly, possibly to several volts, causing deflection of the beam. Although low energy electron diffraction (LEED) guns have been constructed[3.4], and will operate at a few electron volts, they require ultra-high-vacuum conditions, and their electrodes may contaminate when they are operated in close proximity to a specimen of organic resist. It was therefore proposed, for the very low energy exposures, to decelerate a higher-energy beam between two grids, placed 0.5mm apart and 1mm from the specimen.

Using the modified cathode ray tube it was difficult to measure the exposure charge density, because the current density in the spot was not constant. A two-lens system with a magnetic condenser lens focusing onto an aperture and a projection lens focusing an image of the illuminated aperture onto the specimen was then evaluated. This method was not successful because it was not possible to reduce the projection lens aberrations sufficiently, since in a short, low energy column, relatively large solid angles are required to achieve sufficient current density. However, since a relatively large electron spot was required it was decided that this could be obtained simply by illuminating an aperture placed close to the resist specimen. Hence a single lens was used in the final form of the apparatus, described in the next section.

The method of decelerating electrons between two grids was found

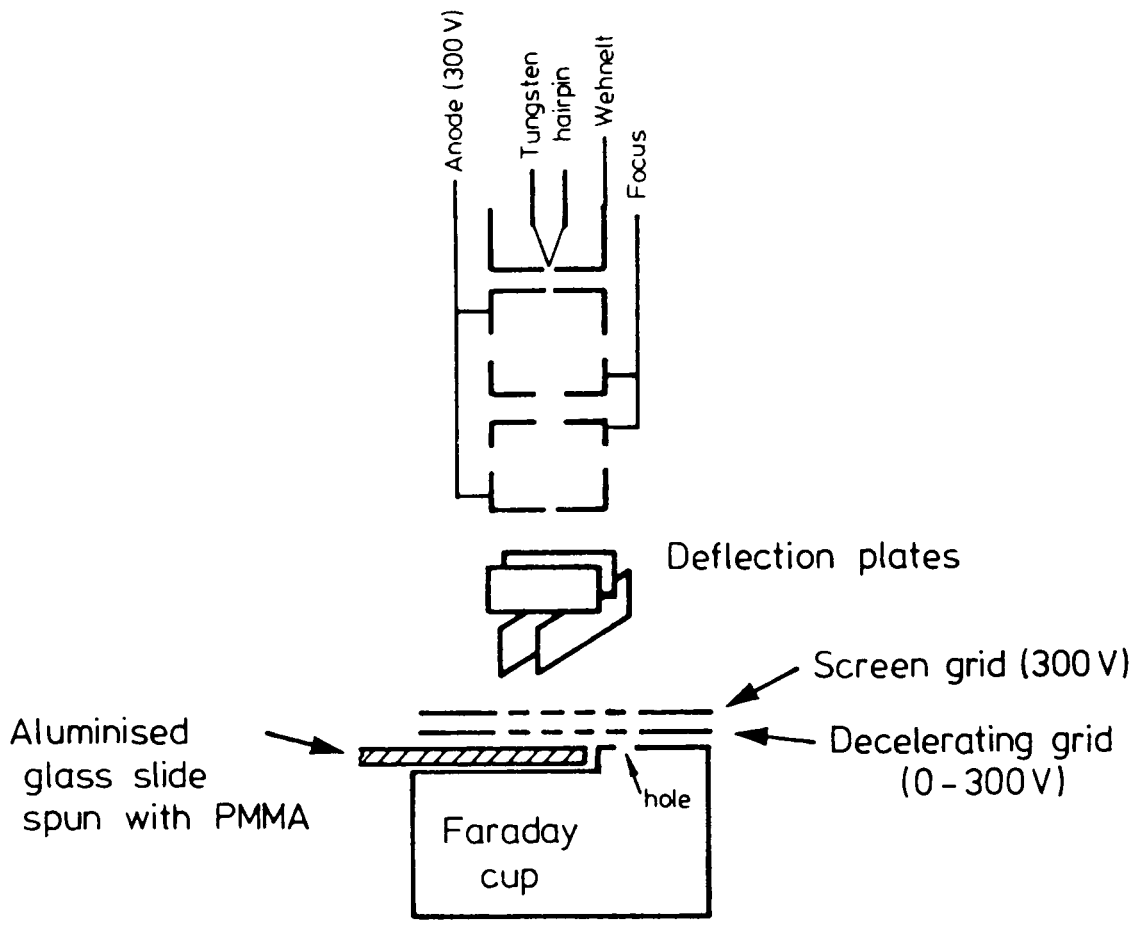

Fig. 3.2 Early form of the low energy electron exposure system, with a tungsten hairpin gun and the electrode structure from a small cathode ray tube.

to be unsatisfactory since the field distribution between the grid bars resulted in uneven current density. When the final electron potential is much lower than the anode potential (ie. for very low energy exposures) electrons travelling at a small angle to the axis before passing through the retarding field will be deflected through a much larger angle afterwards. The exposed area then becomes very large and ill-defined, and the current density becomes small. A more satisfactory electron retarding arrangement employing three apertures was designed, and is described in section 3.3.4.

3.3 Details of the final form of the low energy exposure system

The final form of the apparatus used for the results presented here is shown in figures 3.3 and 3.4. The components of the system are described in this section.

3.3.1. General construction and vacuum system

The low energy exposure system was mounted in an aluminium vacuum collar so that it would be easily demountable from the vacuum system (see figure 3.3). The power supplies, bias unit, and other ancillary equipment were of modular construction; all of the units could therefore be removed easily from the vacuum system, and could be reassembled on another system if necessary.

The specimen holder and Faraday cup were mounted on an X-Y slide arrangement on a central table, which was situated within and supported by the vacuum collar. The electron column was also mounted on the central table, the components of the column being assembled on brass studding. This arrangement was found to be ideal for an experimental system which may have required modification, yet was not very susceptible to mechanical

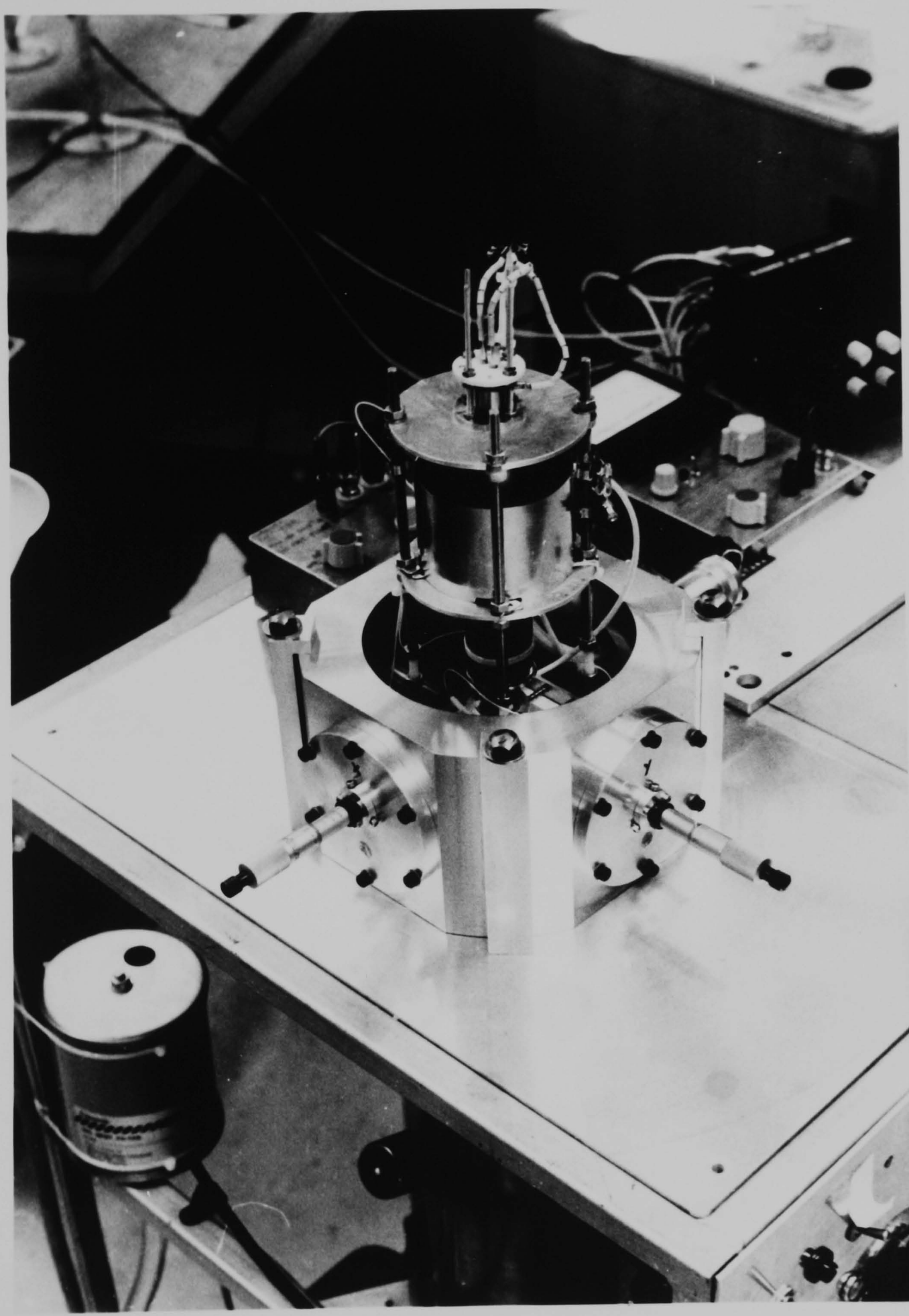

Fig. 3.3 Low energy electron exposure system, evacuated by a liquid nitrogen trapped oil diffusion pump. The electron column and specimen stage are supported by the aluminium collar.

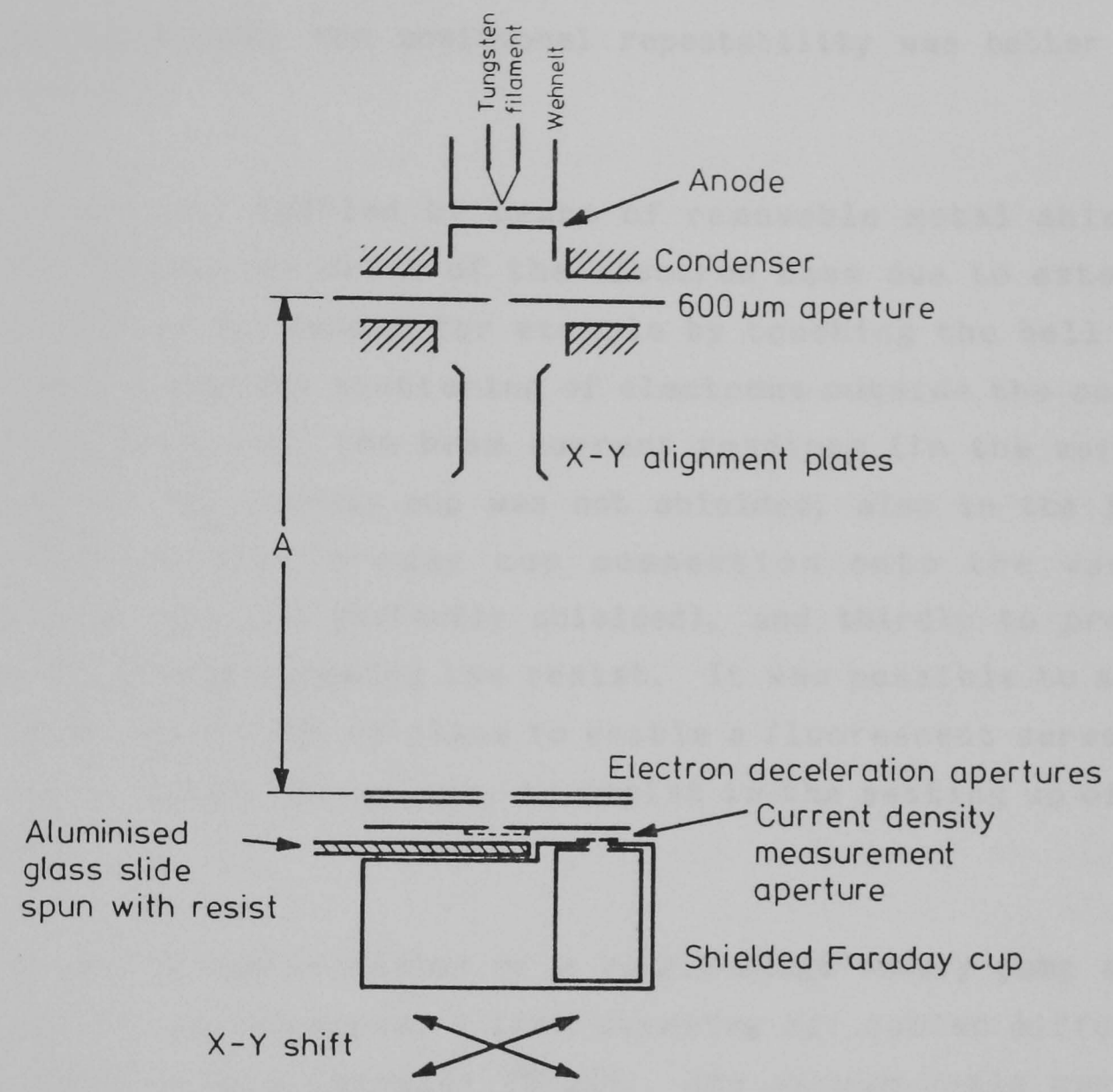

Fig. 3.4 Final form of the low energy electron exposure system. The specimen stage can be moved to expose different areas of the specimen, or to bring the Faraday cup under the beam.

instability and therefore did not require a more rigid structure.

The X-Y specimen stage was shifted by micrometers and spring-biased to prevent backlash. Although the guides themselves were not spring-biased, the positional repeatability was better than 25 microns.

The column was baffled by means of removable metal shields, firstly to prevent drift of the electron beam due to external electric fields, caused for example by touching the bell jar, secondly to prevent scattering of electrons outside the column which might affect the beam current readings (in the earlier arrangement the Faraday cup was not shielded; also in the final arrangement the Faraday cup connection onto the vacuum feedthrough was not perfectly shielded), and thirdly to prevent stray electrons exposing the resist. It was possible to slide the lower shield out of place to enable a fluorescent screen to be placed inside the column, to assist in the setting up of the system.

The vacuum system consisted of a single-stage rotary pump and a liquid-nitrogen-trapped, 2 inch diameter air cooled diffusion pump charged with Convalex 10 oil. The vacuum seals were of viton, and were assembled using as little vacuum grease as possible. Since oil contamination of the system was undesirable, in that it would lead to electron beam drift and other problems, several measures were taken to prevent backstreaming of oil from the pumps, as follows:

(a) A foreline trap filled with sorbtion material was fitted to the rotary pump.

(b) While roughing-out the chamber, dry nitrogen was bled in through a needle valve at the top of the column, as described by Hoffman[3.5]. This ensured that the pressure during roughing was

maintained well into the viscous flow region, to prevent backstreaming, and the dry nitrogen would "sweep" water vapour, carbon dioxide etc. out of the system, enabling the diffusion pump to be started at a higher pressure than would otherwise have been advisable (about 0.1 mbar).

(c) The diffusion pump was never allowed to be hot when the liquid nitrogen cold trap was empty, to minimise backstreaming of oil onto the underside of the baffle valve.

Because the internal arrangement of the system was quite complex, it was found that the pump-down time could be considerably reduced if the column components were heated before opening the system to atmosphere. This was achieved by attaching five 6-watt 12-volt capless bulbs to various points, enabling the column to be heated to about 80°C.

All of the internal wiring of the system was PTFE insulated. Most of the insulating components were of PTFE or machinable ceramic, although some nylon was used, and the lens coil was set in epoxy resin.

The ultimate pressure of the system was about 2×10^{-6}mbar. The system was usually run at any pressure below 8×10^{-6}mbar, which could be attained in about 30 minutes.

3.3.2. Electron gun

The electron gun was similar to those used in electron microscopes, but the Wehnelt cap was smaller since the system was designed to operate at lower potentials. The cathode was an Agar tungsten hairpin filament. The gun had a Wehnelt-to-anode spacing of approximately 0.5mm and could be operated up to 2.5kV. The filament current was usually 2.7-2.9A, from a smooth D.C.

power supply (ripple <1%) which was arranged to float at the cathode potential (the power supply isolation was tested to 3.1kV). It was necessary to stabilise the filament power supply since otherwise the emission current was found to be sensitive to mains fluctuation; the stabilisation was achieved using high-power junction semiconductor devices which appeared to be immune to damage by EHT flashover. The EHT was supplied by a Fluke 3.1kV model 415B power supply with stability better than 0.01% and accuracy 0.25%, and the emission current was monitored by a flashover-protected milliammeter in the EHT line. The emission current at 500eV beam potential was approximately 1mA.

The Wehnelt (control grid) could be either battery-biased up to -75V from the cathode potential, which was sufficient to cut off the emission for any EHT in the range used, or auto-biased by connecting the Wehnelt to the cathode through a large resistance. The latter method is inherently stable since greater emission from the filament results in a higher negative potential on the Wehnelt, which reduces the emission accordingly.

It is possible to control the emission current over a much wider range than the simple passive auto-bias arrangement will allow, by using an active feedback circuit which measures the emission current and controls the Wehnelt potential accordingly; however, the additional complication involved was thought to be unnecessary. One problem associated with emission control circuits is that the beam current is not necessarily linearly related to the emission current, since changing the Wehnelt potential changes the angular distribution of the emission current. Hence it is preferable to sample the beam current, rather than measure the emission current, in order to control the Wehnelt potential. In the system described here it was only possible to do this manually by moving the Faraday cup under the beam, measuring the current collected, and adjusting the gun (or the condenser) accordingly.

To keep the exposure times as short as possible, the gun was usually operated with little or no Wehnelt bias. After an initial warm-up period of about 10 minutes the stability of the exposure current was found to be much more dependent on drift in the beam position, as explained later, than on the emission current, so it was not thought to be necessary to improve the stability of the gun.

A small hole was drilled in the top of the gun ceramic into which a miniature bulb could be placed. This was used to illuminate the hole in the Wehnelt and enabled the gun/anode assembly to be aligned sufficiently accurately with the column. Further alignment was effected by the electrostatic deflection plates.

3.3.3. Magnetic condenser lens

The design of the magnetic electron lens is shown in figure 3.5.

The focal length f of a magnetic lens is given by

$$\frac{1}{f} = \frac{n}{8\phi} \int B_z^2 \, dz \qquad n = \frac{q}{m} \qquad (3.1)$$

where ϕ = electron potential

B_z = flux in the direction of the lens axis

q = electronic charge

m = electron mass

z = axial distance moved by the electrons in the lens field.

Equation 3.1 is an approximation for thin lenses with purely axial magnetic fields[3.6]; however, it provides a useful

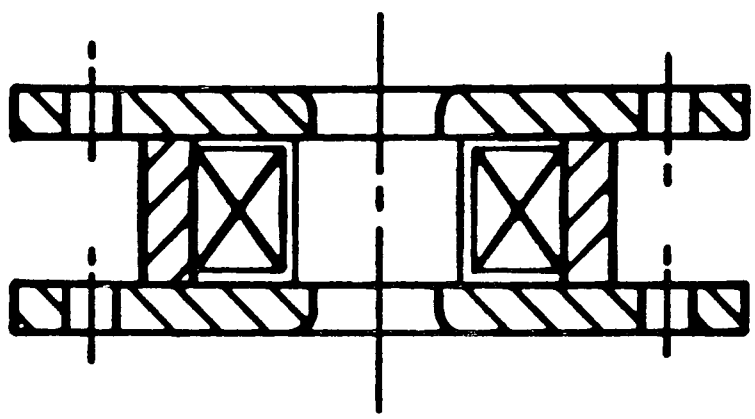

Fig. 3.5 Magnetic condenser lens for the low energy electron exposure system.

approximation for the focal length.

If the permeability of the iron pole-pieces is assumed to be infinite, the magnetic flux between them is given by

$$B = \frac{\mu_o NI}{a} \qquad (3.2)$$

where N = number of turns in the coil, I = current, μ_o = permeability of free space, and a = length of the gap between the pole-pieces (7.6mm).

The lens coil contains 1800 turns and is driven by a 0-100mA constant current supply. Since the lens is placed approximately 2cm from the gun, 100mA lens current should be sufficient to collimate a 2900eV beam. However, because the lens bore is quite large (of the same order as the gap), the magnetic flux on the axis will be less than that given by equation 3.2. It was found that a beam of energy up to about 1500ev could be collimated. At higher acceleration potentials the beam could not be fully collimated but the condenser still provided useful control of the exposure current over the entire range of electron energies used.

The resist exposure area was defined by means of a 400 micron aperture placed close to the specimen, so that the exposed area need not be defined accurately by the lens. Hence lens aberrations and astigmatism were of little consequence; the beam was simply defocused sufficiently for the current density across the defining aperture to be constant. Although lens aberrations were not significant, it was still necessary to stop down the lens by a knife-edge aperture, to prevent scattering of secondary electrons from the inner metal surfaces of the lens and other parts of the column which would otherwise have caused a large energy spread in the beam. The lens was stopped down by a 600 micron aperture, although this diameter could have been increased if necessary to increase the beam current.

3.3.4. Electron deceleration arrangement

The arrangement used in retarding electrons for very low energy exposures (<300eV) is shown in figure 3.6.

For exposures of 300eV and greater energy, all three apertures, and the specimen, were held at anode potential (system earth). In this mode the two 1mm apertures would have no effect. The 400 micron aperture and the mesh served to define the exposure area, and a shadow pattern of the mesh was cast onto the specimen surface. For exposures of less than 300eV, the electron beam was initially accelerated to a higher potential by the anode, usually 500eV. The anode and the upper 1mm aperture were still held at system earth (+500V from the cathode), but the lower 1mm (deceleration) aperture, the exposure defining aperture and grid, and the specimen, were all elevated from the system earth; the difference between the cathode potential and this retarding potential would then determine the final electron potential.

When a retarding potential was applied, the two 1mm apertures would act as an electrostatic lens. It was found that, when decelerating from 500eV, the arrangement produced a focus at the specimen when the final electron potential was 200eV.

If the retarding lens produces a focus close to the specimen or the exposure-defining aperture, the exposure area is reduced and the charge density not constant. It is therefore important to avoid this mode by changing to a different anode potential. If the focus is just above the exposure defining aperture, an enlarged exposure area results, but since the beam current is measured through a 400 micron aperture at the same height as the specimen, the measured charge density will still be correct. This condition occurs for exposures of just above 100eV, and although the image of the grid becomes somewhat blurred, it is

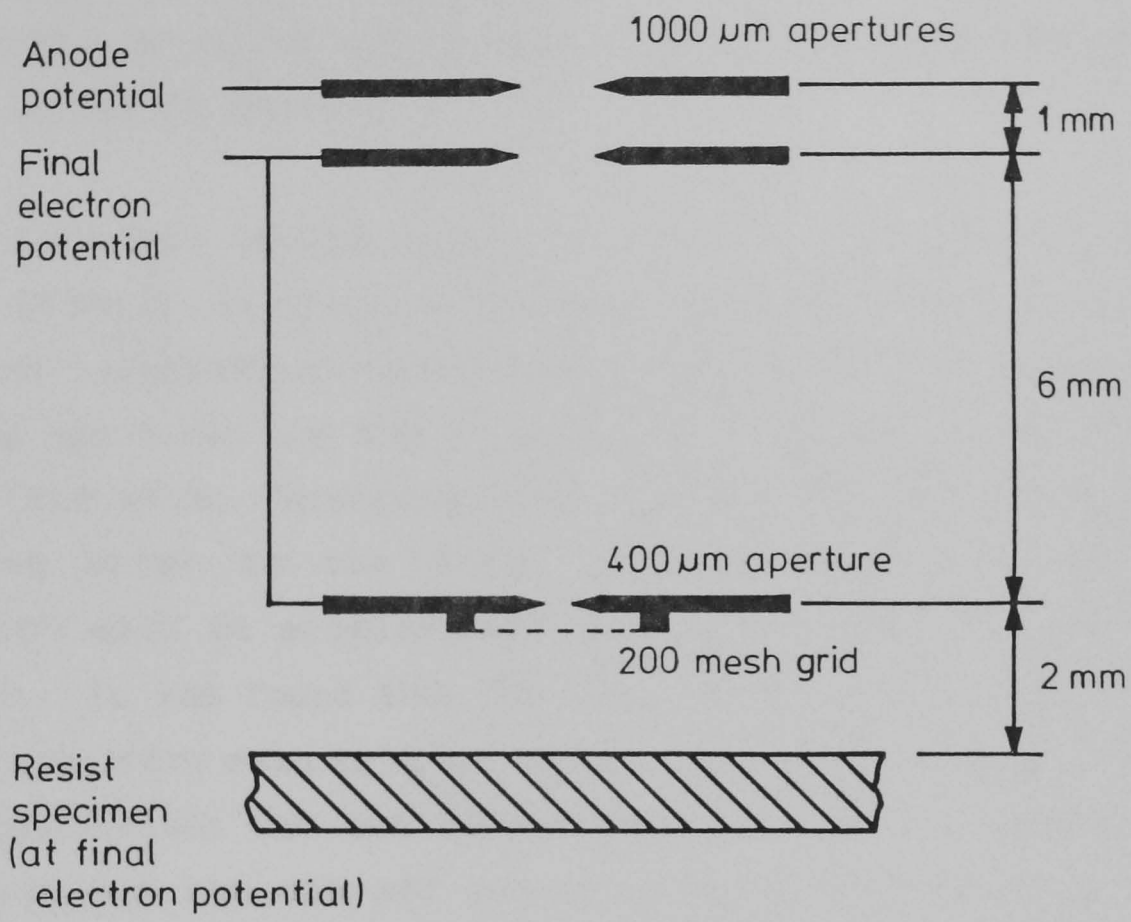

Fig. 3.6 Electron deceleration arrangement for final electron potentials of less than 300eV.

still possible to make useful mark/space depth measurements. Scans of the beam which were produced by the method described in section 3.3.5 are shown in figure 3.7. As the electron energy is decreased below 100eV, the crossover moves further upwards and the beam then diverges as it approaches the defining aperture. The current density for exposures of less than 10eV becomes very small and the exposure time may be as long as 1 hour. However, the system was sufficiently stable to enable exposures of energy as low as 5eV to be made.

The performance of the system at very low energy was found to depend greatly on the build-up of contamination on the lower apertures. Contamination on top of the lower 1mm aperture, the defining aperture, and the grid, will charge to several volts and cut off the beam. Charging of the apertures will not, however, cause an error in the final electron potential since the electrons will be accelerated again once they pass beyond the aperture. It was found that the degree of contamination could be judged by decreasing the final electron energy until the collected current was cut off altogether. If the apertures were newly cleaned the cut-off would be about 4eV, whereas if they were heavily contaminated the cut-off could be as high as 20eV.

3.3.5 Specimen stage and Faraday cup

The PMMA specimens were all spun on 1mm thick aluminised glass microscope slides, which the specimen stage was designed to accept. The slides were clamped under a brass ring to provide an electrical connection to the specimen. Some of the inorganic resist specimens (see chapter 8) were deposited on silicon since the adhesion to glass was poor, and a shim was provided to increase the total thickness to 1mm.

Different exposures on the same specimen were arranged in a 5 x 3

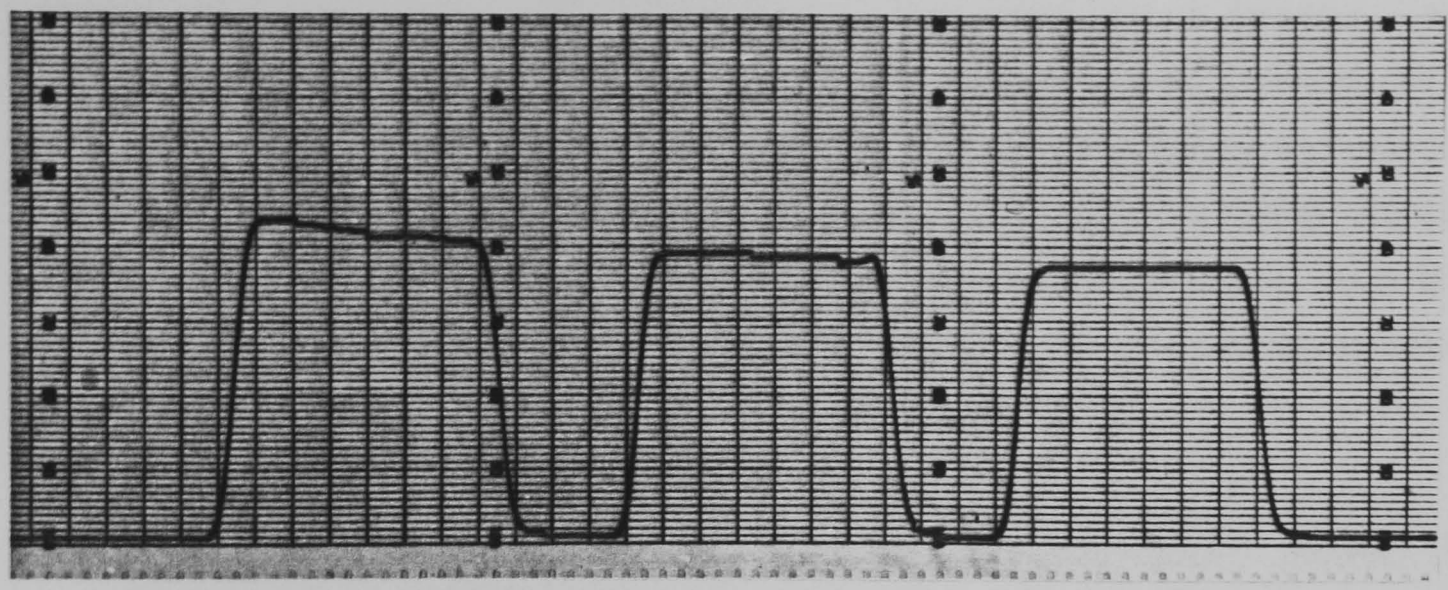

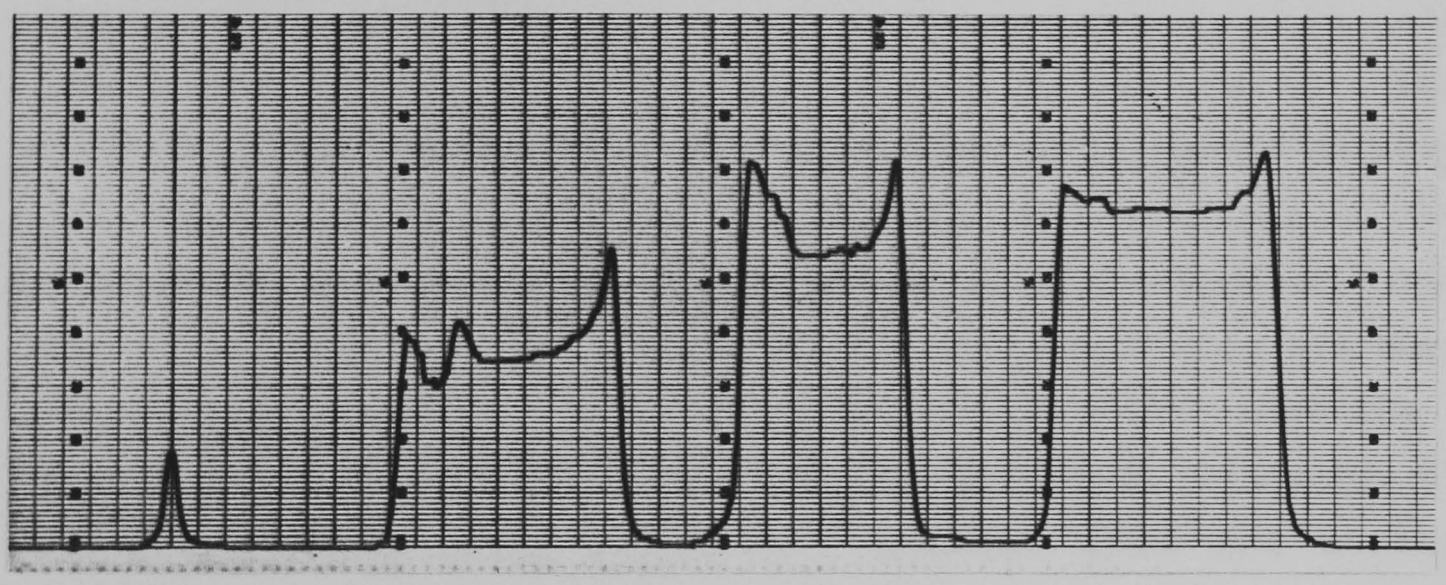

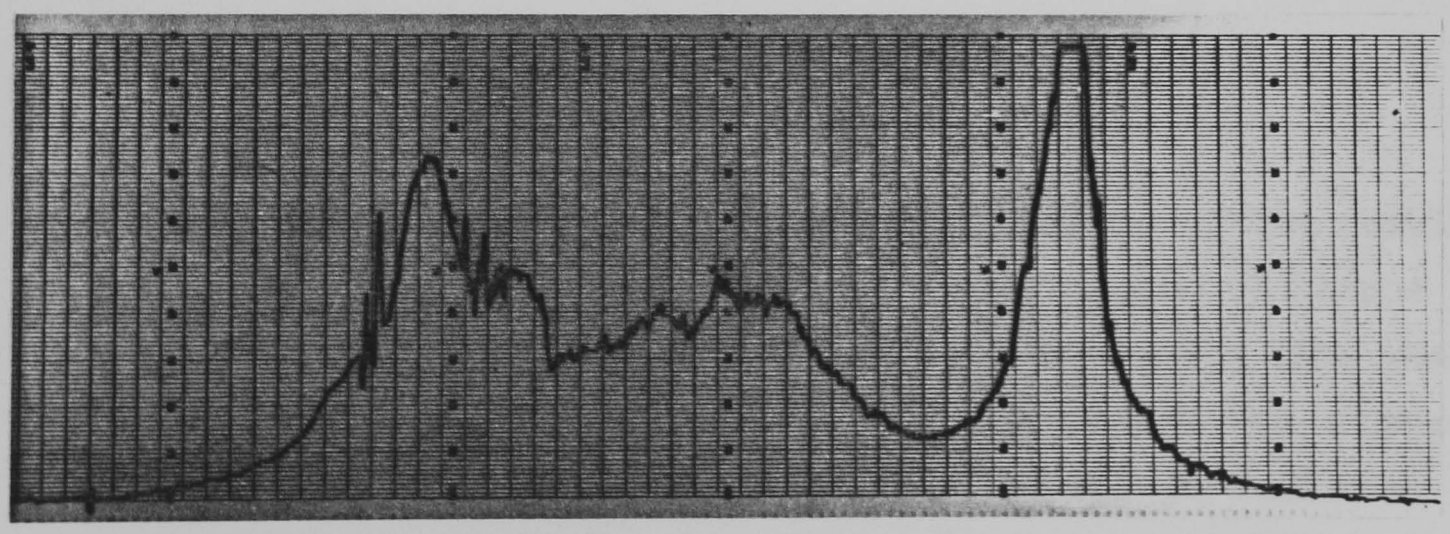

Fig. 3.7 Current density profiles across exposure area, measured by scanning a 10 micron aperture across the beam at a constant rate.

array of locations, all 2mm apart. The developed depths were measured by a Talystep surface profile plotter which incorporated a low power microscope for location of the specimens, and a micrometer-positioned stage. In measuring the developed depths it was only necessary for one exposure to be easily visible through the microscope on the Talystep, the others being located from the first one by means of the micrometers.

The Faraday cup was fully enclosed in the specimen stage to prevent pick-up of stray current. It was connected to the electrical feedthrough by a screened, PTFE insulated wire. The beam current was collected through a 400 micron aperture, with which the Faraday cup could be aligned mechanically. This aperture could be replaced by a 10 micron one, and the stage driven slowly by coupling a geared motor to one of the micrometers, in order to measure the current distribution across the beam. Scans for 500, 100, and 40eV beam potentials are shown in figure 3.7. Below 40eV the current collected through the 10 micron aperture was too small to be measured, although the current density could still be estimated from the current collected through the 400 micron aperture.

3.4 Results

The PMMA specimens were of Elvacite 2041. For all of the results presented here the developer was 1 part methyl isobutyl ketone to 3 parts isopropyl alcohol at 23°C, and the development time was 3 minutes. It was assumed that virtually all of the exposed material had dissolved after 3 minutes, since an increase in depth could not be detected after this time.

Figure 3.8 shows an optical micrograph of an exposed and developed area of PMMA, and a Talystep surface profile trace across a similar area is shown in figure 3.9.

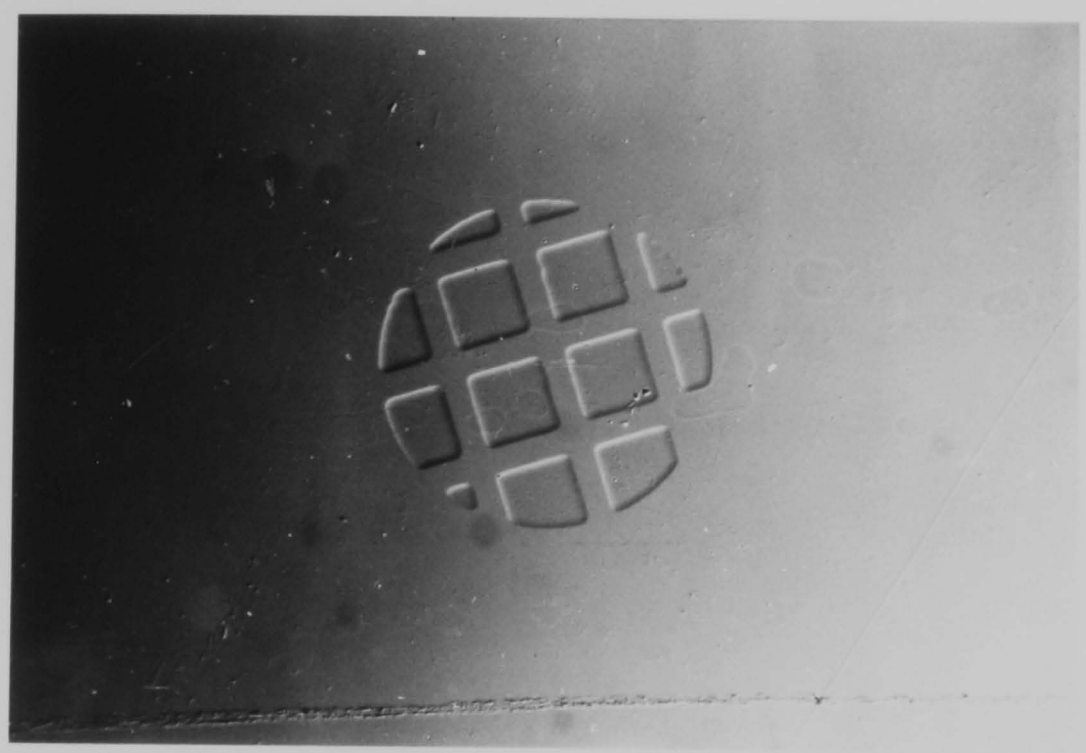

Fig. 3.8 Phase contrast optical micrograph of exposure pattern in PMMA after development. Exposure 5×10^{-5} Ccm^{-2} at 2.2keV. Exposed areas are 170nm deep.

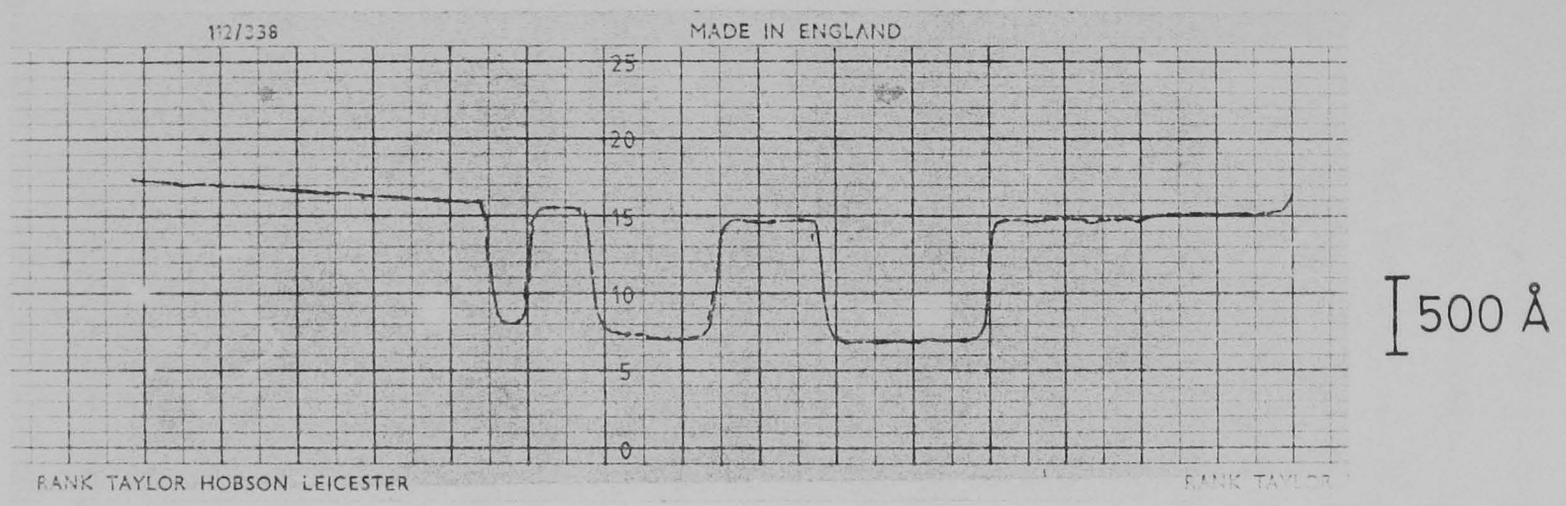

Fig.3.9 Talystep surface profile plot of an exposed and developed area of PMMA. Electron energy 1300eV; exposure dose 5×10^{-5} coulomb cm^{-2}.

A possible cause of error is charging of the resist, which would create an additional decelerating field and hence reduce the final electron energy. It can be seen that potentially charging effects could be very important. If one considers the exposure charge injected into the loss-less capacitor represented by the resist, the surface of the resist would charge up to over 5kV. The validity of the results depends on sufficient leakage of charge occurring to the aluminium layer. There was definite evidence of charging of the 0.24 microns thick PMMA films during exposures at 200 eV and below, in that the developed grid pattern on the resist became distorted. However, this was overcome by exposing PMMA films that were only slightly thicker than the exposure range expected.

Figure 3.10 shows developed depth as a function of charge density for an electron energy of 500eV. The depth is seen to increase with exposure up to about $3x10^{-5}$ Ccm^{-2}. After this the depth remains almost constant and begins to fall beyond about 10^{-4} Ccm^{-2}, when the exposed areas become increasingly irregular due to cross-linked material. The maximum developed depth is assumed to be the exposure range, representing the range over which the electrons are capable of exposing the PMMA. This will be discussed further in chapter 7.

It was found that on greatly overexposing the resist (by, say, an order of magnitude above the exposures given here), swelling of the resist occurred which was clearly visible before development; in some cases the swelling produced thicknesses greatly in excess of the measured ranges. Margolin and Gurov[3.7] report that low energy exposure of PMMA produces films of similar thicknesses to the ranges calculated from the Bethe-Bloch continuous-loss model, but in negative resist the film thicknesses produced are much greater. The swelling was assumed to be due to gassing of the PMMA, but was not investigated further here.

Figure 3.11 shows developed depth as a function of electron

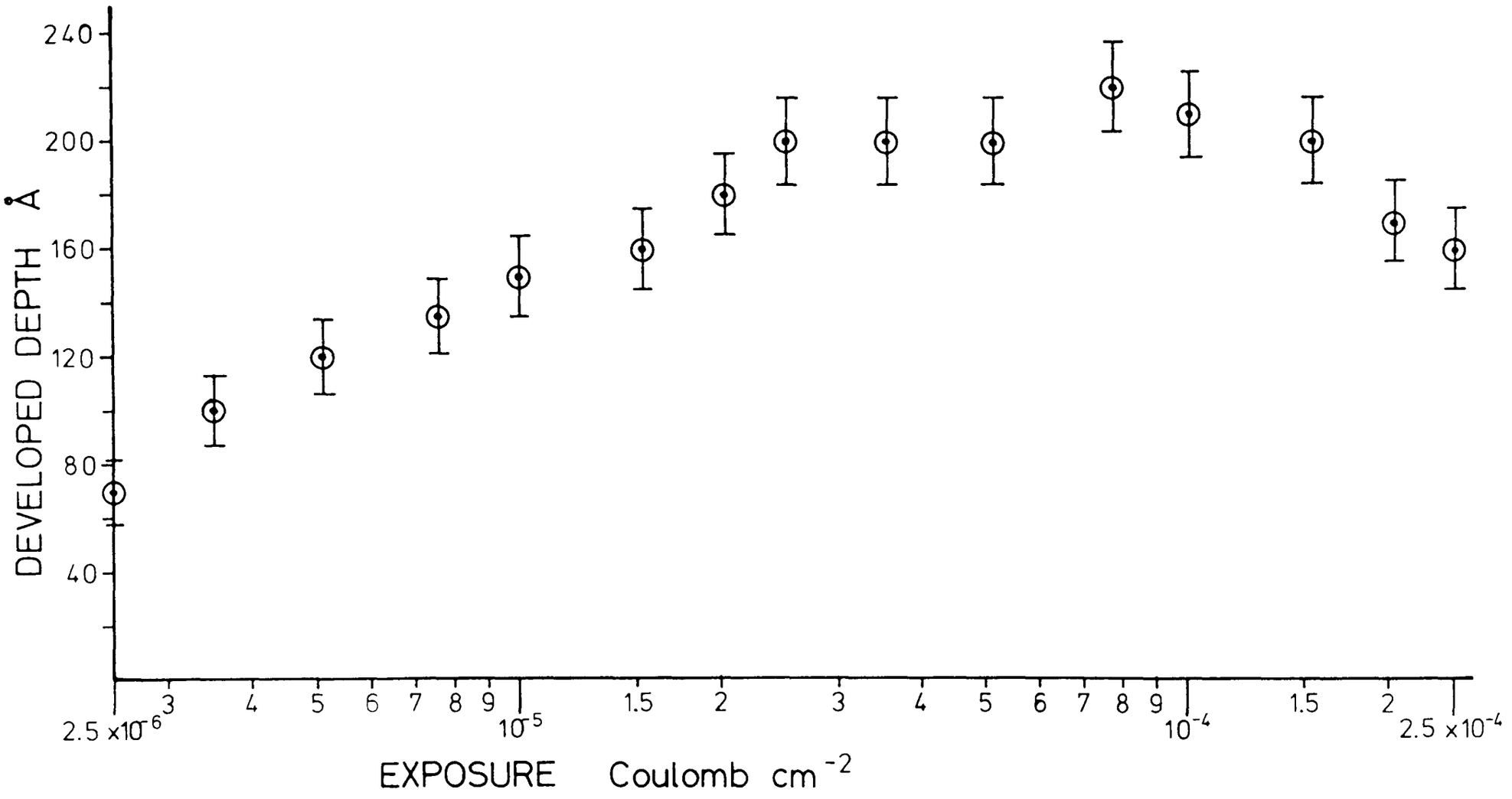

Fig. 3.10 Graph of developed depth against exposure dose, for 500eV electrons. The developed depth reaches a maximum and remains almost constant for a wide range of exposures around 5×10^{-5} Ccm^{-2}. This maximum depth is taken to be the exposure range.

Fig. 3.11 Graph of developed depth against electron energy, with exposure dose constant. Above 400eV the measurements closely follow electron ranges calculated from a model based on the Bethe formula.

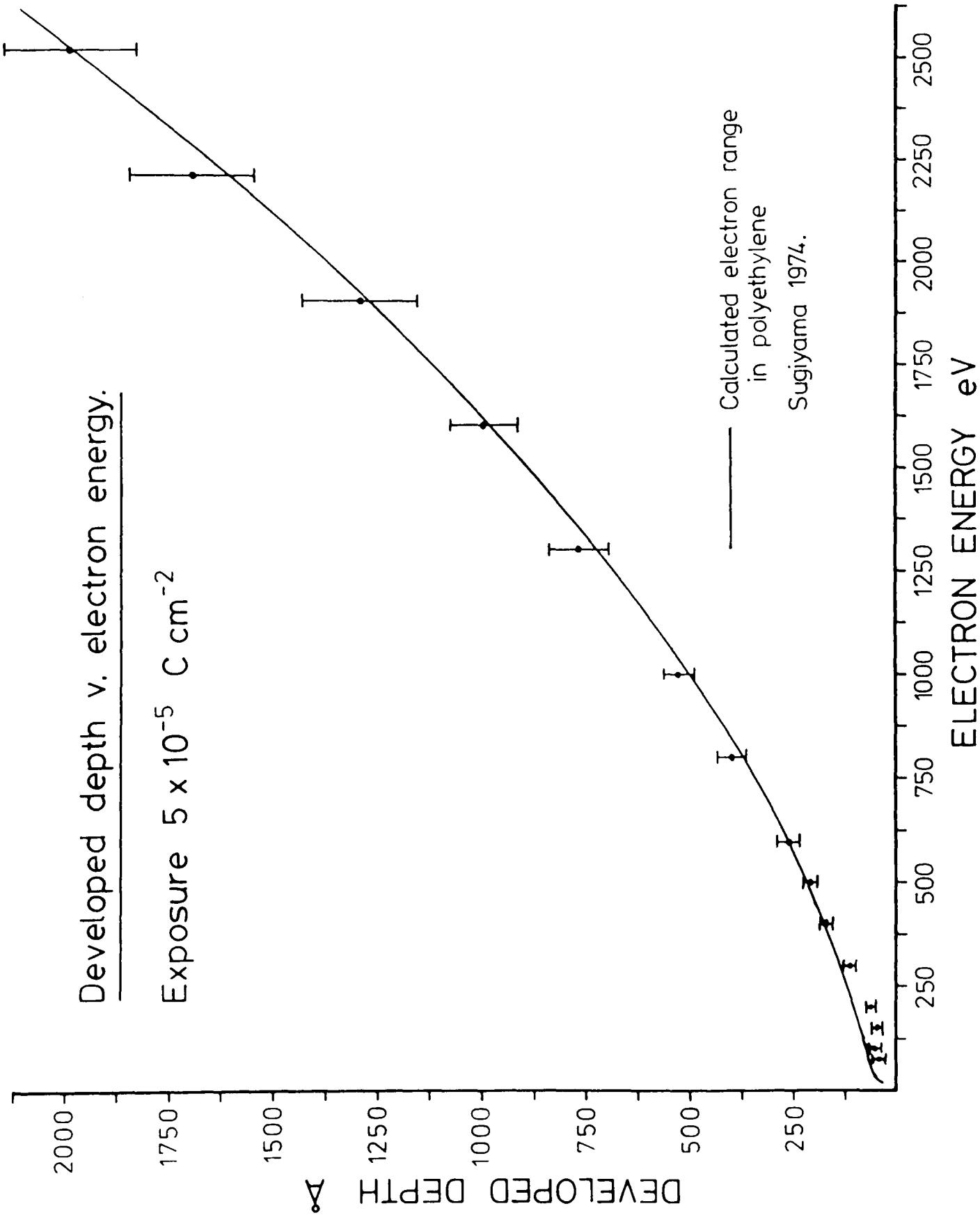

energy from 75 to 2500eV. The charge density is constant at $5x10^{-5}$ Ccm^{-2}. At 400eV and above the results are seen to follow quite closely Sugiyama's calculated data for electron range in polyethylene[3.8]. In this region the developed depth increases with the 1.34th power of electron energy, as can be seen from figure 3.12. The experimental results are seen to depart from the calculated ranges below 400eV.

Very low energy exposures were made, down to 5eV, of resist films less than 10nm thick. There was no evidence that these very low energy exposures produced any measurable effect, even with large doses (up to $5x10^{-4}$ Ccm^{-2}), and so we must assume that the exposure range is negligible.

3.5 Conclusion

A low energy electron exposure system was developed which was capable of exposing resist specimens with electron energies of 5 to 2500eV. For very low energy exposures an electron deceleration arrangement was used, enabling stable exposures of less than 10eV to be given over long periods in a standard, viton-sealed vacuum system containing specimens of organic material.

The exposure ranges of low energy electrons in PMMA have been measured, and are seen to follow published theoretical range data. There is no evidence of any significant increase in the exposure range at very low electron energies, as low as 5eV.

The exposure system described here was also used to investigate arsenic trisulphide inorganic resist, as described in chapter 8.

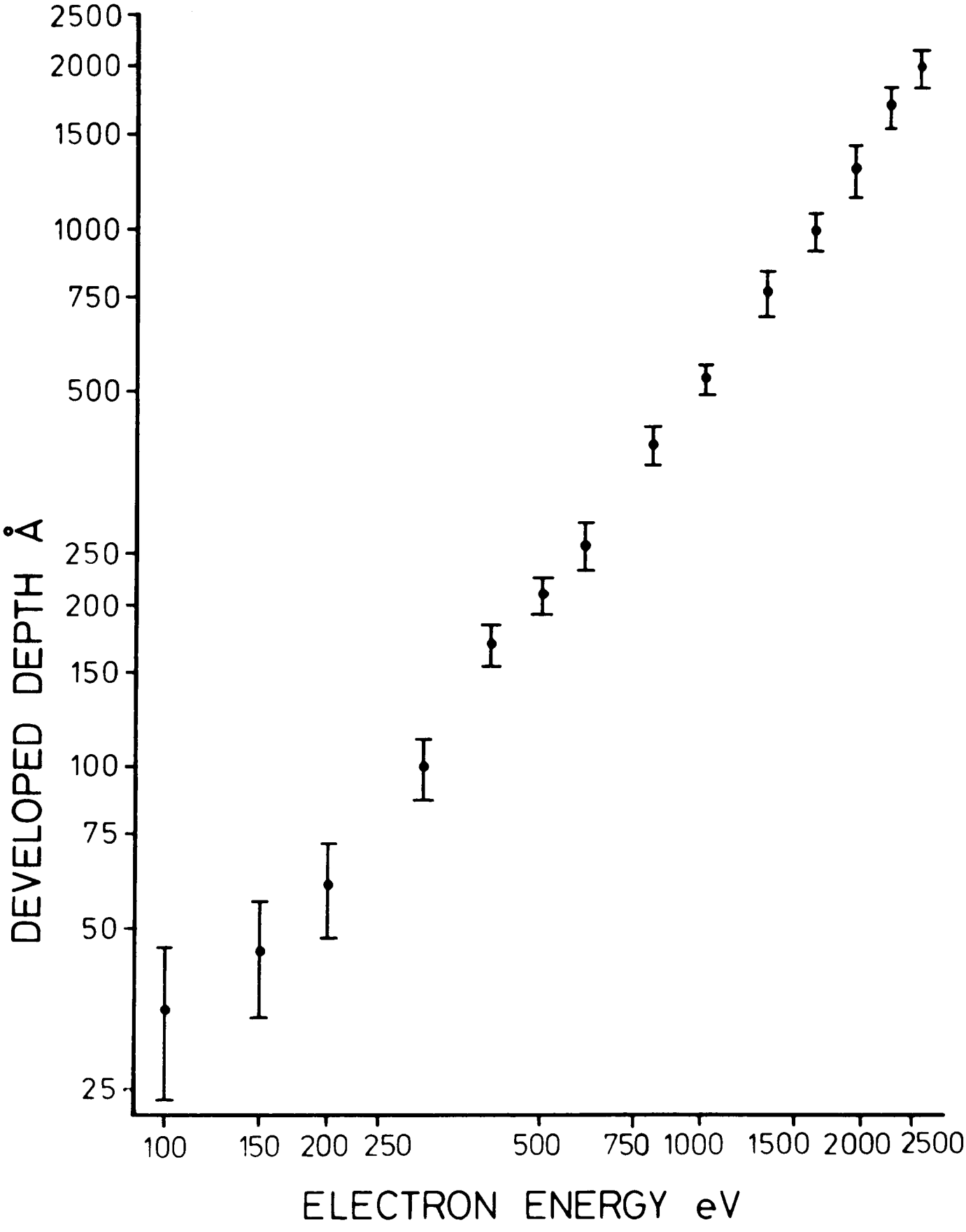

Fig. 3.12 Logarithmic plot of developed depth at $5x10^{-5}$ Ccm^{-2} exposure against electron energy. Above 300eV the developed depth increases with the 1.34th power of electron energy.

References

3.1 K. Murata, D.F. Kyser, C.H. Ting; "Monte-Carlo simulation of fast secondary electron production in electron-beam resists"
J. Appl. Phys. 52(7), 4396-4405, 1981.

3.2 A.N. Broers; "Resolution limits of PMMA resist for exposure with 50kV electrons"
J. Electrochem. Soc. 128(1), 166-170, 1981.

3.3 Burn Jeng Lin; "Deep uv lithography"
J. Vac. Sci. Technol., 12(6), 1317-1320, 1975.

3.4 T.A. Heppell; "A combined low energy and reflection high energy electron diffraction apparatus"
J. Sci. Instrum. 44, 686-688, 1967.

3.5 D.M. Hoffman; "Operation and maintenance of a diffusion-pumped vacuum system"
J. Vac. Sci. Technol. 16(1), 71-74, 1979.

3.6 E.A. Ash; Lecture notes on electron optics.

3.7 V.A. Margolin and S.A. Gurov; "Experimental test of the Bethe-Bloch model in the interaction of a low energy electron beam with an organic resist"
Sov. Tech. Phys. Lett. 5(3), 132-133, 1979.

3.8 H. Sugiyama; "Tables of energy losses and ranges of low energy electrons and positrons"
Bull. Electrotech. Lab. 33, 277-290, 1974.

CHAPTER 4

Electron energy loss spectroscopy of PMMA and silicon nitride.

4.1 Introduction

The ranges over which low energy electrons can expose PMMA resist have been measured (chapter 3). In order to use the low energy electron range data to estimate the energy dissipation profile of the secondary electrons generated in the resist, it is necessary to know the number and energy distribution of secondary electrons that are created by the primary beam. These can be estimated by electron energy loss spectroscopy, where an initially mono-energetic beam of electrons passes through a thin membrane of the material, and the energy distribution of the transmitted electrons is measured by an electron spectrometer.

Energy loss spectra were obtained for unsupported films of both PMMA and silicon nitride. The nitride spectrum was obtained since this material is often used as the support film for very high resolution lithography in PMMA, and its yield of secondary electrons should be included in the Monte-Carlo simulations (chapter 7).

4.2 Specimen preparation

The PMMA membranes were prepared as follows. A thin film (<5nm) of a water-soluble parting material ("Victawet") was deposited by vacuum evaporation onto a glass microscope slide, which was then spun with 35nm of PMMA (Elvacite 2041, molecular weight 360,000) dissolved in xylene. The film was baked at 175°C for several hours, then scribed into small squares and floated off by

immersing the slide slowly at a shallow angle into distilled water, thus dissolving the parting layer. The free PMMA films were then picked up onto 3mm diameter copper grids. Although the membranes so produced were wrinkled and accurate focus of the electron beam could not be maintained if the specimen was moved, this was of no consequence in obtaining the energy loss spectra.

The silicon nitride membranes were identical to those used as substrates for high-resolution lithography, produced by etching back through silicon as described in chapter 6. The nitride membranes were 70nm thick.

4.3 Acquisition of the energy loss spectra

The spectra were obtained by the Vacuum Generators HB5 scanning transmission electron microscope in the Natural Philosophy Department of Glasgow University. This instrument is fitted with an energy analyser and a TOLTEC data acquisition system[4.1]. The primary beam energy was 100keV. The spectra were acquired from 0 to 900eV loss in 1eV steps, the resolution being nominally 1eV. The spectra were later extended up to 1700eV in 2eV steps; the extended spectra were merged with the original ones at 900eV. The collection semi-angle of the detector system was about 27mrad; not all of the electrons with greater losses are collected within this angle, and the spectra must be corrected accordingly (section 4.4.3).

In acquiring the PMMA spectrum, the exposure dose was limited to 1.4×10^{-4} Ccm^{-2}, this dose being insufficient to cross-link the material. Ritsko et al. have produced energy loss measurements of PMMA between 1 and 300eV, and find that the losses around 5eV increase greatly with larger doses than this[4.2]. The exposure area was 0.6 microns square, but the specimen was moved continuously as the spectrum was being acquired, over a total

distance of 140 microns in 56 seconds with a beam current of 5pA. This total measurement period was divided into 1024 timeslots, each measuring a particular 1eV wide "window" in the spectrum. In this case each timeslot would receive approximately $2x10^6$ incident primary electrons.

The energy analyser contains two detectors, one counting individual electrons, acquiring the "pulse" spectrum, the other measuring current, obtaining the "analogue" spectrum. The pulse spectrum is accurate for smaller numbers of electrons, but the count rate of the detection system is limited and this spectrum becomes inaccurate for larger numbers. Here the current detector is preferable, once some correction has been made for dark current in the detector, but the analogue spectrum suffers from noise when small currents are measured. Hence the two spectra are merged at some point, which is determined as described in section 4.4.2.

The output of the analogue detector is digitised to enable it to be processed by the TOLTEC system, and therefore the analogue spectra are expressed in arbitrary analogue "counts".

4.4 Processing of the spectra

The spectra were transferred to the GEC 4070 computer within the department for processing. Programs were written on this machine to correct for dark current, merge the pulse and analogue spectra, correct for electrons scattered outside the collection angle of the detector, and then remove the zero-loss peak and correct for double inelastic scattering, as described below.

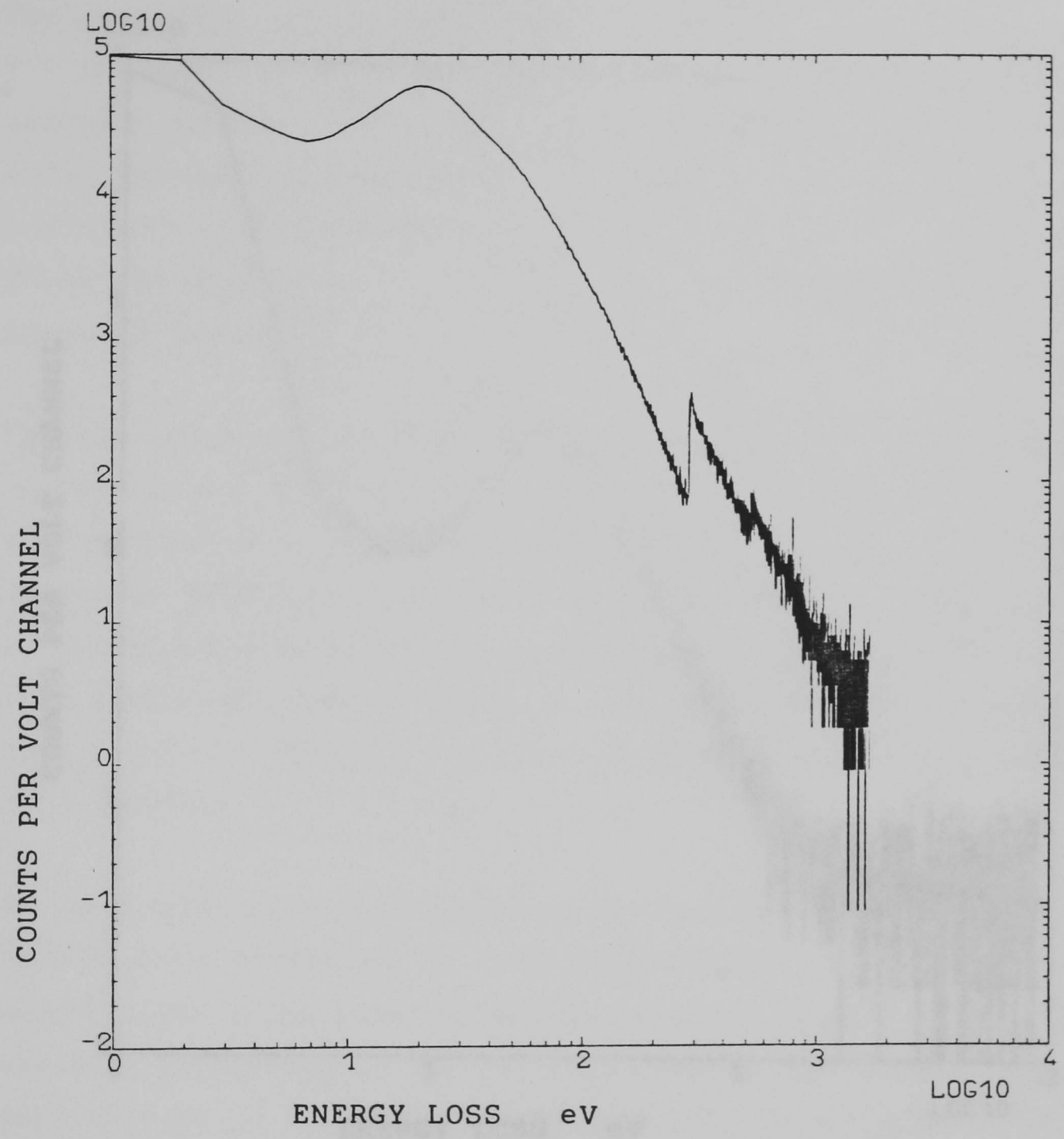

Fig. 4.1 PMMA pulse spectrum, unprocessed.

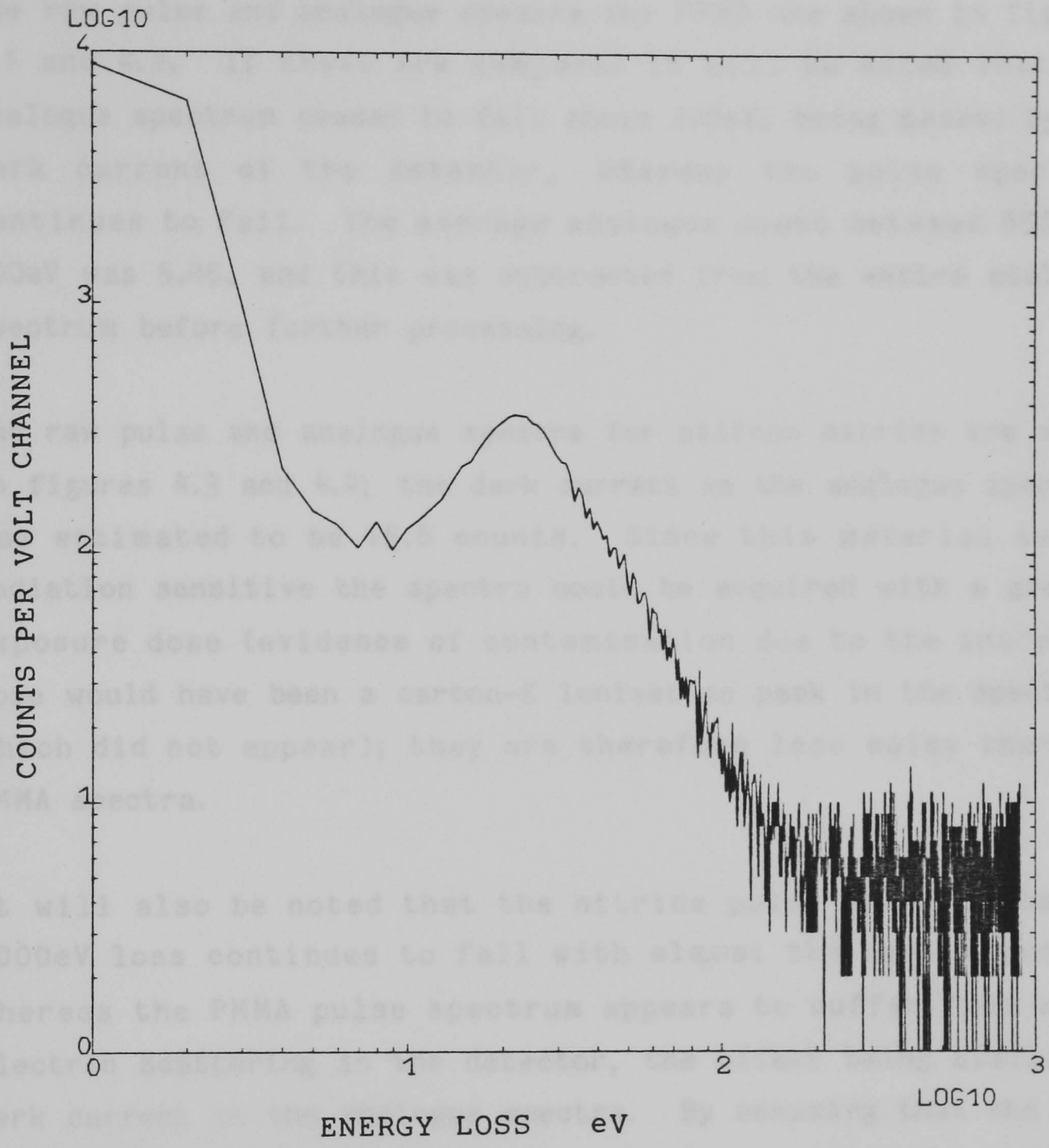

Fig. 4.2 PMMA analogue spectrum, unprocessed.

4.4.1 Dark current correction in the spectra

The raw pulse and analogue spectra for PMMA are shown in figures 4.1 and 4.2. If these are compared it will be noted that the analogue spectrum ceases to fall above 200eV, being masked by the dark current of the detector, whereas the pulse spectrum continues to fall. The average analogue count between 850 and 900eV was 5.45, and this was subtracted from the entire analogue spectrum before further processing.

The raw pulse and analogue spectra for silicon nitride are shown in figures 4.3 and 4.4; the dark current in the analogue spectrum was estimated to be 15.6 counts. Since this material is not radiation sensitive the spectra could be acquired with a greater exposure dose (evidence of contamination due to the increased dose would have been a carbon-K ionisation peak in the spectrum, which did not appear); they are therefore less noisy than the PMMA spectra.

It will also be noted that the nitride pulse spectrum beyond 1000eV loss continues to fall with almost the same exponent, whereas the PMMA pulse spectrum appears to suffer from stray electron scattering in the detector, the effect being similar to dark current in the analogue spectra. By assuming that the PMMA pulse spectrum should continue to fall with the same exponent above 1000eV, just as the nitride spectrum does, it was assumed that the stray scattering accounted for an average of 1.9 pulse counts per electron volt channel, which was subtracted from the PMMA pulse spectrum. In order to prevent negative counts in the PMMA spectrum (caused by noise), counts above 700eV were averaged over 10eV.

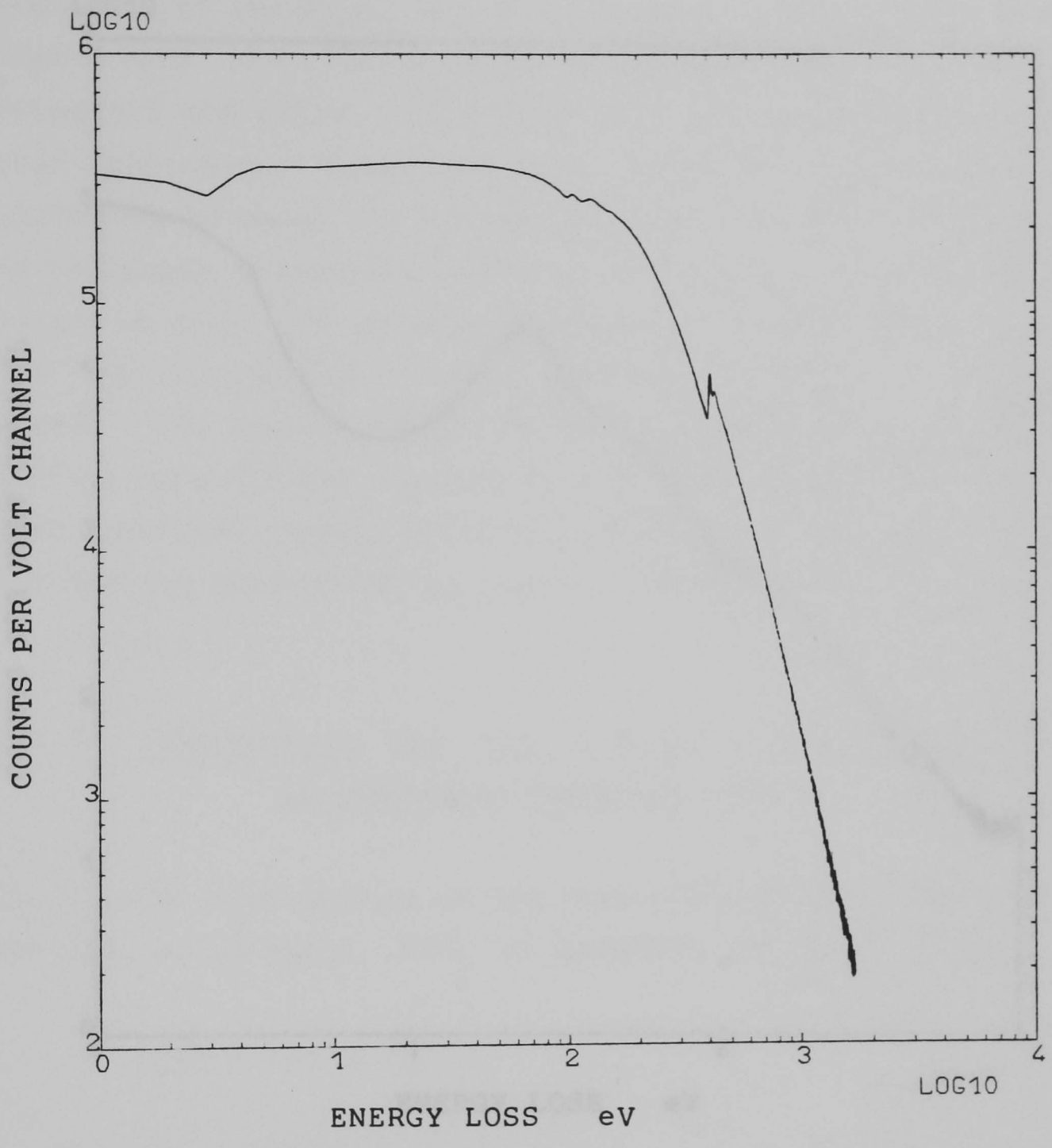

Fig. 4.3 Silicon nitride pulse spectrum, unprocessed

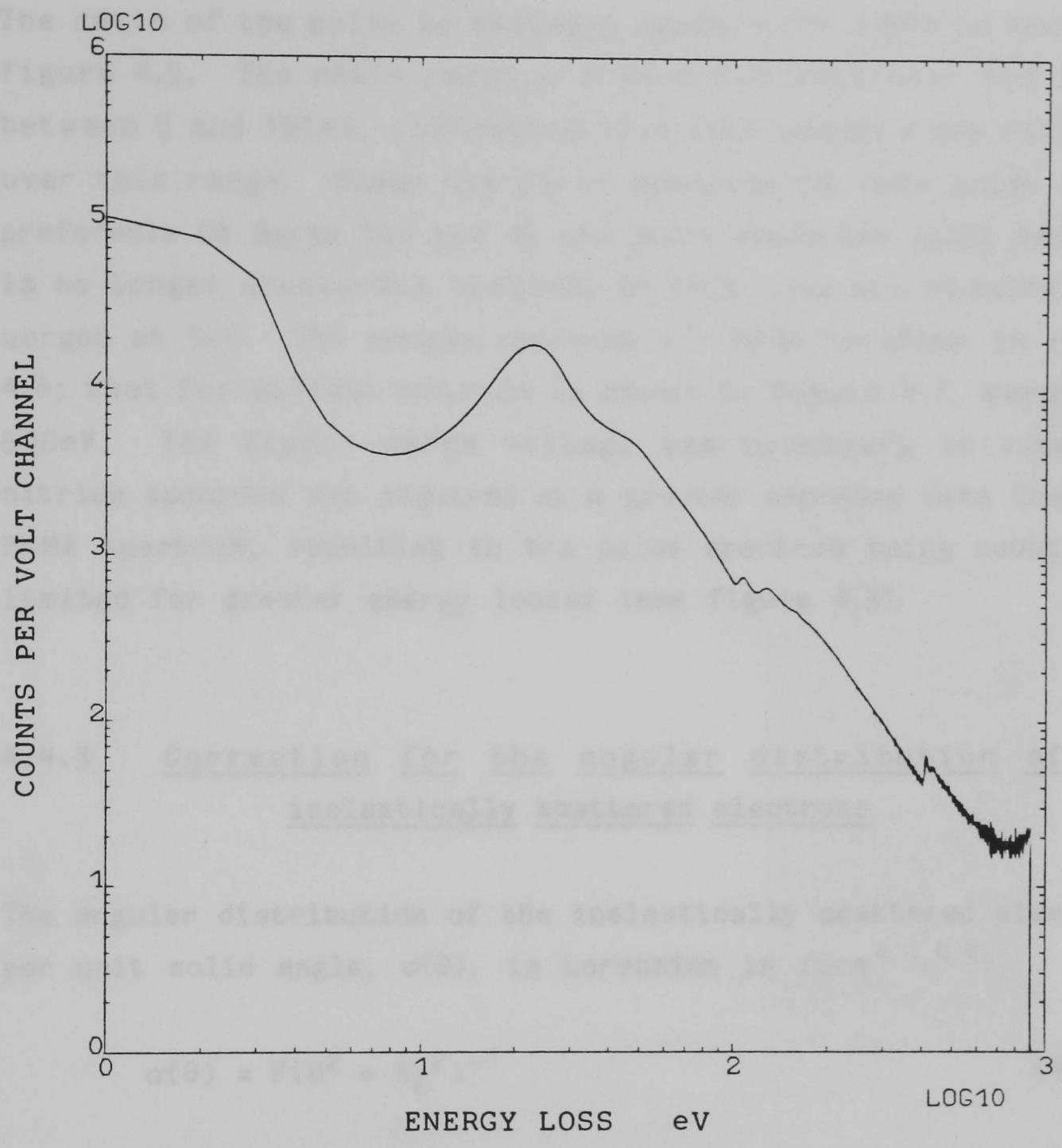

Fig. 4.4 Silicon nitride analogue spectrum, unprocessed.

4.4.2 Merging the spectra

The ratio of the pulse to analogue spectra for PMMA is shown in figure 4.5. The ratio remains almost constant over the range between 5 and 150eV, indicating that both spectra are reliable over this range. Since the pulse spectrum is less noisy it is preferable to merge the two at the point where the pulse detector is no longer count-rate limited; in this case the spectra were merged at 5eV. The merged spectrum for PMMA is shown in figure 4.6; that for silicon nitride is shown in figure 4.7, merged at 590eV. The higher merge voltage was necessary because the nitride spectrum was acquired at a greater exposure dose than the PMMA spectrum, resulting in the pulse spectrum being count rate limited for greater energy losses (see figure 4.3).

4.4.3 Correction for the angular distribution of the inelastically scattered electrons

The angular distribution of the inelastically scattered electrons per unit solid angle, $\sigma(\theta)$, is Lorenzian in form[4.3,4.4]:

$$\sigma(\theta) = F(\theta^2 + \theta_E^2)^{-1} \qquad (4.1)$$

where $\theta_E = \Delta E/2E$,

ΔE = energy loss

E = initial electron energy.

F is a function related to the generalised oscillator strength (GOS), determined by the band structure of the target atoms. The GOS is constant for small deflection angles, and for plasmon excitations (collective valence excitations which account for many of the losses up to about 50eV - see section 4.5) falls abruptly to zero at a cut-off angle $\theta_c = \Delta E/E$; for single electron excitations the fall is more gradual[4.4]. The

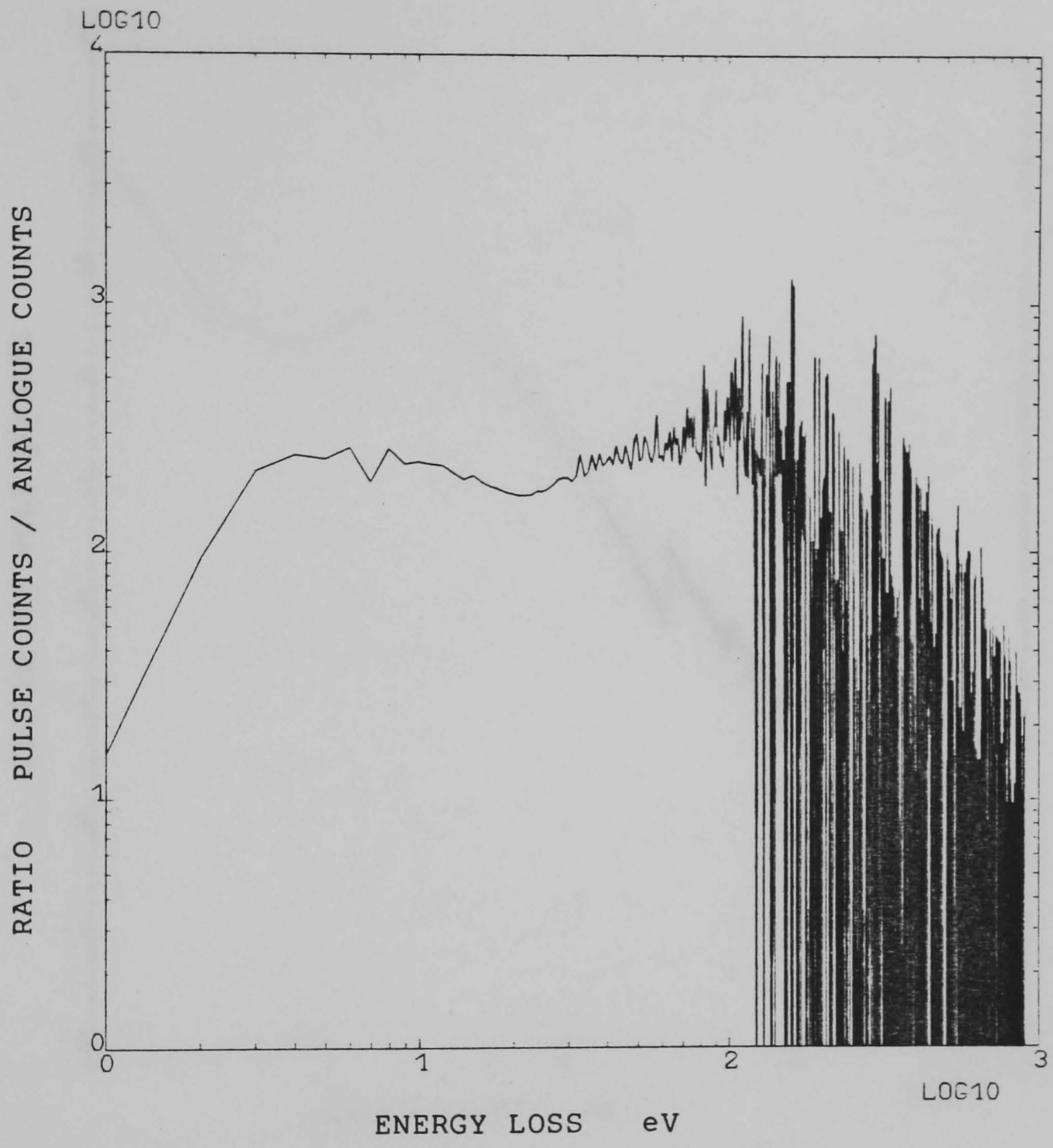

Fig. 4.5 Ratio of pulse to analogue spectra (PMMA), after subtracting the dark current from the analogue spectrum.

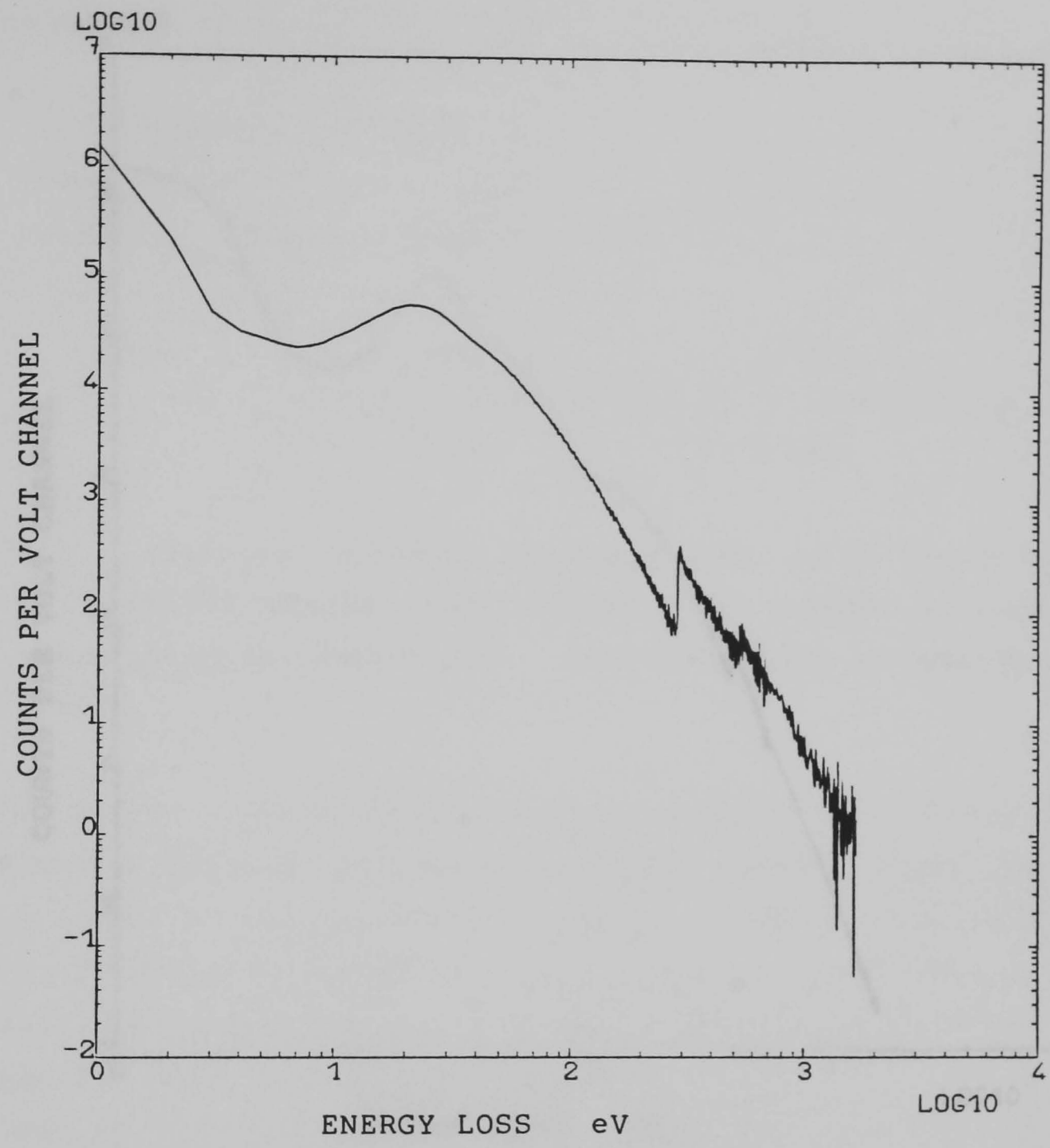

Fig. 4.6 PMMA spectrum merged at 5eV, with dark current correction of 5.45 counts in the analogue spectrum and stray electron correction of 1.9 counts in the pulse spectrum.

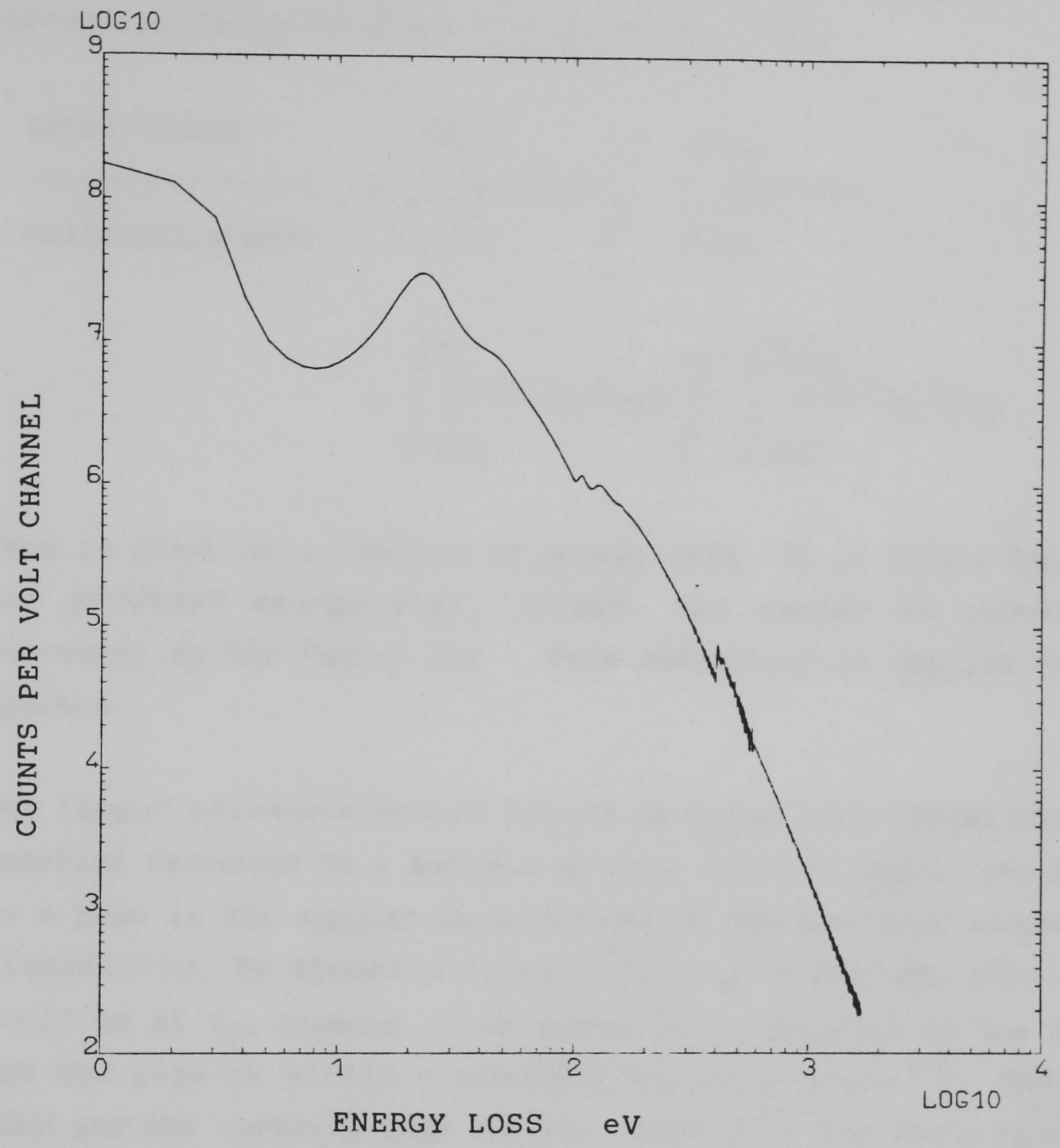

Fig. 4.7 Silicon nitride spectrum, merged at 590eV and corrected for dark current of 15.6 counts in the analogue spectrum.

distribution $\sigma(\theta)$ can be integrated up to the cut-off angle, and up to the collection semi-angle θ_{det} (27mrad), to determine the correction factor to allow for the counts lost:

$$\frac{\text{total counts}}{\text{collected counts}} = \int_{\theta=0}^{\theta_c} \sigma(\theta)\theta d\theta \Big/ \int_{\theta=0}^{\theta_{det}} \sigma(\theta)\theta d\theta$$

$$= \int_{\theta=0}^{\theta_c} \theta(\theta^2+\theta_E{}^2)d\theta \Big/ \int_{\theta=0}^{\theta_{det}} \theta(\theta^2+\theta_E{}^2)d\theta \qquad (4.2)$$

This is shown as a function of energy loss ΔE in figure 4.8. At the greatest energy loss, 1700eV, the number of counts is increased by the factor 2.3. This correction is applied to the spectra.

For larger valence electron losses (greater than 100eV) the GOS function increases to a maximum at some non-zero angle, and there is a peak in the angular distribution of the scattered electrons. Classically, by assuming conservation of momentum, this peak would be at θ_c; however, some momentum is absorbed by the atom, and the peak is within a somewhat narrower angle[4.5]. Between 50eV and the carbon-K edge (280eV), Egerton[4.5] has found that the differential-energy scattering cross section (and hence the loss spectrum) for carbon can be approximated as

$$d\sigma/d(\Delta E) \propto \Delta E^{-r} \qquad (\Delta E = \text{energy loss}) \qquad (4.3)$$

where r is about 4.5 for small-angle scattering (2mrad collection angle), decreasing to about 4.0 when large-angle scattering is included, with a collection angle of 130mrad. For small-angle scattering he found this to agree with Bethe quantum-mechanical theory based on a hydrogenic model, and it was therefore expected to apply to valence electron excitation in atoms other than

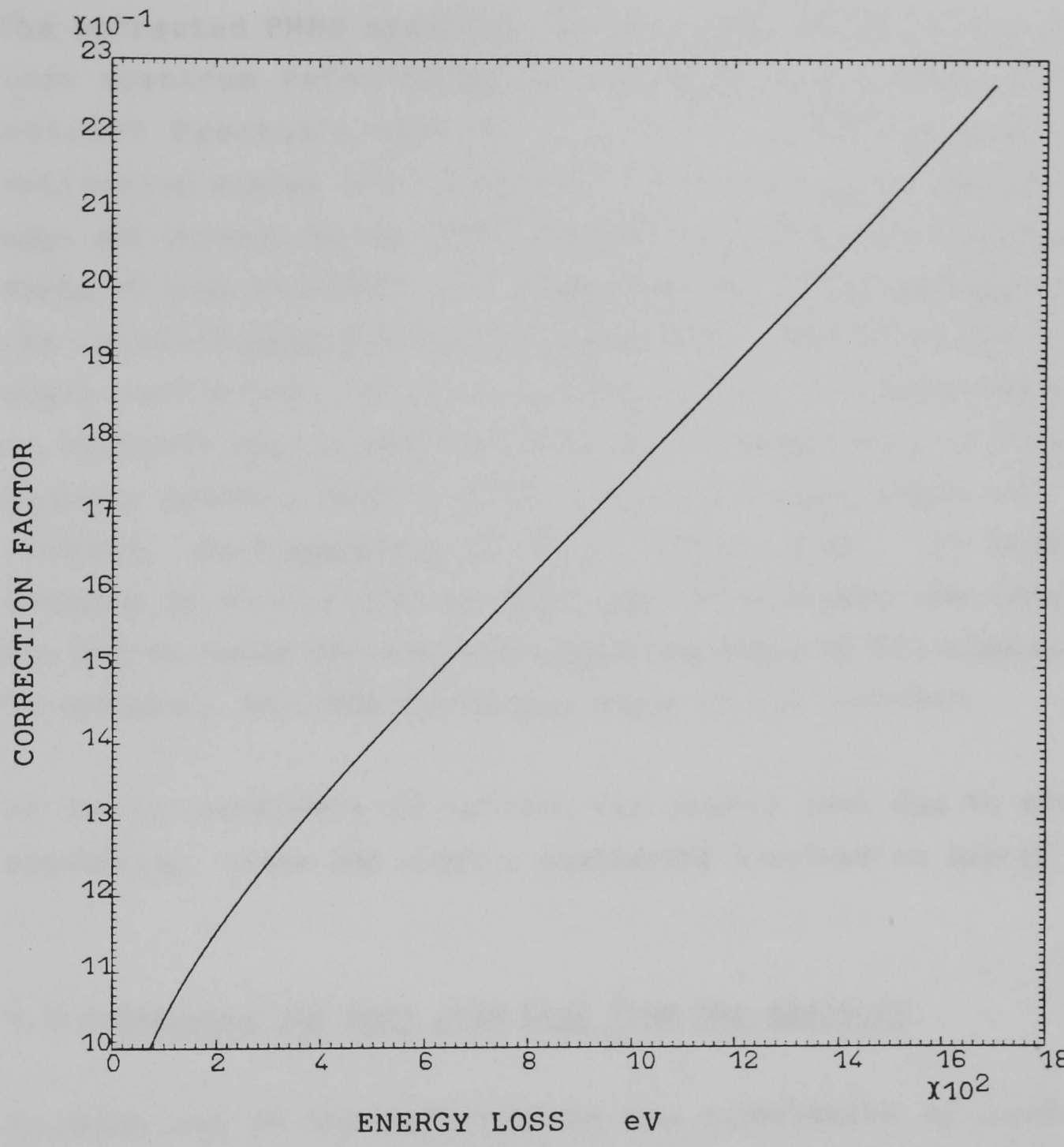

Fig. 4.8 Correction to energy loss spectra, to allow for the finite collection angle of the detection system (27 mrad).

carbon.

The corrected PMMA spectrum, in the relative magnitude of the loss spectrum referred to the plasmon (22eV) peak, closely matches Egerton's spectra for carbon measured with wide collection angles (100-130mrad)[4.4,4.5], both up to the carbon-K edge and beyond, except that the PMMA spectrum also contains the oxygen-K peak at 530eV. The power law, r, of the spectrum below the carbon-K peak agrees with Egerton's value of 4.0 for large-angle scattering. It is therefore thought that equation 4.2 is an adequate approximation, although it would be preferable to acquire spectra over a wide collection semi-angle of, say, 150mrad, corresponding to θ_c at 2250eV loss. It might be possible to arrange this by adjusting the post-specimen lenses of the HB5 to match the maximum scattering angle of the electrons to be detected, into the collection angle of the detector.

It is not necessary to correct for counts lost due to elastic scattering, since the elastic scattering involves no energy loss.

4.4.4 Removing the zero loss peak from the spectrum

To make use of the spectrum in the simulation of inelastic scattering in the material, we derive from the spectrum the inelastic mean free path of the electrons, enabling us to decide, together with a random number, on the inelastic collision point for a particular electron. Having decided where an inelastic collision takes place, we then wish to know the energy loss, which can be determined from the loss spectrum distribution with the zero loss peak omitted.

Although the resolution of the energy analyser is nominally 1eV, the zero-loss peak is very large, and the counts appertaining to it are spread over several electron volts. It is assumed that

the peak is symmetrical, its maximum being at zero volts loss; the peak therefore spreads into negative as well as positive energy loss. The zero-loss peak is removed by subtracting the counts at negative loss values from the equivalent positive ones.

The zero-loss peak in the spectrum obtained from a 35nm thick film of PMMA contains 76.8% of the total counts (ie. 76.8% of the electrons pass through unimpeded). The probability P of an inelastic collision within a distance x is given by

$$P = 1 - e^{-x/a} \qquad (4.4)$$

where a = inelastic mean free path (IMFP).

From equation 4.4, the inelastic mean free path of the 100keV electrons in PMMA was calculated to be 133nm. The IMFP of 100keV electrons in silicon nitride was found to be 130nm.

4.4.5 Correction for double inelastic scattering

A finite number of electrons will be scattered twice, and the spectrum can be corrected to allow for double inelastic scattering events as described here. Since most of the primary electrons pass through unimpeded, it is assumed that the number of electrons being scattered more than twice is negligible. The method is similar to that used by Ritsko et al.[4.2]

After removing the zero-loss peak, the spectrum is normalised, and then convolved with itself to obtain an approximation for the double scattering loss function. Some fraction n of this is then subtracted from the original loss function, and the spectrum is normalised again to allow for the number of counts subtracted, resulting in the corrected loss function.

The fraction n is applied since a true double scattering loss function should be obtained from a spectrum of purely single scattering events. This could be achieved by an iterative process, but since the number of double scattering events is quite small (about 5%) the additional accuracy was not thought to be necessary. The fraction n is calculated as follows.

If the probability that an electron will be inelastically scattered within the film = σ,

then the probability that an electron will be scattered twice within the film is approximately σ^2,

and the probability for single scattering events only is $(\sigma - \sigma^2)$, or $(1-\sigma)$ of the original loss spectrum.

Hence the correction factor n for the double scattering probability function is $(1-\sigma)^2 = 0.768^2 = 0.59$ (calculated for PMMA).

The correction factor n for the silicon nitride spectrum is 0.34.

The compensated spectrum for PMMA is shown in figure 4.9, and it will be noted that the inner shell ionisation peaks (carbon K at 284eV and oxygen K at 532eV) are sharper than in the raw spectrum. The compensated spectrum was checked by convolving it with itself to obtain the double scattering probability function, and adding this to the compensated spectrum. The resulting distribution closely resembled the spectrum before correction.

The fully processed spectrum for silicon nitride (merged at 590eV) is shown in figure 4.10.

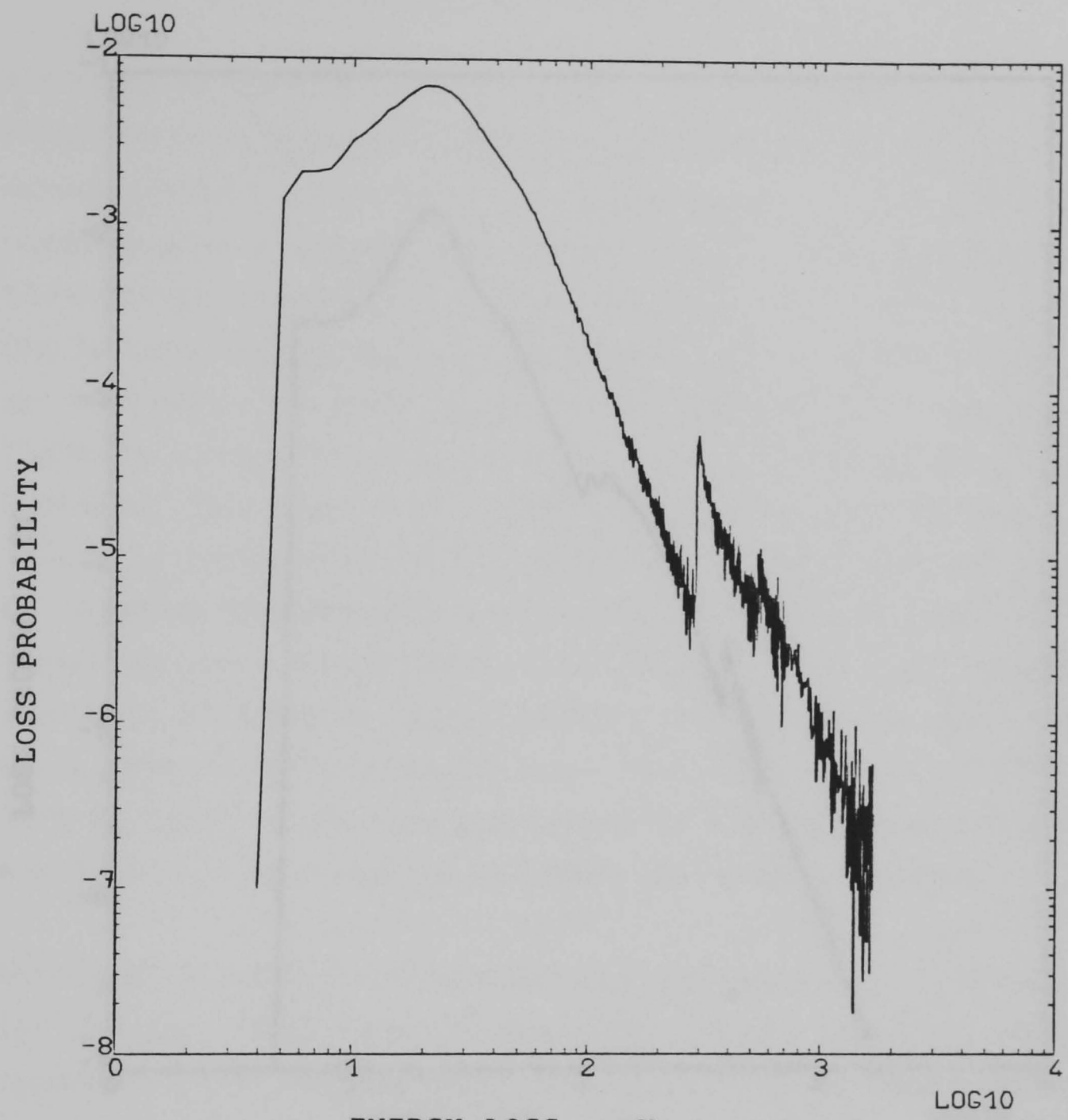

Fig. 4.9 Normalised PMMA energy loss spectrum with the zero loss peak subtracted, corrected for the finite detector collection angle and compensated for double inelastic scattering.

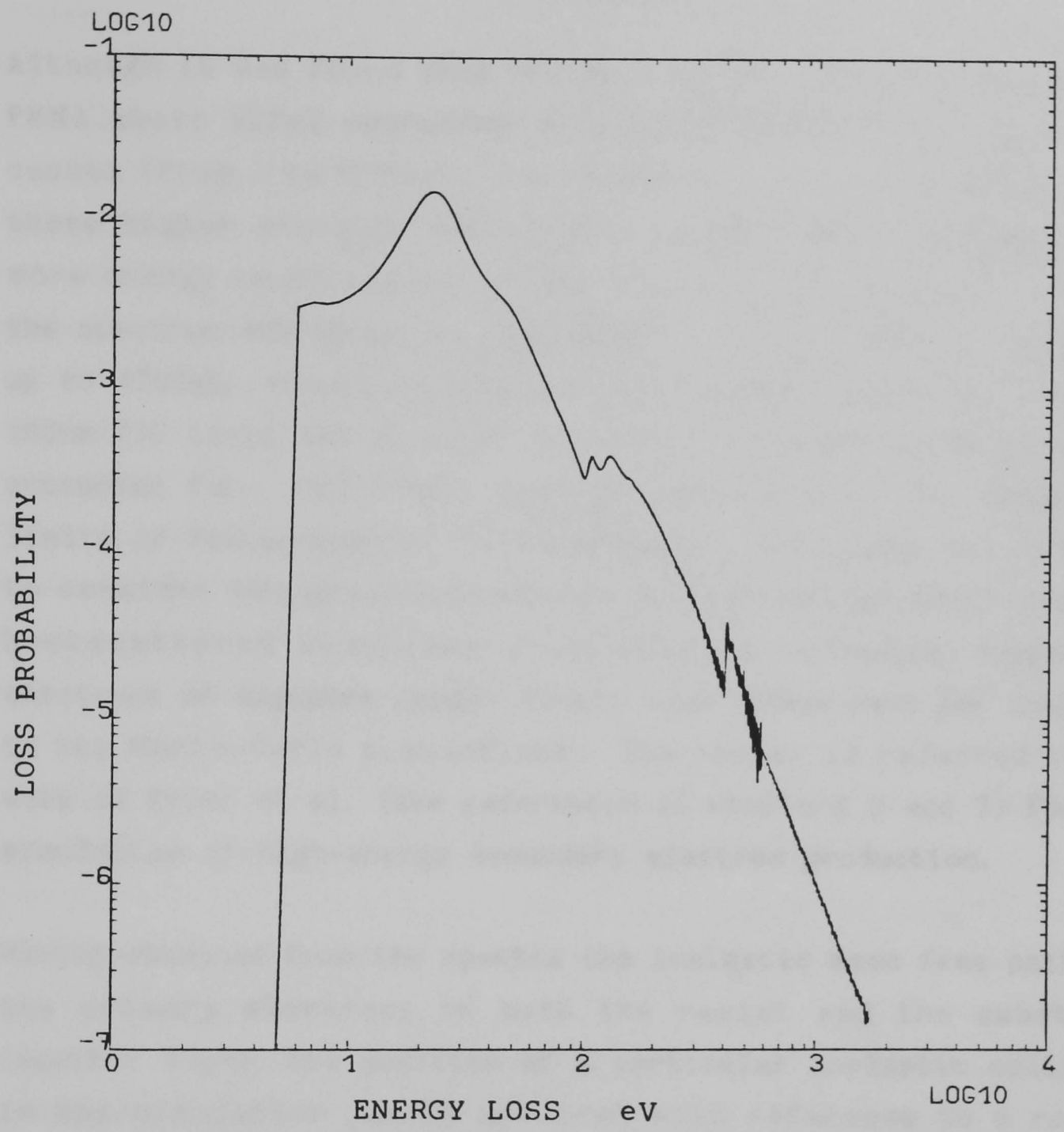

Fig. 4.10 Normalised silicon nitride energy loss spectrum, corrected for the finite detector collection angle and compensated for double inelastic scattering.

4.5 Application of the processed spectra in the Monte-Carlo simulations

Although it was found that the part of the 1700eV spectrum for PMMA above 900eV contained only about 0.7% of the total loss counts (from 1 to 1700eV), the secondary electrons produced at these higher energies have longer ranges and, of course, have more energy to dissipate in the resist; therefore this part of the spectrum may be quite significant. By acquiring the spectrum up to 1700eV, secondary electrons of exposure ranges up to about 100nm (10 times the minimum linewidths achieved in PMMA) can be accounted for. Since this work is applicable to the resolution limits of lithography on thin substrates, and it was not intended to consider the proximity effect of high energy secondary and backscattered electrons from solid substrates, secondary electrons of exposure ranges longer than 100nm were not included in the Monte-Carlo simulations. The reader is referred to the work of Kyser et al. (see references in chapters 3 and 7) for the simulation of high-energy secondary electron production.

Having obtained from the spectra the inelastic mean free paths of the primary electrons in both the resist and the substrate (section 4.4.4), the position of a particular inelastic collision in the simulation can be obtained with reference to a random number. The appropriate loss spectrum then gives the probability distribution for the energy loss suffered by the electron, which can be determined with reference to another random number.

The energy of a secondary electron created in an inelastic collision is then taken to be the energy loss suffered by the primary, less the binding energy of the secondary. Most of the electrons emitted are valence electrons, for which the binding energy is assumed to be 10eV, following Adesida et al.[4.6] Losses of less than the binding energy result in excitation of electrons into unfilled states above the Fermi level, rather than

emission of secondaries; any error in the binding energy is small compared with the energy of secondaries of significant exposure range.

The binding energy for inner shell electrons is taken to be that corresponding to the leading edge of the appropriate peak in the spectrum, even though this may not be perfectly accurate, to avoid difficulties in running the simulation program (the first few eV above the inner shell edges actually represent excitation of electrons into higher bound states, but the inaccuracy is negligible). The assumed inner shell binding energies for PMMA are 289eV for carbon-K and 532eV for oxygen-K. Those assumed for silicon nitride are 408eV for nitrogen-K and 108eV for silicon-L; the silicon K-shell binding energy of about 1840eV is outside the range of the spectrum. The silicon-L loss exhibits the characteristic double peak of L-shell excitations[4.4].

It will be noted from the spectra that the energy loss probability appears to fall with almost the same exponent both before and after the inner shell loss peaks. Egerton[4.5] argues that the valence electron contribution can be extrapolated well into the inner-shell region of the spectrum. The probability of a loss of energy above one of the peaks representing an excitation of the appropriate inner shell electron, rather than one of lower binding energy (eg. a valence electron), can then be approximated simply as the ratio of a few counts averaged just above, to a few counts averaged just below, the leading edge of the peak.

The carbon-K ionisation probability (in the PMMA spectrum) is seen to decrease just above its leading edge (the shapes of the various peaks depend on the density of states in the conduction band[4.5]). To allow for this the relative probability for carbon K-shell ionisation, calculated as described, is multiplied by a factor (0.625) for energy losses above 320eV. Similar

corrections are made, where necessary, to the other ionisation peaks.

The binding energy, which is lost when an inner shell electron is emitted, is liberated as x-rays and auger electrons when the inner shell is filled again by another electron. The energy carried by x-rays is dissipated over very long ranges, and the auger electrons will account for very little energy dissipation[4.7]. Therefore both are neglected in the Monte-Carlo simulation, except that the energy lost by a primary in creating x-rays is automatically noted as not dissipating significantly in the resist.

The energy loss probability distribution for secondary electrons is taken to be the same as the distribution for primary electrons, up to the energy of the particular secondary electron. The justification for this assumption is due to Ritsko et al.[4.2], who obtained loss spectra in PMMA for 20, 40, and 100eV electrons, as well as for high energy electrons. The differences noted were in the fine details of the spectra between 4 and 7eV, caused by differences in the forbidden transitions. Although such differences may be of significance in deciding which energy losses actually result in chain scission in the resist, they do not concern us here in determining the yield of higher-energy secondary electrons.

The large peak at 22eV in the PMMA spectrum is the plasmon excitation, a collective oscillation of the valence electrons. In this region of the spectra (up to about 50eV[4.5]) it is not possible to distinguish the single particle ionisation losses (which create secondaries and may result in chain scission) from the plasmon losses[4.3]. However, the exposure range at this energy is negligible, and so the Monte-Carlo simulation assumes that energy dissipated in this region is local in effect. Whether or not a particular energy loss can can result in chain

scission will be taken into account in the overall G-value that is assumed (chain scissions per 100eV energy dissipation - see chapter 7). The losses in the spectra above 50eV have been shown to be due almost entirely to single-electron collisions, rather than multiple plasmon excitations[4.5].

4.6 Conclusion

Electron energy loss spectra have been obtained for PMMA and silicon nitride, and processed for use in the simulation of secondary electron production in a Monte-Carlo simulation of the exposure of PMMA on thin silicon nitride substrates. Energy losses were recorded up to 1700eV, representing the generation of secondaries of exposure ranges up to about 100nm. Longer range secondaries may be significant in electron beam lithography on solid substrates, but the data is adequate for the simulation of very high resolution lithography on thin substrates, since the maximum exposure range is about ten times longer than the minimum linewidths that can be achieved, and the number of high energy secondaries is very small.

References

4.1 A.J. Craven, P.F. Adam, W.A.P. Nicholson, J.N. Chapman, and R.P. Ferrier; "Obtaining electron energy loss spectra and x-ray emission spectra free of instrumental artifacts"
Submitted 1983 to J. de Physique, Toulouse.

4.2 J.J. Ritsko, L.J. Brillson, R.W. Bigelow, T.J. Fabish; "Electron energy loss spectroscopy and the optical properties of polymethylmethacrylate from 1 to 300eV"
J. Chem. Phys. 69(9), 3931-3939, 1978.

4.3 N. Swanson and C.J. Powell; "Excitation of π electrons in polystyrene and similar polymers by 20keV electrons"
J. Chem. Phys. 39(3), 630-634, 1963.

4.4 R.F. Egerton; "Electron energy loss spectroscopy"
Proceedings of 25th Scottish Universities Summer School in Physics, 1983.

4.5 R.F. Egerton; "Inelastic scattering of 80keV electrons in amorphous carbon"
Philosophical Magazine 31, 199-215, 1975.

4.6 I. Adesida, R. Shimizu, and T.E. Everhart; "Monte Carlo simulation of electron penetration through thin films of PMMA"
Appl. Phys. Lett. 33(10), 849-850, 1978.

4.7 J.B. Pendry; "Low energy electron diffraction"
Academic Press 1974; pp. 28-29.

CHAPTER 5

Characterisation of electron beam resists

5.1 Introduction

It is possible to define resist contrast both in terms of the change in developed depth with exposure after a given development process[5.1], and in terms of the change in dissolution rate with exposure in a given developer[5.2]. The latter is more useful in modelling the development process if a dynamic rather than a simple static (threshold) development model is used; however, by this definition the contrast is difficult to measure accurately and completely, since the dissolution rate may vary as development proceeds.

It has been found that a dynamic development model tends to break down when the resist exposure becomes discontinuous due to the statistical variations in dose through the resist (see chapter 7). It has therefore been necessary to resort to a static model, in which the resist is assumed to be removed completely if it has been exposed to a given energy dissipation per unit volume (ie. a threshold model). Such a model does not take direct account of the resist contrast, and so a method of resist characterisation was required simply to enable the development process to be optimised, and the developed depth/exposure dose definition is adequate for this purpose.

Various electron beam resists were characterised by the method described here, but most of the results presented are for PMMA, along with some additional results for Philips XXL cross-linking positive resist. Although several negative e-beam resists were also characterised, the results are not presented here.

The exposures from which the depth/dose characteristics were measured were made in the form of a 40-step exposure "wedge" by the Cambridge Instruments EBMF-1 microfabricator at British Telecom Research Laboratories. The resist thickness after development was measured by a Talystep surface profile plotter.

5.2 Experimental method

5.2.1 Exposure wedge

The exposure wedge consisted of 40 rectangles, each 50 microns by 500 microns, with 50 micron spaces between each (see figure 5.1). The total length of the wedge was 4mm. This exposure pattern which included spaces between the exposed areas provided an individual reference level for each depth measurement in the Talystep plots. A Talystep is able to cover up to 2mm (half of the wedge) in a single run, and so very detailed resist characteristics could be obtained quickly. The wedge included a scale along the edge to enable individual rectangles to be identified.

The exposure dose of the entire wedge was adjusted by changing the beam current, along with three clock rates which were set in the job files. The wedge used for characterising positive resist provided a linear range of exposure doses. Each rectangle was exposed a different number of times at CLOCK 1, and then once at CLOCK 2. This enabled the minimum and maximum doses in the wedge to be set as required. The scale was exposed at CLOCK 3.

The PMMA specimens were exposed with a linear range of doses from 20 to 215 μCcm^{-2}. The XXL specimens were also exposed with a linear range of doses, from 24.2 to 71.0 μCcm^{-2}. The exposure details are given in table 5.1.

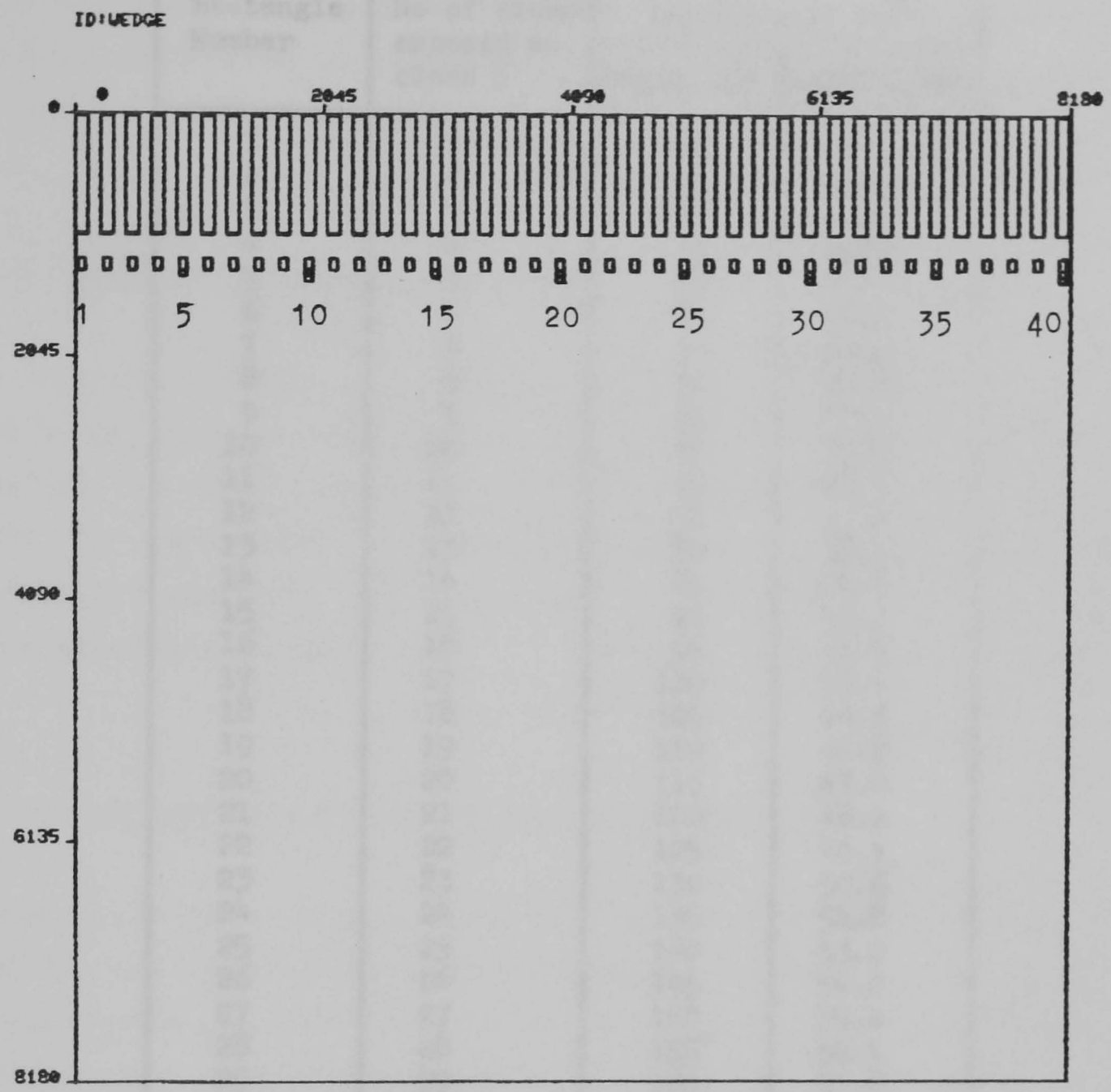

Fig. 5.1 Design of exposure wedge, including a scale for identification of the individual rectangles. The total field size is 4.096 mm square. The numbering along the edges is in pixels.

Rectangle Number	WEDGE. No of times exposed at clock 1	Exposure $\mu C\ cm^{-2}$	
		WEDGE.JOB	WEDGEX.JOB
1	1	20	24.2
2	2	25	25.4
3	3	30	26.6
4	4	35	27.8
5	5	40	29.0
6	6	45	30.2
7	7	50	31.4
8	8	55	32.6
9	9	60	33.8
10	10	65	35.0
11	11	70	36.2
12	12	75	37.4
13	13	80	38.6
14	14	85	39.8
15	15	90	41.0
16	16	95	42.2
17	17	100	43.4
18	18	105	44.6
19	19	110	45.8
20	20	115	47.0
21	21	120	48.2
22	22	125	49.4
23	23	130	50.6
24	24	135	51.8
25	25	140	53.0
26	26	145	54.2
27	27	150	55.4
28	28	155	56.4
29	29	160	57.8
30	30	165	59.0
31	31	170	60.2
32	32	175	61.4
33	33	180	62.6
34	34	185	63.8
35	35	190	65.0
36	36	195	66.2
37	37	200	67.4
38	38	205	68.6
39	39	210	69.8
40	40	215	71.0

Table 5.1 Details of the exposures of the PMMA specimens (job file WEDGE.JOB) and the XXL specimens (job file WEDGEX.JOB). Each rectangle was exposed for the number of times shown at CLOCK 1, and then once at CLOCK 2.

Since the pixel size was 0.5 microns the exposure was made with the beam defocused to about 5 microns diameter, to ensure that the charge density was constant in the exposure area.

5.2.2 Specimen preparation and development

The resist specimens were approximately 0.3 microns thick initially, spun on 10mm square silicon substrates. The solvent used for the PMMA was xylene, and the specimens were baked at 175°C for about one hour before exposure. The development temperature was 21°C. The specimens were rinsed in IPA but not baked after development.

5.2.3 Talystep measurement of the developed depth

It was found that a stylus force of 10mg caused visible damage to PMMA in the rectangles that were almost cleared. A reduced stylus force of 1mg was therefore used for all subsequent measurements. This did not appear to damage PMMA, but damage was apparent in one or two rectangles of the XXL wedges, just below the clearing dose when the resist appeared to be very soft.

5.2.4 Contrast measurement

The contrast (γ) was calculated as described by Bowden[5.1] from the slope of the depth/dose curves (see figure 5.2(a)). In some cases two definitions of γ are used: γ_m is taken from the maximum slope of the curve, and γ_{mc} is the maximum slope of a line which can be drawn through the clearing dose and another point on the curve (figure 5.2(b)).

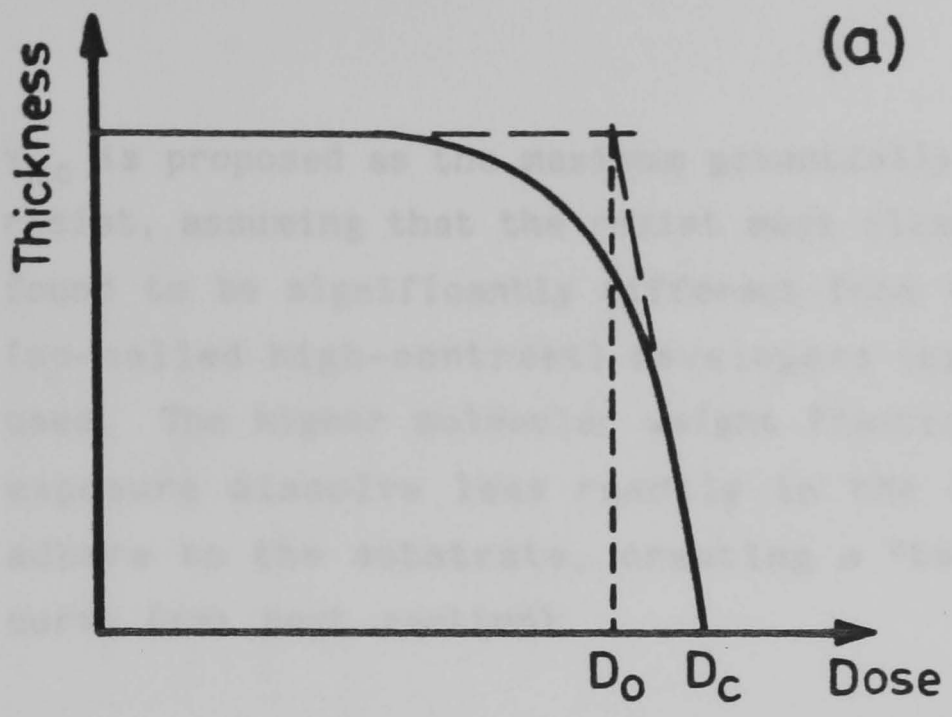

$$\gamma = \left[\log_{10}\left(\frac{D_o}{D_c}\right)\right]^{-1}$$

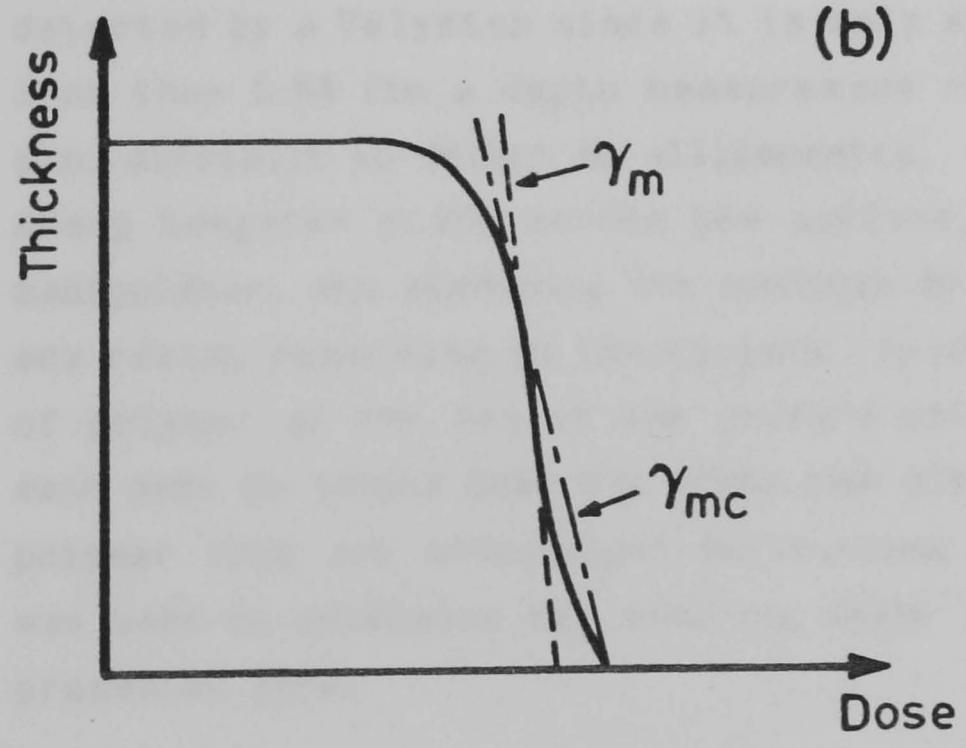

γ_m = maximum slope contrast

γ_{mc} = maximum slope through clearing dose

Fig. 5.2 Definitions of positive resist contrast.

γ_{mc} is proposed as the maximum potentially usable contrast of the resist, assuming that the resist must clear to be usable. γ_{mc} is found to be significantly different from γ_m in PMMA when dilute (so-called high-contrast) developers (eg. 4 IPA : 1 MIBK) are used. The higher molecular weight fractions in the resist after exposure dissolve less readily in the dilute developer, and adhere to the substrate, creating a "tail" in the depth/dose curve (see next section).

5.2.5 Scratch-testing for the clearing point

When a "tail" is evident in the developed depth-exposure dose relationship, the exact clearing dose of the resist can be difficult to determine, since a significant increase in exposure may be required to clear the last 1nm or so of resist which is otherwise deposited on the substrate. This thickness cannot be detected by a Talystep since it is only an increase in depth of less than 0.5% (in a depth measurement of about 300nm); it is also difficult to detect by ellipsometry. However, by stroking a sharp tungsten probe across the surface by means of a micro-manipulator, and examining the specimen by an optical microscope, any resist remaining on the surface could be detected as a heap of polymer at the end of the probe's path. Care was taken in each case to ensure that the probe was clean and did not pick up polymer from the undeveloped surrounding areas. This technique was used to determine the clearing doses in most of the results presented here.

5.3 Results for PMMA

Figure 5.3 shows the developed depth-exposure dose relationship for Elvacite 2041 PMMA (molecular weight 360,000), exposed at 20kV and developed in 2 IPA : 1 MiBK at 21^{o}C. Figure 5.4 shows

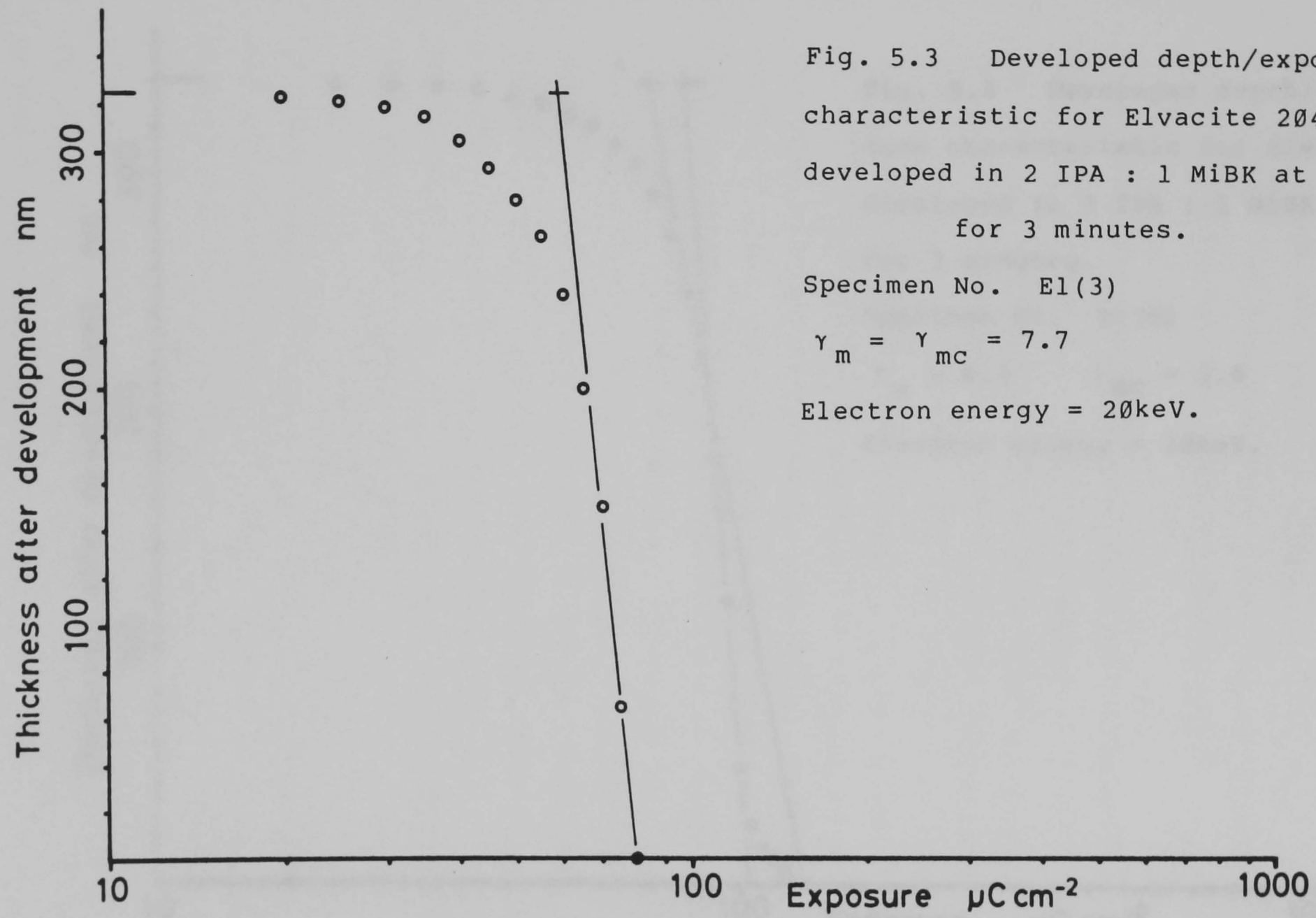

Fig. 5.3 Developed depth/exposure dose characteristic for Elvacite 2041 developed in 2 IPA : 1 MiBK at 21°C for 3 minutes.

Specimen No. E1(3)

$\gamma_m = \gamma_{mc} = 7.7$

Electron energy = 20keV.

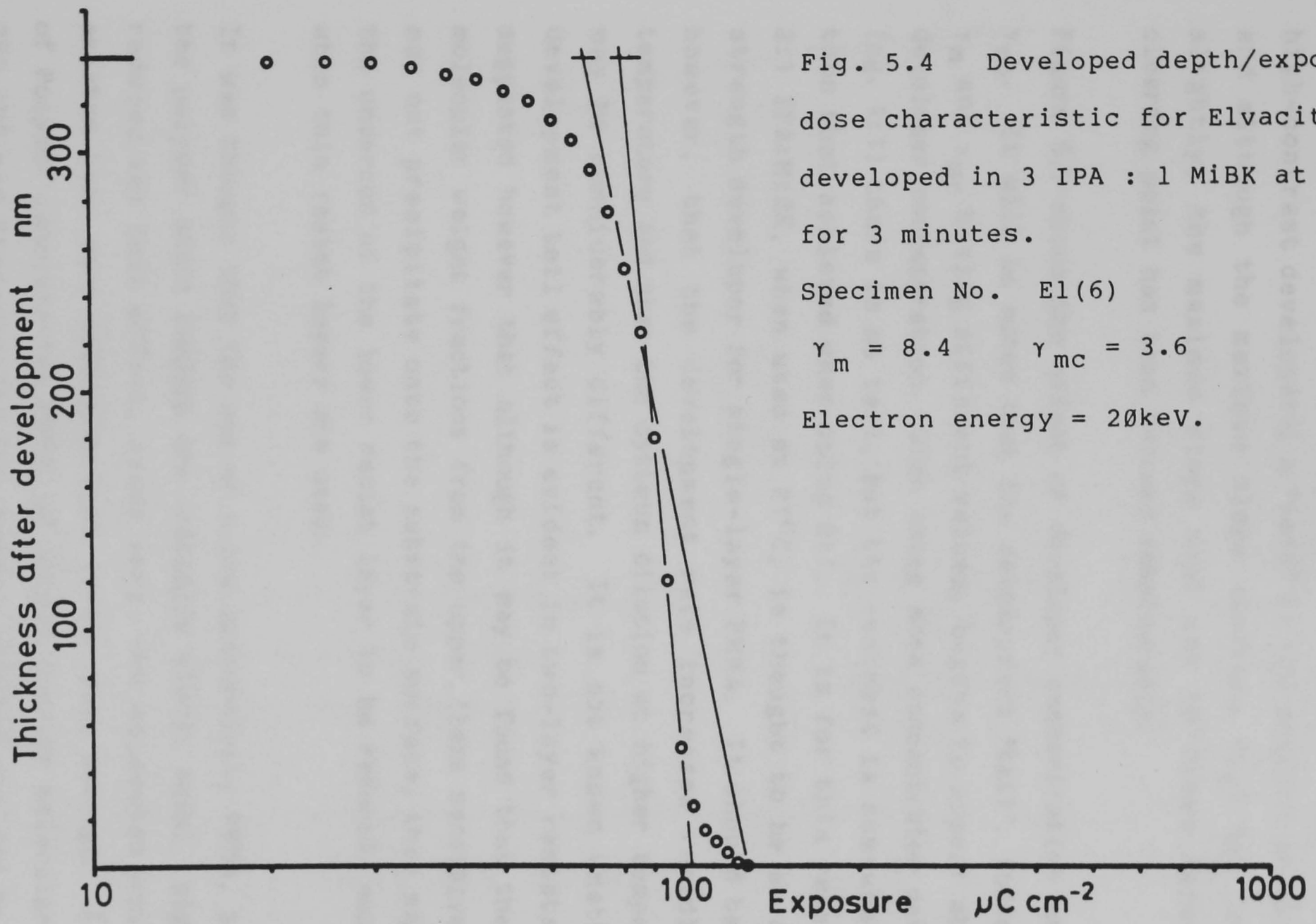

Fig. 5.4 Developed depth/exposure dose characteristic for Elvacite 2041 developed in 3 IPA : 1 MiBK at 21°C for 3 minutes.

Specimen No. E1(6)

$\gamma_m = 8.4$ $\gamma_{mc} = 3.6$

Electron energy = 20keV.

the relationship for another sample of the same batch of resist, also exposed at 20kV, but developed in 3 IPA : 1 MiBK (a standard high-contrast developer); a "tail" is now evident in the curve, and although the maximum slope contrast (γ_m) has increased slightly, the maximum slope that can be drawn through the clearing point has been reduced considerably.

Figure 5.5 shows the effect of developer concentration on γ_m and γ_{mc}. It will be noted that the development "tail", indicated by γ_m and γ_{mc} having different values, begins to appear above 2:1 developer concentration. When using more concentrated developers (eg. 1:1) there is no tail, but the contrast is somewhat lower than that achieved when using 2:1. It is for this reason that 2:1 IPA:MiBK, when used at 21^{o}C, is thought to be an optimum strength developer for single-layer PMMA. It should be noted, however, that the development rate increases rapidly with temperature and that the optimum dilution at higher temperatures may be considerably different. It is not known whether the development tail effect is evident in two-layer resists; it is suggested however that although it may be found that the higher molecular weight fractions from the upper (less sensitive) layer may not precipitate onto the substrate surface, they may cause the undercut of the lower resist layer to be reduced, especially when thin resist layers are used.

It was thought that the use of a low dispersivity PMMA, in which the polymer chain lengths are initially almost equal, might have reduced the tail effect, since very few molecules would have existed that were initially much larger than average. A sample of Polymer Laboratories PMMA, of weight average molecular weight 280,000 and dispersivity (ie. number average divided by weight average molecular weight) 1.15, was developed in the same solution at the same time as a sample of Elvacite 2041 (molecular weight 360,000, dispersivity 1.93), for accurate comparison (samples EX1(14) and PL(1) in table 5.2). The developer was 3:1

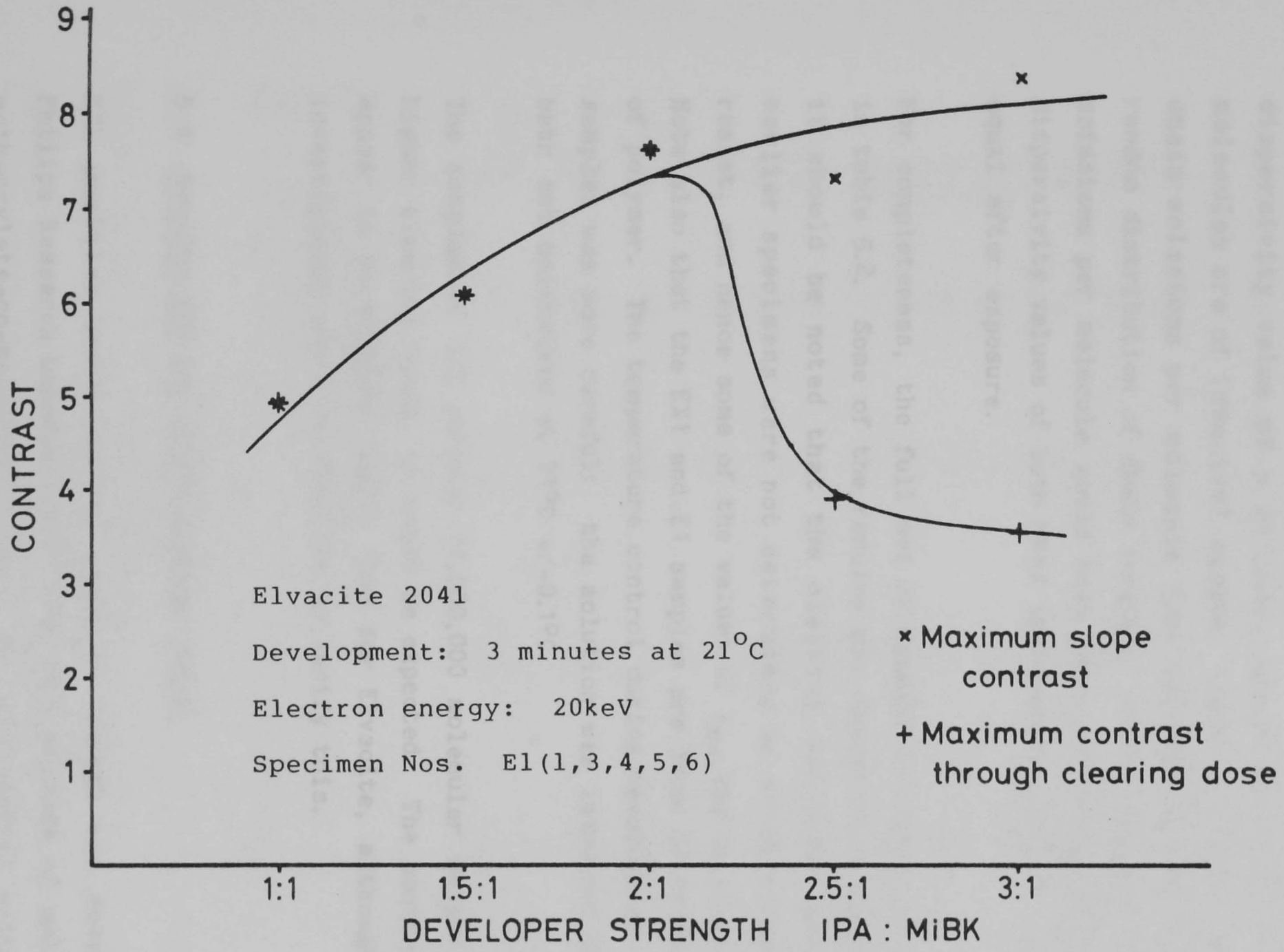

Fig. 5.5 Dependence of resist contrast on developer concentration.

IPA:MiBK at 21°C. It was found that the differences in the values of γ_m and γ_{mc} respectively were negligible. Hence there would appear to be no advantage in terms of resist contrast in using a low-dispersivity polymer. It is known that the dispersivity value of a polymer, which is unity if all the molecules are of identical weight, tends to 2 after about five chain scissions per molecule (see chapter 7), representing a random distribution of chain lengths. Since more than five chain scissions per molecule would have occurred during exposure, the dispersivity values of both PMMA specimens would have been almost equal after exposure.

For completeness, the full set of results for PMMA are presented in table 5.2. Some of the results may appear anomalous; however, it should be noted that the clearing doses for some of the earlier specimens were not determined by scratch-testing the resist, and hence some of the values of γ_{mc} may be overestimated. Note also that the EX1 and E1 samples are from different batches of polymer. The temperature control during development of the E1 samples was more careful: the solution was immersed in a water bath and maintained at 21°C +/-0.1°C.

The samples of ICI polymer (1,000,000 molecular weight) exhibit higher clearing doses, as would be expected. The contrast values appear to be slightly higher than for Elvacite, although further investigation would be required to verify this.

5.4 Results for XXL cross-linking resist

XXL positive cross-linking electron resist was developed at Philips Research Laboratories[5.4] and is a mixture of poly-(methyl methacrylate-co-methacrylic acid) and poly-(methyl methacrylate-co-methacryloyl chloride) containing 10 mol % of potential cross-linking groups. The resist film becomes cross-linked on heating,

Table 5.2 Contrast values and clearing doses for PMMA and XXL specimens

Specimen No	Beam potential (kV)	Developer (IPA:MiBK)	Development time (seconds)	Clearing dose (μCcm^{-2})	γ_m	γ_{mc}
EX1 (1)	20	3:1	45	175	5.8	3.5
(2)	20	3:1	180	165	4.5	2.4
(3)	20	4:1	45	205	11.1	3.2
(4)	30	4:1	45	-	7.0	-
(5)	20	4:1	90	145	11.3	5.6
(6)	20	1:1	45	85	5.9	5.9
(10)	20	4:1	180	145	8.7	4.2
(11)	20	4:1	90	155	9.1	4.5
(12)	20	4:1	45	200	8.4	3.3
(14)	20	3:1	180	185	6.7	2.3
(15)	20	2:1	180	85	7.4	4.2
(16)	20	2.5:1	180	120	7.4	3.1
E1 (1)	20	1:1	180	60	4.9	4.9
(3)	20	2:1	180	80	7.7	7.7
(4)	20	1.5:1	180	70	6.1	6.1
(5)	20	2.5:1	180	110	7.4	3.9
(6)	20	3:1	180	130	8.4	3.6
PL (2)	20	3:1	180	170	6.3	2.1
ICI (1)	20	4:1	45	165	10.3	4.1
(2)	20	1:1	45	80	7.2	7.2
XXL (4)	30	MiBK	120	62.6	19.0	
(6)	20	MiBK	120	36.0	16.3	

EX1 = Elvacite 2041 from BTRL
E1 = Elvacite 2041 from G.U.
PL = Polymer Labs. low dispersivity 280,000 m.w.
ICI = ICI 1,000,000 m.w.
XXL = Philips XXL cross-linking methacrylate resist

EX1(14) and PL(2) developed in same solution at same time.

EX1(4) did not clear at any dose in range given.

Clearing dose was determined by scratch-test only for specimen numbers EX1(6,14,15,16), E1(1,3,4,5,6), and PL1(2). γ_{mc} may be overestimated for other specimens.

and is therefore insoluble until exposure by an electron beam breaks the cross-links. The insolubility of the unexposed resist results in potentially very high contrast, and its properties have been exploited in double layer resist structures[5.5].

After spinning, the resist was baked at 175°C for 15 minutes in an oven with dry nitrogen purge. This procedure is recommended to cross-link the resist fully, although lower baking temperatures can be used to achieve only partial cross linking and hence higher exposure sensitivity[5.6]. Development was in MiBK for 2 minutes at 21°C.

The developed depth/exposure dose curve for exposure at 20kV is shown in figure 5.6. It will be noted that no "tail" effect is evident in the curve and that the contrast value is greater than for PMMA. However, as noted in section 5.2.3, just below the clearing dose the resist appeared to be very soft and was easily damaged by the Talystep probe; it was also found that the probe could become clogged by material from these areas. It has been found[5.7] that very high resolution lithography in this resist is difficult because strands of the material bridge across narrow lines (of the order of 0.1 microns), probably due to the softness of the walls of the resist which receive an exposure just below the clearing dose.

5.5 Significance of the results in thin substrate lithography

The question arises whether the results of resist exposure experiments on solid substrates can be applied to lithography on thin substrates, since backscattering may cause a significant variation in exposure with depth. In order to estimate the effect of backscattering under similar conditions to those of the experiments described here, the secondary electron Monte-Carlo program (chapter 7) was run to simulate exposure of 300nm of PMMA

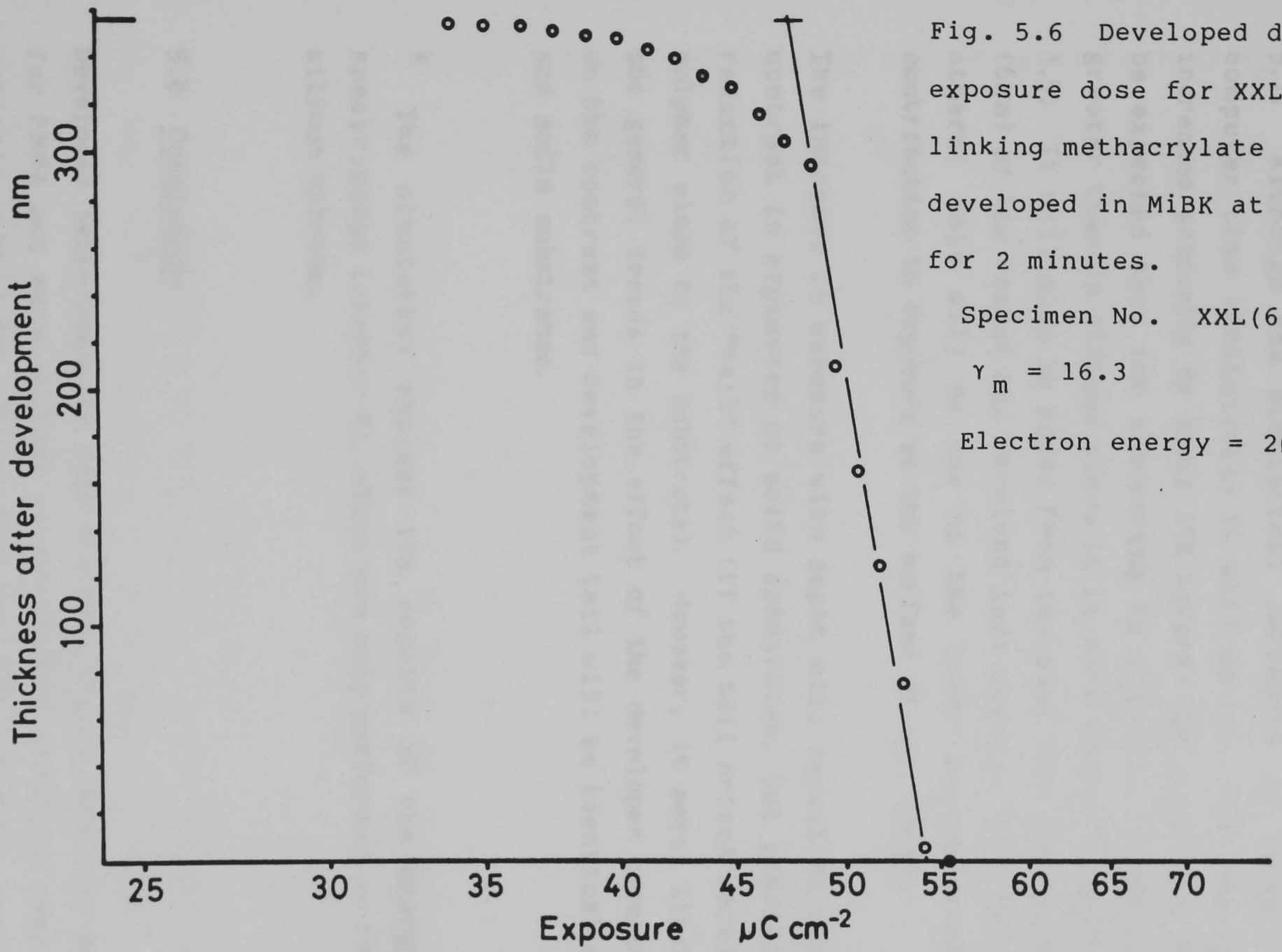

Fig. 5.6 Developed depth/ exposure dose for XXL cross-linking methacrylate resist, developed in MiBK at 21°C for 2 minutes.

Specimen No. XXL(6)

γ_m = 16.3

Electron energy = 20keV.

by 20kV electrons on a solid silicon nitride substrate*.

A plot of the relative exposure with depth is shown in figure 5.7. Although the statistical variation is large (due to computer time limitations) it will be seen that the exposure increases gradually by about 15% towards the substrate. It might be expected that the scattering in silicon nitride would be greater than in silicon since it is more dense, by a factor of 1.5. It will also be noted from the plot that the top element (6nm) of the resist has received less exposure than all of the others; this will be due to the lower secondary electron contribution to exposure at the surface of the resist.

The increase in exposure with depth will result in increased contrast in exposures on solid substrates, but possibly in a reduction of the "tail" effect (if the tail arises mainly from polymer close to the substrate). However, it seems likely that the general trends in the effect of the developer concentration on the contrast and development tail will be identical on thin and solid substrates.

* The simulation employs the results of the energy loss spectroscopy (chapter 4), which was only performed on PMMA and silicon nitride.

5.6 Conclusion

Developed depth/exposure dose characteristics have been measured for PMMA and methacrylate cross-linking positive resists. A reliable method for determining the clearing dose, even when a long "tail" in the depth/dose curve is evident, has been described. The PMMA characteristics show that more dilute developers, which are thought to yield higher contrast, can

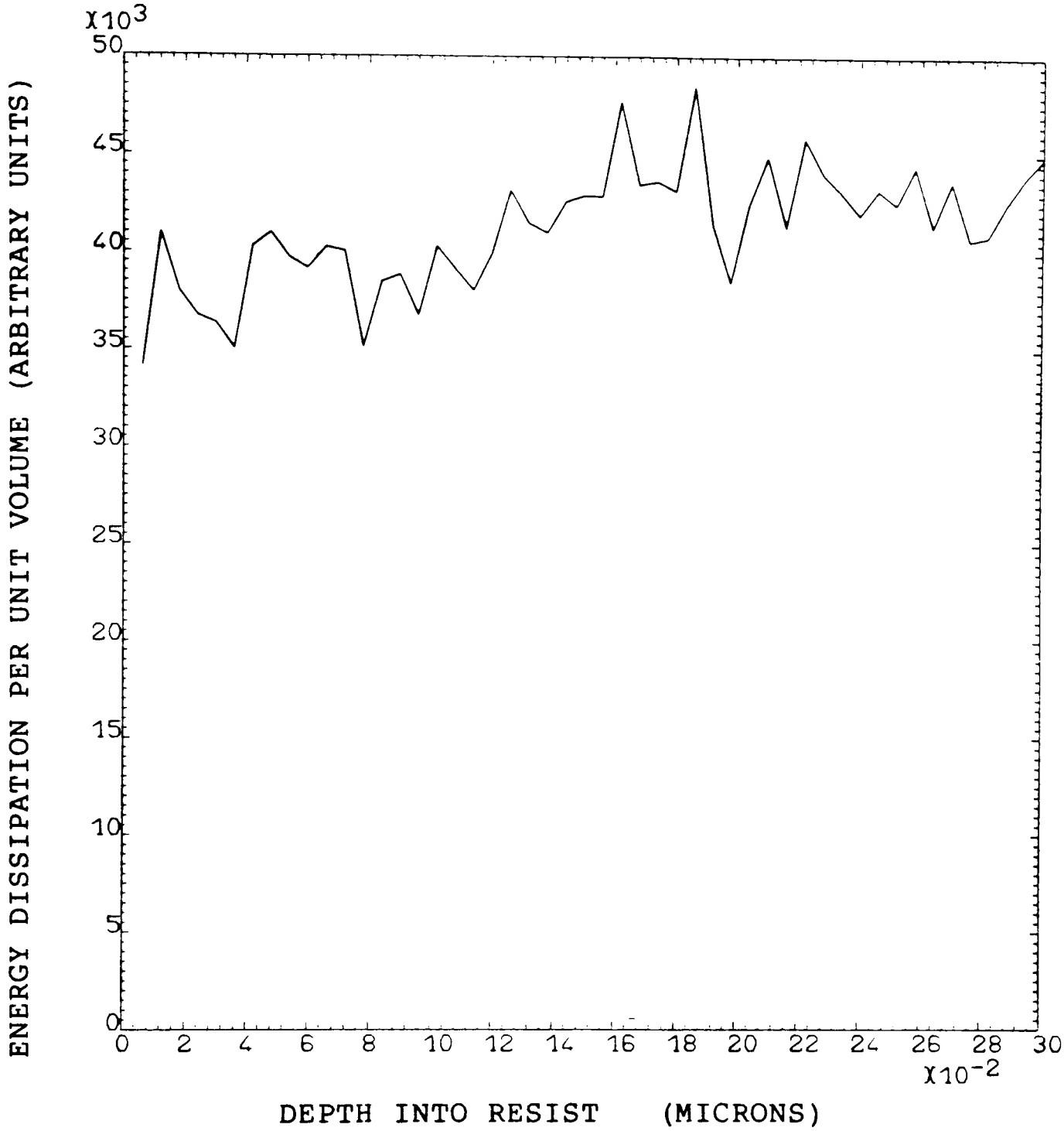

Fig. 5.7 Simulation of large-area exposure by 20keV electrons of 300nm thick PMMA on a solid silicon nitride substrate. The simulation program is described in chapter 7 and includes the effect of energy spreading by secondary electrons. The exposure increases gradually through the resist, and is about 15% greater close to the substrate as it is near the surface.

actually result in a useful contrast which is reduced due to the appearance of a development "tail". At 21°C the optimum developer concentration was found to be 2 IPA : 1 MiBK.

References

5.1 M.J. Bowden; "Electron irradiation of polymers and its application to resists for electron beam lithography"
CRC Critical Reviews in Solid State Sciences, pp223-264, February 1979.

5.2 J.S. Greeneich; "Developer characteristics of Poly-(Methyl Methacrylate) electron resist"
J. Electrochem. Soc.: Solid-State Science and Technology, 122(7), 970-976, 1975.

5.4 E.D. Roberts, Appl. Polymer Symp., No. 23, p.87, 1974.

5.5 C. Dix and P. Hendy; "A double PMMA resist structure for sub-micron lithography using a single developer"

5.6 E.D. Roberts; Data sheet on Methacrylate positive-working cross-linking electron resist Type XXL20
Applied Physics Devision, Philips Reseach Laboratories, Redhill, Surrey.

5.7 The comments of Drs. C. Dix and P. Hendy, British Telecom Research Laboratories, are appreciated.

CHAPTER 6

Linewidth resolution measurements in PMMA

6.1 Introduction

Practical electron beam lithography in two-layer PMMA, both of 0.1 micron linewidths on solid substrates, and of 10nm linewidths on thin substrates, is already in use within the Department for the fabrication of experimental devices. It was thought that a 60nm-thick two-layer resist, although capable of the highest reported resolution achieved in a practical exposure-development process[6.1], would be too thick for the investigation of the fundamental limits of lithography; not only would the lines in the resist have very high aspect ratios, but also they would have complex cross-sections resulting in difficulties in the analysis of the results. The lateral spread of exposure is thought to be indicated by the increase of linewidth with exposure dose, and it was required to measure this in the simplest possible case: exposure by a very fine beam, of resist which was sufficiently thin to result in developed lines of low aspect ratio.

Two-layer resist structures can give undercut profiles on development, and continuous metal structures of useful thicknesses can be produced from them, using lift-off techniques. In the work described here, however, it was thought that developing lines of high aspect ratio even in single-layer resist might result in complex line profiles, possibly due to some flow of the resist after development. It was therefore required to use as thin a resist layer as possible (in practice about 10nm), but it was not necessary to produce continuous metal lines by lift-off.

The equipment usually used within the Department for the electron beam exposure of specimens, a modified Philips SEM 500[6.2], has a gaussian beam of 8nm diameter (verified as described in chapter 2), which is little smaller than the minimum linewidths already achieved. A limited allocation of time was available on the Vacuum Generators HB5 scanning transmission electron microscope in the Natural Philosophy Department, Glasgow University, which has a nominal spot diameter of less than 1nm. It was therefore decided to develop a technique of lithography in 10nm-thick PMMA, along with very thin (about 1nm) metallisation, and possibly lift-off assisted by the discontinuity (ie. granularity) of the metallisation. The technique was to be perfected as far as possible on the Philips SEM 500 before moving to the HB5.

Previous results on the increase of linewidth with exposure dose are shown in figure 6.1, and it was required to repeat these measurements using the smaller electron beam of the HB5. Such measurements are of greater importance than absolute linewidth tests in the modelling of the physical processes involved in lithography.

A JEOL transmission electron microscope was available, again in the Natural Philosophy Department, for examination of the specimens and measurement of linewidths. Examination of specimens in such an instrument entails exposure doses much greater than those used in the lithographic process, which can result in physical changes in the resist. It is thought however that metallisation will indicate the original linewidths.

6.2 Experimental method

6.2.1 Preparation of specimens

The substrates used were 70nm-thick silicon nitride membranes, prepared by preferentially etching through silicon to a layer of silicon nitride on the polished face[6.3]. The method was similar to that described in chapter 2 for the preparation of silicon edge specimens; however, in this case, silicon nitride was used

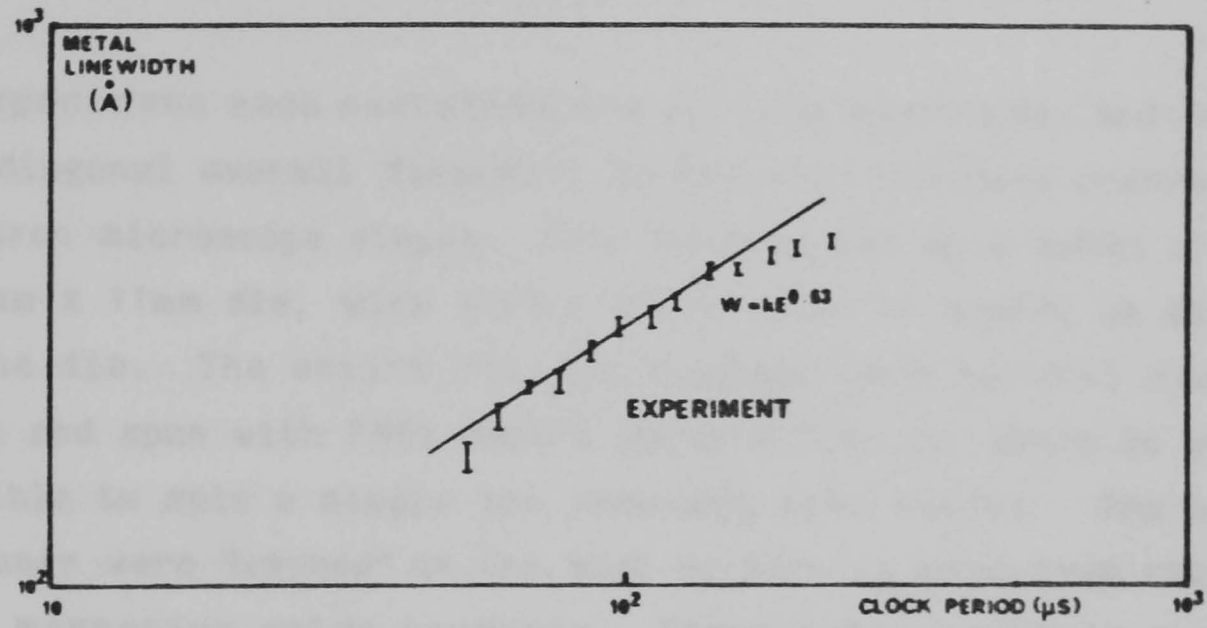

Fig. 6.1 Linewidth-exposure dose relationship measured for 5nm thick lifted-off Au/Pd metal lines, from 50nm thick single-layer PMMA on a thin carbon substrate. The exposure dose is linearly related to the clock period. Exposure was at 50keV, with the 8nm diameter beam of the Philips SEM 500. Development was for 45 seconds in 3 IPA : 1 MiBK at 23°C. Shown with the permission of S.P. Beaumont, Glasgow University.

as the masking layer and was etched in boiling phosphoric acid (95% as supplied, etch rate about 5nm per minute at 154°C), and the silicon preferential etch was boiling sodium hydroxide solution (33% w/w, etch rate about 10 microns per minute at 120°C). The silicon was etched back along the <111> planes to form nitride membrane windows about 100 microns square.

The specimens each contained one nitride membrane, and were of 3mm diagonal overall dimension to fit into standard transmission electron microscope stages. They were etched as a batch of 16 on a 11mm x 11mm die, with etched break lines to assist in dividing up the die. The entire die was mounted on a special clamping chuck and spun with PMMA before being broken up, since it was not possible to spin a single 3mm specimen with resist. The nitride membanes were "smoked" on the back by burning magnesium ribbon to form magnesium oxide crystals. These cubic crystals provided sharp edges to assist in focusing the electron beam.

The PMMA used in these experiments was Du Pont Elvacite 2041 which has a weight average molecular weight of 360,000 and a dispersivity (ie. weight average divided by number average molecular weight) of 1.93 [6.2]. A 1% solution of the polymer in low-particle xylene was spin-coated onto the substrate forming a resist film approximately 10nm thick (measured by a Talystep surface profile plotter), which was then baked at 175°C for at least 2 hours. Such a film appeared to be continuous on both macroscopic (by optical examination of a scratch mark) and microscopic (see figures 6.4 and 6.5) scales.

6.2.2 Exposure of resist

All exposures were of widely-spaced lines. The exposures performed in the Philips SEM were at 50keV primary electron energy, and were made under the control of a microprocessor-based

pattern generator, the exposure being varied by changing the clock rate. The test pattern consisted of 30 sets of lines, having a logarithmically-covered range of exposures between $1.2x10^{-10}$ and $2.0x10^{-9}$ Ccm^{-1}. The beam current (about 5pA) was measured onto a collection plate before the exposures were made, and the timings corrected accordingly. A correction factor was allowed for the current scattered from the collection plate, by comparing the current with that collected by a Faraday cup. (It was later arranged for a Faraday cup to be used for all beam current measurements.)

Exposures performed in the HB5 were less well calibrated. Kratschmer et al.[6.4] state that the field emitter in this instrument exhibits a linear decrease in current of about 20% in 20 minutes, and since they used a digital pattern generator they were able to adjust the timings continuously during lithography. The exposures described here were made under the control of the microscope's analogue scan generator by scanning a 20-line raster, and to compensate for the variation in beam current the current was measured at the beginning and end of the set of exposures; the variation was assumed to be linear with time. The dose vas varied by means of the magnification zoom control, in 20 steps over an estimated range of $2x10^{-10}$ to $1.3x10^{-9}$ Ccm^{-1}. Relative to each other the exposures (after compensating for the change in beam current with time) were expected to be correct to within 10%. By collecting the current on the objective aperture (the beam solid angle being defined by a virtual objective aperture), the beam current was measured to be about 50pA. The absolute beam current may have been considerably greater, possibly up to 100pA, due to scattering of electrons from the collecting surface; however, only the relative exposures are important in measuring the linewidth-dose relationship. Focusing of the beam was checked before each exposure, at high magnification at the centre of each exposure area; all exposures were made at 100keV primary electron energy.

6.2.3 Development and metallisation

All of the specimens were developed in 2:1 IPA:MiBK for 15 seconds at 21°C. The reasons for this choice of developer rather than the more usual 3:1 dilution are explained in chapter 5.

Some samples were metallised by evaporating Au/Pd alloy, and some by ion-beam sputtering of molybdenum. The Au/Pd alloy was evaporated from a source of about 2mm diameter placed 20cm below the specimen. The thickness of the metal was about 1nm, measured by means of a quartz crystal frequency shift thickness monitor. The thickness measurement assumes the bulk density of the metal, and therefore gives the average thickness of very thin, grainy films.

The grain size of the Au/Pd alloy was about 4nm, and it was decided to attempt to coat some samples by ion-beam sputtering of refractory metal. A small ion gun was available, an Ion Tech (Teddington) saddle-field ion source type B13, producing a 4mm beam of argon ions. The electrode potentials were arranged to produce a peak ion energy of about +200eV. The beam was directed to impinge at an angle of about 45° to the refractory metal target; the sample was placed about 10cm above the target, directly above the point at which the beam would impinge. A shutter was used to cover the sample, but not the thickness monitor crystal, so that the target could be sputtered for some time before deposition began in order to clean the surface. Deposition did not begin until some time after the sputtering rate, as measured by the thickness monitor, became constant.

Initially tungsten was used as the refractory metal target, but it was found with this material that the deposited thickness, as measured by a Talystep surface profile plotter, was about ten

times thicker than was estimated by the thickness monitor. It is thought that this was caused by the tungsten adsorbing material as it was being deposited, possibly the argon ions or atoms in the chamber. Sputtered molybdenum was not found to cause this effect, and was used in subsequent experiments. On examination of the specimens, no granularity was observed in the sputtered molybdenum (with an estimated resolution of 1nm).

The sputter deposition was very slow; a thickness of about 0.7-0.8nm could be deposited in 1-2 hours. The B13 ion gun is therefore only suitable for sputtering very thin films of refractory metal and could not be used for device fabrication.

6.2.4 Lift-off technique

On those samples where lift-off was attempted, this was performed by the "shooting" technique described by Beaumont et al.[6.5] The sample was held by tweezers and immersed in a beaker of methanol, a non-solvent for PMMA. A 50ml syringe fitted with a .25mm bore needle was filled with chlorobenzene, a strong solvent for PMMA, which was then sprayed rapidly at the sample surface through the methanol.

6.3 Results

6.3.1 Lines exposed in the Philips SEM 500

Lift-off was attempted with the 1nm Au/Pd films deposited on samples exposed in the Philips SEM. It was not expected that undercut profiles would be produced in the 10nm-thick resist, and it was intended to make use of the granularity of the thin metal layer to enable the solvent to dissolve the resist. It was found that the metal was only removed in the area close to the

developed line, as shown in figure 6.2, the exposure in this case being 1.8×10^{-9} Ccm^{-1}.

The removal of the metal from along the edges of the line was found to occur whether or not lift-off was attempted, and has been noticed previously in thicker (about 60nm) PMMA[6.6], although the effect has not been explained satisfactorily. Since it occurs here in very thin resist and with a well-defined evaporation source (subtending about 1^{o} at the specimen), and the metal on top of the resist appears to have been pulled back from the developed line after the metal deposition has been completed (there is little or no metal in the gaps), the effect is thought to be due to shrinkage of the partially exposed resist along the edges of the developed lines (caused by secondary electrons and the finite beam distribution), which absorbs some solvent during development. The shrinkage probably occurs due to electron beam exposure during examination, drawing back the metal deposited on top of the resist; the opening of the gaps has sometimes been noticed during SEM examination[6.7].

To increase the solubility of the remaining resist in order to assist lift-off, the entire membrane was re-exposed after development but before the metal was deposited. The re-exposure dose was 8.9×10^{-4} Ccm^{-2}. This enabled most of the metal to be removed from the undeveloped regions, as shown in figure 6.3, although completely clean lift-off was not accomplished. The minimum linewidths achieved were about 10nm, with exposure dose 8×10^{-10} Ccm^{-1}, which was less than that required to remove the metal around the lines without re-exposure, by the shrinking back of the partially exposed resist as above. It will be noted in figure 6.3 that the remaining metal has not been pulled back from along the edges of the line; the specimen was not examined by electron microscopy before the remaining resist was removed by lift-off.

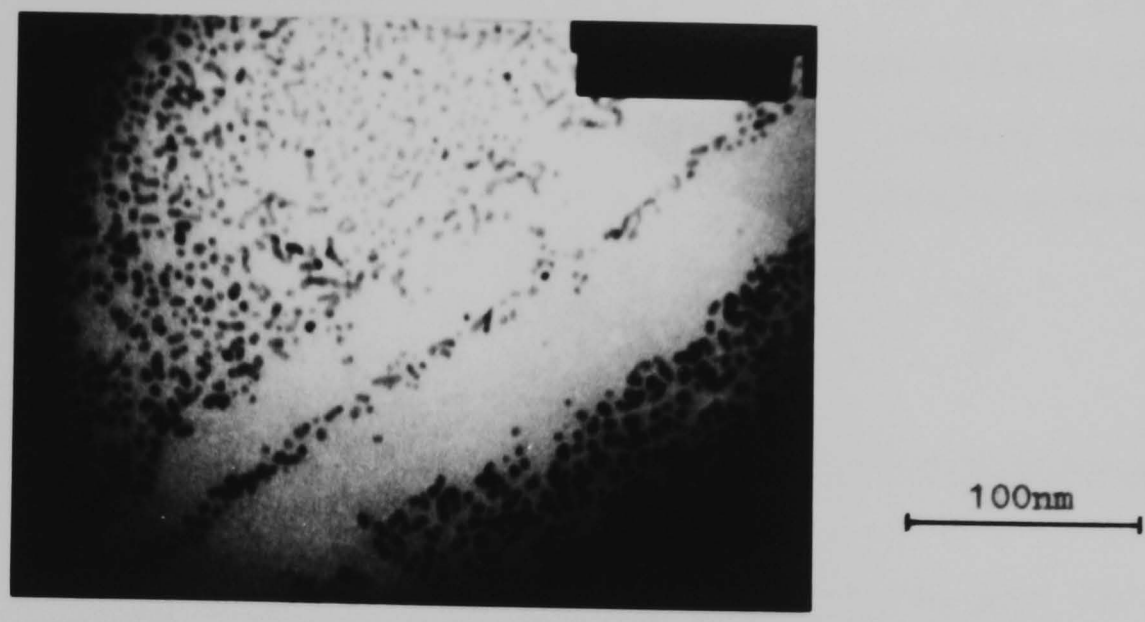

Fig. 6.2 Au/Pd line in 10nm thick resist. Lift-off attempted but not successful. Exposed by 8nm beam at 50keV.

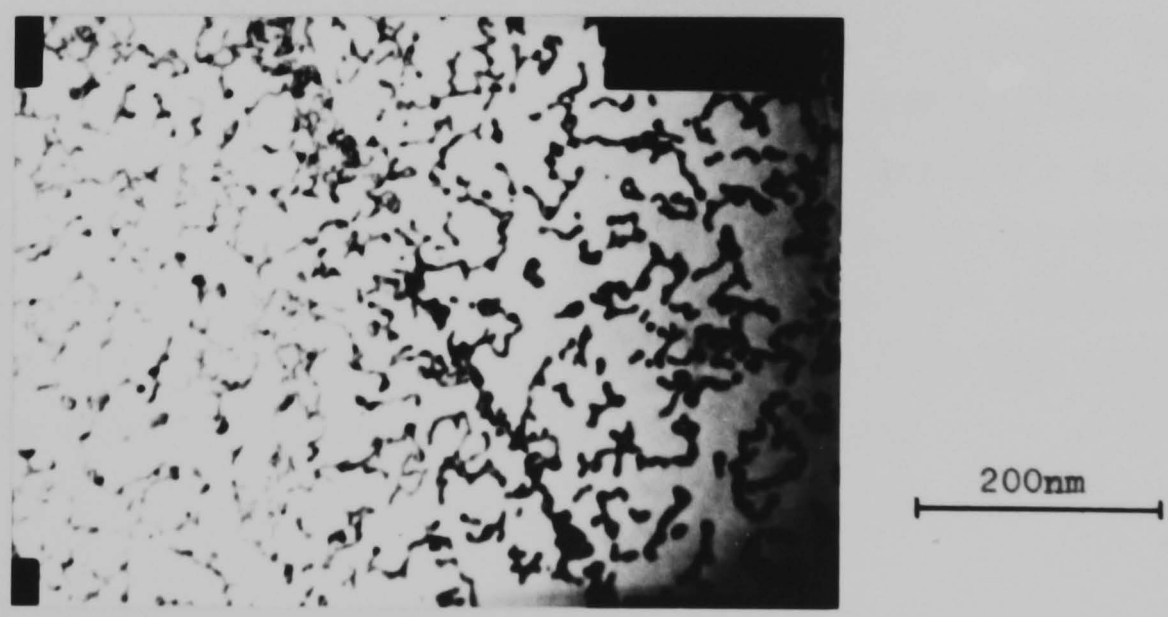

Fig. 6.3 Au/Pd line (average thickness about 1nm) from 10nm thick resist. Lift-off partially successful, assisted by re-exposure of the resist after development.

Lift-off was not successful on samples that were coated with sputtered molybdenum, probably because the metallisation was continuous (ie. grain-free). However, this coating material was found to be useful in observing lines in resist exposed in the HB5, when lift-off was not attempted.

6.3.2 Lines exposed in the HB5 high-resolution microscope

Since the lift-off technique was unreliable, and only a very limited time allocation was available on the HB5, it was decided not to attempt lift-off, but to coat the samples with sputtered molybdenum and observe the lines in resist. The contrast in the transmission electron micrographs was therefore very poor, but despite this it was possible to estimate the linewidths.

Figure 6.4 shows the narrowest lines that were observed, these being approximately 10-12nm wide, the nominal exposure dose being 2.5×10^{-10} Ccm^{-1}. Figure 6.5 shows wider lines (about 36nm) produced at an increased dose of 9.7×10^{-10} Ccm^{-1}. The increase of linewidth with exposure dose is shown in figure 6.6. Over this range, linewidth is seen to increase approximately with the 0.75th power of exposure. The critical exposure dose stated above is less than that found for exposures in the Philips SEM, although it should be noted that the beam current measurement was of current collected onto an aperture and that the actual doses may be greater than the nominal doses stated.

6.3.3 Additional results

Additional results for the linewidth-exposure relationship were later obtained and are shown with the permission of K.Y. Lee. Figure 6.7 shows the linewidth-exposure results for 10nm thick metal (Au/Pd) lifted off from 80nm thick double layer PMMA, in

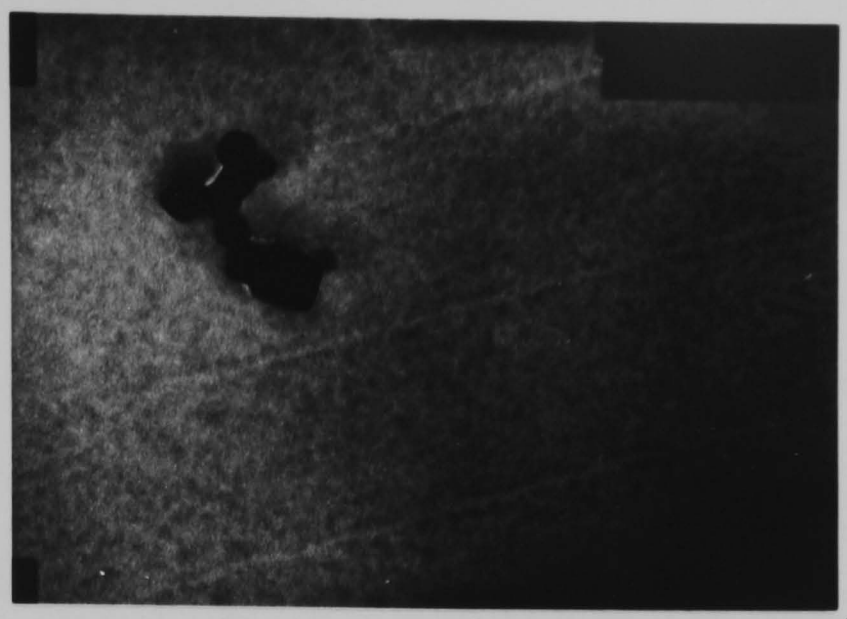

Fig. 6.4 10-12 nm wide lines written in HB5 STEM, developed and metallised with about 0.7nm of sputtered molybdenum. Nominal exposure 2.5×10^{-10} Ccm^{-1}.

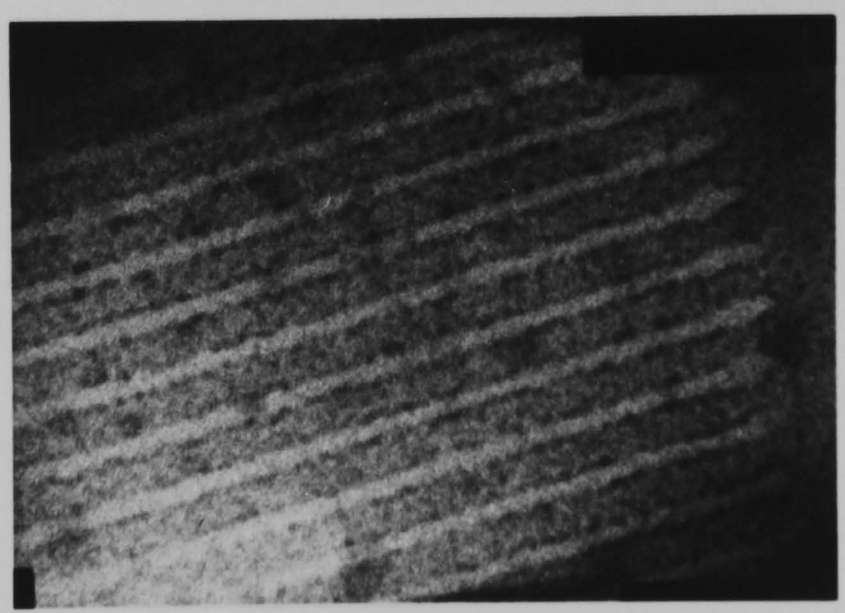

Fig. 6.5 Lines about 36nm wide, written in HB5 STEM, developed and metallised with about 0.7nm of sputtered molybdenum. Nominal exposure 9.7×10^{-10} Ccm^{-1}.

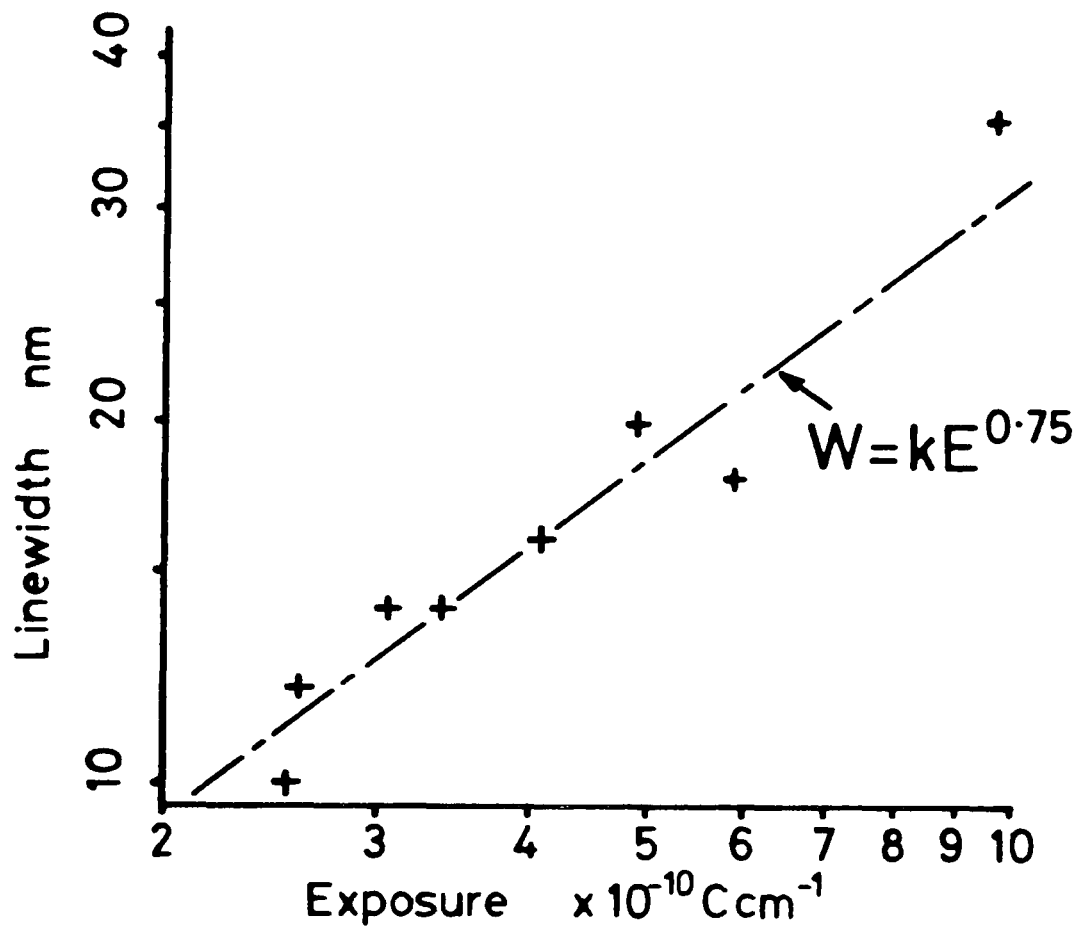

Fig. 6.6 Linewidth-dose relationship obtained by the exposure of 10nm thick PMMA in the HB5 high-resolution STEM, the spot size being less than 1nm.

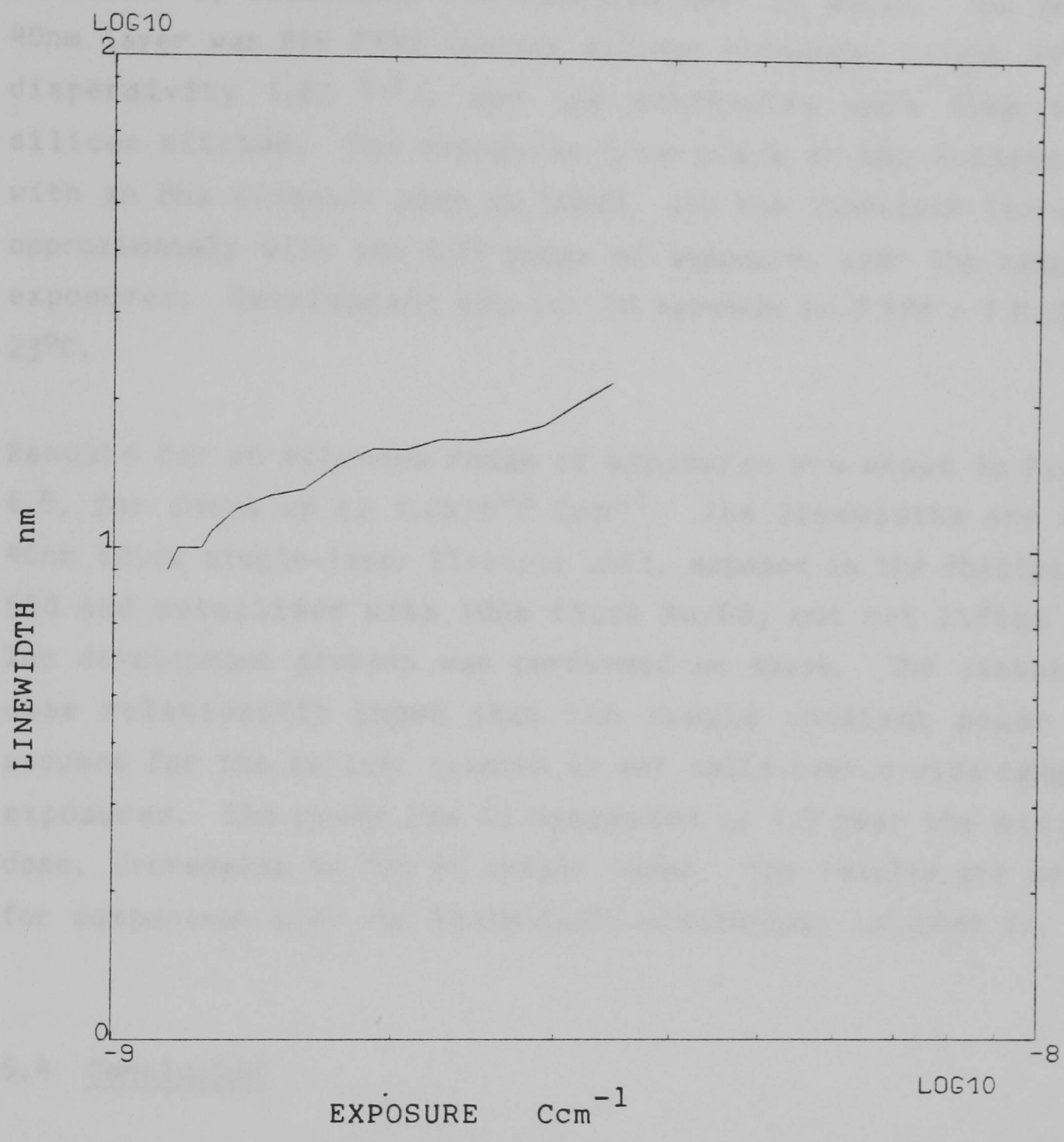

Fig. 6.7 Linewidth-exposure measurements of lifted-off 10nm thick Au/Pd lines, from 80nm thick double layer PMMA. Exposures were made in the Philips SEM 500 with 8nm diameter beam. Results are shown with permission of K.Y. Lee (Glasgow University).

which the top 40nm layer (which determines the deposited linewidth by shadowing) was Elvacite 2041 as above. The bottom 40nm layer was BDH PMMA (weight average molecular weight 137000, dispersivity 1.82 [6.2]), and the substrates were 70nm thick silicon nitride. The exposures took place in the Philips SEM with an 8nm diameter beam at 50keV, and the linewidth increases approximately with the 0.72 power of exposure, over the range of exposures. Development was for 30 seconds in 3 IPA : 1 MiBK at 23°C.

Results for an extended range of exposures are shown in figure 6.8, for doses up to 1.2×10^{-8} Ccm^{-1}. The linewidths are from 40nm thick single-layer Elvacite 2041, exposed in the Philips SEM 500 and metallised with 10nm thick Au/Pd, but not lifted off. The development process was performed as above. The linewidth-dose relationship shows that the simple constant power law assumed for the earlier results is not valid over a wide range of exposures. The power law is estimated as 1.5 near the minimum dose, decreasing to 0.5 at larger doses. The results are useful for comparison with the Monte-Carlo simulations (chapter 7).

6.4 Conclusion

Linewidth resolution measurements have been made in very thin (10nm) single-layer films of PMMA on thin silicon nitride membranes. Although it has not been possible to achieve useful lift-off of metal lines, the use of such a thin resist layer has enabled an investigation of the performance of the resist at its resolution limit, without attempting to produce lines of very high aspect ratio.

The linewidth-exposure relationship has been measured for exposure by a very fine (about 0.5nm) 100keV electron beam. For these exposures the absolute exposure doses are not known

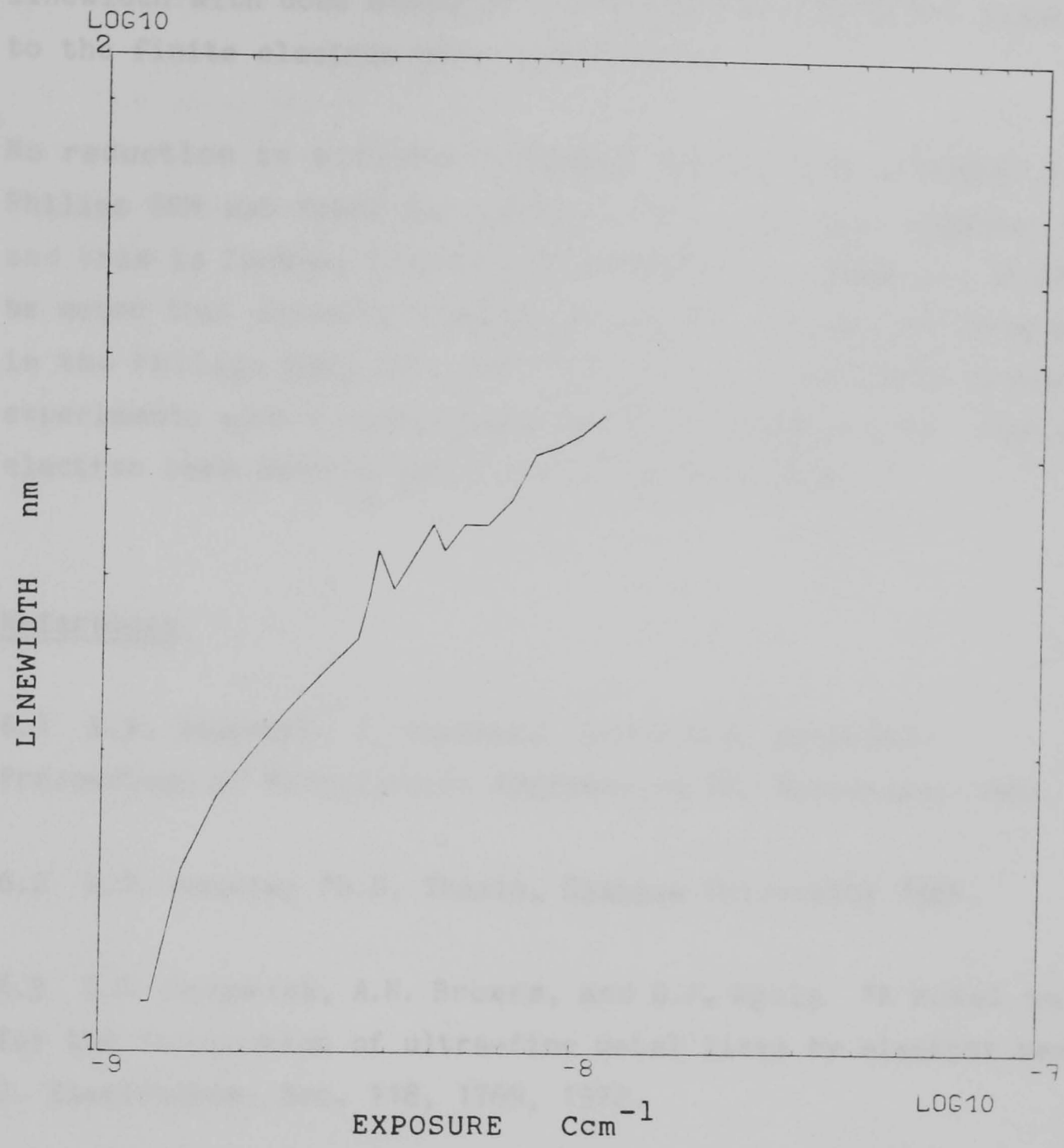

Fig. 6.8 Linewidth-exposure measurements of lines in 40nm thick single layer PMMA (Elvacite 2041), over an extended range of exposures. Exposures were made in the Philips SEM 500. After development the resist was metallised with 10nm of Au/Pd, but lift-off was not attempted. Results are shown with permission of K.Y. Lee (Glasgow University).

accurately; however, the results do show that the increase in linewidth with dose measured in the Philips SEM is not simply due to the finite electron beam distribution.

No reduction in minimum linewidth below that achieved in the Philips SEM was found for exposure by a very fine electron beam, and this is further discussed in chapter 7. However, it should be noted that exposure control in the HB5 was not as accurate as in the Philips SEM, and that it will be possible to repeat the experiments when a more stable and controlable high resolution electron beam machine shortly becomes available.

References

6.1 S.P. Beaumont, T. Tamamura, and C.D.W. Wilkinson
Proceedings of Microcircuit Engineering 80, Amsterdam, 1980.

6.2 W.S. Mackie; Ph.D. Thesis, Glasgow University 1984.

6.3 T.D. Sedgwick, A.N. Broers, and B.J. Agule "A novel method for the fabrication of ultra-fine metal lines by electron beams"
J. Electrochem. Soc. 118, 1769, 1972.

6.4 E. Kratschmer, D. Stephani, and H. Beneking; "High resolution 100keV E-beam lithography"
Proceedings of Microcircuit Engineering 83, Cambridge, 1983

6.5 S.P. Beaumont, P.G. Bower, T. Tamamura, and C.D.W. Wilkinson "Sub-20nm-wide metal lines by electron beam exposure of thin poly(methyl methacrylate) films and liftoff"
Appl. Phys. Lett. 38(6), 436-439, 1981.

6.6 S.P. Beaumont, T. Tamamura, and C.D.W. Wilkinson "Very high resolution electron beam lithography using lift-off processing"

Proceedings of the 9th International Conference on Electron and Ion Beam Science and Technology (ed. R. Bakish), 1980.

6.7 The comments of Dr. S.P. Beaumont, Glasgow University, are appreciated.

CHAPTER 7

Monte-Carlo simulation of the exposure of PMMA

7.1 Introduction

In a Monte-Carlo simulation of the electron beam exposure of resist, many trajectories are calculated of primary electrons passing through the resist layer and, if appropriate, the substrate. The elastic collision points, and the angular deviation of the electrons at these points, are calculated from a model of the scattering process (usually the Rutherford model), with reference to pseudo-random numbers generated by the computer. In earlier simulations the energy dissipation along the electron paths (per unit path length) was calculated according to the Bethe formula (see for example Hawryluk, Hawryluk, and Smith[7.1]); however this "continuous slowing down approximation" (CSDA) leads to inaccuracy due to the effect known as electron "straggling", some electrons having much longer paths through the resist and substrate than others. Some later simulations have used the technique of Shimizu et al.[7.2] in simulating discrete inelastic collision points at which energy is dissipated, using random numbers in a manner similar to the simulation of elastic scattering. Such Monte-Carlo calculations result in a more accurate energy distribution of electrons transmitted through thin films than does the CSDA method[7.15], and can be used in simulating the exposure of resist on solid substrates, enabling the effect of electron backscattering from the substrate to be quantified.

Such a simulation, which included discrete elastic and inelastic collision points (based on the Rutherford scattering model and the Bethe model of energy loss, respectively), was used to

produce the linewidth-exposure relationship shown in figure 7.1 (due to S.P. Beaumont), for a thin film of PMMA on a thin substrate. The power law of 0.29 is much lower than that found in practice for exposure by a beam of negligible diameter, or for exposure by a beam of diameter almost as large as the minimum linewidths obtained (about 0.7; see chapter 6).

The elastic and inelastic mean free path lengths of 100keV primary electrons in PMMA are both of the order of 100nm, so that when passing through a resist layer only 10nm thick there will most probably be only one collision, either elastic or inelastic, or none at all. Since several elastic collisions would usually be required to turn an electron back on its original path and return it to the resist layer (the elastic scattering angles for primary electrons are of the order of tens of milliradians), the amount of backscattering of primary electrons from a substrate only 70nm thick is negligible. Hence almost all of the primary inelastic collisions in the resist will be within the primary electron beam diameter, and it would appear from a simulation based only on following the trajectories of primary electrons that a 1nm electron beam would produce a well-confined energy dissipation profile 1nm wide. In practice, however, the narrowest lines resulting from exposure by a beam of less than 1nm are about 10nm wide (see chapter 6), and it has been proposed that the energy spreading effect of secondary electrons is responsible for the discrepancy.

Attempts to include the effect of secondary electrons in Monte-Carlo programs have relied on various models for the production of secondary electrons and for their ranges in the material[7.3,7.9-7.11]. The differential cross-sections for the production of secondaries are noted as being inaccurate and the models have not been proved experimentally for PMMA. Models for the ranges of low energy electrons in polymeric materials may also be inaccurate. It was therefore decided to attempt a Monte-

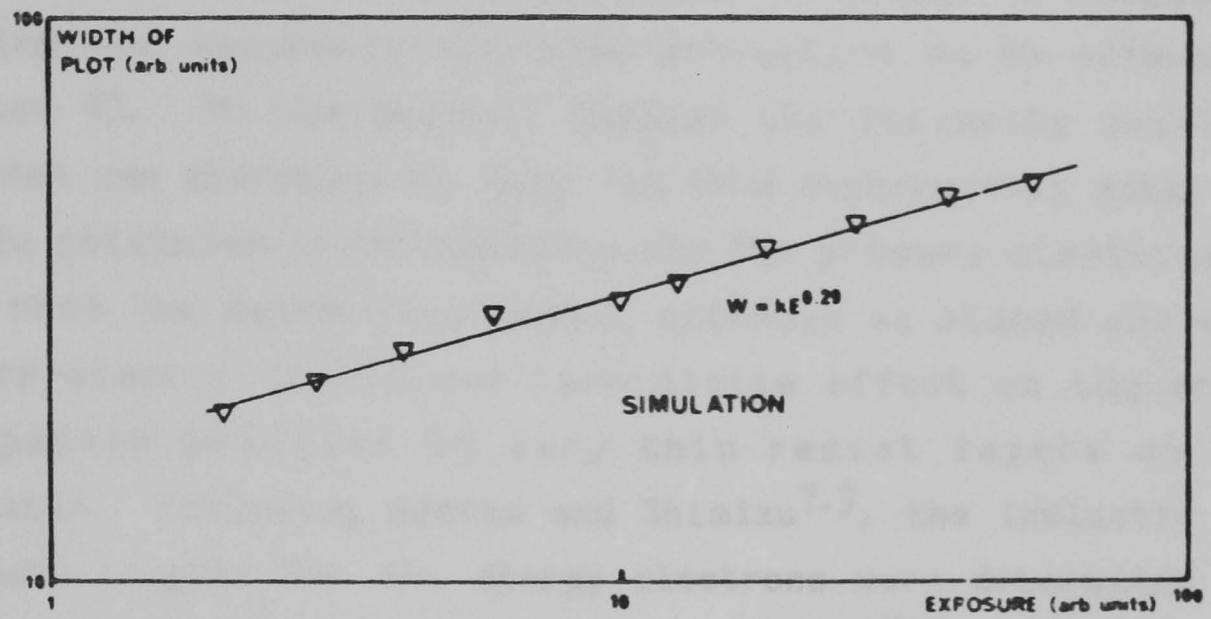

Fig. 7.1 Linewidth-exposure dose relationship resulting from a Monte-Carlo simulation of the exposure at 50keV of thin (50nm) PMMA on a thin carbon substrate. The simulation included discrete elastic and inelastic collision points, but did not include the production of secondary electrons. The incident beam was 8nm in diameter and of gaussian profile. Shown with the permission of S.P. Beaumont, Glasgow University.

Carlo calculation including the effect of secondary electrons, using, as far as possible, experimental data for the various effects involved.

Measurements of low-energy electron exposure ranges have been presented in chapter 3, and electron energy loss spectroscopy has been performed on PMMA and silicon nitride (used as the supporting membrane in the experiments described in chapter 6), enabling the secondary electron production to be determined (chapter 4). In the present chapter the inelastic collision processes can therefore be modelled from experimental data; the elastic collision cross sections for the primary electrons are taken from the Rutherford model, although as stated above the primary elastic collisions have little effect on the energy dissipation profiles in very thin resist layers on thin substrates. Following Samoto and Shimizu[7.3], the inelastic mean free path lengths for low energy electrons were determined from the empirical formulae of Seah and Dench[7.4]. At very low energies the elastic mean free paths predicted by the Rutherford model become very small (of the order of the atom spacings) and would lead to extremely long computation times; the Rutherford model at low energy is also known to be very inaccurate[7.5]. (The Mott cross-section is more accurate but would have to be tabulated for use in a Monte-Carlo calculation, and is still inaccurate at very low energies.) Since the secondary electrons are deflected in a random manner by several inelastic collisions, and almost all of the higher energy secondaries (of significant range) lose their energy in several collisions, the effect of elastic scattering is simulated simply by shortening the inelastic mean free path by a variable factor which is determined by comparing simulated low energy exposures with the experimental exposure range data. This procedure also compensates for any inaccuracy in the Seah and Dench empirical formula as applied to PMMA.

7.2 Monte-Carlo simulation in three dimensions

Monte-Carlo simulations are often reduced to two dimensions, in order to reduce the computation time and simplify the structure of the program. In a program to simulate the line exposure of PMMA, electron trajectories and energy losses can be tracked in three dimensions (x along the line, y across the line, and z vertically), and all losses recorded in a y-z array only, thus integrating the energy dissipation in the x direction along the line. Since the exposure is symmetrical about the centre of the line (taken as y=0), the losses at negative y-coordinates can be superimposed on the positive y-coordinate losses. These techniques reduce greatly the number of incident electrons which must be simulated in order to achieve "smooth" energy dissipation contours.

However, in exposures to achieve the ultimate resolution in PMMA, it is found that the energy dissipation contours are not smooth (see section 7.5.2), and a realistic simulation must take into account the factors influencing the statistical variations in the energy dissipation. In the simulations described here, the dissipation was not integrated in the x-direction or mirrored about the x-z plane. The incident beam of electrons was "scanned" in the x-direction, and the y-coordinate of the entry point of each electron was determined by a random number together with the required beam distribution (both negative and positive y), which could be determined as described in chapter 2 for electron beams of the order of 10nm in diameter, or alternatively could be a delta function representing a very fine beam.

Energy losses were only recorded at central x-elements (ie. in a single y-z array), corresponding to a cross section of the exposed line (figure 7.2). The centre of the electron beam would enter the resist at the centre of the first y-element and

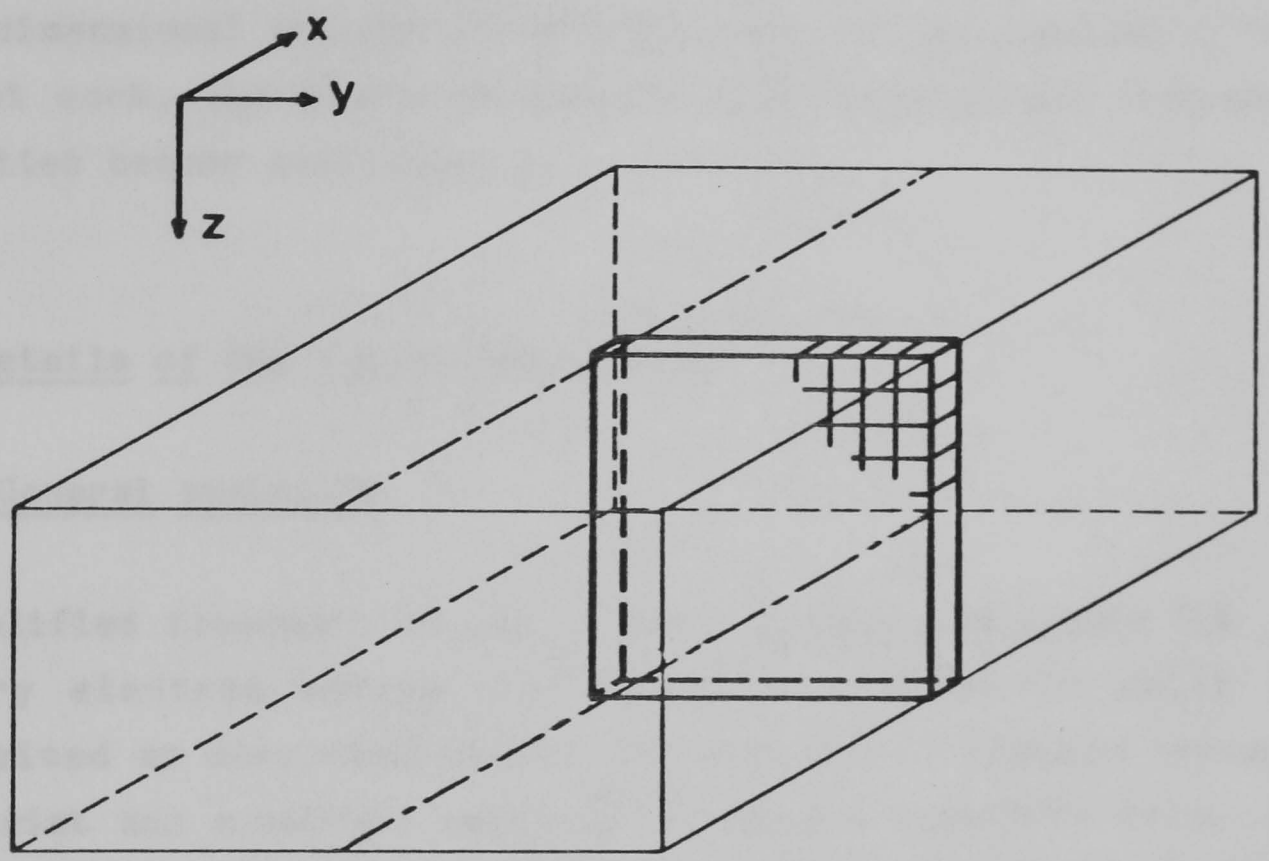

Fig. 7.2 Monte-Carlo simulation in three dimensions. Primary electrons pass through the block of resist indicated by the faint lines, the centre of the beam being scanned along the top centre-line. Secondary electrons are tracked within the resist and substrate, whether inside or outside the block. Energy losses are only recorded if they occur within the cross-sectional y-z array, delineated by the heavy lines.

only one half of the cross section would be mapped in the array. Using three-dimensional graphical display programs and a three-dimensional storage array it would be possible to plot dissipation contours along the exposed line, although it must be remembered that for the energy dissipation to be realistic the exposed line must be extended beyond the recorded array section. Three-dimensional storage and display were not implemented in the present work, but might be incorporated when better computer facilities become available.

7.3 Details of the simulation program

7.3.1 General structure

A simplified flowchart of the program is shown in figure 7.3. A primary electron enters the resist at a position which is determined as described in section 7.2, and is tracked through the resist and substrate until it leaves the composite film. At this point any secondary electrons which were created are tracked until either they have insufficient energy to expose the resist (less than 5eV), or they leave the film. Tertiary electrons can also be created by inelastic collisions of the secondaries, and are tracked in the same manner.

If an electron passes from the resist into the substrate or vice-versa, it is placed at its point of intersection with the interface and its mean free path re-calculated in the new material; it then proceeds in the same direction as before. The same routine is used for tracking both primary and secondary electrons, although the mean free path is calculated differently for low energy electrons.

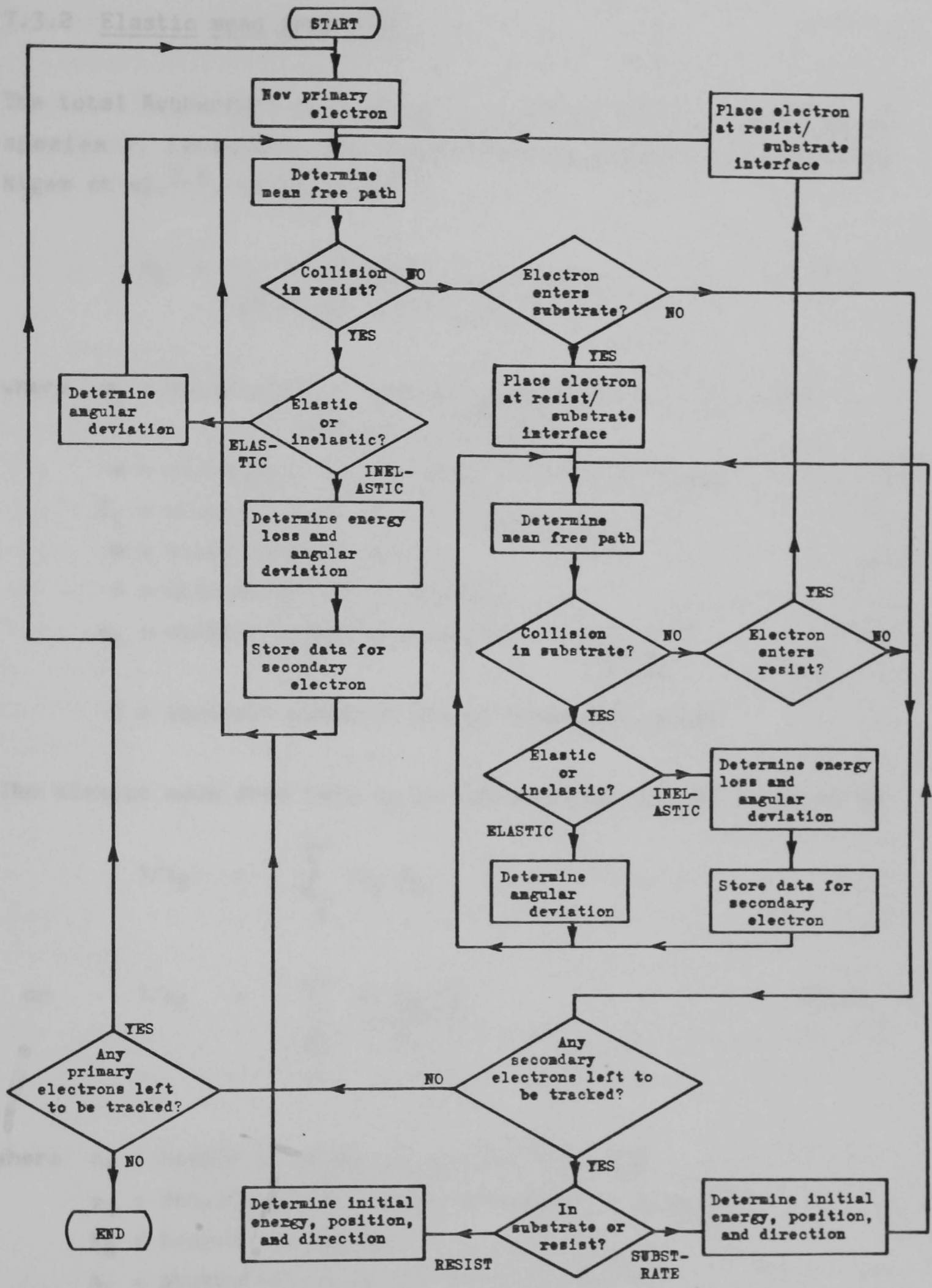

Fig. 7.3 Flowchart of the Monte-Carlo simulation program, including the energy spreading effect of secondary electrons.

7.3.2 Elastic mean free path

The total Rutherford scattering cross section σ_i for each atom of species i, including the atomic screening parameter given by Nigam et al.[7.6], is given by[7.1]

$$\sigma_i = \frac{Z_i^2 \pi e^4}{m^2 v^4 \alpha_i^2 (\alpha_i^2 + 1)} \qquad (7.1)$$

where σ_i = total elastic scattering cross section (in cm^2) per atom of species i

e = electronic charge (esu) = 4.8×10^{-10} esu

Z_i = atomic number of the atom of species i

m = electron mass (grams)

v = electon velocity (cm/sec)

α_i = atomic screening parameter = $\frac{2.33\ Z_i^{1/3}}{E^{1/2}}$

E = incident electron energy (electron volts)

The elastic mean free path λ_E in the material (in cm) is given by

$$1/\lambda_E = \sum_i n_i \sigma_i$$

or

$$1/\lambda_E = \sum_i \frac{\rho_i N_A \sigma_i}{A_i} \qquad (7.2)$$

where n_i = number of atoms of species i per cm^3

ρ_i = density of the atoms of species i (g cm^{-3})

N_A = Avogadro's number

A_i = atomic weight of the atom of species i

The elastic mean free path is calculated according to equation 7.2 only for primary electrons (taken to be those of energy

greater than 1700eV). The effect of random elastic scattering of secondary electrons is included by reducing the inelastic mean free path (see section 7.1), and the elastic path length is therefore set as an arbitrarily large number.

7.3.3 Inelastic mean free path (IMFP) of primary electrons

The inelastic mean free path of 100keV electrons in both PMMA and silicon nitride was derived from the energy loss spectra (as explained in chapter 4). The simulations on thin substrates were run for 100keV primary electrons and since the energy losses in almost all cases in thin substrates are small, it would be reasonable to take the measured values of mean free path for all primary electrons. However, it was also required to run simulations on solid substrates for use in deriving the variation in exposure with depth in the resist (chapter 5), when the primary electrons lose all of their energy within the resist and substrate. Therefore the measured values of mean free path were taken for 100keV electrons, and these were scaled as shown below for electrons of energy lower than 100keV, but above 1700eV, below which the model for secondary electrons was used. This method also allows other beam potentials to be used when necessary.

The inelastic mean free path was scaled by reference to the CSDA Bethe energy loss formula (non-relativistic):

$$\frac{dE}{ds} = \frac{-2\pi e^4 n_i}{E} \ln\left[\frac{E}{I}\left(\frac{e}{2}\right)^{1/2}\right] \qquad (7.3)$$

where dE/ds is the rate of change of electron energy with distance, n_i is the density of atoms of species i, and I is the mean ionisation energy of the material.

Since the inelastic mean free path is inversely proportional to the rate of loss of energy with distance, the IMFP at electron energy E, λ_p, is given by:

$$\lambda_p = \lambda_k \frac{E}{100000} \cdot \frac{\ln(100000.C)}{\ln(E.C)} \qquad (7.4)$$

where λ_k = IMFP at 100keV

$$C = \frac{(e/2)^{1/2}}{I}$$

The value of mean ionisation energy assumed for PMMA was that used by Hawryluk, Hawryluk, and Smith[7.1,7.7] (65.6eV), who also use the empirical result[7.7]

$$I = Z\,(9.76 + 58.8Z^{-1.19}) \quad \text{for } Z \geqslant 13 \qquad (7.5)$$

This formula was used to estimate the mean ionisation energy for silicon nitride (taking the weighted average atomic number) as being 136eV.

It should be noted that these calculations are only used to scale the inelastic mean free path length from its measured value at 100keV. Since most primary electrons lose very little energy within thin films, the scaling routine will have very little effect when the simulation is run for thin resist and substrate films, with 100keV incident electron energy; most of the results reported are taken from such simulations.

7.3.4 Secondary electron inelastic mean free path

Following Samoto and Shimizu[7.3], the secondary electron inelastic mean free paths were calculated from the empirical formulae of Seah and Dench[7.4]. For organic material the IMFP, λ_p (in

nanometres), is given by

$$\lambda_p = \frac{1}{d}\left(\frac{49}{E^2} + 0.11E^{1/2}\right) \qquad (7.6)$$

where d is the density ($g.cm^{-3}$), taken as 1.23 $g.cm^{-3}$ for PMMA[7.3]. For inorganic compounds the IMFP, λ_m (in atomic monolayers), is given by Seah and Dench as

$$\lambda_m = \frac{2170}{E^2} + 0.41(aE)^{1/2} \qquad (7.7)$$

where a is the average atomic monolayer dimension (nanometres) and is taken as 0.213nm for silicon nitride.

The IMFP is calculated according to equations 7.6 and 7.7 for all electrons of energy less than 1700eV, and is then corrected to allow for the effect of random elastic scattering (section 7.4).

7.3.5 Determination of step length and type of collision

The total mean free path is given by

$$\frac{1}{\lambda_T} = \frac{1}{\lambda_{inel}} + \frac{1}{\lambda_{el}} \qquad (7.8)$$

The step length, s, between collisions is then derived from the probability of collision using the Poisson distribution, $(1/\lambda)\, e^{-s/\lambda}$, to be

$$s = -\lambda \ln R_1 \qquad (7.9)$$

where R_1 is a uniform random number between 0 and 1. Following

Shimizu et al.[7.2] another random number R_2 is used to decide whether the scattering is elastic, according to whether the inequality

$$R_2 \leqslant \frac{1/\lambda_{el}}{1/\lambda_T} \tag{7.10}$$

is satisfied; otherwise the scattering is inelastic.

7.3.6 Angular deflection in an elastic collision

The calculation of elastic angular deflection is that of a conventional Monte-Carlo approach (see, for example, Hawryluk, Hawryluk, and Smith[7.1]). The differential Rutherford scattering cross-section into solid angle Ω (with the screening term α) is

$$\frac{d\sigma_i}{d\Omega} = \frac{Z_i^2 e^4}{4 m^2 v^4 (\sin^2(\theta/2) + \alpha_i^2)^2} \tag{7.11}$$

where θ is the deflection angle. The electron is scattered by an atom of species i if a random number R_3 satisfies

$$R_3 \leqslant \frac{n_i \sigma_i}{\sum_i n_i \sigma_i} \tag{7.12}$$

Since a small change of solid angle $d\Omega = 2\pi \sin\theta \, d\theta$, the deflection angle θ can be calculated from a random number R_4:

$$R_4 = \int_0^{\theta} \frac{d\sigma_i}{d\Omega} 2\pi \sin\theta \, d\theta \Bigg/ \int_0^{\pi} \frac{d\sigma_i}{d\Omega} 2\pi \sin\theta \, d\theta \tag{7.13}$$

The denominator is simply the total elastic cross-section σ_i, and we can obtain

$$\cos\theta = \frac{R_4'\,(1 + 2\alpha_i^2) - \alpha_i^2}{R_4' + \alpha_i^2} \qquad (7.14)$$

where $R_4' = 1 - R_4$

By rotational symmetry, the azimuthal angle ϕ of the deflection is obtained from

$$R_5 = \phi / 2\pi \qquad (7.15)$$

The deflection of the electron through angles θ and ϕ is made with respect to a 3x3 transformation matrix which relates the direction of travel of the electron to the direction orthogonal to the surface of the resist, in case the electron has already been deflected from the normal by a previous collision. The members of the transformation matrix are then re-calculated for use in the determination of subsequent collision coordinates and angular deflection.

7.3.7 Angular deflection and energy loss in an inelastic collision, and the generation of secondary electrons

The determination of energy loss from the electron energy loss spectra, and of the energy of secondary electrons that are generated, is described fully in chapter 4. Following Samoto and Shimizu[7.3], the deflection angle of the primary electron θ_p, and the angle of emission of the secondary electron θ_s (with respect to the initial primary electron direction), are calculated according to the simple binary collision model (by conservation of momentum):

$$\sin^2\theta_p = \cos^2\theta_s = \Delta E/E \qquad (7.16)$$

where ΔE is the energy loss.

It is noted in chapter 4 that the deflection θ_p calculated by this method is overestimated since some momentum is absorbed by the atom; however, this inaccuracy is more significant in thick substrate rather than thin substrate lithography, where the primary electrons suffer many inelastic collisions.

The azimuthal angle for primary electrons ϕ_p is calculated as for elastic collisions (equation 7.15), and the secondary azimuthal angle ϕ_s is assumed to be $(\phi_p + \pi)$.

For the subsequent tracking of secondary (and tertiary) electrons, at an inelastic collision the energy loss and the direction of the colliding electron (ie. the transformation matrix) are stored, together with the angles θ_s and ϕ_s. When the secondary is to be tracked its initial energy and direction are calculated. Secondary electrons are not tracked unless they are able to cause chain scission in PMMA (ie. they have at least 5eV energy).

7.4 Simulation of low energy exposures

To test the accuracy of the simulation of secondary electron energy dissipation, the program was run to simulate blanket (ie. large area) exposures by low energy electrons up to 1700eV. The results could be compared with the direct low energy electron exposures of chapter 3.

The energy dissipation was recorded in an array of elements which was sufficiently large to include all lateral spreading of the electrons. It was only necessary for the array to contain single elements in the horizontal direction provided these elements were sufficiently large. The array contained 50 elements in the

vertical direction. This arrangement resulted in the dissipation being integrated horizontally to simulate the effect of a large area exposure, and the energy dissipation could then be plotted against depth.

The exposure latitude of PMMA, representing the factor between the dose which is just sufficient for all of the resist to develop, and the dose at which cross-linking begins to prevent full development, is known to be a factor of 10 (see Hatzakis[7.8]). It will be noted that the developed depth/exposure characteristic of figure 3.10, for low energy exposures, is almost, but not quite, constant over an order of magnitude range of exposures, indicating that the exposure latitude given by Hatzakis also applies to low energy exposures. The simulated dissipation/depth characteristics for low energy exposures (see for example figures 7.6 and 7.7) show that the exposure reaches a maximum at some level below the surface (about half of the secondaries are lost at the surface), below which the dissipation decreases.

It is assumed that the dissipation at the maximum developed depth in figure 3.10 (at 5×10^{-5} Ccm^{-2}) is 1/10 of the maximum dissipation; that is, at the incident exposure for maximum developed depth the resist will develop out to the depth at which it receives 1/10 of the maximum energy dissipation. Given less exposure, the resist will not develop to as great a depth, and with greater exposure a layer of cross-linked material will inhibit the development, and will probably precipitate out into the bottom of the developed areas (as do the higher molecular weight fractions which are thought to cause the development "tails" described in chapter 5). Hence we assume that the simulated "1/10 exposure depth" is the equivalent of the exposure range measured in chapter 3. Since the exposure at this point is falling rapidly with depth, a small error in the assumed exposure latitude of the resist will not cause a large error in the

simulated exposure range.

Figure 7.4 shows the measured exposure ranges of chapter 3, together with the simulated 1/10 exposure depths which used the Seah and Dench formula for the inelastic mean free path, with no allowance for elastic scattering. This is equivalent to the model of Samoto and Shimizu[7.3], and it will be noted that the ranges are overestimated, especially at low energy. It is assumed that the discrepancy is due to random elastic scattering (the elastic mean free path being of the order of the atom spacings), resulting in a reduction of the effective point-to-point inelastic mean free path. In order to correct the low energy IMFP to match the simulated 1/10 exposure depths to the measured exposure ranges, a correction factor was applied to the Seah and Dench IMFP, of 0.6 below 100eV, rising linearly to 0.9 at 900eV, and remaining constant at 0.9 from 900 to 1700eV (see figure 7.5). Figure 7.4 also shows the 1/10 exposure depths after the correction is applied, and these are seen to match the measured exposure ranges.

The dissipation/depth plots of figures 7.6 (at 500eV) and 7.7 (at 50eV) include the correction to the IMFP. Later in this chapter the size of the elements used in most simulations will be $(2nm)^3$, and it is convenient to give energy dissipation values in electron volts per $(2nm)^3$. By integrating to obtain the total dissipation in the resist, the dissipation at the 1/10 exposure depth can be obtained, for an incident dose of $5x10^{-5}$ Ccm^{-2}. For the 500eV simulation this was found to be 97eV per $(2nm)^3$, and for the 50eV simulation it was 96eV per $(2nm)^3$; the dissipation was also very similar at other incident energies, indicating that the maximum developed depth is always reached at the same low energy exposure dose, over the range of incident energies between 50 and 1700eV. The estimation of the exposure threshold for development is used later in determining the development contours of lines exposed by high energy electrons.

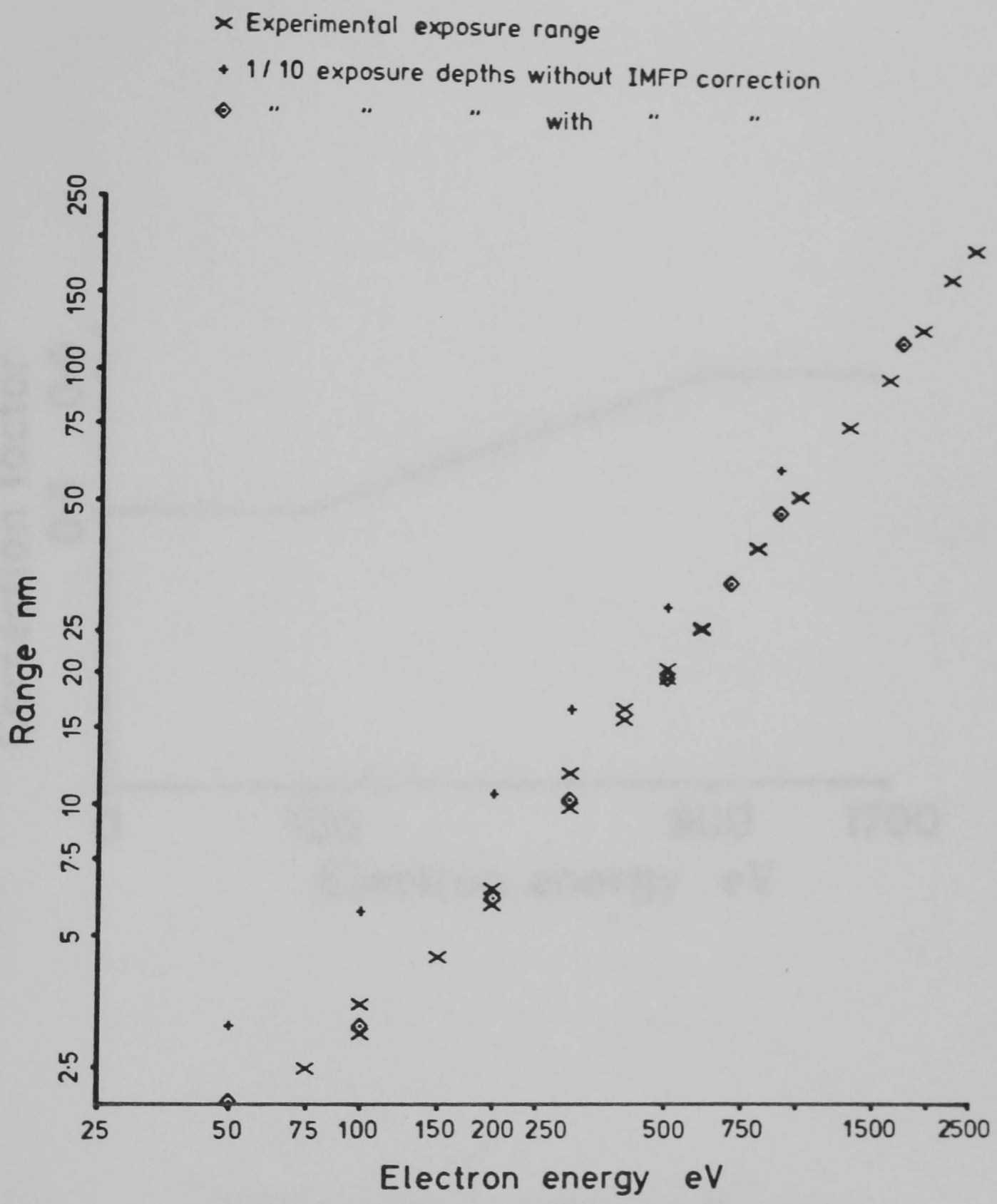

Fig. 7.4 Experimental and simulated exposure ranges of low energy electrons.

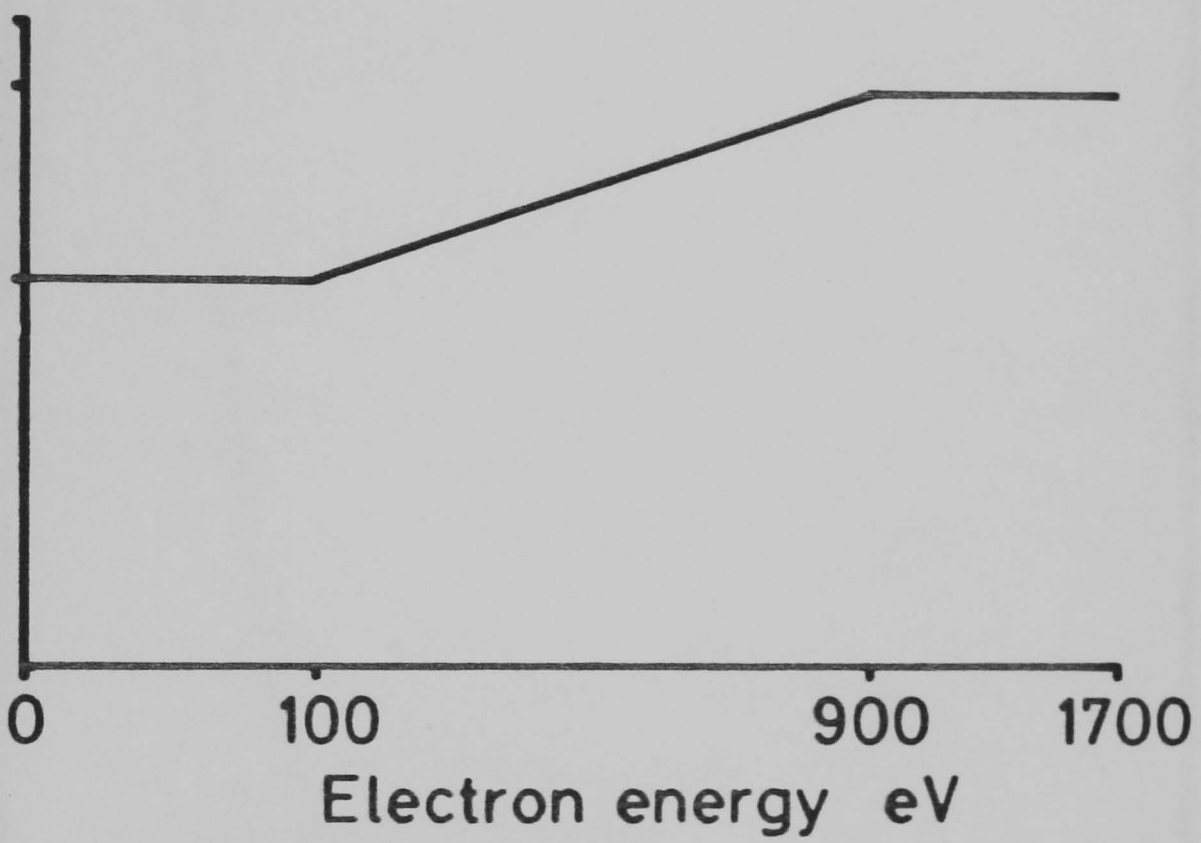

Fig. 7.5 Correction of the inelastic mean free path lengths of the low energy electrons, to allow for the effect of random elastic scattering and any inaccuracy of the Seah and Dench empirical formula, as applied to PMMA.

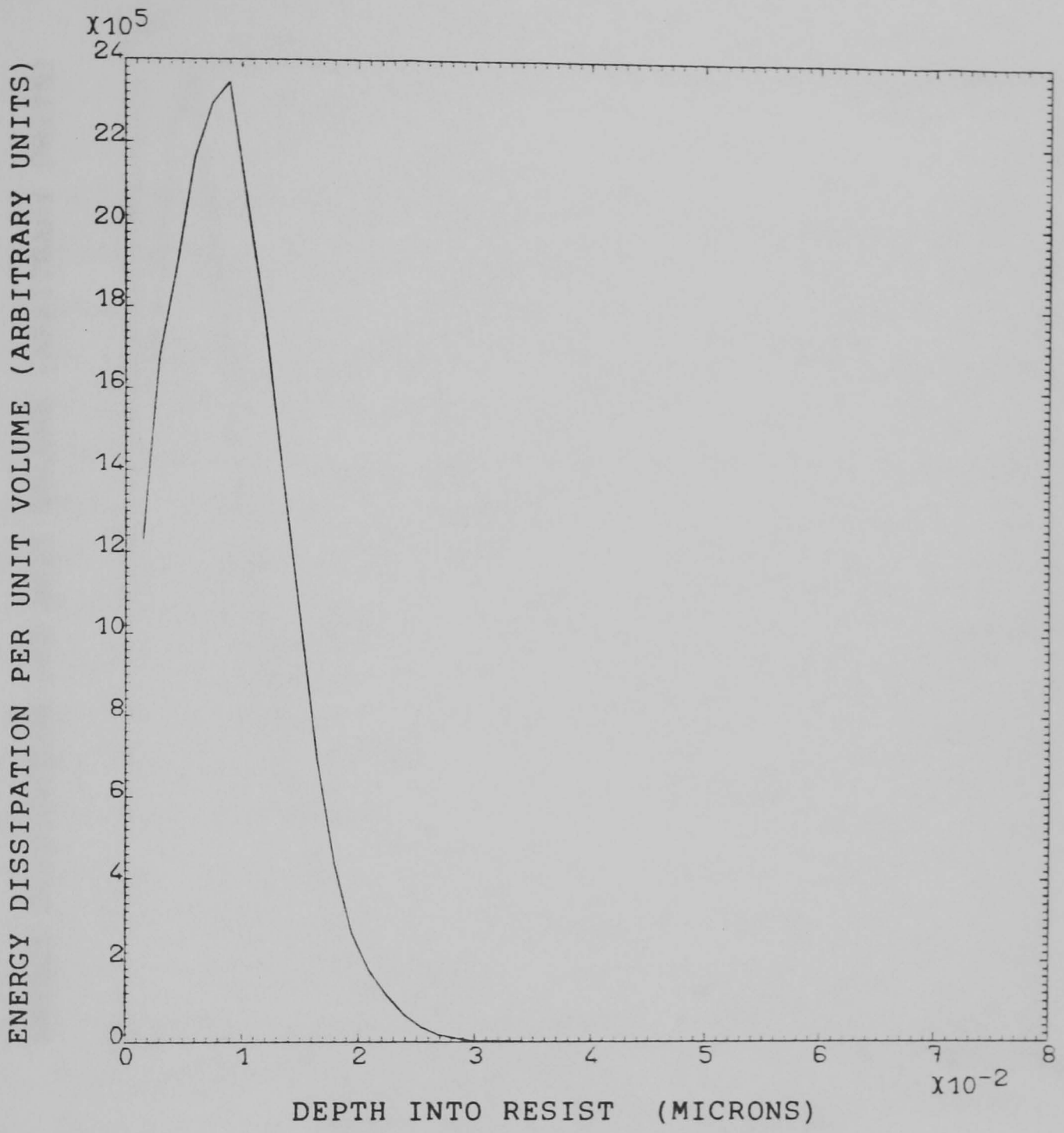

Fig. 7.6 Plot of energy dissipation against depth, for a large-area exposure by 500eV electrons, simulated by the Monte-Carlo program.

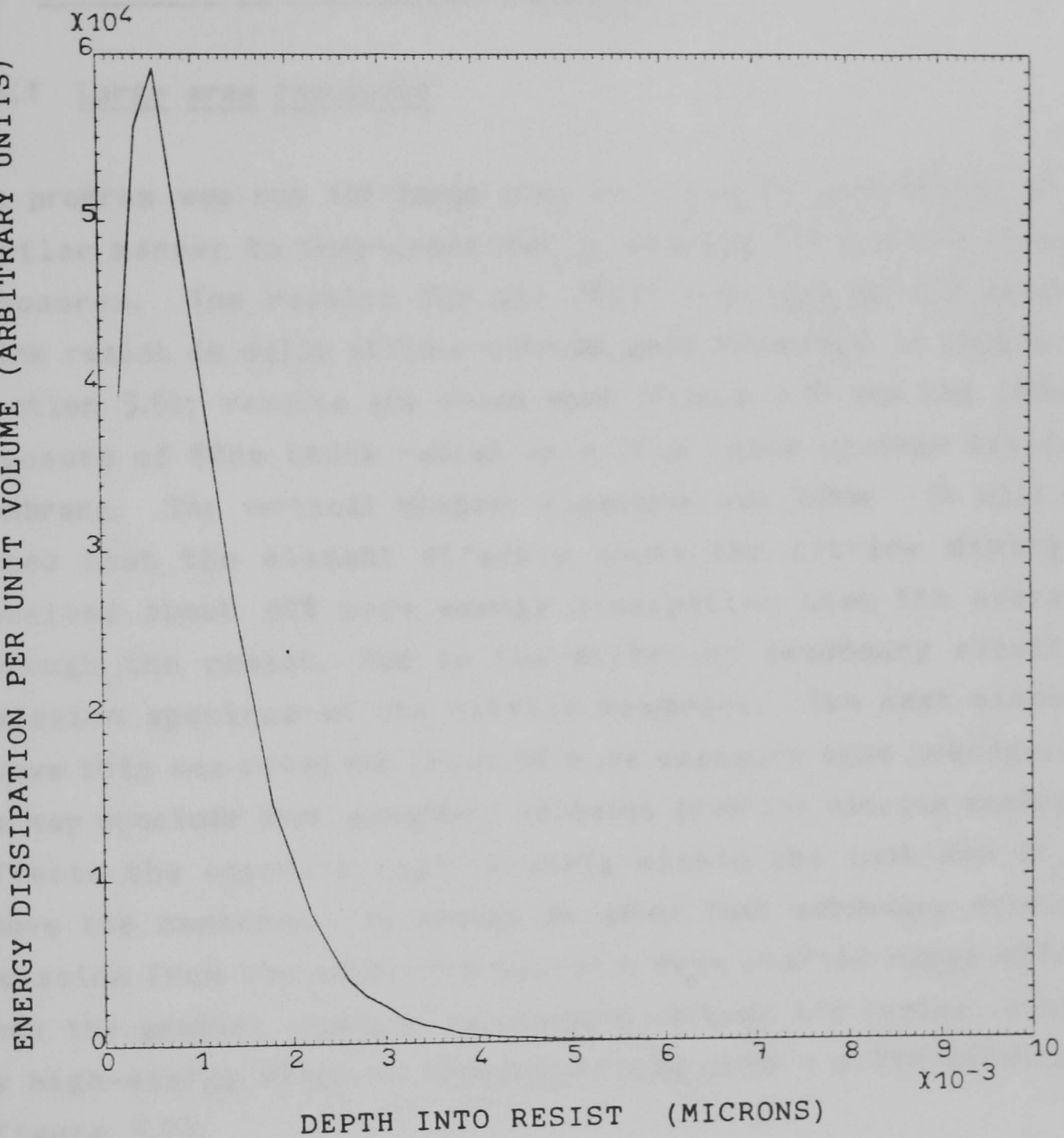

Fig. 7.7 Plot of energy dissipation against depth, for a large-area exposure by 50eV electrons, simulated by the Monte-Carlo program.

7.5 Simulation of high-energy exposures

7.5.1 Large area exposures

The program was run for large area exposures at high energy in a similar manner to that described in section 7.4 for low energy exposures. The results for the 20keV exposure of 0.3 micron thick resist on solid silicon nitride were presented in chapter 5 (section 5.5); results are shown here (figure 7.8) for the 100keV exposure of 60nm thick resist on a 70nm thick silicon nitride membrane. The vertical element dimension was 1.2nm. It will be noted that the element directly above the nitride membrane received about 30% more energy dissipation than the average through the resist, due to the different secondary electron emission spectrum of the nitride membrane. The next element above this one received about 5% more exposure than average, so we may conclude that secondary emission from the nitride membrane affects the exposure significantly within the last 2nm or so above the membrane. It should be noted that secondary electron emission from the substrate causes a much shorter range effect than the gradual increase in exposure through the resist, caused by high-energy electron backscattering from a solid substrate (figure 5.7).

The exposure close to the surface of the resist is about 10% below average, the decrease occurring over the top 10nm or so of resist. Some decrease in exposure would be expected close to the surface since there is no secondary electron contribution from the free space above the resist, and might result in undercutting of fine lines exposed in single layers of the resist (see section 7.5.5).

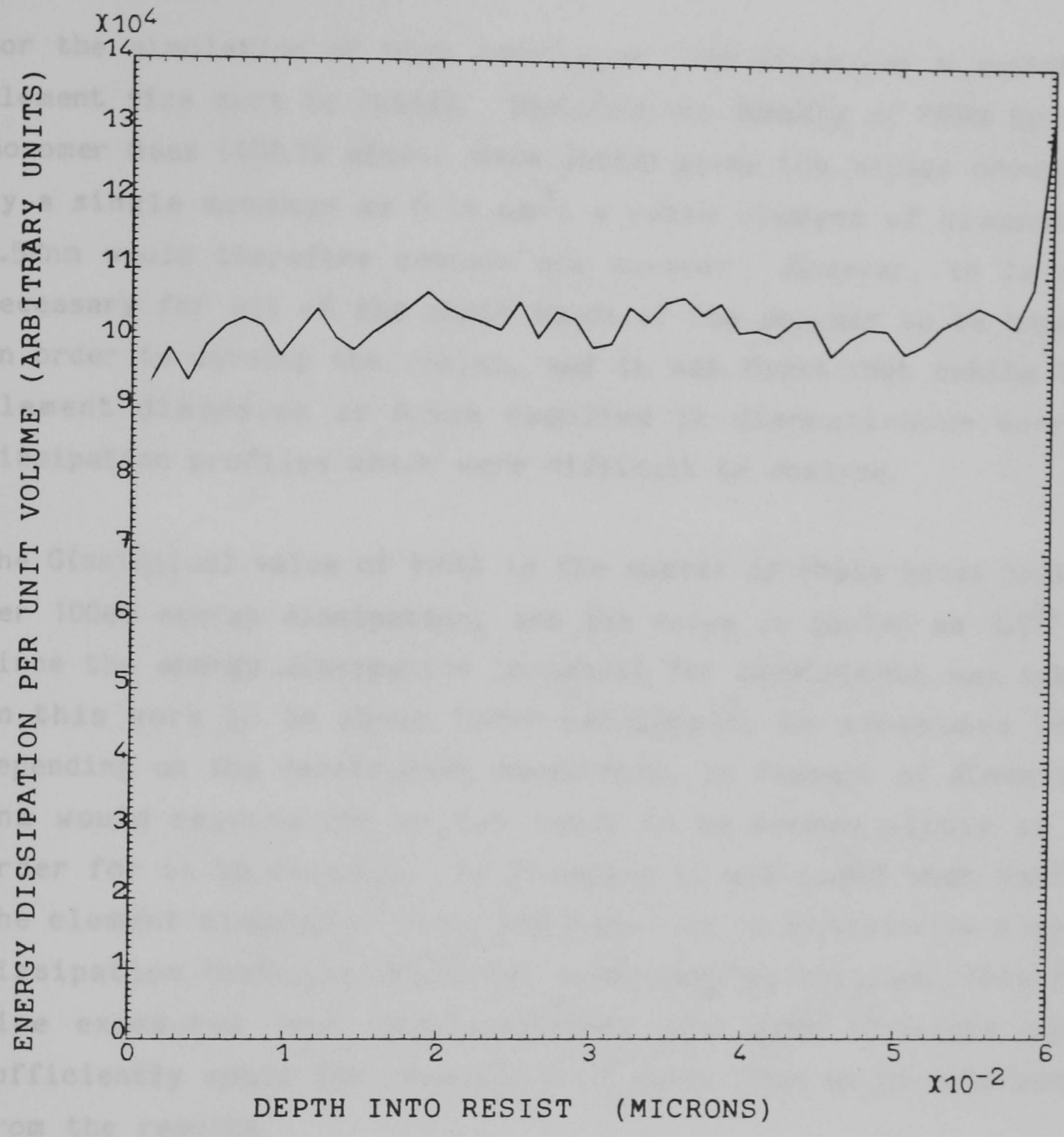

Fig. 7.8 Simulation of large-area exposure by 100keV electrons of 60nm thick PMMA supported by a 70nm silicon nitride membrane.

7.5.2 Energy dissipation and development contours for simulated high-resolution exposures

For the simulation of high resolution line exposures a suitable element size must be chosen. Dividing the density of PMMA by the monomer mass (100.12 atomic mass units) gives the volume occupied by a single monomer as 0.14 nm^3; a cubic element of dimension 0.52nm would therefore contain one monomer. However, it is not necessary for all of the chain bonds of the polymer to be broken in order to develop the resist, and it was found that taking the element dimension as 0.5nm resulted in discontinuous energy dissipation profiles which were difficult to analyse.

The G(scission) value of PMMA is the number of chain bonds broken per 100eV energy dissipation, and its value is quoted as 1.7[7.13]. Since the energy dissipation threshold for development was taken in this work to be about 100eV per $(2nm)^3$, or sometimes less depending on the development conditions, an element of dimension 2nm would require one or two bonds to be broken within it in order for it to develop. In practice it was found that taking the element dimension to be 2nm resulted in continuous energy dissipation contours above the experimental critical dose for line exposures (see next section), and such elements were sufficiently small for linewidths of about 10nm to be determined from the results.

Although the simulations took place in three dimensions, computer data storage was limited and the dissipation was only recorded in one half of a single cross-section through the exposed line (see section 7.2). The results can be plotted as an array showing the elements which receive more than a threshold energy dissipation (see next section) which it is assumed will be dissolved by the developer. A set of threshold plots for various exposures of 20nm thick resist on 70nm thick silicon nitride substrates are shown in figure 7.9; these are for the 8nm beam with tails of the

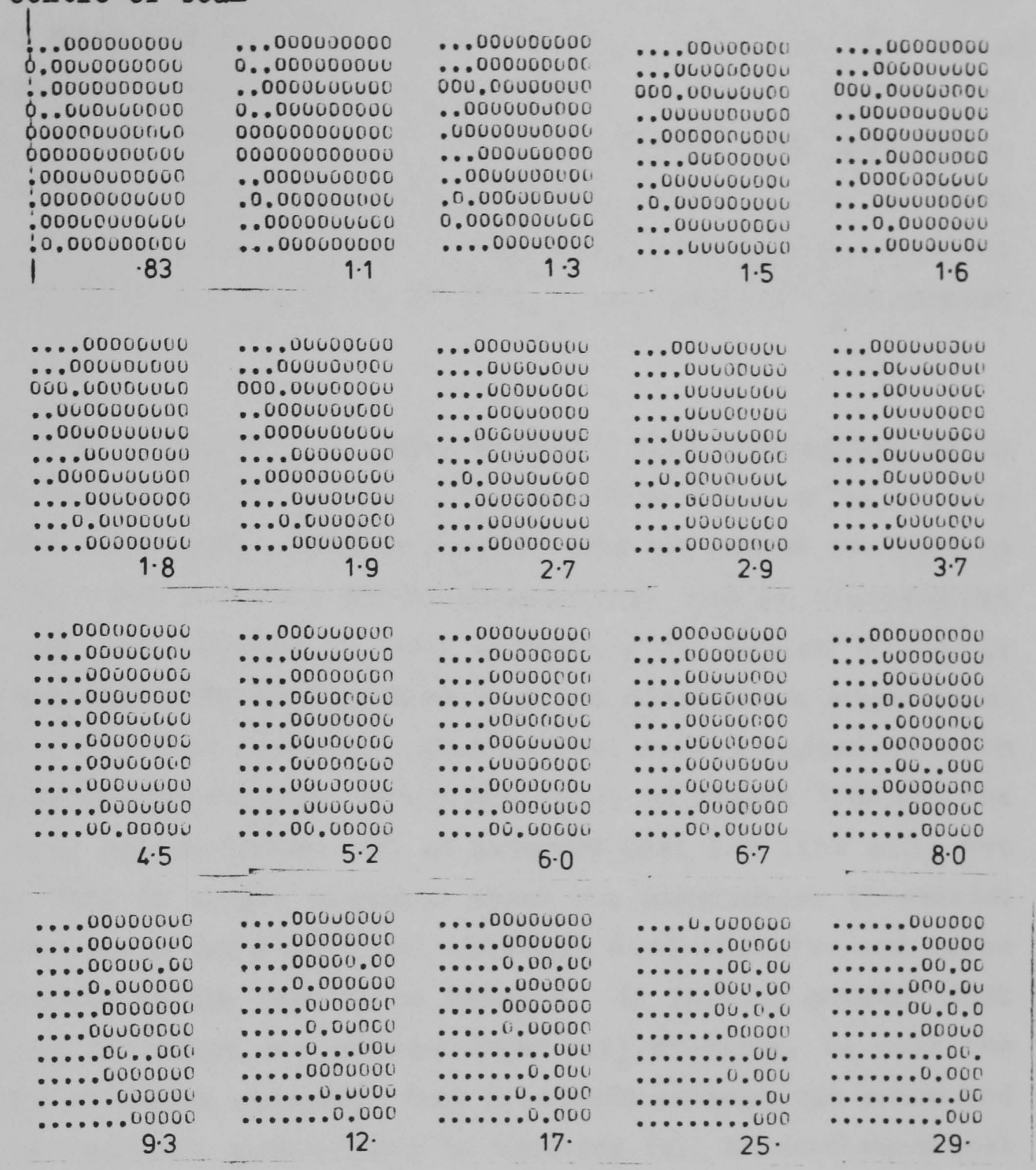

Fig. 7.9 Exposure threshold plots for 20nm thick PMMA on a 70nm silicon nitride substrate, exposed at 100keV by an 8nm beam with tails. Exposures given are $x10^{-9}$ Ccm^{-1}. Elements are 2nm x 2nm x 2nm. Exposure threshold is 100eV per element (a dot indicates that an element is exposed above the threshold). The centre of the beam is at the centre of the first (ie. left-hand) element (see figure 7.2).

Philips SEM (simulated as described in chapter 2), but for 100keV primary beam energy. The sensitivity will therefore be reduced from that for 50keV exposures by a factor which is estimated to be 1.8, because of the increased inelastic mean free path length - see section 7.3.3. Linewidths, however, should not be affected since the backscattering of high energy electrons from the substrate will be negligible at both 50 and 100 keV (see section 7.1).

It would be expected that some elements with dissipation below the threshold would become detached from the walls of the developed line, when elements further into the resist are able to dissolve. Since a full three-dimensional energy dissipation array was not stored it was necessary to devise a fairly arbitrary algorithm to determine from the dissipation array which elements would be removed. This is most easily explained with reference to the results, which are shown in figure 7.10 for the same data set as above. It is assumed that the line will not develop back to single elements above the dissipation threshold; however, two or more adjacent elements will dissolve and cause the elements to the left to be removed. It is also assumed that filaments of resist one element wide will dissolve, as will the elements at convex corners. This treatment is somewhat crude and could be improved considerably by handling full three-dimensional arrays.

Integrating the energy dissipation vertically through the resist (at the largest simulated dose) results in a plot of average energy dissipation against distance from the centre of the exposed line (figure 7.11). This is useful as a rough guide to the lateral variation of energy dissipation at all exposures, but such a plot does not indicate the statistical variation in exposure resulting in undeveloped regions of resist, as do the exposure threshold and development plots.

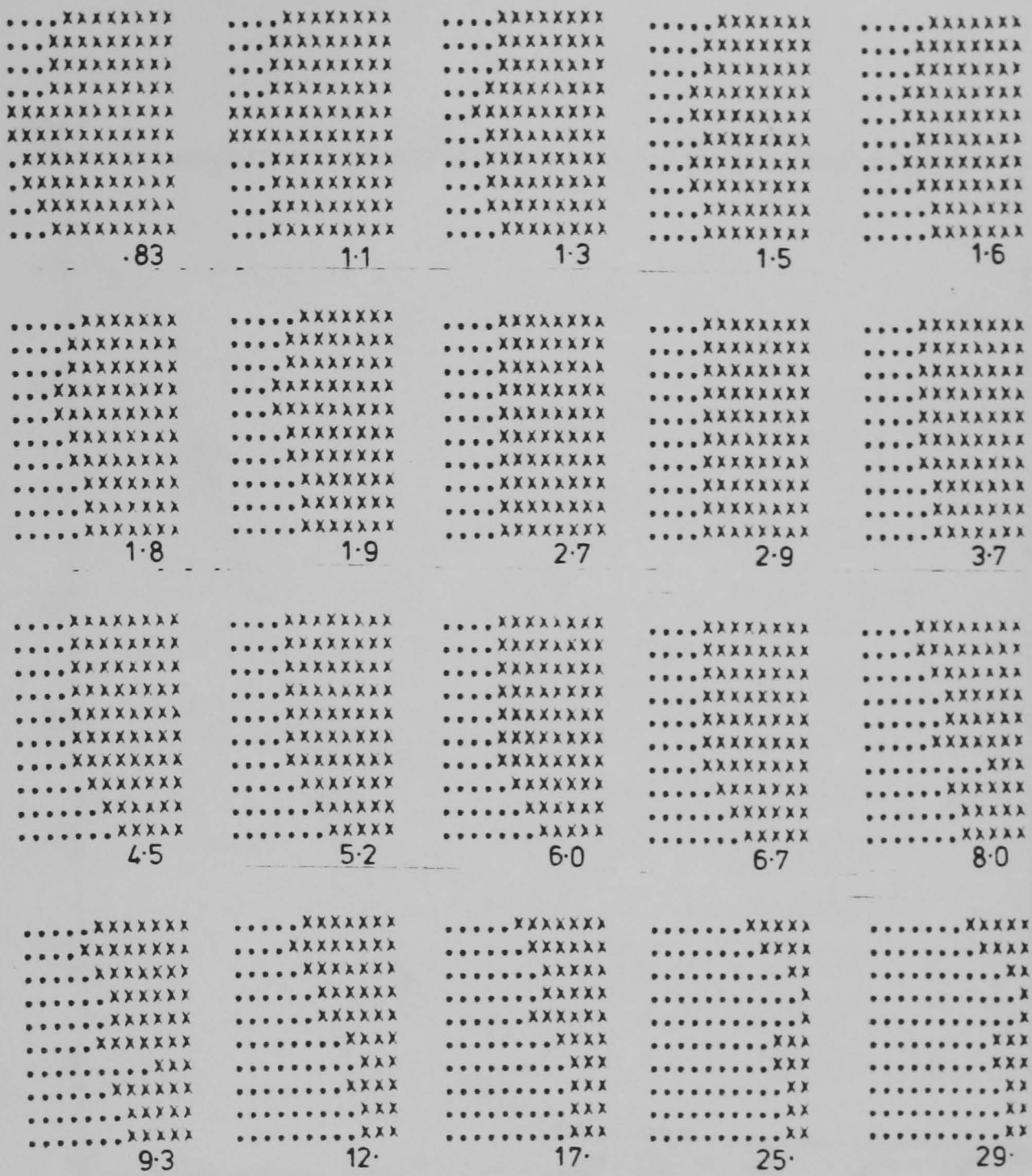

Fig. 7.10 Estimated development contours for the exposures shown in figure 7.9 (see text).

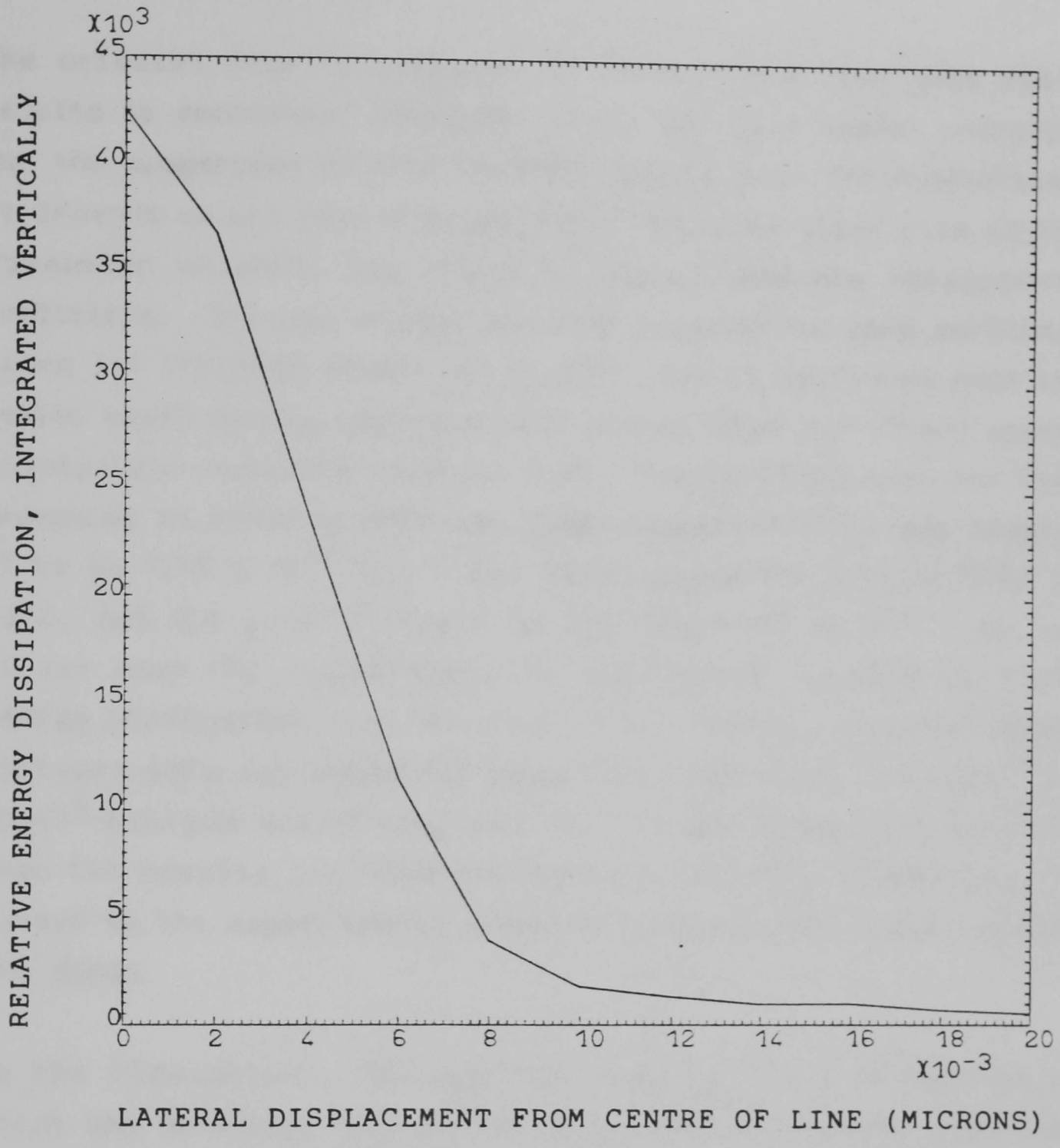

Fig. 7.11 Lateral variation in energy dissipation for exposure at 100keV by an 8nm diameter beam with tails. To achieve a smooth curve the plot is taken from the simulation at 2.9×10^{-8} Ccm^{-1}.

7.5.3 Critical dose

The critical dose is taken to be the minimum line dose which results in continuous developed lines, and is a useful criterion for the comparison of experimental results with the simulations. It depends on the resist sensitivity (related inter alia to the molecular weight), the electron energy, and the development conditions. The low energy exposure experiments were performed using 3:1 IPA:MiBK developer at 23°C, and it was found that the resist would develop approximately to the 100eV per $(2nm)^3$ energy dissipation contours (section 7.4). The critical dose for line exposures in Elvacite 2041 was found experimentally (see chapter 6) to be 1.14×10^{-9} Ccm^{-1} for development in 3:1 IPA:MiBK at 23°C, and 8.9×10^{-10} Ccm^{-1} in 2:1 IPA:MiBK at 21°C; in the former case the resist would be expected to develop to lower energy dissipation contours than in the latter, so development contours were estimated for both 100eV per $(2nm)^3$ and 50eV per $(2nm)^3$ minimum energy dissipation. It was found in most cases that the results for 100eV per element exposure threshold were closer to the experimental data, so usually only these results are shown.

In the simulations, the critical dose is taken to be that at which the developed line (obtained by the development algorithm of section 7.5.1) is continuous vertically in the cross section. Hence the critical dose for the simulations represented in figure 7.10 is approximately 1.3×10^{-9} Ccm^{-1}. This might represent a lower dose than the experimental critical dose, since the line can only be checked for vertical continuity in one cross-section, and not for horizontal continuity.

It is known from viscosity experiments that a critical number average molecular weight exists for entanglement of polymer molecules, M_c, and for PMMA M_c is about 16000 [7.14]. It is

necessary for the molecular weight to be reduced to below M_c in order for the polymer to develop, and of course in the case of random scissions (and considerable dispersivity in the original unexposed polymer) the average molecular weight may have to be reduced well below M_c for the material to be developed fully. If the energy dissipation is 100eV per $(2nm)^3$ and the G(scission) value is 1.7, then the number average molecular weight of Elvacite 2041, which is 186000 before exposure, will be about 3300 after exposure (the decrease in the number average molecular weight is approximately proportional to the number of bonds broken per molecule). Since the dispersivity of the exposed material approaches two after a few bonds are broken[7.14], the weight (and therefore volume) average molecular weight after exposure will be about 6600. This is of some significance which will be discussed later (section 7.7).

7.5.4 Estimation of linewidths

The linewidth can be taken as either the average or the minimum linewidth in the cross section; for the simulation of lift-off processing it might be thought that the latter is preferable since it indicates the width of a thin metal line that would be deposited within the resist line. However, near the critical dose the experimental linewidth is seen to vary considerably along the line, and the cross section only represents one point on the line. In addition, the minimum linewidth estimated from a half cross section (as recorded) can only increase in steps of twice the element size (ie. 4nm); such steps are quite coarse near the critical dose. For these reasons it has been found preferable to take the average linewidths in the development cross sections, although some results for minimum linewidths are also shown for comparison.

7.5.5 Linewidth-dose relationship for 8nm diameter beam

Figure 7.12 shows the average linewidths with increasing dose for 20nm thick PMMA on 70nm thick silicon nitride, at both 100eV and 50eV per $(2nm)^3$ energy dissipation thresholds. The data are taken from the simulation series used for figures 7.9 and 7.10. The beam profile was equivalent to that in the Philips SEM, and figure 7.12 also shows the experimental linewidths for 40nm thick PMMA (Elvacite 2041) exposed in this instrument (see chapter 6, section 6.3.3).

The energy dissipation at 50keV primary beam energy (experimental curve) would be expected to be about 1.8 times that at 100keV (simulations) for the same dose. The overall power law for the simulations is about 0.5; this is equal to the power law for the upper part of the experimental curve. The kink in the simulation curves is caused by different sets of simulations being used for the upper and lower parts of the curves; unfortunately, insufficient computer time was available to repeat the simulations in a single, complete set of runs. However, there does appear to be a more rapid increase in linewidth with dose in the simulations close to the critical dose (1.3×10^{-9} Ccm^{-1} for 100eV per element dissipation threshold).

Figure 7.13 shows the increase of the minimum linewidth with dose at 100eV per element dissipation threshold, for the same set of simulations as represented by figure 7.12; although the absolute linewidths are of course smaller, the power law is similar (about 0.5 overall).

It will be noted from figure 7.10 that undercutting of the resist occurs in the developed line; this has been noticed experimentally in thin single layer resists[7.12], and would be expected from the decrease in exposure over the top 10nm or so of resist (see section 7.5.2).

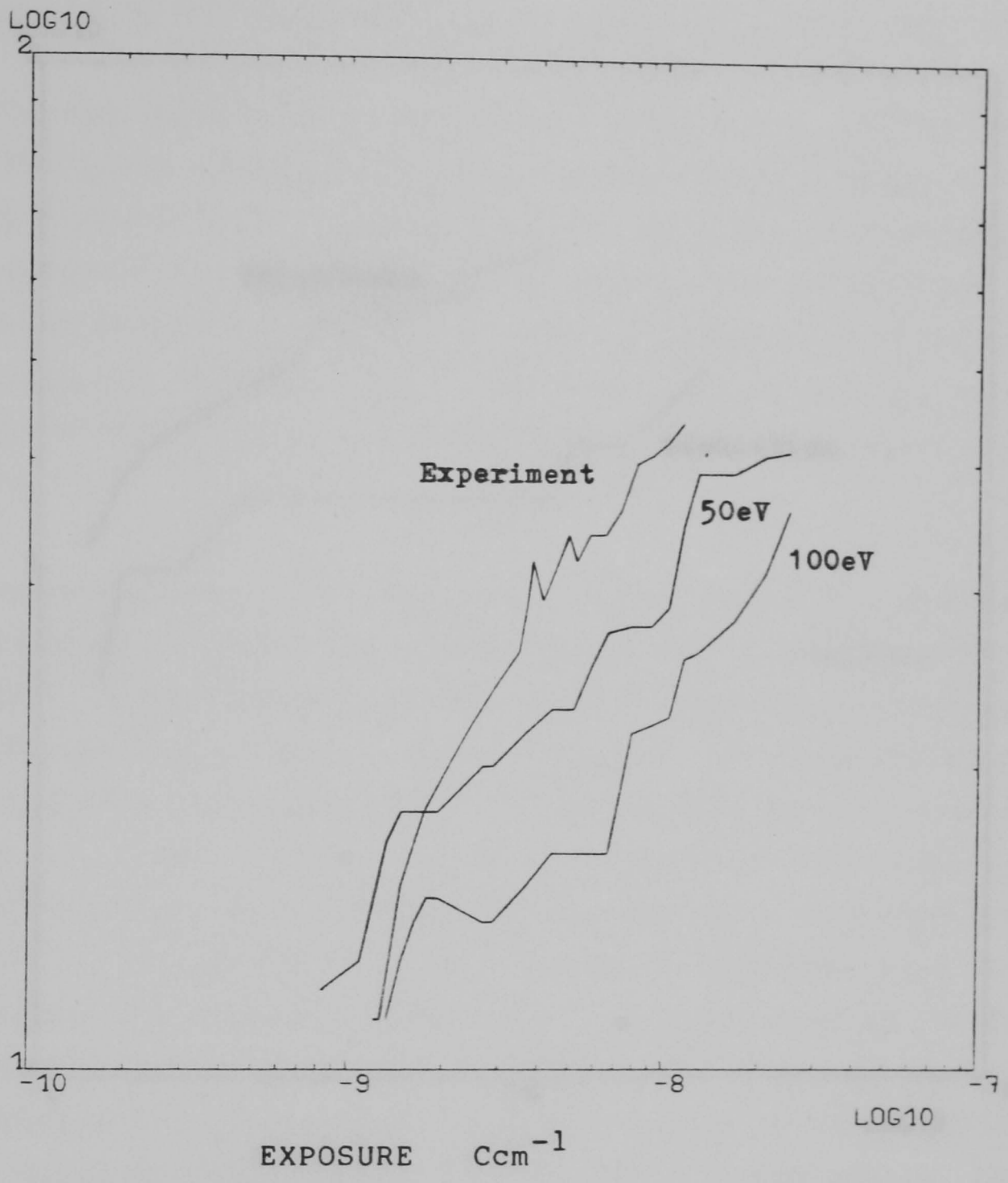

Fig. 7.12 Linewidth-exposure dose relationships for exposure by an 8nm diameter beam with tails, at 50keV (experiment - see figure 6.8) and 100keV (simulations). Simulated results are vertically-averaged linewidths at 50 and 100 eV per $(2nm)^3$ element, as shown in figure 7.10.

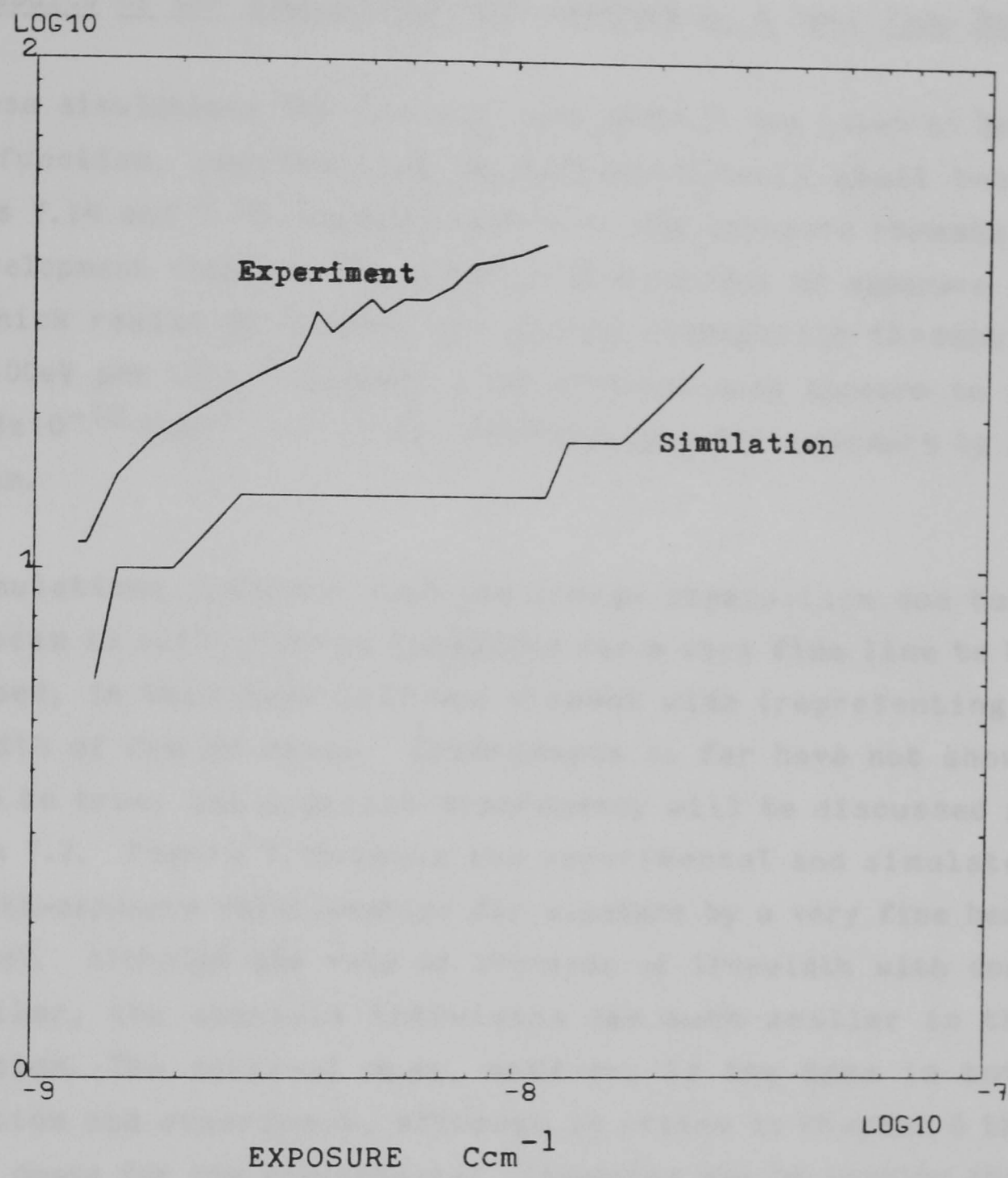

Fig. 7.13 Linewidth-exposure dose relationships for exposure by an 8nm diameter beam with tails. Experimental curve is taken from exposures at 50keV (see figure 6.8), and simulated results represent the minimum linewidths at each exposure in the plots shown in figure 7.10, the energy dissipation threshold being 100eV per element and the primary electron energy 100keV.

7.5.6 Results of the simulations for exposure by a very fine beam

For these simulations the incident beam profile was taken to be a delta function, representing an infinitesimally small beam. Figures 7.14 and 7.15 respectively show the exposure threshold and development contours for a set of simulations of exposure of 20nm thick resist at 100keV, the energy dissipation threshold being 100eV per $(2nm)^3$ element. The critical dose appears to be about $3x10^{-10}$ Ccm^{-1}, which is less than that for exposure by an 8nm beam.

The simulations indicate that the energy dissipation due to a small beam is sufficiently localised for a very fine line to be developed, in this case only one element wide (representing a linewidth of 2nm or less). Experiments so far have not shown this to be true; the apparent discrepancy will be discussed in section 7.7. Figure 7.16 shows the experimental and simulated linewidth-exposure relationships for exposure by a very fine beam at 100keV. Although the rate of increase of linewidth with dose is similar, the absolute linewidths are much smaller in the simulation. The critical dose, however, is the same in both simulation and experiment, although as stated in chapter 6 the nominal doses for the experimental linewidths may be smaller than the actual doses.

Figure 7.17 is a plot of the exposure dose (integrated vertically) against the distance from the centre of the exposed line, at the largest simulated dose. Although the central elements receive much more exposure than the next ones out, it is important to note that overexposure of many of the central elements is necessary in order to ensure that all of them receive more than the critical energy dissipation for development, because of the statistical variation of the exposure with depth.

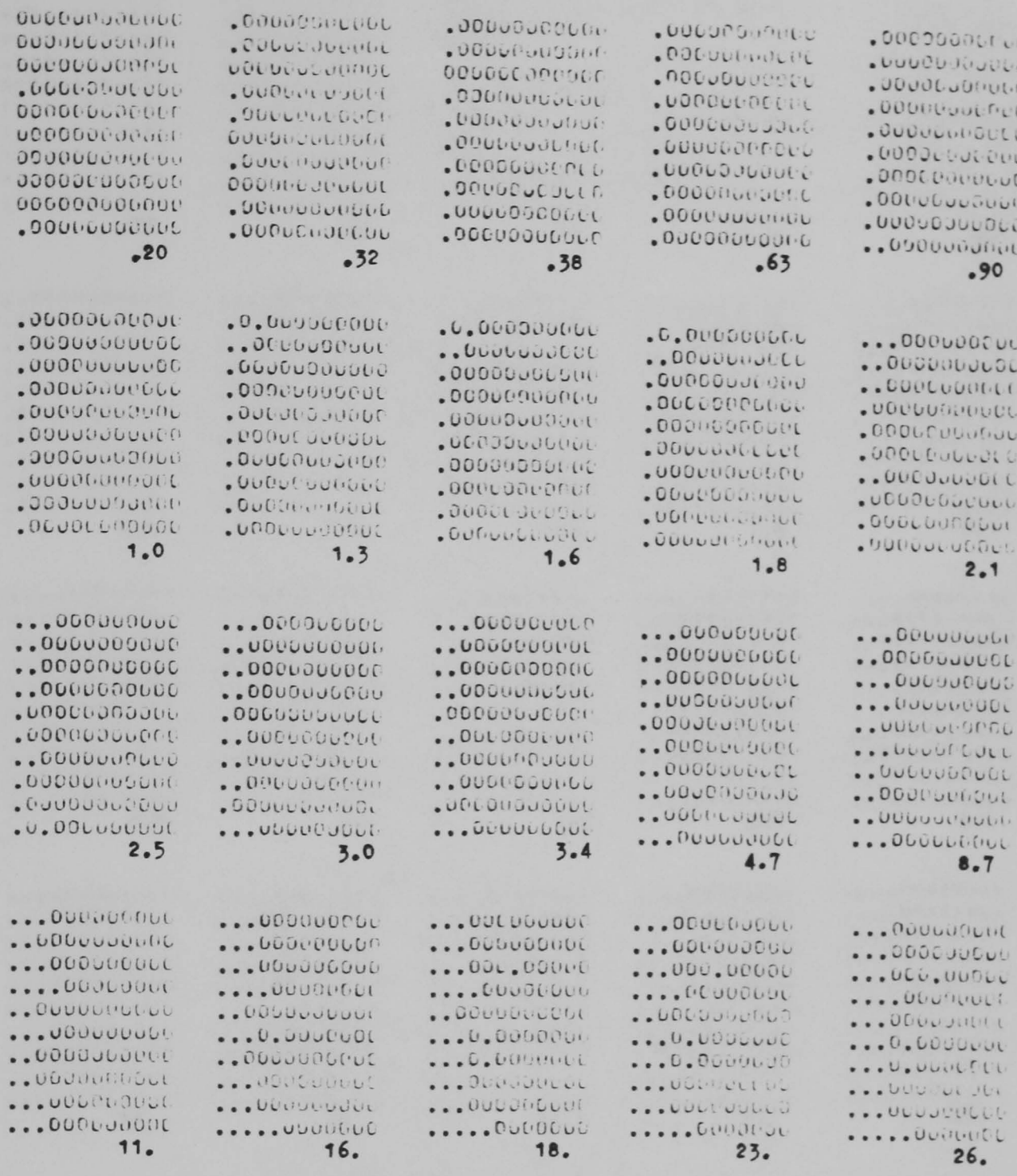

Fig. 7.14 Exposure threshold plots for 20nm thick PMMA on a 70nm silicon nitride substrate, exposed at 100keV by a very fine (ie. delta function) beam. Exposures given are $x10^{-9}$ Ccm^{-1}. Elements are 2nm x 2nm x 2nm. Exposure threshold is 100eV per element. The centre of the beam is at the centre of the first element.

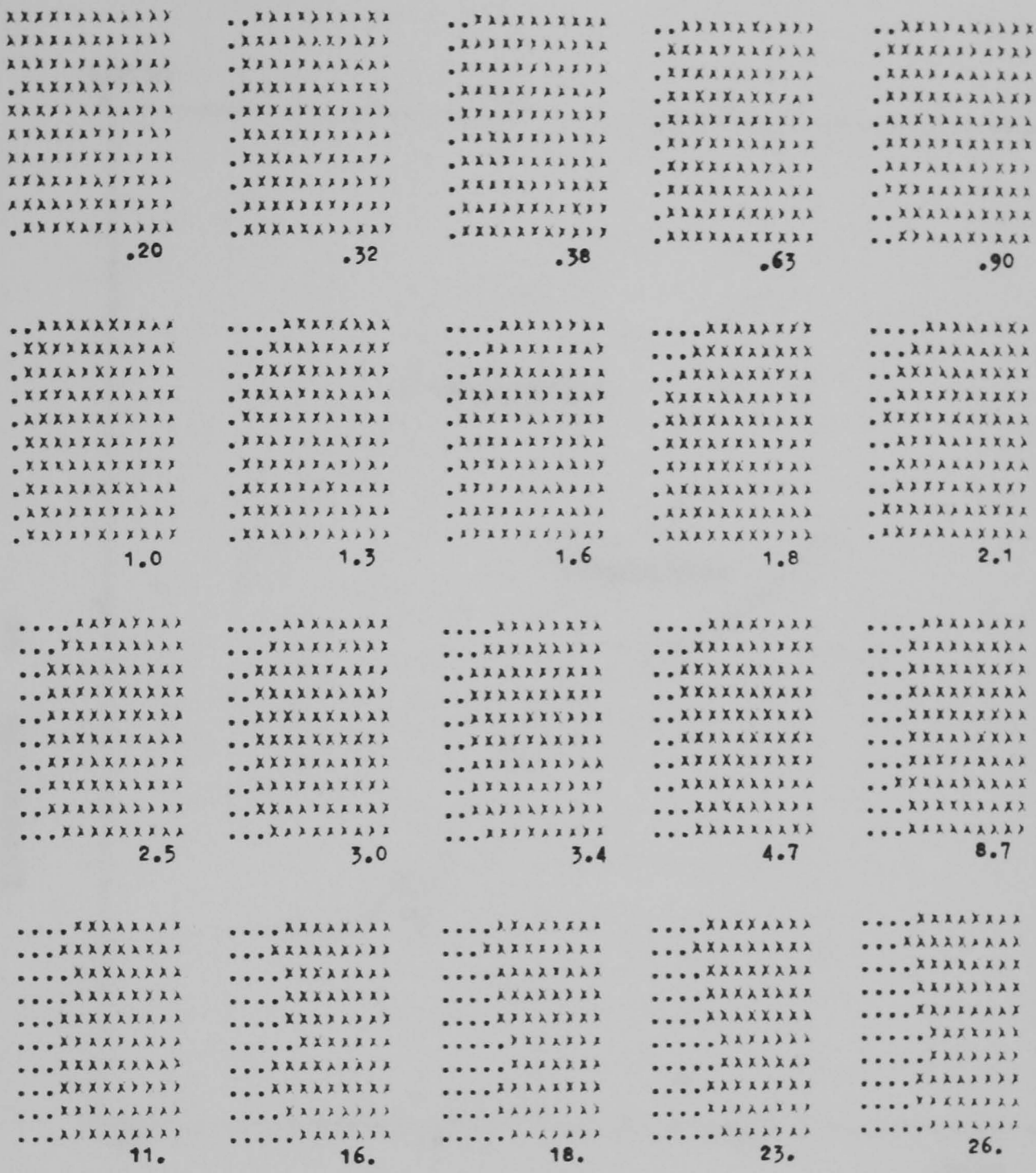

Fig. 7.15 Estimated development contour for the exposures shown in figure 7.14.

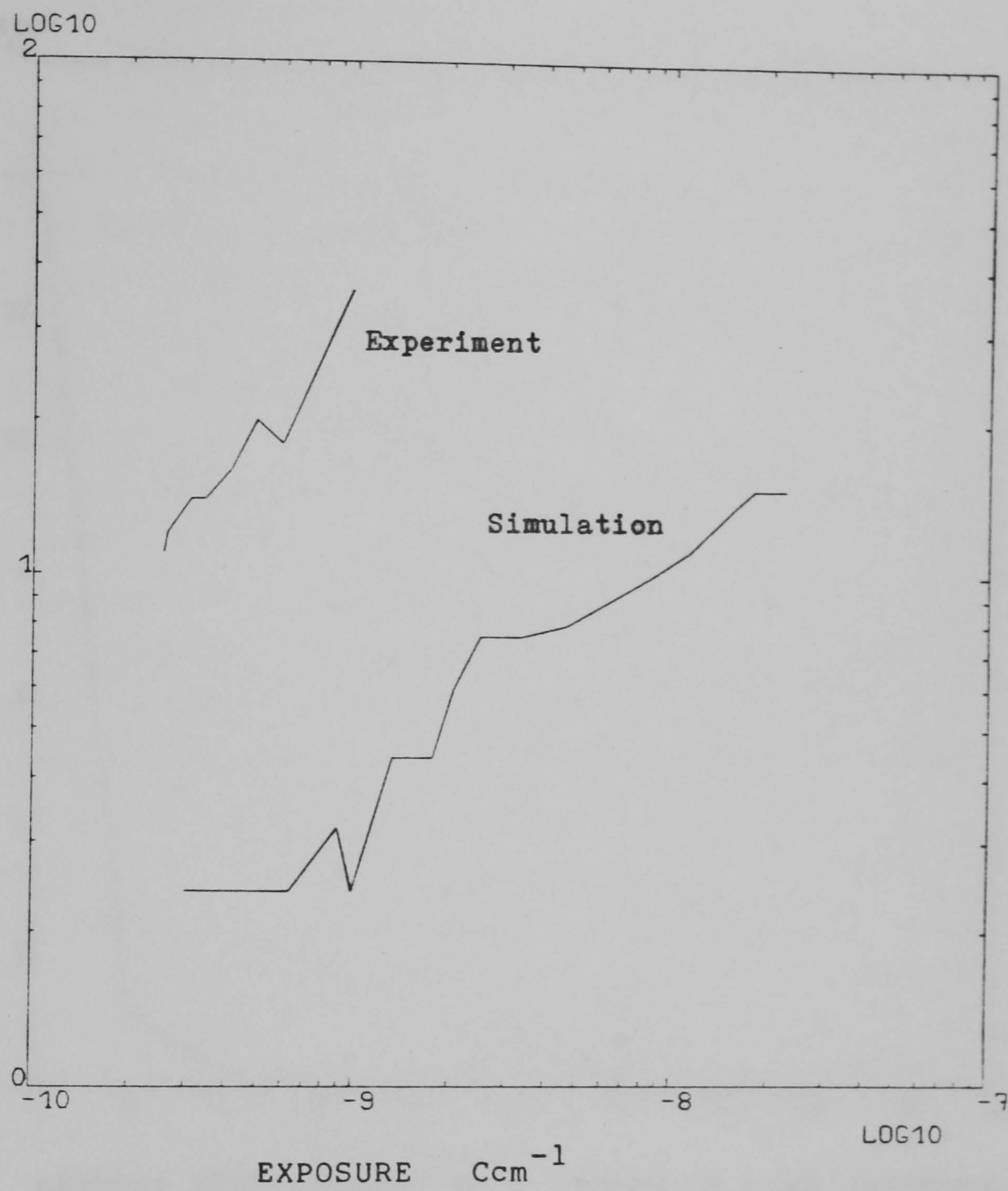

Fig. 7.16 Linewidth-exposure dose relationships for exposure by a very fine beam at 100keV. Experimental results are those shown in figure 6.6. Simulated results are vertically-averaged linewidths at 100eV per $(2nm)^3$ element, as shown in figure 7.15.

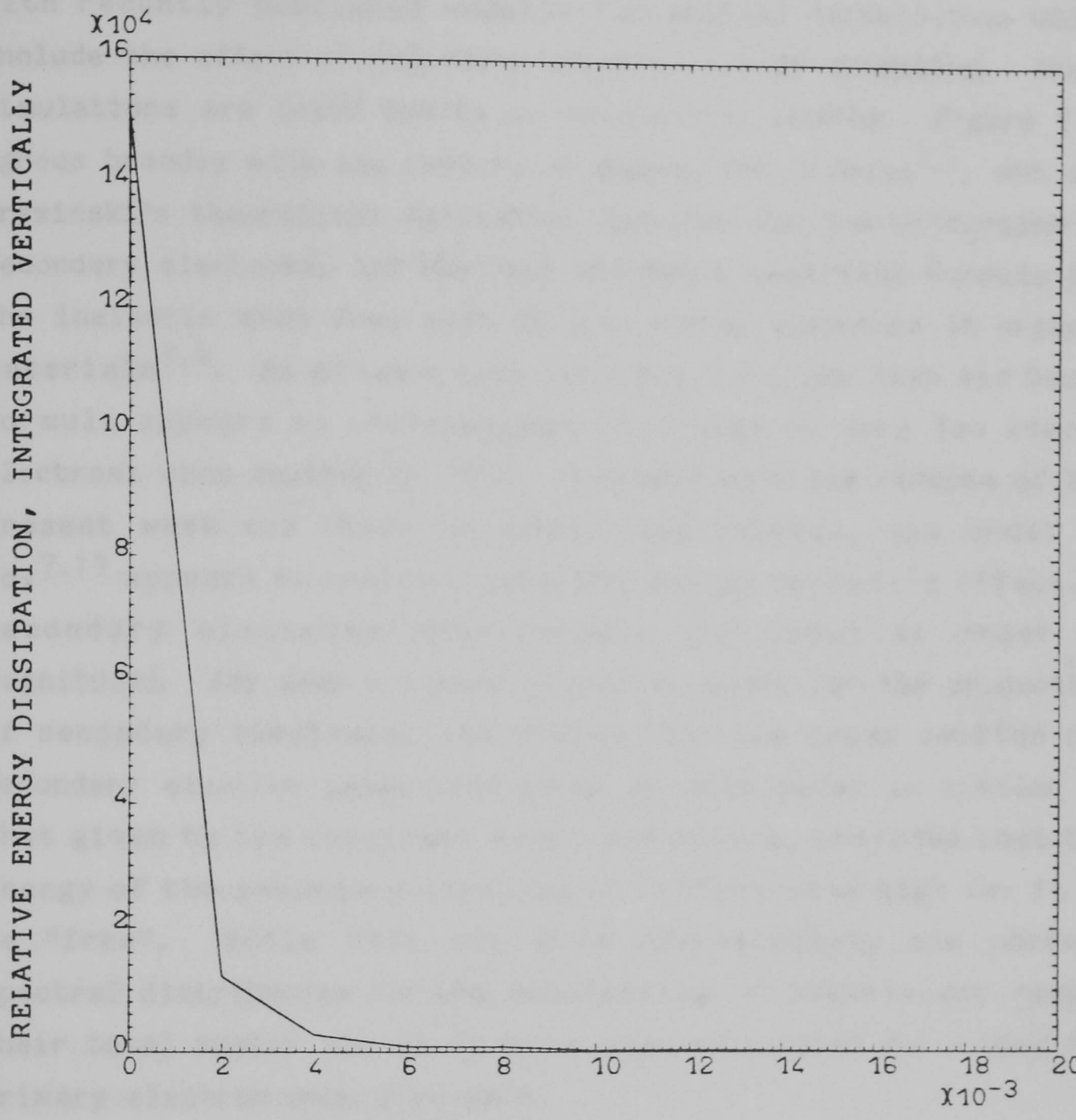

Fig. 7.17 Lateral variation in energy dissipation for exposure at 100keV by a very fine (ie. delta function) beam. The plot is taken from the simulation at 2.6×10^{-8} Ccm^{-1} exposure dose.

Figure 7.17 enables the Monte-Carlo simulation to be compared with recently published results for similar calculations which include the effect of secondary electron energy spreading. These simulations are based mainly on theoretical models. Figure 7.17 agrees broadly with the results of Samoto and Shimizu[7.3], who use Gryzinski's theoretical excitation function for the production of secondary electrons, and the Seah and Dench empirical formula for the inelastic mean free path of low energy electrons in organic materials[7.4]. As we have seen (section 7.4), the Seah and Dench formula appears to overestimate the range of very low energy electrons when applied to PMMA. Compared with the results of the present work and those of Samoto and Shimizu, the model of Joy[7.11] appears to overestimate the energy spreading effect of secondary electrons considerably (by about an order of magnitude). Joy uses a simple classical model for the production of secondary electrons, and states that the cross section for secondary electron production given by this model is similar to that given by the Gryzinski model and others, provided that the energy of the secondary electron is sufficiently high for it to be "free". While this may give approximately the correct spectral distribution for the secondaries of significant range, their total number may be in error when calculated for a specific primary electron mean free path.

7.6 Charging of resist

A Monte-Carlo simulation which includes secondary electrons should result in a more accurate net charge balance in the resist and substrate than one which does not. In the present simulation electrons are tracked until their energy is less than 5eV; below this energy their range may increase considerably, but they would then be influenced by local potential gradients and move in a direction to neutralise charging fields created by higher energy

electrons in an insulating resist or substrate. Accurate determination of charging is therefore very difficult but the simulation can be used to predict the polarity of the charging, and also which situations are more likely to cause charging problems.

The results given here are normalised to the total number of incident primary electrons; since secondary electrons are created in the resist and substrate the (normalised) number of transmitted electrons can therefore exceed unity.

In the simulation of 20keV exposures of 300nm thick PMMA on solid silicon nitride, transmission into the substrate is about 1.05, backscattering from the substrate into the resist 0.5, and loss of electrons from the surface of the resist 0.3. There is therefore a net increase of the number of electrons in the resist of 0.15, and the resist as a whole would charge negatively. However, since the resist is relatively thick and electrons are lost from the top surface, the top of the resist may charge positively by up to 0.3. It has not been found necessary in the exposure of 300nm thick resist on a conducting substrate to overcoat the resist with a thin layer of metal, although insulating substrates are usually metallised. It is therefore presumed that the conduction mechanism in PMMA will neutralise sufficiently the potential gradient through the film, to avoid defocusing of the beam during exposure (which would occur with potentials greater than a few hundred volts).

In the case of thin films of PMMA (20-80nm) on 70nm thick silicon nitride membranes, and exposed at 100keV, the transmission into the substrate is 1.0025, backscattering 0.015, and loss from the top surface 0.002, while 1.015 are transmitted through the entire resist and substrate. At 50keV these values are 1.0045, 0.027, 0.004, and 1.03 respectively (the inelastic mean free path length is shorter than at 100keV so more secondaries are created). It

might be noted that the magnitude of the charging in thin films is at least an order of magnitude less than that in thicker resist on a solid substrate, as above.

In thin substrate work it would be expected that the resist and support film as a whole would charge positively, but since the resist alone gains more electrons than it loses it may charge negatively if the conduction mechanism is insufficient to neutralise the potential gradient through the film during the exposure. It is thought that a very intense beam such as that in the HB5 scanning transmission microscope would be more probable to cause the resist to charge negatively during exposure, hence repelling secondary electrons and increasing their energy spreading effect. This may explain the ability to develop 36nm wide lines using an intense electron beam of diameter less than 1nm (see figure 6.5), despite the simulated lateral distribution of energy dissipation shown in figure 7.17.

Evidence of negative charging of the resist during exposure would be a change in the rate of increase of linewidth with exposure, for different beam currents; however, it might be found that the negative charging of the resist is almost independent of the rate of exposure, since the excitation (and therefore the discharging mechanism) is also related to the beam current. It should also be noted that the use of a thinner substrate would result in less secondary emission into the resist and would therefore reduce the negative charging effect. These points might be investigated further when the new high-resolution electron beam machine becomes available within the Department.

A possible result of positive charging of the membrane is that low energy electrons created during the exposure of a feature might be attracted towards the positive charge deposited at a previously exposed neighbouring feature, for example in the exposure of closely spaced lines.

Although these effects can be suggested, and might be investigated experimentally, they have not been included in the Monte-Carlo calculation since the conduction mechanisms within the resist and subtrate, which are excited during exposure, are very difficult to quantify.

7.7 Discussion and conclusions

It has been shown that the Monte-Carlo simulation described here results in approximately the same critical dose, and rate of increase of linewidth with dose, as the experimental measurements. The agreement of simulation and experiment for an 8nm diameter beam is good, but it is predicted that exposure by a very fine beam will result in continuous lines as narrow as 2nm or less. This was not found in practice, and the use of a very fine beam was found to result in linewidths no less than those produced by an 8nm diameter beam (ie. about 10nm). Although exposure control in the case of the very fine beam was not as accurate, the simulations of exposure by a fine beam indicate a wide exposure latitude for 2nm wide lines.

The weight (and therefore volume) average molecular weight in the experiments was 360000 before exposure (Elvacite 2041) and about 6600 after exposure (section 7.5.3). Not allowing for entanglements, the original molecule might occupy a sphere 8nm in diameter. There are thought to be only a few entanglement points per molecule, so the overall molecular dimension should not be very much larger than this. The molecule might appear as a ball of string, entanglements with other molecules occurring near its perimeter.

If after exposure a molecule is only able to dissolve as a whole, then it would be expected that the narrowest lines produced in

very thin (1-2 molecules thick) resist would vary in width between one and two molecules, or 10-20nm. Linewidth control in practice is better than this (see for example figure 6.2), and it has therefore been thought that the molecules are able to dissolve partially. An explanation for the results presented here, however, could be that it is not possible to cut through the centre of a molecule without the whole of the molecule dissolving, while it is possible to cut through one side of the molecule and much of the other side will remain, supported by its entanglement with other molecules. The minimum linewidth would then be limited approximately to the diameter of the molecule.

The minimum molecular weight necessary for entanglement of PMMA molecules is 16000 (number average); with a low dispersivity value of, say, 1.2 the weight average molecular weight would be about 19000. The diameter of the molecules would then be 3.7nm, assuming that the molecule is sufficiently large (at 190 monomer units) for its shape to be approximately spherical. This may lead to higher resolution, but it might be thought that the resist would then be more sensitive and the exposure could become discontinuous with depth. However, it is estimated that to break down such a polymer to a number average molecular weight of 3300 would require 80eV per 2nm element, rather than 100eV for Elvacite 2041, and reference to figure 7.17 indicates that such a difference in sensitivity should be insignificant.

A number average molecular weight of 16000 should be regarded as a theoretical lower limit for the use of PMMA as a resist; in practice the entanglement of molecules will not be very great and unexposed material will dissolve quite rapidly in the developer. The resist contrast might then be unacceptably low, and although it has not been possible to include the effect of resist contrast in the treatment presented here, it has been assumed that the contrast is sufficient for the resist to develop out to definite energy dissipation thresholds. With carefully controlled

development conditions it might be possible to use a low dispersivity polymer of molecular weight about 48000 (weight average), the molecules in this case being about 5nm in diameter, assuming them to be spherical. This may result in a worthwhile improvement in the minimum linewidth.

In conclusion, the secondary electron Monte-Carlo simulation predicts approximately the correct rate of increase of linewidth with dose, and the correct critical dose for development through a fine line in PMMA. However, the minimum linewidth for exposure by a very fine electron beam appears to be limited by the molecular size of the polymer, and although it is possible to remove some material from a molecule without the entire molecule being dissolved, it does not seem to be possible to expose and develop a fine line through a molecule. Local charging effects might also play some part in the discrepancy between the experimental and simulated results for the exposure of thin PMMA by a very fine electron beam. It is tentatively suggested that some reduction in minimum linewidth may be obtained by the use of a low dispersivity polymer of molecular weight not greatly above that necessary for entanglement.

References

7.1 R.J. Hawryluk, A.M. Hawryluk, and H.I. Smith "Energy dissipation in a thin polymer film by electron beam scattering" J. Appl. Phys. 45(6), 2551-2566, 1974.

7.2 R. Shimizu, Y. Kataoka, T. Ikuta, T. Koshikawa, and H. Hashimoto "A Monte Carlo approach to the direct simulation of electron penetration in solids" J. Phys. D: Appl. Phys. 9, 101-114, 1976.

7.3 N. Samoto and R. Shimizu "Theoretical study of the ultimate

resolution in electron beam lithography by Monte Carlo simulation, including secondary electron generation: Energy dissipation profile in polymethylmethacrylate"
J. Appl. Phys. 54(7), 3855-3859, 1983.

7.4 M.P. Seah and W.A. Dench; Surf. Interface Anal. 1(2); 1979.

7.5 L. Reimer "Quantitative scanning electron microscopy"
Lecture notes, 25th Scottish Summer School in Physics, Glasgow, 1983.

7.6 B.P. Nigam, M.K. Sundaresan, and Ta-You Wu; Phys. Rev. 115, 491, 1959.

7.7 M. Berger and S. Seltzer; Natl. Acad. Sci.-Natl. Res. Council Publ. 1133, 205, 1964.

7.8 M. Hatzakis "Electron resists for microcircuit and mask production"
J. Electrochem. Soc.: Electrochem. Technol.; 116(7); 1033-1037; 1969.

7.9 K. Murata, D.F. Kyser, and C.H. Ting "Monte Carlo simulation of fast secondary electron production in electron beam resists"
J. Appl. Phys. 52(7); 4396-4404; 1981.

7.10 D.F. Kyser "Monte Carlo simulation of spatial resolution limits in electron beam lithography"
Conference proceedings; "Electron beam interactions with solids for microscopy, microanalysis, and microlithography"; Asilomar, 1982.

7.11 D.C. Joy "The spatial resolution limit of electron beam lithography"

Submitted to "Microelectronic Engineering" 1983.

7.12 M.A. Grant; Final year B.Sc.(Eng.) project, Glasgow University, 1983.

7.13 M.J. Bowden "Electron irradiation of polymers and its application to resists for electron beam lithography"
CRC Critical Reviews in Solid State Sciences, pp. 223-264, February 1979.

7.14 V.K. Sharma, S. Affrossman, and R.A. Pethrick "Electron beam lithography - influence of molecular characteristics on the performance of positive resists"
(To be published.)

7.15 I. Adesida, R. Shimizu, and T.E. Everhart "Monte-Carlo simulation of electron penetration through thin films of PMMA"
Appl. Phys. Lett. 33(10), 849-850, 1978.

CHAPTER 8

Low energy electron exposure of arsenic trisulphide inorganic resist

8.1 Introduction

Arsenic trisulphide (As_2S_3) is an amorphous chalcogenide glass resist. Such materials have attracted some attention as photo- or electron beam resists since their amorphous property promises potentially very high resolution[8.1-8.3]. In the most common resist system utilising this material, the arsenic trisulphide is evaporated onto a substrate (in thicknesses of up to 1 micron), and a thin layer of metallic silver (20-50nm) is evaporated onto the surface. The silver acts as a sensitising layer and on exposure to light, by a process known as photodoping or photodissolution[8.4-8.7], silver ions migrate into the resist, rendering it insoluble by an alkaline developer. The use of silver chloride rather than silver as the sensitising layer has been found to result in increased sensitivity[8.8]; however, this resist system is sensitive to yellow light and therefore cannot be handled safely in standard clean-room conditions, and also suffers from poor resolution due to clustering of the dissociated silver[8.10].

It was found that a layer of silver sulphide (Ag_2S) is formed at the interface between silver and arsenic trisulphide, which was thought to be the source of the doping ions[8.7], and later it was discovered that a thin layer of Ag_2S (about 10nm) could be formed directly on the surface of the As_2S_3 by immersing it for a short time in silver nitrate solution. This sensitisation method has been found to result in a stable resist system whose sensitivity at 12keV is about 4×10^{-3} Ccm^{-2} [8.9,8.10].

Experiments have been performed in this Department, by B. Singh, on the electron beam exposure of Ag_2S/As_2S_3 resist, and it was decided to perform some experiments, in collaboration with him, on low energy electron exposure of the material. It was thought that the important electron interactions would take place at or near the interface between the Ag_2S and the As_2S_3, and that there would therefore be a threshold electron energy, corresponding to the range of the electrons in the Ag_2S being just sufficient for them to penetrate to the interface, below which no doping would take place.

The work presented here represents a further use of the low-energy electron exposure system described in chapter 3. It is pointed out in chapter 9 that there may be some advantage for high resolution lithography in the use of an amorphous resist which is sensitive only to higher energy electrons (say above 100eV); the low energy exposure technique enables arsenic trisulphide to be evaluated on this basis, and also elucidates the exposure mechanism of this material.

8.2 Experimental method

About 100nm of As_2S_3 was deposited by vacuum evaporation onto a silicon substrate, at a source temperature of 312°C, which is just above the melting point of the As_2S_3 glass. The deposition rate was 0.1-0.3 nm per minute, and the source temperature was controlled to within 1°C. The film was annealed at 190°C for one hour in nitrogen at atmospheric pressure, to form the stoichiometric compound As_2S_3 [8.10], and was then immersed in silver nitrate solution (concentration 1g:10ml) for 1 minute at 21°C, thereby forming a 10nm-thick layer of Ag_2S on the surface. After exposure the Ag_2S was removed by etching in a solution of iodine and potassium iodide.

The exposures were performed in the low energy electron exposure system as described in chapter 3. All exposures of less than 500eV energy made use of the deceleration arrangement, the anode potential in most cases being 500V. Tests were undertaken to ensure that the resist was not exposed by the light from the cathode filament; no effect was noted over the maximum exposure times involved (about 30 minutes).

The resist was developed in a mixture of 1 part AZ developer, 20 parts isopropyl alcohol, and 30 parts deionised water, as described by Singh et al.[8.9]. The development was usually allowed to proceed until the unexposed areas had just cleared, which was after about 1 minute at 21°C; the specimen was then rinsed in deionised water and blown dry. The resist thickness after development was measured by means of the Talystep surface profile plotter.

The specimens were processed and loaded into the exposure system under yellow light. Further details of the film preparation and development procedures are given by Singh et al.[8.9]

8.3 Results and discussion

It was found that, contrary to our expectation, it was possible to expose the sensitised arsenic trisulphide resist (ie. render it insoluble in the developer) with electrons of all energies in the range 10-2500eV. The minimum exposure dose required to produce a visible effect with incident electron energies of a few hundred electron volts was about 10^{-4} Ccm^{-2}, but the sensitivity was found to vary with electron energy. Figure 8.1 shows the effect of exposure dose on remaining thickness after development, at 300, 100, and 45eV; however, it should be noted that the exposure became difficult to determine accurately below 100eV

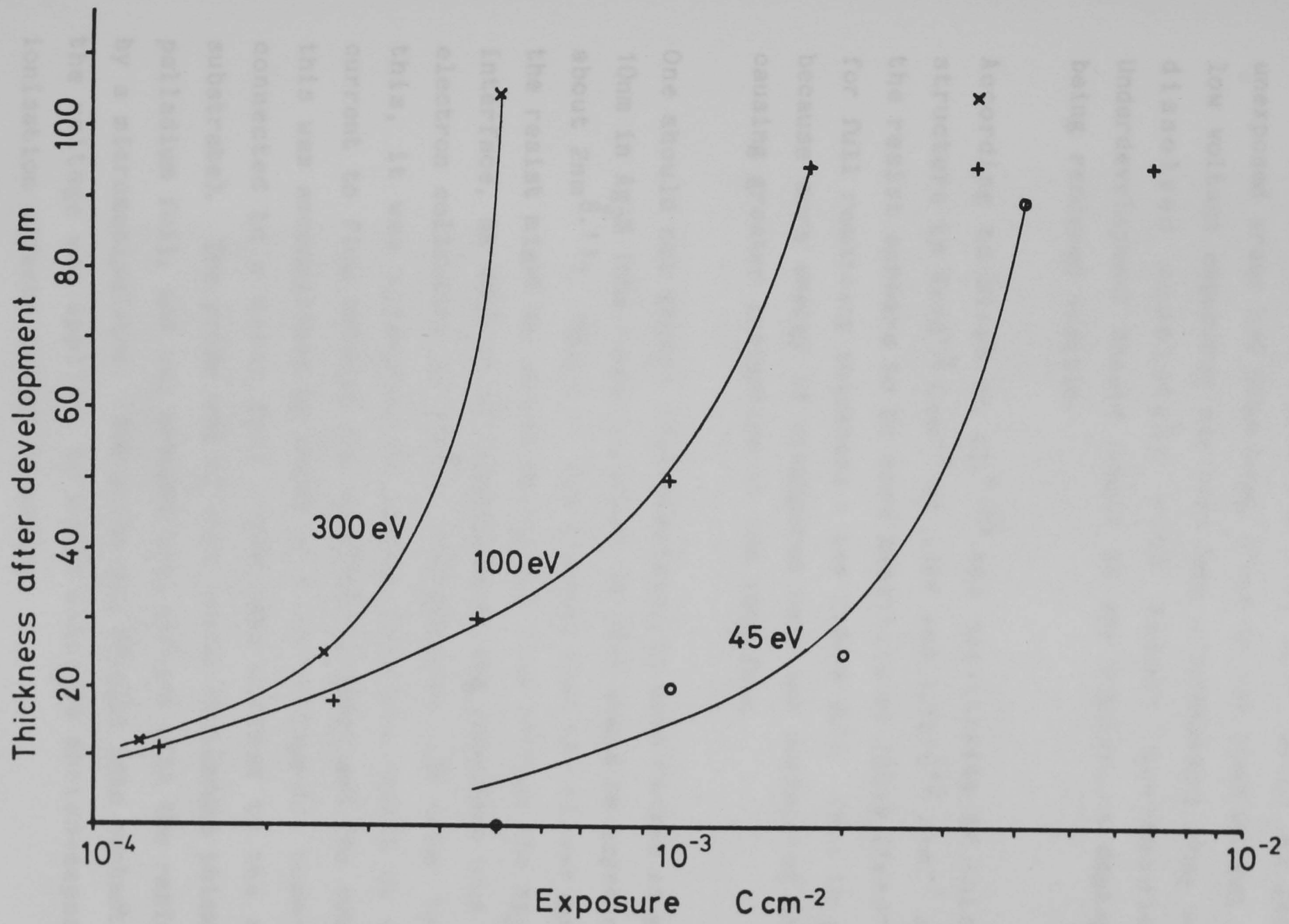

Fig. 8.1 Remaining thickness of arsenic trisulphide resist after exposure by low energy electrons, and development. Initial resist thickness was about 100nm.

since the current density became uneven (see chapter 3). Optical micrographs of exposed and developed areas (at 500eV and 10eV) are shown in figure 8.2. The resist film in figure 8.2(b) (and in figure 8.3) was developed only until about 60-80% of the unexposed areas had dissolved, since it was thought that the very low voltage exposures may have been underexposed; they sometimes dissolved completely with slight overdevelopment. Underdevelopment should result in any significant doping effect being rendered visible.

According to Singh et al.[8.10] the sensitivity of this resist structure is $4x10^{-3}$ Ccm^{-2} at 12kV and $1.3x10^{-2}$ Ccm^{-2} at 25kV; the resist appears to be more sensitive at 300eV ($5x10^{-4}$ Ccm^{-2} for full remaining thickness - see figure 8.1). This is probably because more energy is dissipated near the surface of the film, causing greater ionisation at the interface.

One should not expect 10eV electrons to have ranges as great as 10nm in Ag_2S (the range in silver at 30eV would be expected to be about 2nm[8.11]). Hence it was thought that the silver doping of the resist might be caused by current flow through the Ag_2S/As_2S_3 interface, as well as by ionisation at the interface (due to fast electron collisions or photon interactions). In order to verify this, it was attempted to silver dope the resist by causing current to flow between the sensitising layer and the substrate; this was accomplished by means of a low voltage d.c. power supply connected to a metal foil probe (and earthed to the silicon substrate). The probe was of thin (about 10 microns thick) gold-palladium foil, and was brought into contact with the resist film by a micromanipulator. The probe was brought into contact before the voltage was applied, to avoid possible photon-exposure or ionisation effects caused by arcing.

It was found in many cases that the current flow was unstable, due to mechanical damage of the resist and consequent shorting of

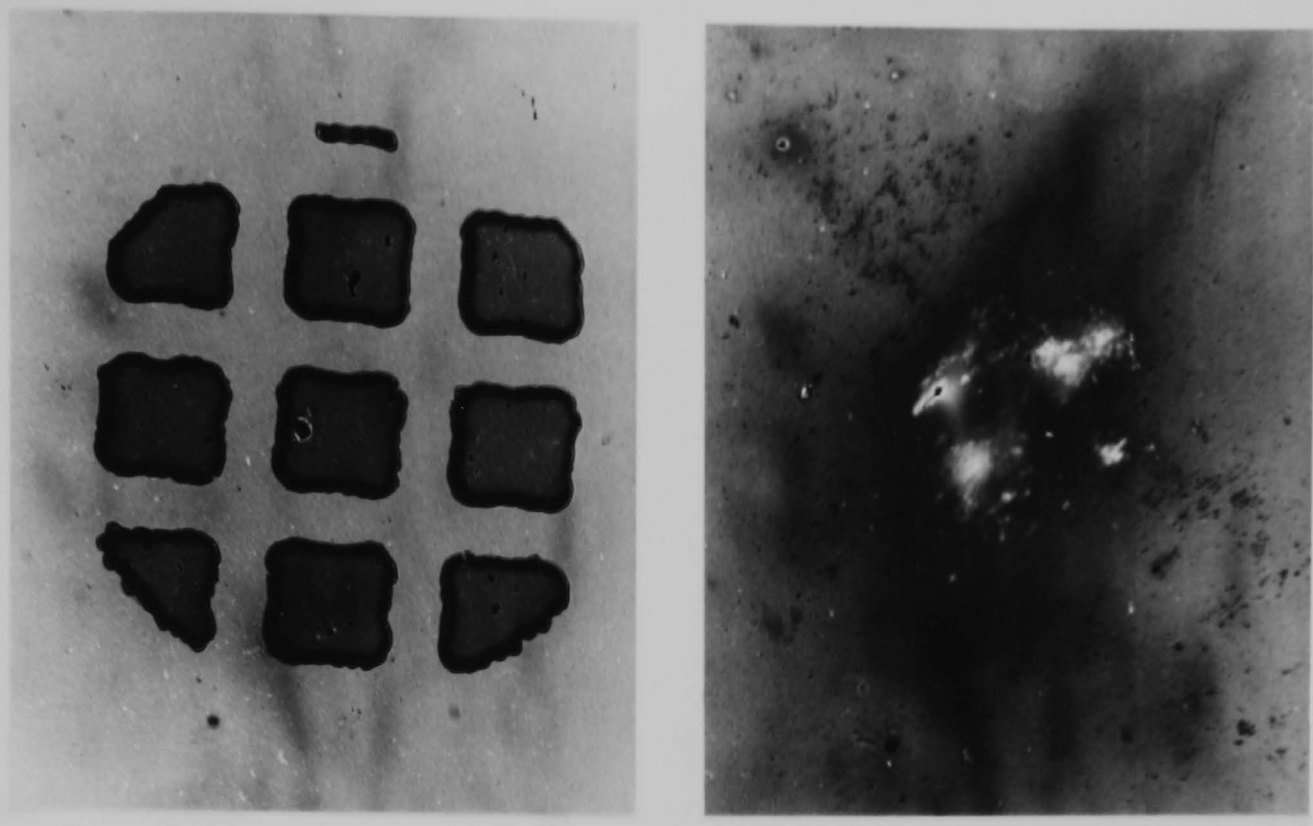

Fig. 8.2 Exposed and developed areas of 0.1 micron thick sensitised As_2S_3 on silicon; (a) at 500eV, exposure $4x10^{-3}$ Ccm^{-2}; (b) at 10eV, exposure approx. $3x10^{-3}$ Ccm^{-2}.

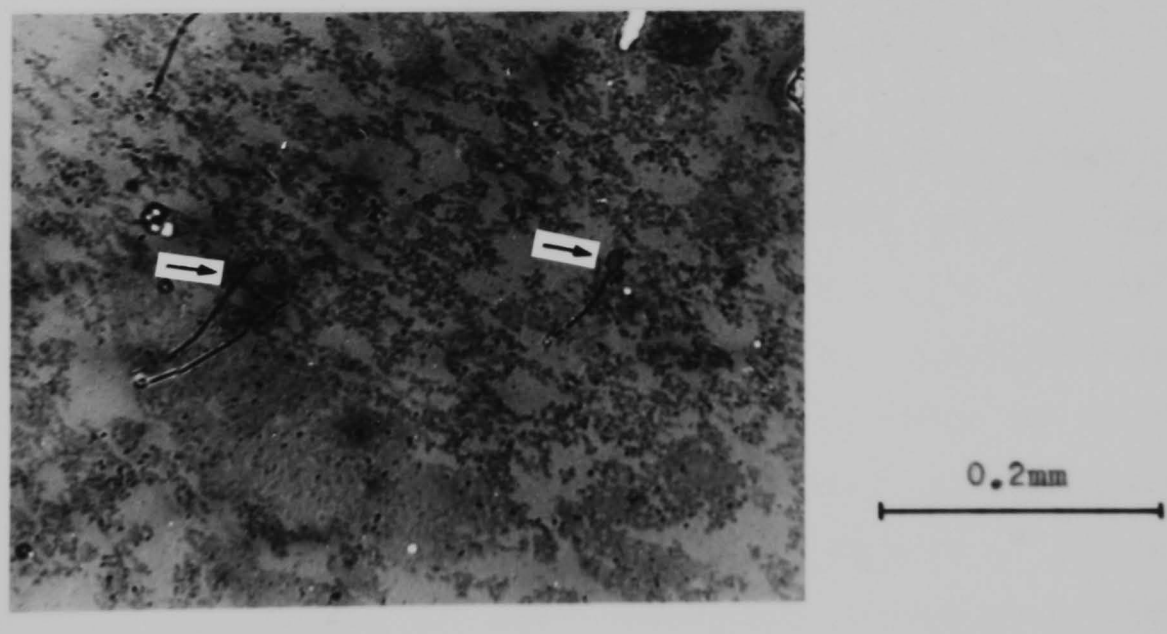

Fig. 8.3 Exposure by current flow of 0.1 micron thick sensitised As_2S_3. The developed tick marks (indicated by the arrows) were exposed by a metal foil probe biased at -10V; exposure charge density approximately $8x10^{-2}$ Ccm^{-2}.

the probe to the substrate. However, if mechanical damage did not occur and the probe was negatively biased, a steady current would flow and silver doping of the resist under the probe would occur, which would be apparent after development (see figure 8.3).

A steady current did not flow from a positively biased probe, and when the probe was negatively biased the current was about $5x10^{-9}$ A for 10V bias, and $5x10^{-4}$ A for 20V bias, although these values are only approximate and an accurate I-V characteristic would be difficult to obtain using the present apparatus. In addition, the current measurement circuit was not sufficiently sensitive to determine whether a forward bias threshold voltage existed. However, the properties would appear to be those of a semiconductor junction between the n-type Ag-S and the p-type As_2S_3 amorphous semiconductor (the silicon substrate was p-type), and the silver doping effect would agree with the model of Suzuki et al.[8.7] who propose that the silver is ionised by holes moving from the As_2S_3 through the junction, and diffuses into the As_2S_3 under the influence of the field created by trapped electrons in this material (in the case discussed here this may occur after the external bias is removed).

The estimated charge density deposited for the exposure shown in figure 8.3 was $8x10^{-2}$ Ccm^{-2}, which is considerably greater than that for the 10eV electron exposure of figure 8.2(b) ($3x10^{-3}$ Ccm^{-2}). However, it was not practical to give a smaller dose than this (or a larger dose in the electron exposure) so it is not known whether the sensitivity in the two cases is identical; it may well be so because the current induced doping of figure 8.3 has appeared to result in more thorough fixation of the resist.

8.4 Conclusion

It has been found that the silver sulphide/arsenic trisulphide inorganic resist system can be exposed by low energy electrons and that no threshold energy for exposure exists, at least above 10eV. The sensitivity of this resist in the hundreds of eV range appears to be higher than in the tens of keV range, indicating that ionisation near the surface is an important mechanism in its exposure. However, it was also found that current flow through the Ag_2S/As_2S_3 interface, which appears to form a rectifying semiconductor junction, can also result in exposure of the resist, and that the sensitivity for exposure by this method may be similar to that for very low energy (10eV) electron beam exposure. Silver doping of the resist by current flow would be in accordance with a proposed model for the photodoping process, in which the silver is ionised by holes passing from the As_2S_3 through the interface.

References

8.1 A. Yoshikawa, O. Ochi, N. Nagai, and Y. Mizushima
Appl. Phys. Lett. 31, 161, 1977.

8.2 K.L. Tai, L.F. Johnson, D.W. Murphy, and M.S.C. Chung
155th Electrochem. Soc. Meeting, Boston, 1979.

8.3 K.D. Kolwicz and M.S. Chang
J. Electrochem. Soc. 127, 137, 1980.

8.4 H. Kokado, I. Shimizu, and E. Inoue "Discussion on the mechanism of photodoping"
J. Non-Crystalline Solids 20, 131-139, 1976.

8.5 D. Goldschmidt and P.S. Rudman "The kinetics of

photodissolution of Ag in amorphous As_2S_3 films"
J. Non-Crystalline Solids 22, 229-243, 1976.

8.6 J. Malinowski and A. Buroff "Photostimulated solid state reactions"
Contemp. Phys. 19(2), 99-108, 1978.

8.7 T. Suzuki, Y. Hirose, and H. Hirose "A model of the photodoping mechanism in the Ag/Ag_2S_3 system"
Phys. Stat. Sol. (a) 72, K165, 1982.

8.8 M.S. Chang, T.W. Hou, J.T. Chen, K.D. Kolwicz, and J.N. Zemel "Inorganic resist for dry processing and dopant applications"
J. Vac. Sci. Technol. 16(6), 1973-1976, 1980.

8.9 B. Singh, S.P. Beaumont, G. Stewart, and C.D.W. Wilkinson "An improved process for introducing silver into As_2S_3 resist"
Proc. 161st Electrochem. Soc. Meeting, Montreal, Canada, 1982.

8.10 B. Singh, S.P. Beaumont, P.G. Bower, and C.D.W. Wilkinson "New inorganic electron resist system for high resolution lithography"
Appl. Phys. Lett. 41(9), 889-891, 1982

8.11 H. Sugiyama
Bull. Electrotech. Lab. 33, 277-290, 1974.

CHAPTER 9

Conclusion

9.1 PMMA on thin membranes

Much of the work presented has been concerned with the modelling of high-resolution lithography processes in thin films of PMMA on thin silicon nitride support membranes. As well as the minimum linewidths that can be obtained, attention has been paid to the simulation of the rate of increase of linewidth with exposure dose, since this is thought to be a good test of the accuracy of the simulation as far as energy distribution is concerned. For larger doses the power law relating linewidth and exposure was found to be about 0.5 in both the experimental and simulated results.

The low energy electron exposure experiments in PMMA have enabled the exposure range of secondary electrons in the material to be measured, the results being directly applicable to high resolution lithography. The apparatus and techniques that have been developed should enable new resists to be evaluated in the future.

The results of the electron energy loss spectroscopy and the low energy electron range experiments compare well in general form with published data on other materials, and some faith is therefore placed in the simulated energy dissipation distributions being close to the truth. The large discrepancy between the experimental and simulated results for the exposure of PMMA by a very fine (ie. less than one nanometre) electron beam are therefore attributed to molecular size and development effects, although charging effects have also been noted and

suggestions have been made on how these might be investigated.

Some suggestions have also been made on how the ultimate resolution might be improved in PMMA. Although a Vacuum Generators HB5 is available at present for limited use, a more stable (and more controlable) high resolution electron beam machine should soon be available within the Department and will be more suitable for such experiments to be carried out.

The simulations in the present work have been restricted to single line exposures, but the Monte-Carlo program that has been developed accepts the incident primary electron distribution in numerical form. It could therefore be used without modification to simulate the exposure of closely-spaced features, gratings for example.

9.2 Other resists

We have seen that the ultimate resolution of PMMA is probably determined by its molecular size, and it is thought that higher resolution might be obtained by the use of an amorphous resist. The work on PMMA, however, points out some other desirable attributes of high resolution resists, which might be investigated in future work.

PMMA is sensitive to low energy electrons, and most secondary electrons, which are created by single primary collisions, will lose their energy in several additional collisions, for each of which there is a finite probability of a main chain bond being broken. Some tertiary electrons will be created by these additional collisions. Since most of the secondary electrons do not move far from their point of origin (a few nanometres), most of the energy dissipation is localised around the primary collision points and hence discontinuities can occur on

development. This is known as "shot noise" when seen as variations along an exposed and developed line (often in more sensitive resists than PMMA), but it has been shown in the present work on Monte-Carlo simulations that discontinuities occur with depth, just below the critical dose for the development of narrow lines in PMMA. The necessity of exposing the resist sufficiently to clear these discontinuities results in a narrow exposure latitude for the exposure of fine lines, and hence difficulties in the lithography of closely-spaced features.

Hence it would appear that an amorphous resist that is insensitive to low energy electrons should be ideal for very high resolution lithography. The amorphous chalcogenide glass resist arsenic trisulphide is very sensitive to low energy electrons and is also sensitive to current flow (see chapter 8); this resist has not proved to be suitable for very high resolution work on the same scale as PMMA. Resists of the direct-cutting type (see chapter 1) are thought to be insensitive to low energy electrons, but are very much less sensitive than those of the exposure-development type. Depending on resist thickness, the sensitivity of sodium beta-alumina has been found[9.1] to be about 6×10^{-2} Ccm^{-1} for the exposure of 2nm wide lines, which is about eight orders of magnitude below the sensitivity of PMMA. Even PMMA is considered to be too insensitive for many lower-resolution purposes.

For more practical lithography on a nanometre scale, an amorphous, exposure-development type resist would seem to be required, in which the chemical or physical change necessary for development is the result of a fairly high-energy-loss collision, perhaps of the order of 100eV. If the efficiency of the higher energy loss collisions for causing the required change were high, then the sensitivity would be considerably better than the direct-cutting materials. Although some of the higher energy secondary electrons would be capable of exposing the resist, most

of them would lose their energy in several steps and would not cause exposure. Unlike PMMA, therefore, most of the exposure would be the result of the primary electron, rather than the secondary electron, collisions, and although the resist would be much less sensitive than PMMA, the problem of exposure localisation would not occur.

Reference

9.1 M.E. Mochel, C.J. Humphreys, J.A. Eades, J.M. Mochel, and A.M. Petford "Electron beam writing on a 20 angstrom scale in metal beta-aluminas"
Appl. Phys. Lett. 42(4), 392-394, 1983.